

Development of advanced protic ionic liquid-based electrolytes for energy storage devices

Dissertation

(kumulativ)

Zur Erlangung des akademischen Grades doctor rerum naturalium

(Dr. rer. nat.)

Vorgelegt dem Rat der Chemisch-Geowissenschaftlichen Fakultät der
Friedrich-Schiller-Universität Jena

von: M. Sc. Timo Stettner

geboren am 22.03.1992 in Frankfurt am Main

Gutachter:

1. Prof. Dr. Andrea Balducci

2. Prof. Dr. Martin Oschatz

3. Prof. Dr. Stefano Passerini

Tag der Verteidigung: 21.03.2022

Selbstständigkeitserklärung

Ich erkläre, dass ich die vorliegende Arbeit selbstständig und unter Verwendung der angegebenen Hilfsmittel, persönlichen Mitteilungen und Quellen angefertigt habe

Ort, Datum

Unterschrift der Verfasserin/des Verfassers

Erklärung zu den Eigenanteilen der Promovendin/des Promovenden sowie der weiteren Doktorandinnen/Doktoranden als Co-Autorinnen/Co-Autoren an den Publikationen und Zweitpublikationsrechten bei einer kumulativen Dissertation

Für alle in dieser kumulativen Dissertation verwendeten Manuskripte liegen die notwendigen Genehmigungen der Verlage („Reprint permissions“) für die Zweitpublikation vor.

Die Co-Autorinnen/-Autoren der in dieser kumulativen Dissertation verwendeten Manuskripte sind sowohl über die Nutzung, als auch über die oben angegebenen Eigenanteile der weiteren Doktorandinnen/Doktoranden als Co-Autorinnen/-Autoren an den Publikationen und Zweitpublikationsrechten bei einer kumulativen Dissertation informiert und stimmen dem zu (es wird empfohlen, diese grundsätzliche Zustimmung bereits bei Einreichung der Veröffentlichung einzuholen bzw. die Gewichtung der Anteile parallel zur Einreichung zu klären).

Die Anteile der Promovendin/des Promovenden sowie der weiteren Doktorandinnen/Doktoranden als Co-Autorinnen/Co-Autoren an den Publikationen und Zweitpublikationsrechten bei einer kumulativen Dissertation sind in der Anlage aufgeführt.

Name der Promovendin/ Datum Ort Unterschrift
des Promovenden

Ich bin mit der Abfassung der Dissertation als publikationsbasierte Dissertation, d.h. kumulativ, einverstanden und bestätige die vorstehenden Angaben.

Name der Betreuerin/ Datum Ort Unterschrift
des Betreuers

Erklärung zu den Eigenanteilen der Promovendin/des Promovenden sowie der weiteren Doktorandinnen/Doktoranden als Co-Autorinnen/Co-Autoren an den Publikationen und Zweitpublikationsrechten bei einer kumulativen Dissertation

Publikation 1: Protic ionic liquids in energy storage devices: Past, present and future perspective		
T. Stettner (A1), A. Balducci (A2)		
Energy Storage Materials (Volume 40, September 2021, Pages 402-414)		
Beteiligt an		
	Autor 1	Autor 2
Konzeption des Forschungsansatzes	x	x
Planung der Untersuchung	x	x
Literaturrecherche	x	
Schreiben des Manuskriptes	x	x
Vorschlag Anrechnung Publikationsäquivalente	0.5	

Publikation 2: Water in Protic Ionic Liquids: Properties and Use of a New Class of Electrolytes for Energy-Storage Devices					
T. Stettner (A1), S. Gehrke (A2), P. Ray (A3), B. Kirchner (A4), A. Balducci (A5)					
ChemSusChem 12.16 (2019): 3827-3836					
Beteiligt an					
	Autor 1	Autor 2	Autor 3	Autor 4	Autor 5
Konzeption des Forschungsansatzes	x	x		x	x
Planung der Untersuchung	x	x	x	x	x
Datenerhebung	x	x	x		
Datenanalyse und -interpretation	x	x	x		
Schreiben des Manuskriptes	x	x	x	x	x
Vorschlag Anrechnung Publikationsäquivalente	1				

Publikation 3: Water in Protic Ionic Liquid Electrolytes: From solvent separated ion pairs to water clusters					
S. Gehrke (A1), P. Ray (A2), T Stettner (A3), A. Balducci (A4) B. Kirchner (A5)					
ChemSusChem 14.16 (2021): 3315.					
Beteiligt an					
	Autor 1	Autor 2	Autor 3	Autor 4	Autor 5
Konzeption des Forschungsansatzes	x			x	x
Planung der Untersuchung				x	
Datenerhebung	x	x	x		
Datenanalyse und -interpretation	x	x			
Schreiben des Manuskriptes	x	x	x	x	x
Vorschlag Anrechnung Publikationsäquivalente			0.5		

Publikation 4: Mixtures of glyme and aprotic-protic ionic liquids as electrolytes for energy storage devices					
T. Stettner (A1), P. Huang (A2), M. Goktas (A3), P. Adelhelm (A4), A. Balducci (A5)					
The Journal of Chemical Physics 2018, 148 (19), 193825					
Beteiligt an					
	Autor 1	Autor 2	Autor 3	Autor 4	Autor 5
Konzeption des Forschungsansatzes	x	x		x	x
Planung der Untersuchung	x	x			
Datenerhebung	x	x			
Datenanalyse und -interpretation	x	x			
Schreiben des Manuskriptes	x				x
Vorschlag Anrechnung Publikationsäquivalente	0				

Publikation 4 ist vorwiegend im Rahmen meiner Masterarbeit entstanden und wird deshalb in der Dissertation nur als inhaltliche Unterstützung verwendet. Sie ist jedoch weder relevant für die Publikationsäquivalente noch für die Vollkommenheit der Arbeit.

Publikation 5: Imidazolium-Based Protic Ionic Liquids as Electrolytes for Lithium-Ion Batteries			
T. Stettner (A1), F.C. Walter (A2), A. Balducci (A3)			
Batteries & Supercaps 2.1 (2019): 55-59.			
Beteiligt an			
	Autor 1	Autor 2	Autor 3
Konzeption des Forschungsansatzes	x		x
Planung der Untersuchung	x	x	x
Datenerhebung	x	x	
Datenanalyse und -interpretation	x	x	
Schreiben des Manuskriptes	x		x
Vorschlag Anrechnung Publikationsäquivalente	1		

Publikation 6: Enabling safe and stable Li metal batteries with protic ionic liquid electrolytes and high voltage cathodes					
G. Lingua (A1), M. Falco (A2), T. Stettner (A3), C. Gerbaldi (A4), A. Balducci (A5)					
Journal of Power Sources 481 (2021): 228979.					
Beteiligt an					
	Autor 1	Autor 2	Autor 3	Autor 4	Autor 5
Konzeption des Forschungsansatzes	x		x	x	x
Planung der Untersuchung	x		x	x	x
Datenerhebung	x	x	x		
Datenanalyse und -interpretation	x	x	x		
Schreiben des Manuskriptes	x		x	x	x
Vorschlag Anrechnung Publikationsäquivalente			0.5		

Publikation 7: Ionic Liquid-Based Electrolytes for Calcium-Based Energy Storage Systems				
T. Stettner (A1), R. Dugas (A2), A. Ponrouch (A3), A. Balducci (A4)				
Journal of The Electrochemical Society 167.10 (2020): 100544				
Beteiligt an				
	Autor 1	Autor 2	Autor 3	Autor 4
Konzeption des Forschungsansatzes	x	x	x	x
Planung der Untersuchung	x	x	x	x
Datenerhebung	x	x		
Datenanalyse und -interpretation	x	x		
Schreiben des Manuskriptes	x	x	x	x
Vorschlag Anrechnung Publikationsäquivalente	0.75			

Publikation 8: Silica based ionogels: interface effects with aprotic and protic ionic liquids with lithium								
A. Marie (A1), B. Said (A2), A. Galarneau (A3), T. Stettner (A4), A. Balducci (A5), M. Bayle (A6), B. Humbert (A7), J. Le Bideau (A8)								
Physical Chemistry Chemical Physics 22.41 (2020): 24051-24058.								
Beteiligt an								
	A 1	A 2	A 3	A 4	A 5	A 6	A 7	A 8
Konzeption des Forschungsansatzes		x			x			x
Planung der Untersuchung		x						x
Datenerhebung	x	x	x	x		x	x	
Datenanalyse und -interpretation	x	x	x	x		x	x	
Schreiben des Manuskriptes	x	x	x	x	x	x	x	x
Vorschlag Anrechnung Publikationsäquivalente	0.5							

Publikation 9: Protic Ionic Liquids-Based Crosslinked Polymer Electrolytes: A New Class of Solid Electrolytes for Energy Storage Devices
 T. Stettner (A1), G. Lingua (A2), M. Falco (A3), A. Balducci (A4), C. Gerbaldi (A5)
 Energy Technology 8.11 (2020): 2000742.

Beteiligt an					
	Autor 1	Autor 2	Autor 3	Autor 4	Autor 5
Konzeption des Forschungsansatzes	x	x		x	x
Planung der Untersuchung	x	x		x	x
Datenerhebung	x	x	x		
Datenanalyse und -interpretation	x	x	x		
Schreiben des Manuskriptes	x	x		x	x
Vorschlag Anrechnung Publikationsäquivalente	0.75				

Acknowledgement

First, I want to thank Prof. Dr. Andrea Balducci for giving me the opportunity and his support to realize this work. But also, for the many possibilities to present my projects on an international stage and to meet other researchers to exchange thoughts and ideas.

I also thank Prof. Dr. Oschatz for reviewing my thesis as second reviewer.

Furthermore, I thank all my co-workers for the great atmosphere in our group. The coffee breaks, the diverse get-togethers, and the willingness to operate as a team facilitated and enriched the daily work immensely.

Moreover, I want to thank the colleagues of the ITUC, especially Saskia Sabrina Thieme and Beate Fähndrich. Their organizational skills and their experience regarding the sometimes very complex university business was invaluable in many cases.

Finally, I want to thank my family and friends for all the positive energy I could draw from the shared adventures and experiences, helping to stay on course for this whole journey.

Summary

This thesis is dedicated to the development of alternative electrolytes for electrochemical energy storage devices which have become a crucial part of modern society and infrastructure. Conventional electrolytes for supercapacitors or batteries are usually based on a combination of conducting salt and flammable or volatile solvents. Replacing them with inflammable and very low volatile ionic liquids (ILs), molten salts with a melting point below 100 °C, can increase the safety of the devices, which is an imperative for mobile as well as stationary applications.

While there are many different types of ILs, the works within this thesis focus on protic ionic liquids (PILs), bearing an available proton in their structure. They have the advantage of an easier, thus often cheaper synthesis as well as the possibility of an additional charge transport mechanism besides conventional vehicular ion transport. Both points address the most often cited drawbacks of ionic liquids, meaning the cost as well as bad transport characteristics, i.e., high viscosity and low ionic conductivity.

The implementation of PILs in electrochemical energy storage devices is yet not as advanced compared to their aprotic counterparts. This is related to the presence of an easily reducible, available proton in their structure. Nevertheless, their application in supercapacitors as well as batteries documented in the literature so far show promising results. They are summarized in the introduction part of this thesis, which is based on Publication 1 (review article).

The first part of the work covers the implementation of PILs in electrical double layer capacitors (EDLCs). In Publication 2, the investigated PIL 1-butylpyrrolidinium bis(trifluoromethanesulfonyl)imide ([Pyr_{H4}][TFSI]) was mixed with small amounts of water to increase the transport properties drastically as well as lowering the melting point below room temperature. While the addition of water comes for the price of a lower operating voltage compared to the neat PIL, the power capability of EDLC employing these PIL-water-based electrolytes could be increased significantly. Furthermore, the investigations were supported by classical molecular dynamics simulations, which give insight on the interactions between water and PIL molecules. Continuing this work, Publication 3 is focusing on the simulations, going even more into detail of the analysis of the interactions.

Publication 4 also concerns the implementation of PILs in EDLCs, in this case a sodium-ion-based system. Electrolytes for sodium-based systems are often glycol ether (glyme) based, offering the possibility to employ electrode materials like graphite. Unlike lithium-ions, sodium-ions are stored in these intercalation materials via co-intercalation together with solvent molecules. Thus, the PIL used in this work ($[\text{Pyr}_{\text{H4}}][\text{TFSI}]$) was mixed with bis(2-methoxyethyl) (diglyme). Additionally, a comparison with an aprotic ionic liquid (AIL) was carried out, using 1-butyl-1-methyl-pyrrolidinium bis(trifluoromethanesulfonyl)imide ($[\text{Pyr}_{14}][\text{TFSI}]$). The optimal ratio of glyme to IL was determined by investigating chemical-physical characteristics of the electrolytes as well as the performance of EDLCs employing these diglyme-IL-mixtures.

The second part of the thesis is comprised of publications related to the employment of PILs in battery devices. More specifically, Publication 5 is about the synthesis of imidazolium-based PILs and their application in lithium-ion batteries. Four different PILs were synthesized, fully characterized, and employed in combination with lithium iron phosphate (LFP, LiFePO_4). While LFP electrodes could successfully be cycled in all PILs, the best performance was achieved in 1-2-Dimethylimidazolium bis(trifluoromethanesulfonyl)imide as well as 1-2-Dimethylimidazolium bis(fluorosulfonyl)imide.

The effect of additives in PIL based electrolytes, e.g., for an effective solid-electrolyte-interphase formation, was researched in Publication 6. $[\text{Pyr}_{\text{H4}}][\text{TFSI}]$ and 1-butylpyrrolidinium bis(fluorosulfonyl)imide ($[\text{Pyr}_{\text{H4}}][\text{FSI}]$) were combined with $\text{Li}[\text{TFSI}]$ and $\text{Li}[\text{FSI}]$, respectively, as well as vinyl ethylene carbonate (VEC). These electrolytes were successfully employed in lithium-metal cells using LFP but also lithium-nickel-manganese-cobalt-oxide as cathode material. Furthermore, it could be shown that with the addition of VEC, even the reversible cycling of lithium-metal electrodes is possible in these PIL-based electrolytes, which are usually prone to reduction when combined with elementary lithium.

Another post-lithium system in combination with PIL-based electrolytes has been examined in Publication 7. In this work, calcium-ion-based electrolytes, utilizing $[\text{Pyr}_{\text{H4}}][\text{TFSI}]$ as well as $[\text{Pyr}_{14}][\text{TFSI}]$ respectively, were compared and their application in an EDLC as well as in a battery setup was investigated. While activated carbon-based electrodes could be cycled in both electrolyte systems, TiS_2 -based electrodes could only be successfully cycled in the aprotic electrolyte. The results make clear that more investigations are necessary to establish PILs in

calcium-based systems, for example employing additives to achieve a reversible storage of calcium-ions in battery materials.

The final part of the thesis is about the confinement of PILs in host structures. This way, the safety of an electrolyte can be increased in terms of leakage but also to enable flexible energy storage devices. Publication 8 focusses on the chemical-physical changes of an AIL ([Pyr₁₄][TFSI]) and PIL ([Pyr_{H4}][TFSI]) when encompassed in a silica based material, resulting in ionogels. Furthermore, the influence of the addition of a lithium salt has been assessed. Depending on the nature of the ILs, these influences differ, mainly due to the presence/absence of the protic network in an IL, leading to different changes within the ILs.

Finally, a polymer based on polyethylene oxide combined with the PIL [Pyr_{H4}][TFSI] was examined in Publication 9. First, its conductivity as well as flammability were investigated, revealing high conduction as well as high resistance towards ignition. Afterwards it was employed in an EDLC and in a battery system. While the former is able to achieve capacitance values comparable to an EDLC system employing neat [Pyr_{H4}][TFSI], the power performance needs to be improved in the future. The battery system, on the other hand, was showing not only good energy densities, but also power performance.

Zusammenfassung

Die vorliegende Doktorarbeit befasst sich mit der Entwicklung von alternativen Elektrolyten für elektrochemische Energiespeichergeräte, welche zu einem wichtigen Bestandteil der modernen Gesellschaft als auch der Infrastruktur geworden sind. Konventionelle Elektrolyte für Superkondensatoren oder Batterien basieren normalerweise auf einer Kombination aus Leitsalz und brennbaren oder flüchtigen Lösungsmitteln. Das Ersetzen dieser Lösungsmittel mit unbrennbaren und schwerflüchtigen ionischen Flüssigkeiten (ILs), geschmolzene Salze mit einem Schmelzpunkt unter 100 °C, kann die Sicherheit der Speichergeräte erhöhen. Diese letztgenannte Eigenschaft ist nicht nur zwingend notwendig für mobile, sondern auch für stationäre Anwendungen.

Es gibt viele verschiedene Typen von ILs, der Fokus der meisten Arbeiten in dieser Doktorarbeit liegen jedoch auf protischen ionischen Flüssigkeiten (PILs), welche ein verfügbares Proton in ihrer Struktur beinhalten. Sie haben den Vorteil einer einfacheren, dadurch oftmals günstigeren Synthese als auch die Möglichkeit eines weiteren Ladungstransportmechanismus neben der konventionellen einfachen Bewegung von Ladungsträgern. Beide Punkte betreffen die meistgenannten Nachteile von ILs, nämlich die Kosten als auch die schlechten Transporteigenschaften, im speziellen eine hohe Viskosität und geringe ionische Leitfähigkeit.

Die Implementierung von PILs in elektrochemischen Energiespeichergeräten ist noch nicht so weit vorangeschritten verglichen mit ihren aprotischen Gegenstücken. Dies liegt an der Anwesenheit eines leichtreduzierbaren Protons in ihrer Struktur. Nichtsdestotrotz zeigen die bisher vorliegenden Veröffentlichungen mit Anwendungen in Superkondensatoren als auch Batterien vielversprechende Ergebnisse. Diese sind in der Einleitung der vorliegenden Doktorarbeit zusammengefasst, welche auf Publikation 1 (Review Artikel) basiert.

Der erste Teil der Arbeit befasst sich mit der Implementierung von PILs in elektrochemischen Doppelschichtkondensatoren (EDLCs). In Publikation 2 wurde die untersuchte PIL 1-Butylpyrrolidinium Bis(trifluormethansulfonyl)imid ($[\text{Pyr}_{\text{H4}}][\text{TFSI}]$) mit geringen Mengen Wasser gemischt, um die Transporteigenschaften drastisch zu verbessern als auch den Schmelzpunkt unter Raumtemperatur zu verringern. Während die Zugabe von Wasser zwar zu einer niedrigeren Betriebsspannung führt, konnte das Leistungspotential von EDLCs mit diesen PIL-Wasser-basierten Elektrolyten, verglichen mit der reinen PIL, erheblich verbessert werden. Weiterhin wurden die Untersuchungen mit klassischen molekularen dynamischen

Simulationen unterstützt, welche Einblicke in die Interaktionen zwischen Wasser und PIL Molekülen geben. Diese Arbeit weiterführend wird der Fokus in Publikation 3 auf die Simulationen gelegt, mit detaillierteren Analysen bezüglich der Molekülinteraktionen.

Publikation 4 betrifft ebenfalls die Implementierung von PILs in EDLCs, in diesem Fall ein natriumionenbasiertes System. Elektrolyte für natriumbasierte Systeme sind oftmals glykoletherbasiert (glyme), was die Möglichkeit eröffnet Elektrodenmaterialien wie Graphit zu nutzen. Anders als Lithiumionen werden Natriumionen in diesen Interkalationsmaterialien durch „co-Interkalationen“ zusammen mit Lösungsmittelmolekülen eingelagert. Deswegen wurde die in dieser Arbeit untersuchte PIL $[\text{Pyr}_{\text{H4}}][\text{TFSI}]$ mit Bis(2-methoxyethyl)ether (diglyme) gemischt. Zusätzlich wurde ein Vergleich mit einer aprotischen ionischen Flüssigkeit (AIL) durchgeführt. Hierfür wurde 1-Butyl-1-Methylpyrrolidinium Bis(trifluormethansulfonyl)imid ($[\text{Pyr}_{14}][\text{TFSI}]$) verwendet. Das optimale Verhältnis zwischen glyme und IL wurde durch Untersuchungen der chemisch-physikalischen Eigenschaften der Elektrolyte als auch der Leistungsfähigkeit von EDLCs, die diese diglyme-IL-basierten Elektrolyte nutzen, bestimmt.

Der zweite Teil der Doktorarbeit setzt sich aus Publikationen zusammen, die sich mit der Anwendung von PILs in Batterien beschäftigen. Genauer gesagt behandelt Publikation 5 die Synthese von imidazoliumbasierten PILs und deren Anwendung in Lithium-Ionen-Akkumulatoren. Vier verschiedene PILs wurden synthetisiert, vollständig charakterisiert und mit Lithium-Eisenphosphat (LFP, LiFePO_4) Elektroden kombiniert. Während diese Elektroden in allen vier PILs zyklisiert werden konnten, wurden die besten Ergebnisse in 1-2-Dimethylimidazolium Bis(trifluormethansulfonyl)imid und 1-2-Dimethylimidazolium bis(fluorsulfonyl)imid erzielt.

Der Einfluss von Additiven in PIL-basierten Elektrolyten, um zum Beispiel eine effektive „solid-electrolyte-interphase“ aufzubauen, wurde in Publikation 6 untersucht. $[\text{Pyr}_{\text{H4}}][\text{TFSI}]$ und Butylpyrrolidinium Bis(fluormethansulfonyl)imid ($[\text{Pyr}_{\text{H4}}][\text{FSI}]$) wurden jeweils mit $\text{Li}[\text{TFSI}]$ und $\text{Li}[\text{FSI}]$, als auch mit Vinylethylencarbonat (VEC) gemischt. Diese Elektrolyte wurden erfolgreich in Lithiummetall-Zellen mit LFP- aber auch Lithium-Nickel-Mangan-Cobalt-Oxid-Kathoden verwendet. Weiterhin konnte gezeigt werden, dass durch die Addition von VEC sogar das reversible Zyklisieren von Lithiummetallelektroden in diesen PIL-basierten Elektrolyten

möglich ist, welche normalerweise anfällig für Reduktionsreaktionen sind, wenn sie mit elementarem Lithium in Kontakt kommen.

Ein weiteres „post Lithium“-System in Kombination mit PIL basierten Elektrolyten wurde in Publikation 7 untersucht. In dieser Arbeit wurden calciumionenbasierte Elektrolyte verglichen, jeweils basierend auf $[\text{Pyr}_{\text{H4}}][\text{TFSI}]$ und $[\text{Pyr}_{14}][\text{TFSI}]$, und deren Anwendung in einem EDLC- als auch Batteriesetup untersucht. Während Elektroden basierend auf aktiviertem Kohlenstoff in beiden Elektrolytsystemen zyklisiert werden konnten, war dies mit TiS_2 basierten Elektroden nur im aprotischen Elektrolyt möglich. Die Ergebnisse verdeutlichen, dass weitere Untersuchungen nötig sind, um PILs in calciumbasierten Systemen zu etablieren, zum Beispiel durch das Einsetzen von Additiven, um ein reversibles Einlagern von Calciumionen in Batteriematerialien zu ermöglichen.

Im letzten Teil der Doktorarbeit geht es um das Einschließen von PILs in geeigneten Trägerstrukturen. Dadurch kann die Sicherheit eines Elektrolyten in Bezug auf Auslaufen erhöht, aber ebenso flexible Energiespeichersysteme ermöglicht werden. Publikation 8 legt dabei den Fokus auf die Änderungen der chemisch-physikalischen Eigenschaften einer AIL ($[\text{Pyr}_{14}][\text{TFSI}]$) und einer PIL ($[\text{Pyr}_{\text{H4}}][\text{TFSI}]$) die durch das Einschließen in einem siliziumbasierten Material verursacht werden, wodurch „Ionogels“ resultieren. Weiterhin wurde der Einfluss der Zugabe eines Lithiumsalzes untersucht. Abhängig von der Art der IL fallen die Einflüsse und dadurch verursachte Veränderungen unterschiedlich aus. Dies ist hauptsächlich auf die Anwesenheit/Abwesenheit des protischen Netzwerkes zurückzuführen.

Schließlich wurde ein Polymer basierend auf Polyethylenoxid, welches mit der PIL $[\text{Pyr}_{\text{H4}}][\text{TFSI}]$ kombiniert wurde, in Publikation 9 untersucht. Zunächst wurde dessen Leitfähigkeit und Entflammbarkeit untersucht, wobei ein hohes Leitvermögen als auch eine niedrige Brennbarkeit festgestellt worden sind. Anschließend wurde es in einem EDLC- als auch Batteriesystem eingesetzt. Obwohl Ersteres fähig ist elektrische Kapazitäten vergleichbar mit einem EDLC-System in Kombination mit reinem $[\text{Pyr}_{\text{H4}}][\text{TFSI}]$ zu erreichen, muss dessen Leistungsfähigkeit jedoch weiter verbessert werden. Das Batteriesystem wiederum zeigte nicht nur gute Energiedichten, sondern auch eine hohe Leistungsfähigkeit.

Table of Contents

1.	Introduction	1
1.1.	Ionic Liquids.....	1
1.2.	Properties of Protic Ionic Liquids	5
1.2.1.	Thermal Properties	6
1.2.2.	Transport Properties	10
1.2.3.	Electrochemical Stability	12
1.3.	Synthesis of Protic Ionic Liquids.....	12
1.4.	Common Protic Ionic Liquids	14
1.4.1.	Cations.....	14
1.4.2.	Anions.....	15
1.5.	Mixtures of Protic Ionic Liquids.....	15
1.6.	Electrochemical Energy Storage Devices	17
1.6.1.	Electrical Double Layer Capacitors.....	18
1.6.2.	Pseudocapacitors	24
1.6.3.	Alkali Metal-Ion Batteries	26
1.7.	PILs in Chemical Energy Storage Devices	30
1.7.1.	PILs in Supercapacitors.....	30
1.7.2.	PILs in Alkali Metal-Ion Batteries	32
1.8.	The development of new PIL-based electrolytes.....	34
1.8.1.	Publication 1: Protic ionic liquids in energy storage devices: past, present and future perspective	36
2.	Results and Discussion	49
2.1.	PILs in EDLC systems	49
2.1.1.	Publication 2/Publication 3: Water in Protic Ionic Liquids: Properties and Use of a New Class of Electrolytes for Energy-Storage Devices / Water in Protic Ionic Liquid Electrolytes: From Solvent Separated Ion Pairs to Water Clusters.....	49

2.1.2.	Publication 4: Mixtures of glyme and aprotic-protic ionic liquids as electrolytes for energy storage devices	73
2.2.	PILs in Battery Systems	85
2.2.1.	Publication 5: Imidazolium-Based Protic Ionic Liquids as Electrolytes for Lithium-Ion Batteries	85
2.2.2.	Publication 6: Enabling safe and stable Li metal batteries with protic ionic liquid electrolytes and high voltage cathodes.....	92
2.2.3.	Publication 7: Ionic Liquid-Based Electrolytes for Calcium-Based Energy Storage Systems	102
2.3.	Confinement of PILs	110
2.3.1.	Publication 8: Silica based ionogels: interface effects with aprotic and protic ionic liquids with lithium	110
2.3.2.	Publication 9: Protic Ionic Liquids-Based Crosslinked Polymer Electrolytes: A New Class of Solid Electrolytes for Energy Storage Devices.....	120
3.	Conclusion	131
4.	Outlook.....	135
5.	References.....	136
6.	Appendix	I

Figure Index

Figure 1 Phase diagram of a AlCl_3 in ethyl pyridinium bromide system.	2
Figure 2 Development of IL related publications over the years.	3
Figure 3 Possible classification for different types of ionic liquids.	4
Figure 4 Walden Plot for different kinds of ionic liquids.	6
Figure 5 Influence of the ΔpK_a between acid and base of a PIL on the boiling point of the respective PIL.	7
Figure 6 Optimization of the mobility of the acidic proton in a PIL by adjusting the ΔpK_a value	11
Figure 7 Reaction pathways for the synthesis of hydrophobic and hydrophilic PILs.	13
Figure 8 Common types of cations and anions for PILs.	14
Figure 9 Improvement of transport properties of a PIL via mixing with a solvent.	16
Figure 10 Schematics of both a classical capacitor and an electrochemical double layer capacitor.	19
Figure 11 Approximate OPVs of different electrolyte systems for EDLCs.	23
Figure 12 Voltage profiles of different supercapacitor systems.	25
Figure 13 Schematic of a lithium-ion battery based on a graphite anode and a LiCoO_2 cathode.	28

Table Index

Table 1 Correlation of different pseudocapacitor systems to their specific thermodynamic relations.....	24
---	----

List of Abbreviations

AC	Activated Carbon
ACN	Acetonitrile
[AcO] ⁻	Acetate
AIL	Aprotic ionic liquid
b.p.	Boiling point
2-D	2-Dimensional
3-D	3-Dimensional
DEC	Diethyl carbonate
DMC	Dimethyl carbonate
EC	Ethylene carbonate
EDLC	Electrical double layer capacitor
emf	Electromotive force
ESW	Electrochemical stability window
[1-Et-3-Melm][BF ₄]	1-Ethyl-3-methylimidazolium tetrafluoroborate
[Et ₄ N][BF ₄]	Tetraethylammonium tetrafluoroborate
[EtNH ₃][NO ₃]	Ethylammonium nitrate
[Et ₃ NH][TFSI]	Triethylamine bis(trifluoromethanesulfonyl)imide
[1-EtOH-3-Melm][TFSI]	1-Ethanol-3-methylimidazolium bis(trifluoromethanesulfonyl)imide
FD	Formation degree
[FSI] ⁻	Bis(fluorosulfonyl)imide
2G	Bis(2-methoxyethyl) ether
HC	Hard carbon
[HCOO] ⁻	Formate
HPyr	0.5 M Lithium bis(fluorosulfonyl)imide in 1-butylpyrrolidinium bis(trifluoromethanesulfonyl)imide
IL	Ionic liquid
[Im _H] ⁺	Imidazolium
[Im _H][TFSI]	Imidazolium bis(trifluoromethanesulfonyl)imide
LFP (LiFePO ₄)	Lithium iron phosphate
LIB	Lithium-ion battery

LTO	Lithium titanate oxide
[1-2-Me ₂ Im _H] ⁺	1-2-Dimethylimidazolium
[1-MeIm _H][FSI]	1-Methylimidazolium bis(fluorosulfonyl)imide
[1-MeIm _H][TFSI]	1-Methylimidazolium bis(trifluoromethanesulfonyl)imide
[2-MePy _H][TFA]	α-Picoline trifluoroacetic acid
m.p.	Melting point
NMC (LiNi _x Mn _y Co _z O ₂)	Lithium nickel manganese cobalt oxide
NMR	Nuclear magnetic resonance
[NO ₃] ⁻	Nitrate
OPV	Operating voltage
PC	Propylene carbonate
PEMFC	Proton exchange membrane fuel cell
PEO	Polyethylene oxide
PEO_HPyr	0.5 M Lithium bis(fluorosulfonyl)imide in 1-butylpyrrolidinium bis(trifluoromethanesulfonyl)imide encompassed in polyethylene oxide
PIL	Protic ionic liquid
[Pip _H] ⁺	Piperidinium
[Py _H] ⁺	Pyridinium
[Pyr _H] ⁺	Pyrrolidinium
[Pyr _{HH}][NO ₃]	pyrrolidinium nitrate
[Pyr _{H4}][TFSI]	1-Butylpyrrolidinium bis(trifluoromethanesulfonyl)imide
[Pyr ₁₄][TFSI]	1-Butyl-1-methylpyrrolidinium bis(trifluoromethanesulfonyl)imide
QSPR	Quantitative structure-activity relationship
RT	Room temperature
SEI	Solid-electrolyte-interphase
[TFA] ⁻	Trifluoroacetic acid
[TFSI] ⁻	Bis(trifluoromethanesulfonyl)imide
T _g	Glass transition temperature
UV	Ultraviolet
VEC	Vinyl ethylene carbonate
wt.%	Weight percent

1. Introduction

1.1. Ionic Liquids

Ionic liquids (ILs) are a class of compounds well-known by most chemists nowadays and established in many fields of chemistry. Their nature may appear rather trivial on the first look, being molten salts with a melting point below 100 °C. Nevertheless, the very reason for their multiple applications, the interplay between anions and cations, is nowhere close from being completely understood and predictable. Therefore, they still appear as attractive and interesting compounds, even 20 years after their enormous rise in publicity in the research community but also in the industry.[1]

Although this exposure was taking place at the beginning of the 21st century, the principle of ILs, or rather molten salts, was known for much longer. In the early 19th century, it was Sir Humphry Davy who isolated a series of alkali and alkaline earth metals using molten salt electrolysis, admittedly with salts having very high melting points.[2] Until today, this use of molten salts is a very important method to produce aluminum, amongst others.[3] The first molten salt with a melting point (m.p.) below 100 °C was a “syrupy liquid” reported by W. Ramsay in 1876 when synthesizing different picoline allyl compounds, e.g., 1-allyl-2-methylpyridinium chloride, with a melting point of 93.9 °C.[4]

This quite unexciting note is not surprising, considering that at this stage, molten salts were very hot melts, in which anything other than temperature insensible electrochemistry was not possible. How should one visualize sensible chemical reactions or materials in such a torrid medium? This was exactly the problem Paul Walden was facing in 1914 when he tried to investigate the electric conductivity and molecular sizes of water free molten salts. In order to utilize methods and apparatuses suitable for these investigations only applicable at mild conditions, he needed to find salts with very low melting points. The solution was moving from inorganic to organic salts, more precisely ammonium salts, e.g., ethylammonium nitrate ([EtNH₃][NO₃]) with a melting point of 12 °C.[5]

Despite this first utilization of a room temperature (RT) molten salt, the main application of these ionic media remained in electrochemistry at rather high temperatures until the second half of the 20th century. This slowly changed with investigations about different alkyl

pyridinium halide – AlCl_3 mixtures from different research groups.[6, 7] The melting point of these mixtures could be lowered even to $-40\text{ }^\circ\text{C}$, depending on the composition (Figure 1). Only a few research groups picked up on this development and employed these low melting AlCl_3 systems e.g., as electrolyte in thermal batteries or even as reaction media for organic chemistry.[8-10] Nevertheless, the idea to perform chemical reactions as well as analyze sensible compounds in these ionic, aprotic molten salts started to grow. Furthermore, the yet rather undefined term ionic liquid instead of molten salt started to be used more and more.[11]

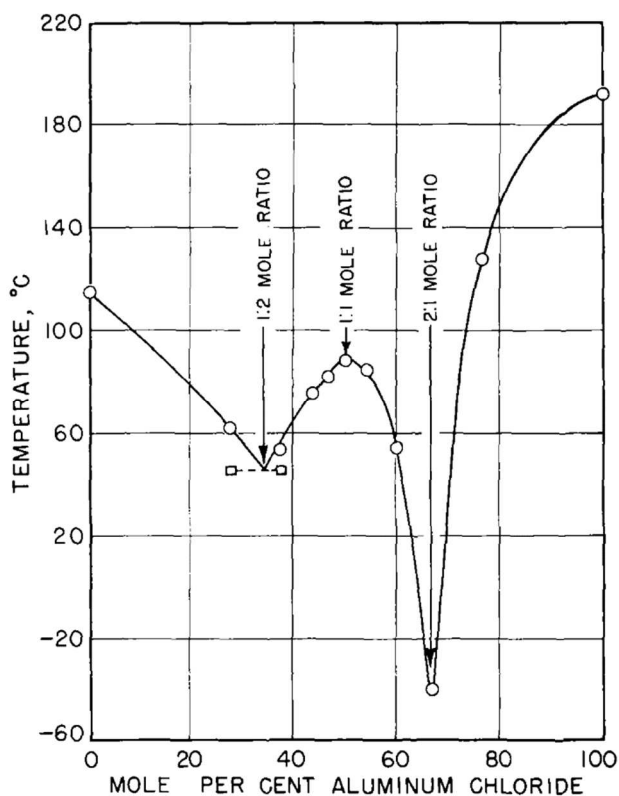


Figure 1 Phase diagram of a AlCl_3 in ethyl pyridinium bromide system. Figure taken from [6] with permission of publisher IOP Publishing, Ltd.

It still took almost 20 years until ILs had their breakthrough in the chemical society. One big obstacle was the instability of the AlCl_3 compounds towards air and water, which was solved by the introduction of the 1-ethyl-3-methylimidazolium cation by Wilke et al. in 1992 and also by the bis(trifluoromethylsulfonyl)imide anion by Bonhôte et al. in 1996.[12, 13] These works opened up the possibilities for far more cation and anion combinations resulting in RT ILs, each with specific, somewhat tunable properties. Combined with the shifting attitude of the chemical industry at that time, towards environmental friendlier and more sustainable

production, this new “class” of compounds drew massive attention as green solvent, both from the research community as well as from the industry.[14, 15] Of course, other factors contributed to this rise, e.g., the commercial availability of ILs or the better connection of researchers.[16] Worth mentioning here should also be the sometimes unjustified claims or hopes with such a kind of hype, like nonexistent vapor pressure or low- to non-toxicity, which have gotten disproven over time.[17-20]

Nevertheless, the true benefits and characteristics of ILs, discussed in chapter 1.3, were more and more recognized and sufficiently understood. Gradually, they were implemented in a large variety of applications, including reaction media or even as catalyst for organic as well as inorganic chemistry, cellulose processing, chemical analysis, biocatalysis, CO₂ capture and as electrolytes in chemical energy storage devices.[21-27]

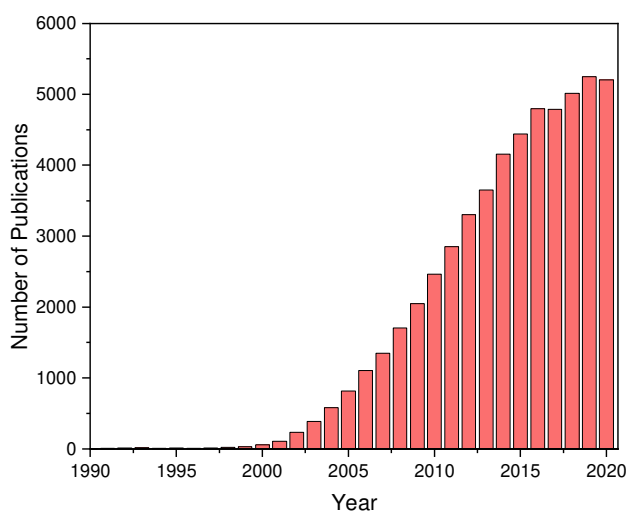


Figure 2 Development of IL related publications over the years. Created with Web of Science™ searching for the topic “ionic liquid”.

As already mentioned, and perfectly highlighted by this broad list of applications (Figure 2), ILs are very versatile, and their manifold of characteristics makes it necessary to classify and distinguish different types of ILs (Figure 3). This does not only make it easier to discuss their properties and their influences, but also to filter more efficiently for specific applications in the sheer mass of ILs.

The most prominent representatives of ILs are aprotic ionic liquids (AILs), which are the most studied as well as industrial employed ILs.[16, 28] Representatives of this class usually have the characteristics generally associated with ILs, including very low vapor pressures, broad

electrochemical as well as thermal stabilities but also relatively poor ionic transport properties.[29]

Another group of ILs consists of polymeric ionic liquids. Here, either the anion or the cation, or even both, are connected to a polymer. Thus, flexible and electrochemical stable polymers can be synthesized with the possibility to shape them individually. While the main field of application of polymeric ILs lies in electrochemical energy storage devices as solid electrolyte, they are more and more employed for other tasks, e.g., osmotically driven processes or as optical sensors.[30-32]

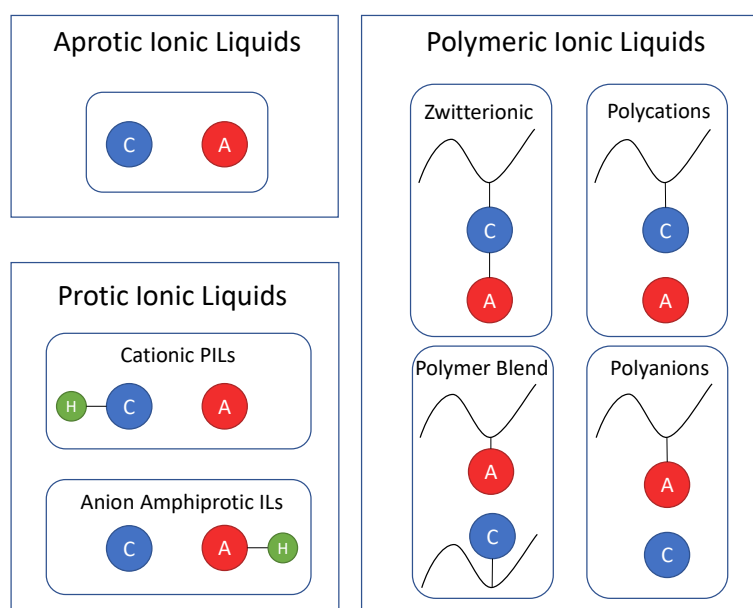


Figure 3 Possible classification for different types of ionic liquids.

Finally, as the group of aprotic ionic liquids already indicates, ILs with an available proton, either on the cation or the anion, can be classified as protic ionic liquids (PILs). In general, PILs and AILs have rather similar properties in terms of transport and thermal properties compared to conventional solvents, as opposed to polymeric ILs. When looking closer however, there are fundamental differences in almost all characteristics with the available proton being the source of most of them. [33] Although less used than AILs in research and industry, PILs cover a large variety of application areas. Obviously, they are applicable when a protic environment is necessary, in contrast to AILs.[34, 35]

Since most investigations during this thesis have been focused on cationic protic ionic liquids, the next chapters will focus on their properties in detail, with comparisons to AILs when appropriate.

1.2. Properties of Protic Ionic Liquids

The chemical-physical properties of PILs differ from their aprotic counterparts mostly because of the presence of a proton acceptor-donor system. While AILs are only governed by Coulombic and some cohesion or dispersion forces, anions and cations in PILs experience much stronger interactions in the form of hydrogen bonds. [36-39] Due to this, the strength of the employed acid and base have a dramatic influence on the overall properties of a PIL.[34, 40] This is true not only because of the changing hydrogen network, but also owing to the degree of protonation, a property expressible by the ionicity of a PIL.

$$(\eta * \Lambda)^\alpha = \text{constant} \quad (1)$$

The term ionicity in the context of PILs was first introduced by Angell et al. in 2003.[41] The original intent was to describe the degree of ion dissociation within a PIL, with a higher ionicity meaning lower amounts of paired ions. Using the Walden rule (see Equation 1), stating that the product of ionic conductivity (Λ) and viscosity (η) of a solution should be constant, a prediction about the ionicity of a PIL can be made. Most often a comparison with an aqueous 0.1 M KCl reference line is performed, in which the ions are expected to be fully dissociated. ILs close to this line are also expected to have fully dissociated cations and anions, while ILs below the line experience ion pairing. This of course, influences the transport properties, as less charge carriers are available, with the ionic conduction becoming more and more dependent on the viscosity. The third case, in which ILs lay above the reference line, occurs when charge transport mechanisms take place which are independent from the viscosity. The Grotthuss mechanism is one example, possible only in PILs, which has been investigated over the years and will be explained in a later section.[42, 43]

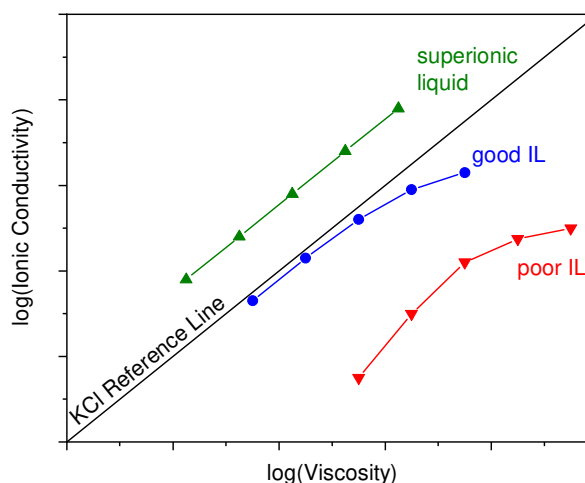


Figure 4 Walden Plot for different kinds of ionic liquids. The ionic conductivity is plotted against the viscosity in a logarithmic scale. The ionicity of an IL is evaluated by referencing it to an aqueous KCl reference line.

Although quite sound for simple mixtures, this method has been discussed and questioned by several groups regarding PILs.[44, 45] One problem associated with the whole concept of ionicity is the thought of only having either dissociated ions or ion pairs. The difficulty with PILs however, is the often-incomplete reaction of acid and base or the back reaction to the precursors, depending on the ΔpK_a value of the PIL. The proton transfer can be illustrated by the Formation Degree (FD):

$$FD = \frac{[A^-] + [HB^+] + [A^-HB^+]}{[A^-] + [HB^+] + [A^-HB^+] + [HA] + [B]} \quad (2)$$

The added neutral components in the mix act almost as solvents with lower viscosities compared to the PIL. Regarding the ionicity, Mariani et al. thus suggest using a “reduced” ionicity when discussing the quality of a PIL, basically taking every component in the liquid in consideration.[46]

1.2.1. Thermal Properties

One of the most important characteristics of ILs, making them attractive for most applications, is the very low vapor pressure, sometimes even claimed to be nonexistent.[17, 47] While this claim has been disproven over time, it is a fact that AILs display extremely high vaporization enthalpies depending on the coulombic interactions of the ion pairs, which are still present in

the gas phase.[48, 49] For PILs on the other hand, the vapor pressure as well as the composition of the gas phase are depending on several factors.

As already explained, the ΔpK_a value of the PIL influence the FD and thus the composition of a PIL. In the case of a low ΔpK_a , the concentration of neutral species, precursor acid and base molecules, is rather high. When increasing the temperature, these molecules will start to vaporize much earlier than the ion pairs, leading to a reduced boiling point. This means, the boiling point of the precursors is an important factor for the thermal attributes of a PIL. When increasing the ΔpK_a of a PIL by using stronger acids/base, less neutral species will be present. However, this amount is also temperature dependent, resulting in lower FD values at higher temperatures. Thus, even PILs with relatively high ΔpK_a can have neutral species evaporating. When increasing the ΔpK_a even further, the vapor will consist only of ion pairs, resembling a more typical IL behavior.[50] Nevertheless, the vaporization enthalpies of PIL are still lower compared their aprotic counterparts, since the hydrogen bonds still present in the gas phase contribute to this energy.[51] While the boiling points (b.p.s) of AILs lay between 450 to 700 °C, PILs generally display much lower b.p.s between 100 and 300 °C.[33, 52]

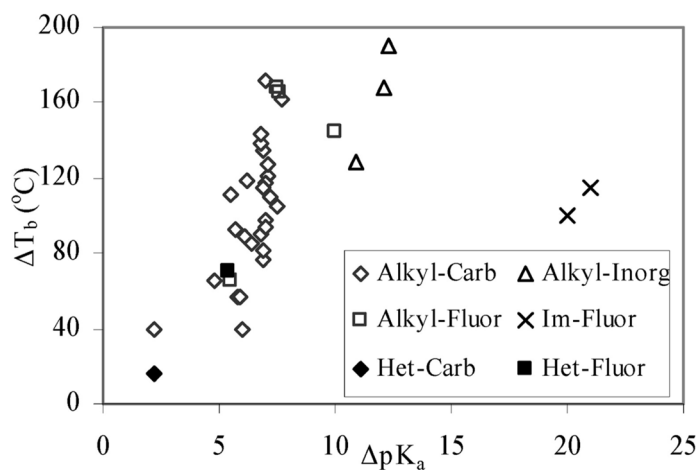


Figure 5 Influence of the ΔpK_a between acid and base of a PIL on the boiling point of the respective PIL. Alkyl stands for alkylammonium cations, Carb for carboxylate anions, Fluor for fluorinated anions and Inorg for inorganic anions. Figure taken from [33] with permission of publisher American Chemical Society.

Regarding the thermal properties it is of course of most importance to consider the thermal stability of both cations and anions, the latter one being the limiting factor in most cases. The stability is dependent e.g., on the coordinating nature, nucleophilicity or the presence of good leaving groups in the anion. Contrary, changes in the cation, e.g., chain length or alkylation

usually have only a limited impact.[53, 54] If the ΔpK_a of a PIL is too high, they decompose before the b.p. is reached, since vaporization enthalpy will be too high.[36]

Besides the low vapor pressure, ILs are often considered as alternative for conventional solvents due to their non-flammability. This is true when evaluating the flammability of ILs with conventional flash point measurements, i.e., heating the liquid and ignite it. However, when reaching the decomposition temperature of an IL, the resulting vapors are most likely flammable.[55, 56] This low, but existent, flammability paired with their low vapor pressure makes their use in laboratories rather safe. In other circumstances, however, ILs still pose a hazard in terms of fire, e.g., large amounts of heat released in large scale processes.[57]

On the other side of the temperature window, all ILs undergo a glass transition when they are cooled rapidly below the melting point. Since the glass transition temperature (T_g) is dependent on cohesive energies within a liquid, lowering the attracting or increasing the repulsive forces, e.g., increasing anion size or the cations asymmetry, will lead to a lower T_g . [58, 59]

The m.p.s of PILs have been shown to be relatively low compared to their T_g , with no certain explanation found yet. It is assumed, that it is due to a very uniform distribution of negative and positive charge carriers.[36] When comparing m.p.s of AILs and PILs, it is hard to make a statement about differences in regard to the presence of a proton, since the mass difference when changing from a protic to an aprotic ionic liquid is rather high. This alone has a large impact on the m.p.[60] As it is the case for the T_g , lower cohesive forces will lead to lower m.p.s, achievable by worse stacking efficiency, e.g., through bulky, asymmetrical ions. Too large ions on the other hand, will lead to higher m.p.s, since the attractive forces, e.g., van der Waals forces will increase disproportionate at a certain point.[59, 61] In contrast to the boiling point, the m.p.s and T_g s of PILs do not correlate well with the ΔpK_a , hinting at additional or more important factors than just the state of the hydrogen network.[40, 59] Both, for AILs and PILs, the m.p. is varying strongly even with small changes in anion and cation composition, but values below 0 °C are possible. [33, 62]

One critical point regarding the m.p.s of PILs is the amount of residual water. It has been shown, that already as small amounts of water as 100 ppm can lower the m.p. drastically.[63]. Considering that this residual water is not even recognized in electrochemical measurements, it is of high importance to assure a completely dry PIL when measuring the m.p.[64]

The density of PILs and AILs behave in a similar way. The bulkier and less symmetric the ions, the lower the density.[65, 66] However, for PILs also the strength of the hydrogen bond effects the density, with stronger bonds leading to higher densities.[34]

As for conventional solvents polarity is an important property of ILs, since it has an influence on many parameters, e.g., solvation capability, reaction rates, absorption bands and chemical equilibria. Polarity itself is not a simple value to measure and it depends on a variety of interactions, including the polarizability, the dipole moment as well as hydrogen-bond capability and electron pair exchanges.[67, 68] For ILs specifically, the coulombic and van der-Waals interactions play an important role for the polarity and different approaches have been used to measure it.[69, 70]

The character of the anions and cations is strongly affecting the polarity of ILs. For example, the presence of long alkyl chains, meaning a less polar character, will lead to less polar ILs. Usually large and bulky, thus soft, cations are chosen for ILs. Paired with soft anions, which are easily polarized, it will lead to an overall less polar, more covalent binding. On the other hand, employing hard anions will lead to lower electron density within the binding, leading to more polar compounds. An additional factor is the steric hindrance of the ions. More interaction between the ions, due to higher vicinity, will lead to less polar compounds. [71, 72]

In AILs, the cation appears to have the biggest influence on the polarity, since the hydrogen-bond donating ability, stemming from the cation and much lower compared to PILs, is more important compared to the hydrogen-bond acceptance from the anion.[73] In PILs the basicity of the anion for the cation governs the covalent character of the binding. While very polarizable anions can lead to very little polar PILs, the introduction of a oxyanions will result in large hydrogen networks, thus generating highly polar PILs.[74]

1.2.2. Transport Properties

May it be the transport of charge carriers within an IL or the flow behavior in a pipe, conductivity as well as viscosity are critical parameters to evaluate the suitability of an IL for any application. For ILs this is an especially sensitive topic, since they are known for their rather restrained transport properties compared to conventional solvents or electrolytes owing to their high coulombic interactions. Furthermore, the ΔpK_a , in the case of PILs, plays a special and important role, as it does for the thermal properties.

The viscosity of an IL, whether AIL or PIL, is primarily dependent on the ions' structures, resulting in specific cation-anion electrostatic interactions. Contributing to this are hydrogen bonds, especially in PILs as well as van der Waals forces.[75] Some works are concluding that the structure of the anion has a greater influence on the viscosity .[34, 66] However, this has been doubted in the past, with no clear trend spotted.[76, 77] Nevertheless, reducing van der Waals forces by using complex and highly fluorinated anions as well as short alkyl chains overall can be used as a rule of thumb to decrease the viscosity.[29, 78] Additionally, in the case of PILs, worse stacking cations and charge delocalization on the anion will reduce the strong hydrogen bonds and thus the viscosity.[79, 80].

While the ionic conductivity of an IL primarily depends on the viscosity of the fluid, the amount of available charge carriers and/or the presence of a non-vehicular charge transport strongly influences the conduction as well. As already explained, the ionicity is a parameter to describe the amount of ion pairing in an IL. Having a high ionicity, meaning a low amount of ion pairs, will result in a higher conductivity. This is true for both AILs and PILs, with the latter being more complicated due to the already mentioned "reduced" ionicity. Thus, it is imperative to design weakly coordinating ions, and in the case of PILs, high ΔpK_a to maximize available charge carriers.[81-83] Nevertheless, It should be mentioned that the concept of ionicity, thus drawing conclusions from conduction and viscosity about the amount of ion pairing, has been criticized lately.[45, 84]

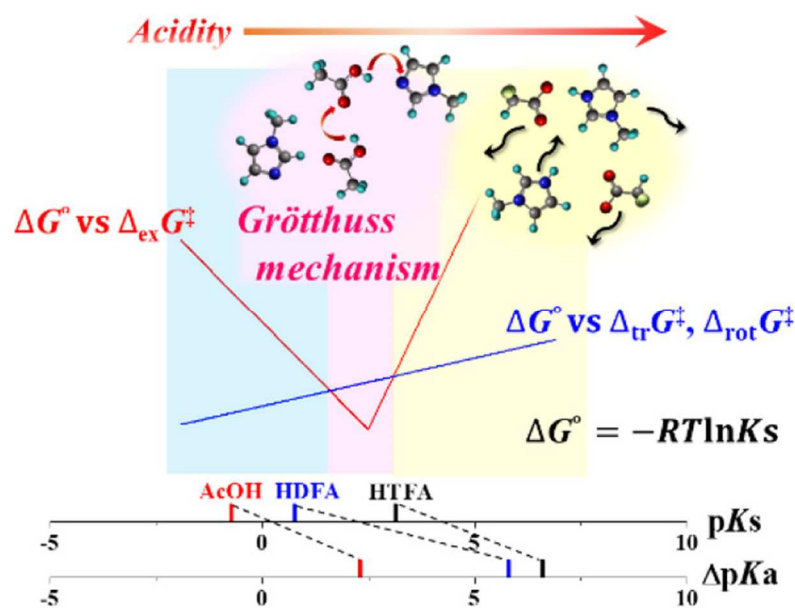


Figure 6 Optimization of the mobility of the acidic proton in a PIL by adjusting the ΔpK_a value. Figure taken from [85] with permission of publisher American Chemical Society.

An interesting example for which this popular concept cannot be successfully applied is that of the non-vehicular charge transport in PILs. The original concept of the Walden Plot only ascribes such a phenomenon to “superionic” liquids, meaning ILs laying above the reference KCl line. Since most PILs are found below this line, they should be categorized as “poor” ionic liquids with low ionic conductions compared to their viscosity.[33] However, exactly such poor protic ionic liquids have been found to exhibit a proton conduction mechanism in the form of the Grotthuss diffusion.[43] Within these PILs, the protons can travel, or rather hop, between a chain of ions, increasing the conductivity of the system significantly.[86] This mechanism is impossible in AILs due to the absence of the proton donor-acceptor system. The most important factor for this type of diffusion is the ΔpK_a of a PIL. Watanabe et al. concluded a “sweet spot”, in which the energy for the proton transfer between ions is lower compared to the translational and rotational energy of the proton carriers. Basically, to enable the Grotthuss diffusion, the ΔpK_a needs to be high enough for a minimum of protonated cations, and low enough to prevent a too strong binding of these protons (see Figure 6).[85]

1.2.3. Electrochemical Stability

The electrochemical stability window (ESW) of an IL is of utmost importance when employed as electrolyte in electrochemical energy storage devices or energy converters. In some works the ESW is derived from the highest occupied molecular orbital (HOMO) and lowest unoccupied molecular orbital (LUMO) of the isolated electrolyte molecules.[87, 88] However, this has been criticized and one should only refer to potentials of electrolyte reduction/oxidation at negative/positive potentials.[89]

When AILs are compared to conventional electrolytes, they appear as very attractive alternative, since they enable higher operating voltages (OPVs) up to 3.7 V and, by this, high energy devices.[90] Unfortunately, this is not true for most PILs, when the cation bears the proton. In these cases, this available proton is easily reduced at potentials around 2 V vs. Li^+/Li , forming H_2 amongst others, while the anions show similar stabilities as in AILs.[91, 92] Thus, optimizing the ESW of a PIL is mostly about choosing the most stable anion. Highly fluorinated anions with good charge delocalization, e.g., hexafluorophosphate ($[\text{PF}_6]^-$), tetrafluoroborate ($[\text{BF}_4]^-$) or bis(trifluoromethylsulfonyl)imide ($[\text{TFSI}]^-$), have proven to be highly oxidation resistant enabling ESWs for PILs (but not OPVs) of up to 3.5 V.[93, 94]

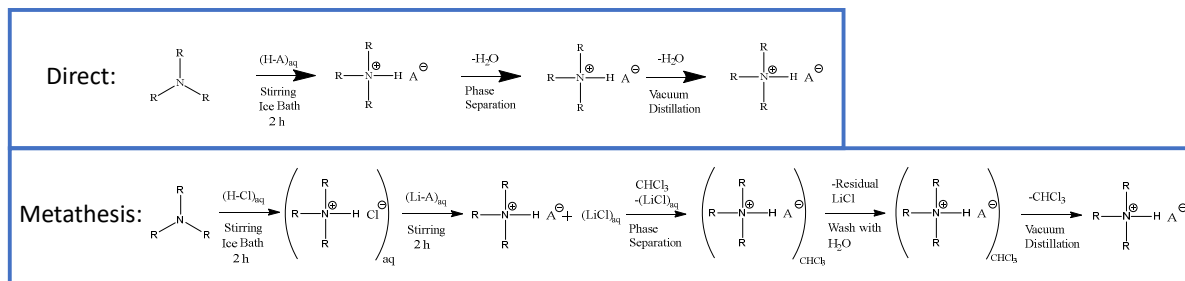
1.3. Synthesis of Protic Ionic Liquids

As mentioned in chapter 1.1, Paul Walden was working with $[\text{EtNH}_3][\text{NO}_3]$ in 1914. This is one of the first documented uses of an IL and also of a PIL.[5] This document shows one of the main advantages of PILs compared to their aprotic counterparts: a very easy accessibility due to a simple synthesis path.

PILs can easily be obtained by the neutralization of a base and an acid. To prevent thermal decomposition during this exothermic reaction, the reaction is cooled by an ice bath. Furthermore, the deployed base should be purified by distillation in advance. This way, the only byproduct is water, which can be removed via phase separation (only in the case of hydrophobic PILs) and vacuum distillation.[95] A complete drying is important since water drastically influences the properties of PILs and is detrimental in most applications. During this drying step, the PIL usually will change color due to the heat leading to minor thermal decomposition of the components. While this change of color can appear significant, the

concentration of impurities is negligible and difficult to detect by mass spectrometry and NMR spectroscopy.[96]

Hydrophobic



Hydrophilic

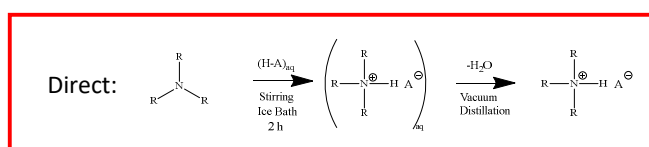


Figure 7 Reaction pathways for the synthesis of hydrophobic (blue) and hydrophilic (red) PILs.

If the anion of the desired PIL is the base of a superacid, the neutralization of the precursor base can also be done in an advanced neutralization, to prevent drastic exothermic energy. For this, a standard acid, e.g., HCl can be used, leading to an intermediate salt of the precursor base with $[\text{Cl}]^-$ as anion. Afterwards, a metathesis of the $[\text{Cl}]^-$ anion with the desired anion, by simply adding a water-soluble salt of the superacid will result in the desired PIL. Especially hydrophobic PILs are suitable for this approach since the separation from the residual salts can be done by simple washing with water. In the case of hydrophilic PILs, the use of, e.g., silver salts are necessary to precipitate the anion of the substitute acid.

The more theoretical considerations in chapter 1.2 must be understood as broad guidelines when designing PILs. Each specific ion combination has unique interactions, making it impossible to define precise rules for the synthesis of PILs but rather trends for certain anions and cation types with common functionalities. While computational approaches regarding the design of ILs, e.g., quantitative structure-activity relationship (QSPR) are becoming more frequent, the most regular approach to find suitable ILs for certain applications is still a trial-and-error principle.[97] This means synthesizing a variety of ILs based on the established trends and characterize them, what lead to large lists of ILs and (in the best case, all) their properties.[33, 98]

1.4. Common Protic Ionic Liquids

To give a better impression about the characteristics of PILs, in this subchapter, the common employed anions and cations will be considered, with special focus on their properties related to electrochemical applications.

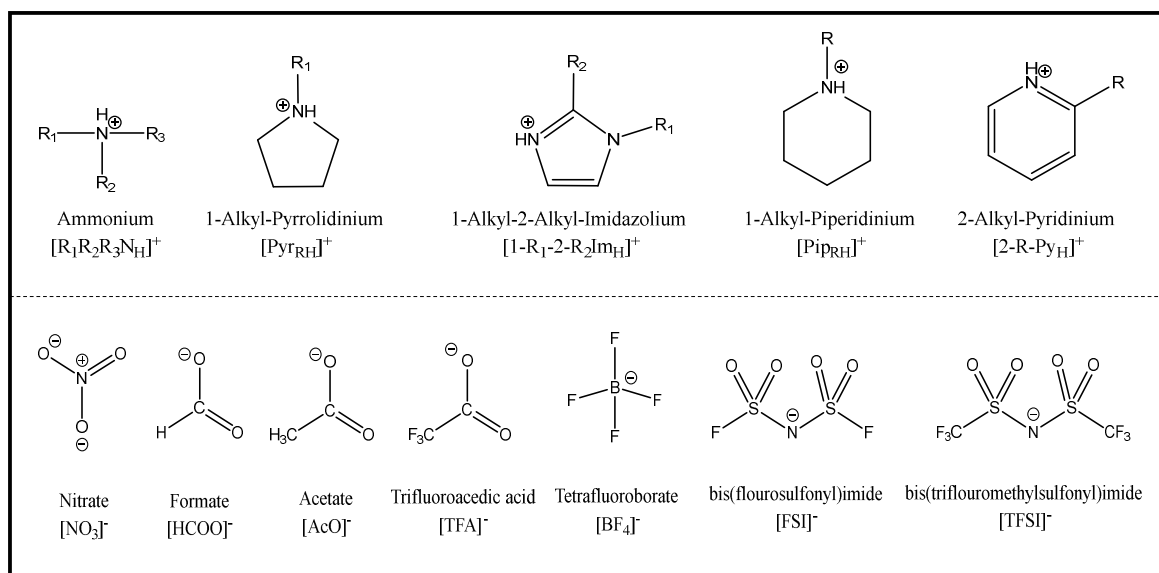


Figure 8 Common types of cations (top) and anions (bottom) for PILs. Figure taken from [99] with permission of publisher Elsevier.

1.4.1. Cations

As already mentioned, in most PILs the cation will bear the proton. Thus, not fully alkylated amines ([NRH]⁺) are a viable option as cation, contrary to AILs. For PILs based on primary, secondary or tertiary amines, the degree of alkylation influences the melting point as well as viscosity. Higher degrees as well as longer alkyl chains lead to higher melting points and viscosities. On the other hand, less available protons, meaning higher alkylation degrees, will result in PILs with higher ESWs.[34]

Although also nitrogen-based, most other employed cations for PILs are heterocycles, e.g., imidazolium ([Im_H]⁺). While the alkylation degree affects the resulting PILs in a similar way as in amine based PIL, meaning more and longer alkyl chains lead to more ion interactions, there seems to be a minimum of sterically hindrance to prevent too efficient ion stacking. In short, ethyl groups lead to less ion-ion interaction compared to methyl groups, while elongating the chain further, will lead to stronger interactions again.[76] Due to its planarity, imidazolium

cations are displaying higher conductivities compared to the similar pyrrolidinium ($[\text{Pyr}_\text{H}]^+$).^[100] However, without the aromatic character, pyrrolidinium cations achieve lower m.p.s, which is the same case when comparing pyridinium ($[\text{Py}_\text{H}]^+$) and piperidinium-based PILs ($[\text{Pip}_\text{H}]^+$).^[33, 97] The viscosity of imidazolium-based PILs is slightly lower compared to pyridinium- and pyrrolidinium-based ones, while piperidinium-based PIL display much larger viscosity, in spite of comparable m.p.s.^[94, 101, 102]

1.4.2. Anions

While PILs with anions like nitrate ($[\text{NO}_3]^-$), formate ($[\text{HCOO}]^-$), acetate ($[\text{AcO}]^-$) and trifluoroacetic acid ($[\text{TFA}]^-$) can display low m.p.s and reasonable transport properties, they have the drawback of a low thermal as well as electrochemical stability compared to higher fluorinated compounds.^[35, 54]

Among these, the tetrafluoroborate anion ($[\text{BF}_4]^-$) is often employed. Although resulting in relatively high m.p.s, PILs based on $[\text{BF}_4]^-$ usually show good conductivities, even close to the m.p.^[33] Lower melting, less viscous and even higher electrochemical and thermal stable PILs are possible with the bis(trifluoromethylsulfonyl)imide ($[\text{TFSI}]^-$) anion. The excellent charge delocalization leads to weakened hydrogen-bonding and overall interaction with the cation, resulting in the superior transport properties.^[13, 101] When shortening the molecule by exchanging the methyl groups with fluor, resulting in the bis(fluorosulfonyl)imide ($[\text{FSI}]^-$) anion, the viscosity and m.p.s of the resulting PILs can even be further lowered, for the price of less electrochemical and thermal stability.^[103]

1.5. Mixtures of Protic Ionic Liquids

As already explained, the rather high viscosity and thus low conductivity of ILs are a result of anion-cation interactions. Weakening these interactions lead to an increased ion mobility. While the perfect but not easy approach for this problem are weak interactions via proper selection of ions, the use of solvent molecules to disrupt these interactions, has been proven to be a feasible alternative solution. The most often employed solvents for these mixtures are conventional organic solvents.^[104]

Compared to AILs, the hydrogen-bond in PILs plays a crucial role in the selection of solvent. While in the former, low to moderate polar solvents are sufficient to disrupt ion interactions and pairing, the strong hydrogen-bonds in PIL make highly polar solvents necessary to yield

solvent-separated ion pairs.[105] Thus, while all mixtures of PILs with solvents will improve transport properties simply due to the lower viscosity of the latter, the highly polar solvents will also increase the ionicity of PILs.[106] A positive side effect of these solvent-PIL mixtures, is a decreased m.p., occurring already with small amounts of solvent.[107]

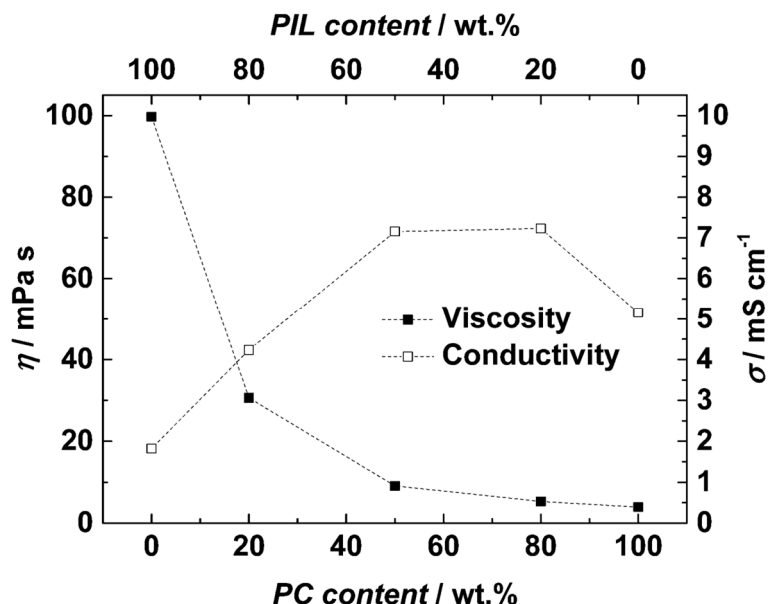


Figure 9 Improvement of transport properties of a PIL (here: butylpyrrolidinium bis(trifluoromethylsulfonyle)imide) via mixing with a solvent (here: propylene carbonate). Figure taken from [108] with permission of publisher Royal Society of Chemistry.

Unfortunately, these improved transport properties come for the price of reduced safety properties. Obvious, the organic solvents in the mixtures will inevitably lead to higher vapor pressures as well as higher flammability compared to the pure ILs. Nevertheless, up to a certain minimum of IL, the mixtures retain a comparatively low flammability.[109]

While mixtures of PILs with water will also have higher vapor pressures, stemming from the evaporating water molecules, the flammability will stay low. Additionally, due to the polarity of water, the ionicity of hydrophilic PILs when mixed with water will increase drastically due to a larger hydrogen-bond network.[110] Furthermore, the charge transport mechanism of a PIL-water mixture can be influenced by the amount of water. High amounts of water will lead to an increased fraction of Grotthuss like proton hopping within the mixture.[111]

However, as it is the case with PIL-solvent mixtures, PIL-water mixtures combine not only advantages but also disadvantages. In this case, the water brings its intrinsic low electrochemical stability of only 1.23 V, even smaller than the ESW of PILs, limiting the OPV when employed as electrolyte in electrochemical energy storage devices.[112]

A special form of PIL mixture is the adjustment of base to acid ratio, resulting in an excess of either base or acid. Practically, there will always be some residual water molecules left inside a PIL. The excess of either base or acid leads to an increased or decreased pH value of the PIL, which can thus be tweaked for the specific application.[113] This method, however, is limited by the amount of residual water, operating as corresponding acid or base. When increasing the excess of acid or base further, they merely act as a kind of solvent, e.g., reducing viscosity due to less ion-pairing.[93]

Lastly, the combination of two PILs can lead to binary mixtures. Within these mixtures, the concentration or packing of the ions as well as their interactions change depending on the ratio of components. Stronger interactions and better packing of the different ions will lead to lower molar volumes, while the opposite is true for weaker interactions and worse stacking. This, in turn, changes the thermal as well as transport properties. With the right composition, the m.p. of a PIL binary mixture can be lower than for the pure components with increased conduction and viscosity, due to eutectic effects.[114] Furthermore, it can lead to a stronger hydrogen-bond network with increased viscosity but also higher conductivity.[115]

1.6. Electrochemical Energy Storage Devices

There are many aspects which led to an increased demand for energy storage devices in our society. Ranging from small gadgets like cell phones or tablets, over larger applications like electric mobility or electric assisted machines, to large scale energy storage, stabilizing electrical grids in times of more and more instabilities caused by an increasing amount of renewable energies. These devices can be categorized in terms of their energy and power supply. While batteries are the perfect candidate for high energy demands, converting chemical energy to electrical energy, they lack in power due to the slow reactions compared to physical energy storage processes. A technology making use of these fast and very reversible processes, is the supercapacitor. Over the years, two different types of supercapacitors have been established, which will be introduced in the next chapters.

1.6.1. Electrical Double Layer Capacitors

As the name already suggests, the electrical double layer capacitor (EDLC) is based in principle on the classic capacitor, forming a potential difference between two electrodes, yielding high power output paired with a very large cycle life. However, in a capacitor, these electrodes are separated by an electric insulating layer (dielectric), resulting in an electrical field in between the electrodes storing the applied energy. This field (E_i) is proportional to the amount of stored charge (Q) and the voltage between the electrodes (U_i).

$$E_i = U_i * Q_i \quad (3)$$

A special characteristic of capacitors is the capacitance (C), expressing the amount of charge it can store at any given voltage.

$$C = \frac{Q}{U} \quad (4)$$

The total energy stored by a capacitor (W) is the sum of all subsets during charge, which are changing due to the increasing voltage.

$$W = \int_0^Q U(q) * dq = \int_0^Q \frac{q}{C} * dq = \frac{1}{2} * \frac{Q^2}{C} = \frac{1}{2} * C * U^2 \quad (5)$$

Contrary to conventional capacitors, the space between the electrodes is not filled with a dielectric but an ionic conducting electrolyte. Thus, one electric field between both electrodes is no longer possible since charge is moved by ions. Instead, two electric double layers are formed directly on each surface between electrodes and electrolyte, with the solvent molecules functioning as dielectric between charged surface and ions. This means the whole system does not consist of one, but two capacitors, which are in serial connection. The total voltage in such a serial connection is:

$$\Delta V_{total} = |\Delta V_1| + |\Delta V_2| \quad (6)$$

With Equation 3 follows:

$$\Delta V_{total} = \frac{Q}{C_1} + \frac{Q}{C_2} = Q \left(\frac{1}{C_1} + \frac{1}{C_2} \right) \quad (7)$$

And finally:

$$\frac{1}{C_{total}} = \frac{1}{C_1} + \frac{1}{C_2} \quad (8)$$

This shows that the total capacitance of the system is dependent on the capacitance of the double layers on each electrode and will always be lower compared to the individual capacitances.

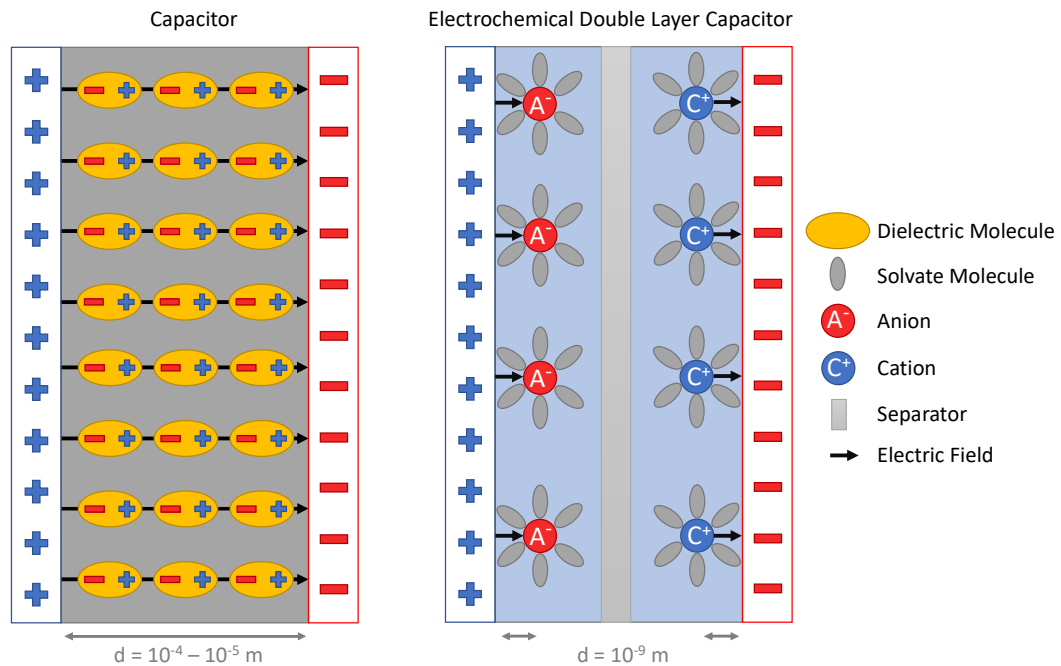


Figure 10 Schematics of both - a classical capacitor (left) and an electrochemical double layer capacitor (right).

Unfortunately, the electrolyte inside an EDLC is limiting the OPV due to its electrochemical decomposition at certain potentials. The voltage window ranges from 1.23 V for aqueous systems to 3.0 - 3.2 V for solvent based electrolytes, while regular ceramic capacitors can build up voltages up to 10^3 V , depending on the material of the dielectric.[116, 117] Nevertheless, the energy density of an EDLC is still much higher compared to a capacitor, with the former showing values between 2 to 8 Wh kg^{-1} and the latter only around 0.1 Wh kg^{-1} . [118] This difference results from many order of magnitudes higher capacitances. While the capacitance of ordinary capacitors usually ranges from 10^{-12} to 10^{-6} F , EDLCs can reach capacitances of 10^3 F . [119, 120] This difference can easily be explained by Equation 9.

$$C = \frac{\epsilon_0 * \epsilon_r * A}{d} \quad (9)$$

As it can be seen, higher permittivity ($\epsilon_0 * \epsilon_r$) of the dielectric or electrolyte result in higher capacitances. However, the permittivity of materials used in capacitors as dielectric, e.g., BaTiO₃ is higher compared to the permittivity of electrolytes in EDLCs.[121, 122] Instead, the higher capacitances of EDLCs are a result of vast specific surface areas of the electrodes (A) as well as much smaller distances (d) of the double layer. In conventional capacitors the electrodes' surface is limited by the dielectric, ranging around $10 \text{ m}^2 \text{ g}^{-1}$, since the electrodes are directly plated onto it.[123] The surface area of carbon-based electrodes, on the other hand, ranges around $10^3 \text{ m}^2 \text{ g}^{-1}$. [124] Additionally, the distance of electrodes in a capacitor is in the order of magnitude 10^{-4} to 10^{-5} m, while in an EDLC it is 10^{-9} m.[125]

Electrodes

One key element of EDLCs, the high-surface area electrodes, is usually achieved by using activated carbon (AC) based electrodes. This abundant and relatively cheap material can be produced by several methods, usually either by a physical or chemical activation of biomass (e.g., coconut husk, olive pits or bamboo) derived charcoal.[126, 127] The physical activation is carried out via heat treatment in presence of oxidizing agents. In a first step, the precursor in the form of biomass is heated to 400-700 °C in an inert atmosphere to remove volatile, non-carbon species (N₂, O₂, H₂). Thus, during this carbonization the carbon content is increased, and pores are created which are still blocked by tarry substances at this stage. The biochar is then heated to 800-1000 °C in a second step, while being exposed to oxidizing gases (Steam, CO₂, Air). This burns off the residuals blocking the pores and even creates new pores. This process can also be carried out in a single step, utilizing medium temperatures, and switching from inert to oxidizing atmosphere without cooling in-between.

Chemical activation, on the other hand, is a combination of oxidizing agents, e.g., NaOH, ZnCl₂ or H₃PO₄, and relatively low temperatures from 250-600 °C. Depending on the employed chemical this activation is a one- or dual-step process, due to different abilities to penetrate non-porous materials. While NaOH and KOH need a prior carbonization for effective penetration, H₃PO₄ or K₂CO₃ can be used in a single step. Advantages of the chemical activation lie in better results in terms of quality of the resulting ACs and economic viability, while the handling of the chemicals can be seen as drawback as well as an additional, necessary washing step.[128, 129]

A large variety of factors contribute to the results of all these processes. Amongst others are the employed precursor materials, temperature, time, oxidizing agents and many more. In the end, most ACs' surface areas range in the order of $2000 \text{ m}^2 \text{ g}^{-1}$ and their pore size lies between 2 and 50 nm.[130]

Unlike graphitic materials, AC displays poor electronic conductivity due to its porous structure without π -electron delocalization.[131] Thus, conductive agents are added to the electrode composition to connect individual particles of the AC to create a better comprehensive network with improved conductivity. Therefore, the added particles need to be smaller compared to the AC and, of course, display high conductivity by themselves. Conductive agents fulfilling these requirements are carbon black, carbon nanotubes or graphene.[127]

Another component of electrodes used in EDLCs is a binder, basically holding together all the particles and attaching them to the current collector. For this task, polymers with low densities, good flexibility, overall inertness and varying solubilities are employed. To prevent dissolving of the electrodes in the electrolyte, a polymer insoluble in the respective solvent must be chosen. Depending on the chosen polymer, the electrodes can either be freestanding which can be shaped like a dough, or are coated directly onto the current collectors in form of a slurry. [132, 133]

The electrodes are connected via metal-based current collectors to an outer electric circuit. These metal foils also provide stability to the electrodes, basically acting as foundation of the electrodes. The most utilized material for current collectors in EDLCs is aluminum, since it is very light and stable even at high potentials due to the formation of a passivation layer in combination with anions like $[\text{PF}_6]^-$ or $[\text{BF}_4]^-$. [134]

Separator

Since in an EDLC the dielectric is replaced with a conducting electrolyte, physical separation of the electrodes is necessary to prevent short circuits and enable the buildup of potentials differences. This is done by a separator, usually natural or synthetic polymers like cellulose or polyolefins (e.g., polypropylene, polyethylene). Rather trivial on the first look, a separator has many requirements. To prevent contact and or penetration even at high pressures, it must be thick and firm enough. On the other hand, since it is only a passive component, it needs to be as thin as possible to lower cost and increase gravimetric as well as volumetric performance of a device. Furthermore, while it needs to be insulating, ions must be able to penetrate the

polymer to ensure charge compensation during operation of the device and it does not stop here. There are many more requirements for this easily overlooked component, e.g., easy processibility, thermal stability, wettability and more.[135, 136]

Electrolyte

Another key element of an EDLC is the electrolyte. Together with the electrodes, it is crucial for a fast and reversible formation of the electric double layer at the electrode/electrolyte interface. Since the ions need to move towards this interface, through the porous system of the electrodes, better transport properties of the electrolyte will yield a higher power output. Thus, electrolytes with low viscosity as well as high ionic conductivity are employed, which is generally valid for aqueous electrolytes, meaning a mixture of water and a conducting salt, e.g., Na_2SO_4 or KOH . This is due to a high dielectric constant of water, ensuring a large number of dissociated ions, thus charge carriers, paired with its low viscosity providing high ion mobility together with the general high mobility of H_3O^+ and OH^- ions. And while water can be handled safely and is inexpensive, there are several drawbacks related to its application, preventing the use as state-of-the-art electrolyte. A drawback is its relatively narrow temperature window, especially at lower temperatures. More importantly however, is the limitation related to the narrow ESW (1.23 V), caused by the early oxidation of $\text{H}_2\text{O}/\text{OH}^-$ and reduction of H_3O^+ .

Since the energy density is regarded as most critical weak point of EDLCs, electrolytes with much broader ESWs compared to water have been established therefore as state-of-the-art. This is typically achieved by the combination of a low viscous solvent and electrochemically resistant salts with good solubility in the selected solvent. The most common employed solvents are acetonitrile (ACN) and propylene carbonate (PC) with the former being more hazardous but less viscous.[90] As conductive salt, quaternary ammonium salts, especially tetraethylammonium tetrafluoroborate ($[\text{Et}_4\text{N}][\text{BF}_4]$), are favored due to their excellent dissociation ability, leading to high amounts of charge carriers in the electrolyte and thus high conductivities.[137] Furthermore they display excellent thermal as well as electrochemical stabilities, enabling high OPVs of 3 V.[138]

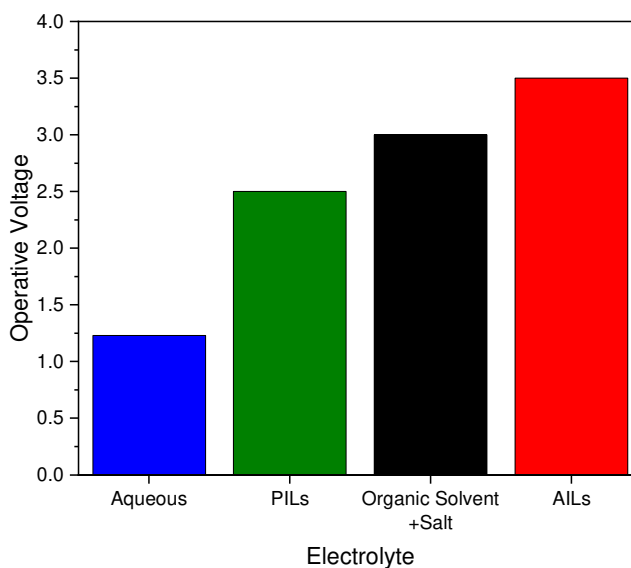


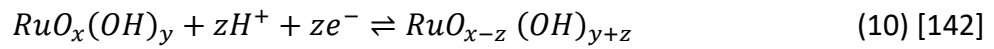
Figure 11 Approximate OPVs of different electrolyte systems for EDLCs.

While this is already much higher compared to aqueous electrolytes, research and industry are trying to improve the OPV even further to catch up in energy density compared to battery systems. One strategy relies on employing neat ILs as electrolyte due to the high redox resistivity of the ions.[139] Furthermore, their intrinsic safety properties would even increase the safety of the EDLC in terms of evaporation and inflaming of the electrolyte.[140] Unfortunately, as already explained in chapter 1.2.2, the transport properties of ILs are underwhelming, thus limiting the power performance of an EDLC.[141] Nevertheless, they have been successfully introduced in EDLCs and strategies to improve their application, with the focus on PILs, will be discussed in chapter 1.7.1.

1.6.2. Pseudocapacitors

The lack of energy density of EDLC systems compared to batteries lies in the different storage mechanisms: On the one hand, fast and reversible non-faradic processes limited to the surface area of the electrodes in the EDLCs. On the other hand, slower but energy intensive electrochemical redox reactions with large potential differences, involving the whole bulk of the electrode in batteries. A special type of supercapacitor, the pseudocapacitor, combines fast surface limited mechanisms with the highly energetic redox reactions, yielding higher energy densities compared to EDLCs and higher power densities compared to batteries.

The faradic reactions involved in these pseudocapacitors are in most cases unlike the ones occurring in 3-dimensional (3-D) materials like graphite. These have a distinct chemical potential and include phase conversion of the whole electrode bulk. Instead, 2-dimensional (2-D) and quasi-2-D processes take place, which involve electrosorption and redox reactions (with some exceptions of 3-D intercalation via charge transfer). A prime example for a 2-D process is the redox reaction of RuO₂:



Unlike most batteries but similar to EDLCs, the potential of these processes is not steady but continuous, since they depend on different changing thermodynamic relations, summarized in Table 1.

Table 1 Correlation of different pseudocapacitor systems to their specific thermodynamic relations. Modified from [143].

System Type	Thermodynamic Relation
Redox System $Ox + ze^- \rightleftharpoons Red$	$E = E_0 + \left(\frac{RT}{zF}\right) \ln \left(\frac{[Ox]}{[Red]}\right)$
Underpotential deposition (Electrosorption) $M^{z+} + S + ze^- \rightleftharpoons S \times M$ (S=surface lattice sites)	$E = E_0 + \left(\frac{RT}{zF}\right) \ln \left(\frac{\Theta}{1 - \Theta}\right)$ (Θ =2-dimensional site occupancy fraction)
Intercalation System Li^+ into MA_2	$E = E_0 + \left(\frac{RT}{zF}\right) \ln \left(\frac{X}{1 - X}\right)$ (X=occupancy fraction of layer-lattice sites)

Over the years, a large variety of active materials have been investigated and recognized as suitable material for these fast surface restrained charge-transfer-reactions. Carbonaceous materials with enriched surface functionalities can deliver higher capacitances compared to

“pristine” carbons because of additional faradic reactions, changing from a pure EDLC to a more pseudocapacitive behavior. However, the higher density and gravimetric capacitance of metal oxides, like MnO_2 or RuO_2 , lead to cheaper devices offering higher capacitances, thus energy densities. Of course, this comes with the tradeoff for power.[144] There are many more materials, amongst others hydroxide materials, conductive polymers, sulfide as well as nitrites, Mxenes and many more. Additionally, the number of possible shapes and compositions of different materials are vast and strongly impact the performance of a pseudocapacitor.[145]

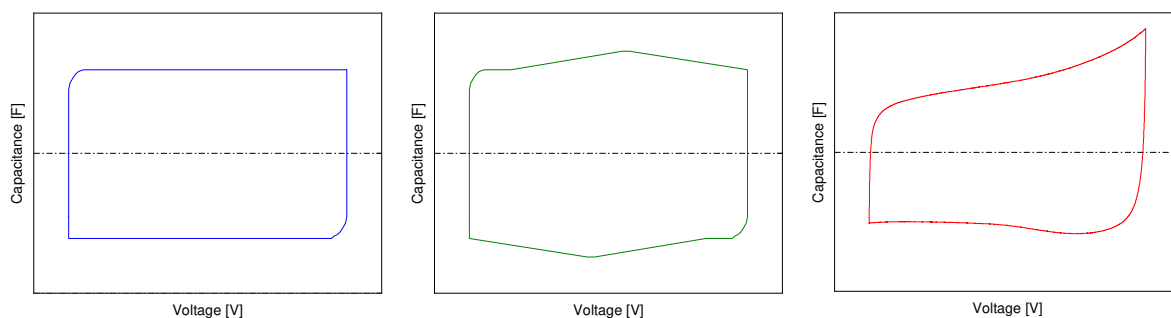


Figure 12 Voltage profiles of different supercapacitor systems. Left: EDLC; Middle: Pseudocapacitor; Right: EDLC with faradic contributions.

Nevertheless, the general composition of a pseudocapacitor is very comparable to that of EDLCs. Two electrodes, coated onto current collectors, are ionically connected via an electrolyte but separated physically through a separator. Although these components have the same task in both systems, they differ very much in requirements.

Starting with the electrode composition, depending on the material, binder and conductive agent are not always necessary. While MnO_2 has a low conductivity, thus dependent on conductive additives, RuO_2 can be used without them. Binders become only necessary, if the active material is shaped into loose forms to maximize the surface area, e.g., into nanoparticles. Furthermore, the current collector is either a plain foil based on carbon or metals, e.g., titanium, or it is a structured network with high porosity, e.g., Ni-foam, to minimize the active materials' thickness while maximizing the mass loading of the electrodes.[145]

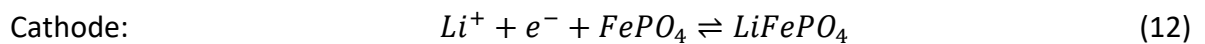
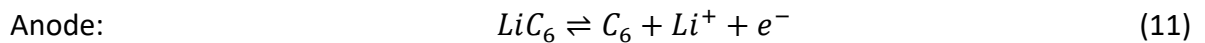
In both systems, EDLC and pseudocapacitor, the task of the electrolyte is the transport of charge in the form of ions to the electrode surfaces. Nevertheless, the composition of the electrolyte in each system is depending on various factors with different weightings.

For instance, any solvated ions will lead to the double layer formation in an EDCL. This process is highly optimized by the right choice of salt and solvent in terms of transport properties, ion fitting etc.

For pseudocapacitors, however, the active material dictates the nature or composition of the electrolyte. Since each material undergoes a specific reaction, the requirements for these must be fulfilled to function at all, i.e., specific ions or available protons must be present. This means for certain materials, only protic electrolytes can be deployed, excluding many standard electrolytes or even the whole “class” of AILs. Thus, aqueous electrolytes or PILs, usually a niche electrolyte in EDLCs, are rather common or at least much more attractive, respectively. The use of PILs in pseudocapacitors will be further highlighted in chapter 1.7.1.

1.6.3. Alkali Metal-Ion Batteries

As already mentioned, a battery system can deliver much higher specific energy compared to supercapacitors, due to chemical redox reactions involving the whole electrode bulk at defined potential ranges. Separated from each other, the reduction takes place at one electrode while the oxidation takes place at the other electrode. Whereas primary batteries are based on irreversible reactions, thus are limited to one discharge, secondary batteries take advantage of reversible processes, and can be used several hundreds of times. An example for a reversible redox reaction pair is given below:



Both reactions have their own Gibbs energy (ΔG), the maximum reversible work that may be performed, which can be expressed by Equation 13, with (z) as number of electrons participating in the reaction, (F) as Faraday constant and (E_0) as electromotive force (emf).

$$\Delta G = -zFE_0 \quad (13)$$

$$E_0 = -\frac{\Delta G^0}{zF} - \frac{RT}{zF} \ln \left(\frac{a_i}{a_{ii}} \right) \quad (14)$$

Together with the Gibbs energy at standard conditions (ΔG^0) and the Nernst equation (Equation 14), the voltage of the cell reaction can be expressed as:

$$E_0 = E_{00} - \frac{RT}{zF} \ln \left(\frac{a_i}{a_{ii}} \right) \quad (15)$$

Here, (E_{00}) is the standard emf, which is a fixed value for each redox reaction. As can be seen, the emf depends on each activity of the involved components in the chemical reaction (a_X). However, since the electrode component involved in the reaction is a solid and the concentration of the $\text{Li}^+_{(\text{solV})}$ can be seen as constant due to high concentrations, the activity terms can be defined as 1. Thus, the potential is stable over the course of the reaction, apart from rising overpotentials due to diffusion and penetration limits.

For the whole device, the cell voltage results from each half reaction potential:

$$U = \Delta E_0 = E_{0,Positive} - E_{0,Negative} \quad (16)$$

Since the resulting cell voltage can also be regarded as stable, each charge stored during the charge process experiences the same electrical potential. Contrary to supercapacitors (Equation 5), the energy is thus easily calculated with Equation 17.

$$W = U * Q \quad (17)$$

Regarding the setup of a battery device, it is very similar to supercapacitors. This includes two electrodes, consisting of active material, conductive agent, binder and current collector, as well as an electrolyte and separator. As shown in Equation 16, high energy values for the device are achieved by a large potential difference between the electrodes, i.e., different active materials performing redox reactions with a large potential distance from each other. These materials can be classified as anode or cathode material if the reaction occurs at low or high potentials, respectively.

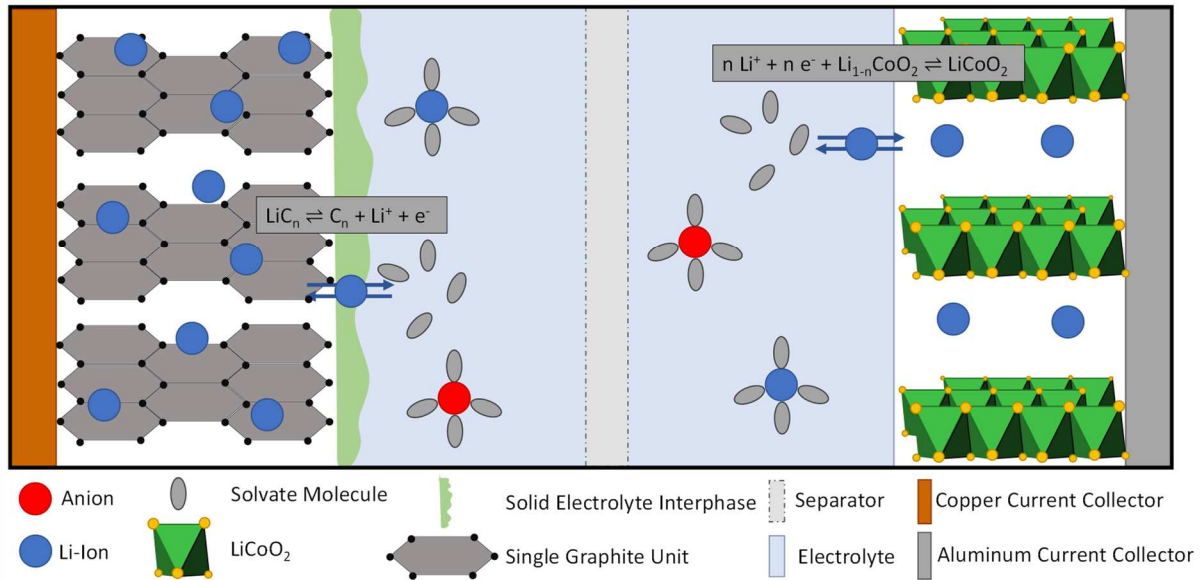


Figure 13 Schematic of a lithium-ion battery based on a graphite anode and a LiCoO₂ cathode.

For lithium-ion batteries (LIBs), the state-of-the-art anode material is graphite, offering high specific capacity (372 mAh g⁻¹) and relatively low cost, working close to 0 V vs. Li⁺/Li. Another carbon anode material are hard carbons (HCs) which, unlike graphite, are disordered and amorphous in structure. They yield higher capacities but come with a rather slopy charge/discharge profile, undesirable for most applications, down to almost 0 V vs. Li⁺/Li. Nevertheless, HCs have been proven as suitable anode material especially for sodium ion batteries, since the larger sodium-ions, compared to lithium-ions, do not intercalate reversibly into graphite. The latter is only functioning via co-intercalation of solvated sodium-ions, e.g., by glycol ether-based solvents.[146]

As cathode materials, metal oxides composed of lithium, nickel, manganese and cobalt, i.e., LiNi_xMn_yCo_zO₂ (NMC) or the structurally similar LiCoO₂ are employed. The former comes for a lower price and can nowadays even exceed the theoretical capacity of LiCoO₂ (274 mAh g⁻¹), depending on the composition. Both materials work around 3.8 V vs. Li⁺/Li. Another, much safer cathode material with the drawback of lower theoretical capacity (170 mAh g⁻¹) and working potential only around 3.4 V vs. Li⁺/Li is LiFePO₄ (LFP).[147]

The mentioned anode materials present a problem for nearly all established electrolytes since their potentials lie outside the ESW of the latter. Therefore, in all batteries small amounts of electrolyte are reduced during the first charge, with the decomposition products forming a

thin layer on the surface of the anode. This layer called solid-electrolyte-interphase (SEI) is necessary in most metal-ion batteries. It is electronically insulating the rest of the intact electrolyte from the electrode, thus preventing any further decomposition. At the same time, it is still possible for alkali metal-ions to move from the electrolyte through the SEI, to the electrodes. This transport is achieved by interstitials and vacancies inside the SEI.[148]

As for supercapacitors, the electrolyte is usually composed of a solvent and salt and requires primarily high solubility of the salt in the solvent as well as good ion mobility. This is why organic carbonates, e.g., PC, which are also used in supercapacitors, have been identified as promising solvents. However, in alkali-metal ion batteries the ability to form an SEI is another important characteristic. This is not the case for PC, leading to very low efficiencies when combined with graphite electrodes. Instead, another organic carbonate, ethylene carbonate (EC), was recognized as being able to form an effective SEI. The drawback of EC, however, is its high melting point and therefore high viscosity at ambient temperatures, limiting the power performance of batteries drastically. Thus, linear aliphatic carbonates with lower m.p.s, like dimethyl or diethyl carbonate (DMC/DEC), are added to the electrolyte to improve the mobility of alkali metal-ions.[149]

Since alkali metal-ion batteries rely on the reduction/oxidation of the respective alkali metal-ion storage compound, the cation of the conductive salt is limited to this ion type. On the other hand, the anion is basically only required to limit the mobility of the cations as little as possible as well as having a high enough anodic stability to enable high voltage cathode materials. Both requirements can be achieved by strong charge delocalization, which is present in highly fluorinated ions, e.g. LiPF_6 or NaPF_6 . [150, 151]

Coming with the usual drawback of high flammability and vapor pressure, the solvent-salt electrolyte composition for batteries is sometimes combined with flame retardants to minimize the risk potential. This is especially important for batteries applied in electrical vehicle (EVs), due to the risk of traffic accidents. Another strategy is the substitution of the solvent-salt-mixture with ILs due to their increased safety properties. However, AILs have been proven as rather limiting for the lithium-ion mobility due to strong interactions with the ILs' anions. In this regard, PILs have been proven to be advantageous which will be further discussed in chapter 1.7.2.

1.7. PILs in Chemical Energy Storage Devices

In 1981, the first PILs rediscovered in modern research, $[\text{EtNH}_3][\text{NO}_3]$, was investigated by Evans et al. due to similar thermodynamic properties of its solutions with nonpolar gases compared to such solutions based on water, and the ability to form micelles.[152] This resemblance to water led 20 years later to the first application of PILs in energy related devices. Susan et al. introduced imidazolium bis(trifluoromethylsulfonyl)imide ($[\text{Im}_\text{H}][\text{TFSI}]$) in a fuel cell.[153] They deliberately chose a PIL instead of the much more prominent AILs at this time, since the proton exchange membrane fuel cell (PEMFC) is dependent on a protic electrolyte. Compared to the regular aqueous electrolytes for these fuel cells, PILs display a much broader temperature and ESW, leading to intensive applications of PILs in PEMFCs.[154] And although fuel cells are no energy storage devices but energy converters, this was the first example of the use of PILs as electrolyte, which eventually also led to the introduction in the former system.

1.7.1. PILs in Supercapacitors

In 2006, AILs have already been successfully established in EDLCs, even in combination with solid electrolytes.[155, 156] On the other hand, PILs have not been considered for any energy storage device at this point, which can mainly be attributed to their lower ESW due the available proton. As in the case of the PEMFC however, it was this proton leading to the introduction of PILs in pseudocapacitors. To benefit from the larger temperature tolerance and ESW of ILs compared to aqueous electrolytes, Rochefort et al. employed for the first time a PIL, α -picoline trifluoroacetic acid ($[\text{2-MePy}_\text{H}][\text{TFA}]$), in a RuO_2 -based pseudocapacitor. In this system, AILs like 1-ethyl-3-methylimidazolium tetrafluoroborate ($[\text{1-Et-3-Melm}][\text{BF}_4]$) yield much lower and no faradic currents, resulting in very low capacitances, since the redox reaction of RuO_2 is dependent on protons (see Equation 10).[157] Even protons attached to AILs, e.g., by hydroxy groups, do not facilitate these pseudocapacitive redox reactions, as shown by the combination of MnO_2 with 1-ethanol-3-methylimidazolium bis(trifluoromethylsulfonyl)imide ($[\text{1-EtOH-3-Melm}][\text{TFSI}]$), since the ability to form hydrogen bonds in these AILs is too low.[158] Over the years, several materials have been identified as suitable pseudocapacitive electrode material in combination with PILs. Amongst others, metal oxides, nitrides and conducting polymers have been employed.[159, 160]

In order to further increase the safety of a PIL-based pseudocapacitor and enable a flexible device, Ketabi et al. investigated for the first time the use of a solid electrolyte in combination with RuO₂- and Ti-based electrodes. For this, they incorporated an eutectic PIL mixture into a polyethylene oxide (PEO), which enables energy storage even at high current densities, attributed to high proton conduction within the electrolyte.[161]

Although primarily employed in EDLCs, AC has also been shown to generate high faradic capacitance in combination with PILs, enabled through oxygen surface functionalities and enhanced through proton hopping near the electrode surface.[162] To further increase the pseudocapacitance of supercapacitors based on AC, the pH value of a PIL can be increased by the addition of small amounts of base, as already explained in 1.5. Demarconnay et al. ascribed this effect to higher mobilities of the hydroxyl ions as well as higher activities of the oxygenated surface groups in alkaline media.[113] Another approach to increase the pseudocapacitance of AC-based supercapacitors is the attachment of redox active species like anthraquinone on the surface of the carbon or in the case of hydroquinone even dispersed in the electrolyte.[162, 163]

PILs employed in AC-based EDLC systems without faradic contribution will lead to the same double layer formation as with other electrolytes (conventional solvent-salt-combinations or AILs). As it is the case in the latter electrolytes, the capacitance depends on the porosity of the AC, i.e., higher surface areas and good pore size distribution will lead to high capacitances.[113] Furthermore, EDLCs based on PILs display high cycle life as well as a broad operational temperature window, which can even be further increased by the mixture with different PIL species to form eutectic mixtures or solvents.[114, 164] The mixture with solvents is also drastically improving a key drawback of PILs i.e., their high viscosity, which is usually limiting the power capability of PIL-based EDLCs, as already explained in chapter 1.6.[165] This power improvement can even be further pronounced when mixed with water, e.g., due to a faster proton transport through the Grotthuss effect.[43] However, this specific effect is dependent on a relatively high concentration of water, with weight percent (wt.%) higher than 50 wt.%.[111]

Several groups were able to improve another critical drawback of PIL-based EDLCs - the small OPV. While Aradilla et al. employed diamond-coated silicon nanowires, Oyedotun et al. utilized oxygen-functionalized carbon nanofibers to achieve OPVs of 4 V and 3 V,

respectively.[166, 167] Nevertheless, classical AC-based EDLCs only function with a much smaller OPV compared to AIL-based devices, ranging from 2 to 2.5 V compared to ~3.5 V, and thus yield much lower specific energy (see Equation 5).[168] Since broader OPVs and higher specific energy was the main motivation for the introduction of ILs in EDLCs, this appears as contradicting. It shows that the preferable application of PILs in supercapacitors lies in pseudocapacitive instead of EDLC devices.

1.7.2. PILs in Alkali Metal-Ion Batteries

Several years after the introduction of PILs into supercapacitors, this subclass of ILs was also considered as electrolyte for LIBs (AILs were already introduced as early as 1999 in these secondary battery systems).[169] Contrary to supercapacitors, the main motivation for IL-based electrolyte in alkali-metal ion batteries has been safety improvements and not OPV increases, since most battery active materials work outside of the ESW of the electrolyte anyway (see chapter 1.6.3).[170] Thus, the small ESW of PILs should not be of concern for the implementation in alkali-metal ion batteries. Nevertheless, the activity towards elemental alkali metals, i.e., the reduction of the cation resulting in hydrogen evolution has certainly delayed attempts for their application in these systems.

In 2013, a PIL-based electrolyte mixed with PC has been employed by Böckenfeld et al. They successfully cycled LFP electrodes in this pyrrolidinium nitrate-([Pyr_{HH}][NO₃]) based electrolyte, presenting a proof-of-concept for PIL-based LIBs.[171] Not much later, the first full cell LIB utilizing a neat PIL-based electrolyte combined with a LFP cathode and lithium titanate oxide (LTO) anode was shown by Menne et al.[172] The anode material was deliberately selected since it lays within the ESW of the employed triethylamine bis(trifluoromethylsulfonyl)imide ([Et₃N_H][TFSI]), unlike carbonaceous materials like graphite or soft carbon. However, since these materials offer much higher energy densities due to lower potentials, the same group subsequently tried to cycle electrodes based on carbonaceous materials in PIL-based electrolytes. And just like for conventional electrolytes before, this was achieved by the formation of an effective SEI. Unlike EC however, PILs alone are not able to form an SEI, which is why an additive, in this case vinyl ethylene carbonate (VEC), needs to be employed.[173] Remarkably, the PIL-based electrolyte, utilizing 1-butylpyrrolidinium bis(trifluoromethylsulfonyl)imide ([Pyr_{H4}][TFSI]) outperformed its aprotic counterpart, 1-butyl-1-methylpyrrolidinium bis(trifluoromethylsulfonyl)imide ([Pyr₁₄][TFSI]) in

combination with graphite- or hard carbon-based electrodes in both specific power as well as energy. Menne et al. later investigated this difference in performance via Raman spectroscopy, revealing a beneficial coordination, i.e., lower coordination number, for the lithium-ions by anions in the PIL-based electrolyte. This is caused by stronger interactions between the protic $[\text{Pyr}_{\text{H4}}]^+$ cation and $[\text{TFSI}]^-$ anion compared to the aprotic $[\text{Pyr}_{14}]^+$ cation.[174] It should be mentioned that unlike graphite and soft carbon, the combination of PIL-based electrolytes with hard carbon does not yield better performance compared to AIL-based electrolyte. Thus, other effects than lithium-mobility within the electrolyte seem the limiting factor in combination with this material.[175]

As for the PIL-based electrolytes in supercapacitors, the high viscosity of PILs is a limiting factor in terms of power performance. Thus, Vogl et al. tried to improve the viscosity by choosing the best suited anion. They found that the $[\text{FSI}]^-$ anion offers lower viscosities compared to the $[\text{TFSI}]^-$ anion while still capable of forming an SEI with the addition of additives.[176] Another approach, already applied in supercapacitors, is the mixture of PILs with solvents. Since the increased safety of PIL-based electrolytes for LIBs is a main incentive, it is important to keep the flammability and vapor pressure of such a mixture at a minimum. Menne et al. used PC as solvent in combination with $[\text{Pyr}_{\text{H4}}][\text{TFSI}]$, showing that up to a specific amount of solvent, the safety properties of the PIL are retained. They primarily improved the transport properties of this PIL-based electrolyte via this method. However, they also diminished a typical problem related to $[\text{TFSI}]^-$ -based electrolytes, the corrosion of aluminum current collectors due to dissolution of $\text{Al}([\text{TFSI}]^-)_3$, making it prone to capacity fading at prolonged cycling. Interestingly, $\text{Al}([\text{TFSI}]^-)_3$ seems to be hardly soluble in the employed PIL-PC mixture, resulting in a drastic increased cycle life at elevated temperatures.[177]

Eutectic mixtures of PILs have also been employed in LIBs, increasing the operative temperature of these devices down to 0 °C.[178]

Unfortunately, research concerning PIL-based electrolytes in combination with alkali metal ion batteries other than lithium-based ones, has been relatively spare, even though these systems are an essential part of modern battery related research. Vogl et al. were the first to employ a PIL-based electrolyte in a sodium-ion hybrid device utilizing a polyanionic cathode and AC-based negative electrode. As in the case of graphite and soft carbon in LIBs, a PIL-based electrolyte displayed better performance compared to its aprotic counterpart. Nevertheless,

they were not able to reversibly insert/extract sodium-ions into/from layered metal oxide cathodes within this PIL-based electrolyte.[179] Furthermore, a carbonaceous anode material, in this case HC, has been investigated by Arnaíz et al. for both, sodium as well as potassium ion-based batteries. Even with the addition of VEC, the employed PIL-based electrolyte could not enable a reversible cycling of this anode material neither for the sodium ion- nor the potassium ion-based system.[180]

1.8. The development of new PIL-based electrolytes

While PILs have been established in various systems over the years, these implementations are far from being optimized. A prime example would be the EDLC, in which the use of PILs appears very unfavorable or even questionable. As already mentioned, the high viscosity and low OPV of PILs drastically limit the performance of such a device, especially when compared to state-of-the-art electrolytes.

Still, devices employing these latter electrolytes have to compete with battery systems, especially in terms of capacity. And even with their much higher OPVs compared to PILs, these state-of-the-art-electrolyte-based EDLCs will hardly reach the energy density of batteries or at least the price per kWh. Thus, this system must excel in its low price for power.

A moderate OPV paired with excellent transport properties would be very desirable. For that, PILs seem to be suitable candidates, coming with intrinsic safety properties as well as sufficient OPVs. However, the transport properties need to be drastically improved with strategies already been discussed in the previous chapters, with the mixtures with water appearing as a very promising one.

While the proof-of-concept for PILs as electrolytes in LIBs has been established the optimization of this system is far away from being complete. One of the most important tasks is the growth of the catalogue of applicable PILs in this system. Not to mention the possible benefits merely by identifying better PILs in terms of transport or thermal properties, this would expand possible investigations in general. While one method to increase the performance of a LIB system, e.g., via additives, might not work for a given PIL, it might work for another one.

In contrast to lithium-ion systems in combination with PILs, with an already successful implementation, the combination with alternative systems, e.g., sodium- or calcium-based

have been rather unexplored. In the last years, research has taken large steps in these systems, employing mostly conventional electrolytes. All this has been pushed by the concerns regarding the availability and prices of lithium, making alternatives necessary. With the foundations being laid, research concerning the electrolyte in these systems is more and more diversifying, e.g., employing AILs to increase the safety. Thus, it seems reasonable also trying to establish PILs as electrolytes, which have already proven to be advantageous in lithium-based systems compared to AILs, hopefully transferring the benefits to these alternative systems.

Another highly promising usage for PILs lies in the immobilization, e.g., in polymers, thus creating solid electrolytes. These offer increased safety properties by eliminating the risk of leakage and allowing flexible devices. Naturally, the vehicular transport of ions in these polymers is rather hampered compared to liquids, making additional transport mechanisms highly desirable. Capable of such mechanisms, PILs appear as perfect candidate for a solid electrolyte. Nevertheless, their use in electrochemical storage devices has been only very scarce compared to AILs, which have been employed already for many years.

In this work, the mentioned applications for PILs will be investigated and analyzed, with the aim to develop safe and effective electrolyte systems for advanced electrochemical energy storage devices. To accomplish this aim, a variety of methods will be employed, ranging from the synthesis of new PILs, innovative mixtures with several solvents but also the immobilization within polymers. While the main investigations will be carried out via electrochemical measurements, also more classical analytical techniques, physical characterization as well as theoretical molecular dynamic simulations will be employed.

1.8.1. Publikation 1: Protic ionic liquids in energy storage devices: past, present and future perspective

Energy Storage Materials 40 (2021) 402–414



Contents lists available at ScienceDirect

Energy Storage Materials

journal homepage: www.elsevier.com/locate/ensm

Protic ionic liquids in energy storage devices: past, present and future perspective



Timo Stettner, Andrea Balducci*

Institute for Technical Chemistry and Environmental Chemistry and Center for Energy and Environmental Chemistry Jena (CEEC Jena), Friedrich Schiller University Jena, Philosophenweg 7a, 07743 Jena, Germany

ARTICLE INFO

Keywords:

Protic ionic liquids
Protic electrolytes
Batteries
Supercapacitors

ABSTRACT

The development of new and especially safer electrolytes is an important task in the development of modern electrochemical energy storage devices. One promising approach to reach this goal is the deployment of ionic liquids as electrolyte. In this review-perspective article we are considering protic ionic liquids (PILs) and we are critically comparing their characteristics, syntheses as well as benefits and drawbacks to the more prominent aprotic ionic liquids. Furthermore, we analyzed in detail the use of PILs as electrolytes in supercapacitor as well as battery. In the last part of the manuscript an outlook regarding the challenges of improving and expanding the use of PILs as electrolytes in energy storage devices, including established and prospective systems and materials, is given.

1. Introduction

Electrochemical energy storage devices such as lithium-ion batteries (LIBs) and supercapacitors (SCs) have become essential in our society during the last decades. Nowadays these devices are used in a multitude of different applications, and their massive introduction in electric vehicles and stationary applications will further strengthen their importance in our daily life [1–3]. The use of safe and high-performance devices is required in several key applications, e.g., transportation [4]. One major task in developing these electrochemical storage devices, besides the enhancement of the performance, is therefore the realization of safe systems.

In the state-of-the-art LIBs and, to a lesser extent SCs, a large hazard potential is associated with the electrolyte of these devices, typically consisting of a mixture containing one or more organic solvents (mainly carbonates and nitriles), a conductive salt (in most of the cases including a fluorinated anion) and a task specific additive, e.g., solid electrolyte interphase (SEI) film-forming agents [5]. The implementation of these electrolytes allows the realization of high performance devices but, at the same time, increases the risk of incineration and bursting of the device in case of overheating or improper opening of the device [6,7]. Consequently, in the past years large efforts have been dedicated towards the development of alternative electrolytes.

Among the various classes of alternative electrolytes proposed so far, ionic liquids (ILs) can be certainly considered as one of the most interesting. By a general definition, ILs are molten salts displaying a melt-

ing point (m.p.) below 100 °C. It has been estimated that 10⁶ different salts are belonging to this category of chemical compounds [8–10]. Clearly, this enormous number of possible ILs makes it extremely difficult to generalize the properties of this class of compounds. Nevertheless, it has been shown that there are many ILs displaying good transport properties, high thermal stabilities, large electrochemical stabilities, low flammability, and low volatility. Clearly, this potential set of properties makes ILs very interesting as electrolyte candidates for LIBs and SCs, especially because their use could allow a direct substitution of the conventional solvents, which are typically flammable [11]. Consequently, a large number of studies have been dedicated to the implementation of ILs in electrolytes for batteries and SCs over the last years [12–17].

Depending on their chemical structure, ILs can be divided into different classes. Among them, two of the most important are aprotic (AILs) and protic (PILs) ionic liquids. ILs belonging to either of these two classes can display the favorable properties mentioned above, while the main difference between them resides on the presence of one (or more) available proton on the cation (or anion) of the PILs. Most of the studies dedicated to the use of ILs in energy storage devices have been carried out utilizing AILs [18–20]. Nevertheless, the interest on the use of PILs in energy storage devices steadily increased in the last years and this class of ILs is now regarded with high interest by the scientific community [21–23]. The aim of this review is to critically analyze the properties of PIL-based electrolytes as well as the advantages and drawbacks related to their use in energy storage devices, specifically alkali/alkaline earth metal-ion batteries as well as supercapacitors.

* Corresponding author.

E-mail address: andrea.balducci@uni-jena.de (A. Balducci).<https://doi.org/10.1016/j.ensm.2021.04.036>

Received 24 February 2021; Received in revised form 9 April 2021; Accepted 21 April 2021

Available online 25 April 2021

2405–8297/© 2021 Elsevier B.V. All rights reserved.

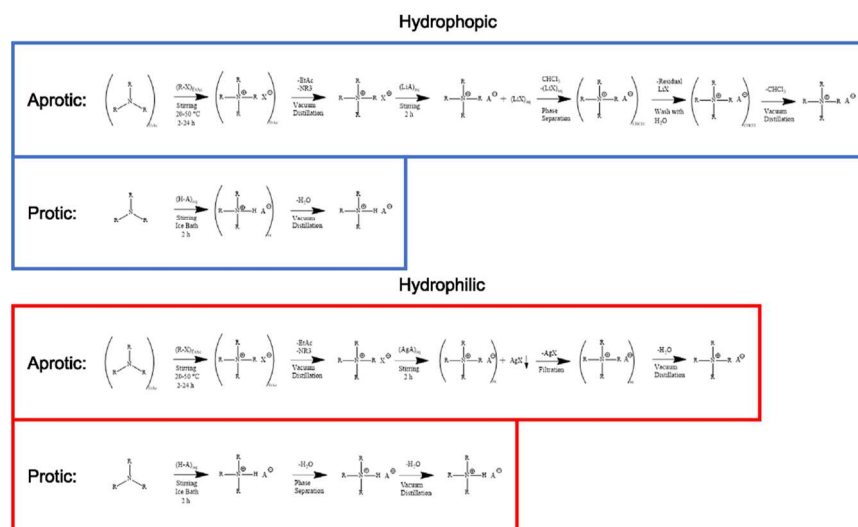


Fig. 1. Schematic synthesis paths for hydrophobic and hydrophilic aprotic and protic ionic liquids. In these examples a tertiary amine is employed as cation, whereas the anion is symbolized by the A.

2. Protic vs. aprotic ionic liquids: synthesis and chemical physical properties

As mentioned above (Chapter 1), and suggested by the name, PILs display an available proton either on their cation or their anion. The cation and anion act as proton-donor and -acceptor, respectively, adding another source of ion-ion interaction within the ILs structure besides the regular Coulombic and dispersion forces [24–27]. In general, this leads to stronger binding forces between anions and cations compared to AILs. These forces are influencing the transport and the thermal properties, as well as electrochemical stabilities, of PILs [28,29].

Although AILs have been the main class of ILs for most applications, it is interesting to note that the first documented use of an IL has been with a protic one. Of course, the classification of an IL has not even been established in 1914 when Paul Walden was working with $[\text{NH}_4][\text{NO}_3]$, investigating the properties of molten salts at room temperature [30]. Anyway, this example highlights the feasible accessibility of PILs, which will be discussed in the following.

The synthesis of ILs is, in most of the cases, based on an ion-exchange process (Fig. 1). AILs, on the one hand, are typically synthesized through a multistep process (normally two steps) involving alkylation, anion-exchange as well as time-intensive purification of not only educts and product but also intermediates [31,32]. PILs, on the other hand, due to the principle of proton donor and acceptor, can be synthesized in a single step reaction, by simply neutralizing an acid with a base [33]. For this reason, the synthesis of PIL is often considered easier compared to that of AILs and, thus, more suitable for the establishment of mass production. Furthermore, it has been reported that the synthesis of PILs can be cheaper compared to that of AILs [34–37]. This latter point, however, needs careful consideration. The biggest difference in term of cost between PILs and AILs is observed for the synthesis of hydrophilic ILs. In the case of PILs, water is the only byproduct that must be removed during the synthesis, whilst for AILs it is necessary to remove also soluble byproducts. The removal of these byproducts requires the use of expensive silver salts, which are increasing the overall cost of the synthesis [38,39]. Nevertheless, it must be remarked that the final cost of all ILs (PILs and AILs) is mostly dependent on the cost of precursors. When

cheap precursors are used, the possibility to synthesize PILs in one step will ultimately make their cost lower than that of AILs. This is also true when expensive precursors, e.g., HTFSI as acid or 1-butylpyrrolidine, are used. In this case, however, the final cost of the PIL will be high anyway.

In view of their use as electrolytes in electrochemical energy storage devices, the optimization of the transport and thermal properties, as well as of the electrochemical stability of ILs is of crucial importance.

It has been shown that the conductivity of AILs and PILs based on similar anion-cation combinations is rather comparable [40,41]. Nevertheless, it is important to remark that the conduction mechanism taking place in these two classes of ILs can be different. In AILs the ion transport is only performed via a vehicular mechanism, and the mobility of the ions is influenced and limited by ion-ion interactions or viscosity [42]. In PILs, due to the presence of the proton, a second mechanism might occur. It is assumed, that through the proton-acceptor and -donor system the protons have the ability to hop through the electrolyte, in a process similar to the Grotthuss effect observed in water [43,44]. The intensity of this latter effect is enhanced by the presence of high amounts of water within the PIL. Furthermore, this effect is influenced by the temperature, and at the glass transition temperature of a PIL it might even dominate the overall conduction process taking place in the IL. In the best scenario, this means that the conduction can be partially decoupled from the viscosity [45]. Recently, Watanabe et al. have illustrated that the pK_a value of the employed acid in a PIL has a significant effect on the predominant conduction mechanism of the ions (Fig. 2). It needs to be adjusted so that the lifetime of the species $[\text{H-B}]^+$ becomes short enough while having a relatively low binding strength between H-A compared to the rotational and translational of the acid. In other words, a too weak or too strong acid will only lead to vehicular conduction mechanisms due to too strong bonding strengths between proton carriers [46,47].

As suggested by Angell, a convenient and elegant way to observe these differences is the Walden plot (see Fig. 3.), in which the conductivity is plotted against the viscosity, using a 1 M KCl solution as reference. [24] ILs that lie beneath the reference line are expected to be not fully dissociated, thus having a low ionicity. Depending on the position re-

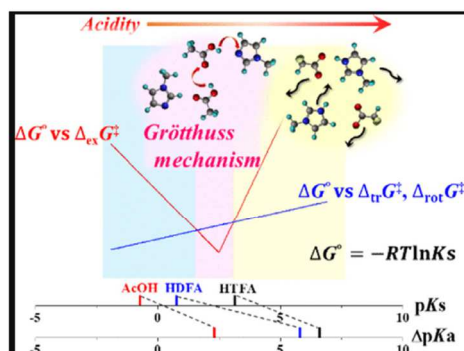


Fig. 2. Optimization of the mobility of the acidic proton in a PIL by adjusting the ΔpK_a value. Figure taken with permission from [47].

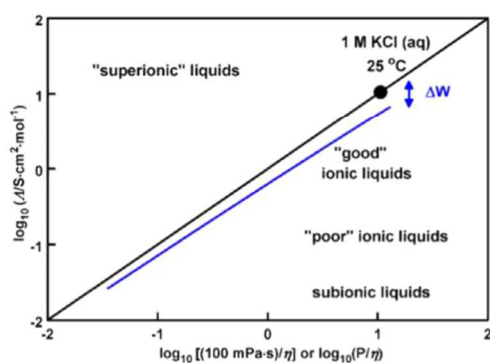


Fig. 3. Classical Walden Plot for a "good" ionic liquid (blue line). The conductivity is plotted against the fluidity and a 1 M KCl aqueous solution is used as reference point. The ionicity of an IL is evaluated by the shift of the IL from the reference (ideal) line, ΔW . Figure taken with permission from [49].

garding the reference line, they are considered as good, poor or subionic ILs. ILs that lie above the line might also be not fully dissociated, but they might display an additional mechanism of ion transportation. In case of PILs, this can be in the form of a proton network, resembling the already mentioned Grothuss mechanism. In the past years the Walden plot has been widely used to describe the properties of ILs but, recently, this method has been critically reviewed by several groups. [48] Harris et al. discussed the problems related to simple molten salts at high temperatures, showing that the Walden plot misleadingly predicts these salts as super-ionic, even if they are associated salts. As an alternative, it is suggested to calculate Laitly resistance coefficients to examine ion association within ILs [49]. Very recently, Mariani et al. discussed the principle of ionicity itself and the way it is derived. They argued that for PILs, instead of using only ion pairing or charge transfer between ions, one must keep in mind possible proton back transfer or even an incomplete reaction overall when calculating ionicity values. Since the precursors usually have a lower viscosity compared to the resulting IL, this would wrongly lead to a higher ionicity for a given IL. To solve this problematic, they suggest using a "reduced ionicity", simply involving all species within a system, neutral as well as charged. This will lead to lower ionicities, thus the terminology "reduced" ionicity [50].

Several studies showed that one of the main drawbacks associated to the use of ILs as electrolytes in energy storage devices is their relatively

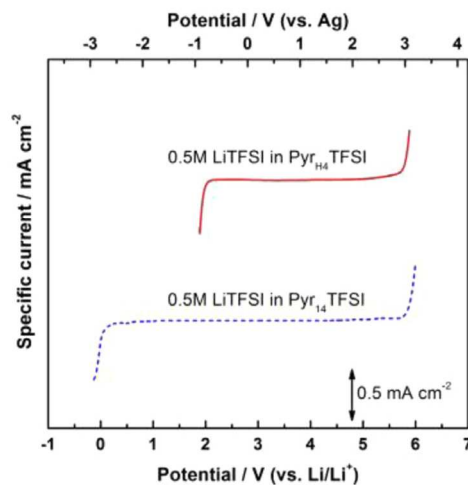


Fig. 4. Comparison of the electrochemical stability of an AIL (blue) vs. PIL (red), measured against a Pt working electrode, both containing 0.5 M LiTFSI. The PIL shows a typical cathodic limitation of around -1 V vs. Ag, due to the reduction of the acidic proton. Figure taken with permission from [70].

high viscosity [51]. It has been reported that AILs and PILs based on similar anion-cation combinations display comparable viscosities, and that for both of them the most straightforward approach to lower the viscosity is to lower the strength of the interactions occurring between anion and cation. Unfortunately, to this date it is not possible to exactly predict the impact of specific ion combinations on the properties of ILs (of any type). Thus, a very large number of ILs, both aprotic and protic, have been synthesized and characterized with the aim to understand the influence of several parameters, e.g., cation ring sizes, alkyl chain lengths, anion size and degree of fluorination, on their properties. Amongst others, the work of Susan et al. supplies useful information about a large number of different PILs, allowing to state some general trends, which indicates the following: [52,53] (1) It has been shown that the use of strong bases as well as strong acids (e.g. bis(trifluoromethane)sulfonimide (TfSI), HBF₄) is leading to the realization of PILs with a high ionicity; [54] (2) In the case of PILs the anion seems to impact the viscosity more than the cation, which is not the case for AILs; [33,55,56] (3) Complex as well as highly fluorinated anions can reduce the Van-der-Waals forces, while long alkyl chains on the anion will increase the viscosity; [51,56] (4) Weak hydrogen bonds in the PIL will overall lead to an improved ion mobility [29]. This latter point has been found to be the most important parameter for PILs in general. Reducing it, e.g. by worse stacking cations or charge delocalization on the anion, will ultimately reduce the ion-ion interactions [57].

In order to be effectively used as liquid electrolytes in energy storage devices the liquidous range of ILs should be as broad as possible. Several studies showed that the thermal stability of PILs and AILs is rather comparable and significantly higher than that of organic solvents. Thus, ILs appear well suited for high temperature applications. In order to be used at low temperatures, also a low melting point (m.p.) is necessary. The m.p. is influenced by several factors, e.g. packing efficiency of the cation or strength of the employed acid, and it has been reported that many AILs can display m.p.s below 0 °C, e.g., 1-Butyl-1-methylpyrrolidinium bis(trifluoromethylsulfonyl)imide ([Pyr₁₄][TfSI]) [21,54]. Overall, the m.p. of PILs appears higher than that of AILs. Considering the m.p., it is important to remark that the amount of residual water present inside a PIL after synthesis is strongly affecting the m.p. of these ILs, especially in

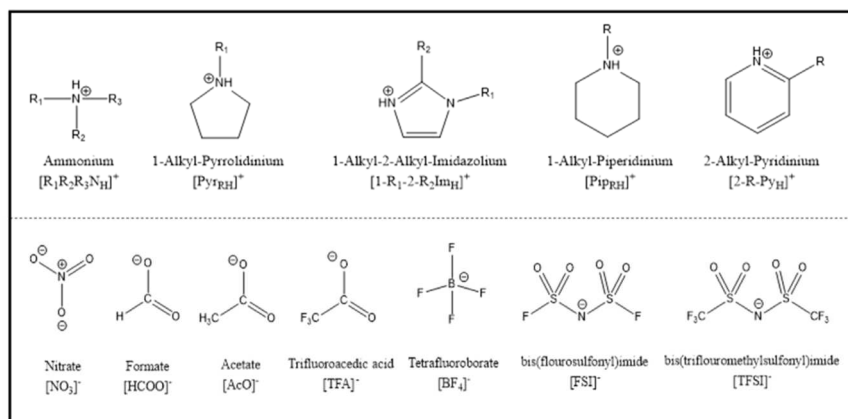


Fig. 5. Structures of the most commonly used cations (top) and anions (below) for the realization of PILs suitable for energy storage devices.

the case of hydrophilic PILs [58,59]. Relatively small amounts of water, e.g., 100 ppm, can lower the m.p. drastically while being not recognizable in electrochemical measurements [21,58,60,61]. Since the amount of water left in a PIL is often not stated in the literature, it is important to carefully consider this point and to correctly identify the m.p. of “dry” PILs in order to have a precise and reliable indication about the liquidous range of PILs and, thus, about their applicability in energy storage devices.

A broad electrochemical stability is mandatory for the realization of high energy LIBs and SCs. AILs can display very large electrochemical stabilities, e.g., larger than 5 V, and they have been largely utilized for the realization of high voltage LIBs and SCs [62–65]. The acidic proton of PIL is easily reducible (as the protons in water), and it is only stable to ca. 2 V vs. Li/Li^+ limiting the cathodic stability of PILs and, consequently, reducing their overall electrochemical stability [66–68]. In order to increase the electrochemical stability of PILs as much as possible, fluorinated anions with a highly delocalized charge, thus with a high oxidative resistance, need to be employed [69]. With these anions, it is possible to synthesize PILs with electrochemical stabilities in the order of 3.5–4 V.

Fig. 5 shows the structures of most often used cations and anions in PILs presently applied in energy storage devices, while Table 1 is reporting a comparison of some properties of these PILs.

Among the cations, imidazolium $[ImH]^+$, pyrrolidinium $[Py^+R_1H]^+$ and ammonium $[NH_4]^+$ have been the most utilized. Typically, imidazolium-based PILs display higher conductivity but lower electrochemical stability compared to pyrrolidinium-based ones. [71,72] The melting point of pyrrolidinium-based ILs are often lower compared to imidazolium- and ammonium-based ILs. For the latter, the alkylation degree is especially crucial, with primary and secondary ammonium showing lower melting points compared to non-alkylated and tertiary compounds. The highest electrochemical stability for ammonium compounds is achieved with tertiary ones, since they lack more easily reducible hydrogens, besides one available proton. Pyridinium-based ILs show even higher melting points compared to the mentioned cations. [21,73] Among the anions, bis(trifluoromethanesulfonyl)imide $[TFSI]^-$ and bis(fluorosulfonyl)imide $[FSI]^-$ are two of the most utilized. Their use allows the realization of PILs with good conductivity and large electrochemical stability, what is typical for fluorinated anions. While tetrafluoroborate $[BF_4]^-$ is also fluorinated, ILs containing this anion often show a rather high melting point. [21] Nevertheless, once liquid, their conductivity is reasonable high, even in the proximity of the melting point. Another advantage of fluorinated anions is their high

thermal stability. In contrast, carboxylates and trifluoroacetate based ILs are decomposing at lower temperatures, forming CO_2 [21,74].

3. Application of PILs in energy storage devices

As mentioned above in the previous sections, PILs are known since decades. However, their use in energy storage devices has been investigated relatively late compared to AILs. The reason for this delay is most likely related to the presence of the proton in the PIL structure, which was seen as an obstacle for their use in these systems. On the other hand, because of their ability to act as proton-donor and -acceptor, their negligible volatility and their electrochemical stability, PILs have been rather soon considered as interesting candidate for the realization of proton exchange membrane fuel cells (PEMFCs). In 2003, Susan et al. were the first to introduce a PIL, based on HTFSI, as electrolyte in a PEMFC. Since then several studies investigated the use of PILs in these systems. [52,88] As reported in a recent review of Elwan et al., PILs can nowadays be considered as an established alternative electrolyte for PEMFCs [89].

In the last years, an increasing number of studies showed that PILs can also be successfully utilized in energy storage devices and the subsequent part of this review will analyze these results in detail. Following the chronological development of these studies, the use of PILs in SCs will be considered at first. Afterwards, the use of PILs in batteries will be addressed.

3.1. PILs in supercapacitors

Supercapacitor is a term utilized to indicate a large number of high-power devices and, depending on the active material utilized for their realization, they can be divided in two main groups: electrochemical double layer capacitors (EDLCs) and pseudocapacitors [90]. In EDLCs the charge is stored through a physical process, the double layer formation, taking place at the interface between electrodes and electrolyte. In pseudocapacitors the charge is chemically stored through fast electrochemical reactions taking place on the surface of the electrodes [91]. Activated carbon (AC) is the most employed active material in EDLCs, while metal oxides, e.g. ruthenium and manganese oxides, are the most utilized active materials in pseudocapacitors [92]. The reactions occurring in these latter materials are based on a proton-electron transfer at the electrode-electrolyte interface, and are occurring in a protic environment (typically aqueous electrolytes) [93]. With the aim to take advantage of the proton mobility of PILs and of their broader electrochemical

Table 1
Comparison of the chemical physical properties of PILs utilized in energy storage applications.

Acronym	Melting Point [°C]	Electrochemical Stability [V]	Conductivity [mS cm ⁻¹]	Viscosity [mPa s]	Density [g cm ⁻³]	Source
[Et ₃ N _H][NO ₃]	-15	3.3	-20 (25 °C)	23.1	1.23 (25 °C)	[75,76]
[Et ₃ N _H][MsO]	24	2.47	1.91 (25 °C)	100 (25 °C)	1.14 (25 °C)	[77]
[Et ₃ N _H][TFSI]	-1	3.8	5.75	29	-	[78]
[iProp ₂ MeN _H][HCOO]	-100 (T _g) ¹	2.7	8.23 (25 °C)	25 (25 °C)	-	[79]
[iProp ₂ EtN _H][HCOO]	-103 (T _g) ¹	2.7	5 (25 °C)	18 (25 °C)	-	[79]
[EDA _H][AcO]	-71 (T _g) ¹	2.45	0.6 (25 °C)	958 (25 °C)	1.10 (25 °C)	[77]
[Py _{rr} H ₄][TFSI]	30	3.6	3.6	43	1.4	[80]
[Py _{rr} H ₄][FSI]	20	3.3	7.4	39	1.32	[81]
[Py _{rr} H ₄][TFSI]	37	3.4	3.7 (40 °C)	62i	1.62	[82]
[Py _{rr} H ₄][HSO ₄]	-30	3	6.8 (25 °C)	174	1.34 (25 °C)	[83]
[2-OxoPy _{rr} H ₄][BF ₄]	24	3	2.1	151.7	1.32	[84]
[dPy _{rr} H ₄][TFSI]	-58	1.2	0.9	159	1.45	[82]
[1-Melm _H][TFSI]	-30	2.75	3.1	67 (35)	1.63	[85]
[1-Melm _H][FSI]	-20	2.75	9.5	34	1.58	[85]
[1-Etlm _H][TFSI]	9	3	4.2	46	1.6	[82]
[1,2-Me ₂ Im _H][TFSI]	-50	2.75	11.0 (50 °C)	28.3 (50 °C)	1.56 (50 °C)	[85]
[1,2-Me ₂ Im _H][FSI]	-30	2.55	6.1	38.6	1.51	[85]
[Pip _H][TFSI]	41	3.4	1.2	176	1.59	[79,82]
[Pip _H][BF ₄]	25	3.2	8.2	139.8	1.27	[84]
[2-MePy _H][TFA]	-87 (T _g) ¹	2.4	3.4 (27 °C)	25.1 (27 °C)	1.32 (27 °C)	[86,87]
[2-EtPy _H][TFA]	-90 (T _g) ¹	2.3	3.1 (27 °C)	20.3 (27 °C)	1.25 (27 °C)	[84,86]
[2-PentPy _H][TFA]	-83 (T _g) ¹	2.4	1.1 (27 °C)	33.9 (27 °C)	1.17 (27 °C)	[86]
[2-MethoxyPy _H][TFA]	Below RT	2.2	1.79 (20 °C)	31.4 (20 °C)	-	[87]
[3-EtPy _H][TFA]	Below RT	2.5	3.9 (27 °C)	22.6 (27 °C)	1.25 (27 °C)	[86]
[Mor _H][BF ₄]	29	3.2	3.1	287.3	1.35	[84,86]
[Mor _{H2}][BF ₄]	21	3.2	3.2	216.2	1.29	[84]

¹ - No melting or crystallization temperature detectable. Direct change from liquid to glassy state. [Et₃N_H][NO₃] (triethylamine nitrate), [Et₃N_H][MsO] (triethylamine mesylate), [Et₃N_H][TFSI] (triethylammonium bis(trifluoromethanesulfonyl)imide), [iProp₂MeN_H][HCOO] (diisopropylmethylammonium formate), [iProp₂EtN_H][HCOO] (diisopropylethylammonium formate), [EDA_H][AcO] (ethylenediamine acetate), [Py_{rr}H₄][TFSI] (1-butylpyrrolidinium bis(trifluoromethanesulfonyl)imide), [Py_{rr}H₄][FSI] (1-butylpyrrolidinium bis(fluorosulfonyl)imide), [Py_{rr}H₄][TFSI] (pyrrolidinium bis(trifluoromethanesulfonyl)imide), [Py_{rr}H₄][HSO₄] (pyrrolidinium hydrogen sulfate), [2-OxoPy_{rr}H₄][BF₄] (1-methyl-2-oxopyrrolidinium tetrafluoroborate), [dPy_{rr}H₄][TFSI] (1,1'-carbonyl-pyrrolidin-pyrrolidinium bis(trifluoromethanesulfonyl)imide), [1-Melm_H][TFSI] (1-methylimidazolium bis(trifluoromethanesulfonyl)imide), [1-Melm_H][FSI] (1-methylimidazolium bis(fluorosulfonyl)imide), [1-Etlm_H][TFSI] (1-ethylimidazolium bis(trifluoromethanesulfonyl)imide), [1,2-Me₂Im_H][TFSI] (1,2-dimethylimidazolium bis(trifluoromethanesulfonyl)imide), [1,2-Me₂Im_H][FSI] (1,2-dimethylimidazolium bis(fluorosulfonyl)imide), [Pip_H][TFSI] (piperidinium bis(trifluoromethanesulfonyl)imide), [Pip_H][BF₄] (1-methylpiperidinium tetrafluoroborate), [2-MePy_H][TFA] (2-methylpyridinium trifluoroacetic acid), [2-EtPy_H][TFA] (2-ethylpyridinium trifluoroacetic acid), [2-PentPy_H][TFA] (2-pentylpyridinium trifluoroacetic acid), [2-MethoxyPy_H][TFA] (2-methoxypyridinium trifluoroacetic acid), [3-EtPy_H][TFA] (3-ethylpyridinium trifluoroacetic acid), [Mor_H][BF₄] (4-methylmorpholin-4-ium tetrafluoroborate), [Mor_{H2}][BF₄] (4-ethylmorpholin-4-ium tetrafluoroborate).

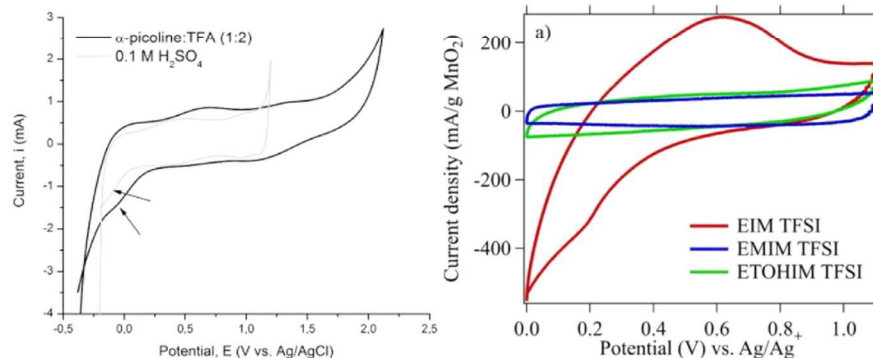


Fig. 6. Pseudocapacitive behavior of RuO₂ (left) and MnO₂ (right) electrodes in PILs. Figures taken with permission from [94] (left) and [95] (right).

stability with respect to water, Rochefort et al. were the first to utilize a PIL, 2-methylpyridinium trifluoroacetic acid ([2-MePy][TFA]), in combination with RuO₂ based electrodes (Fig. 6) [94]. In their pioneering work they showed that in this PIL, RuO₂ is displaying capacitances comparable to that observed in aqueous electrolytes, while AILs cannot be used. The group of Rochefort was also the first to show that PILs can be successfully used in combination with MnO₂ [87]. As in the case of

RuO₂, also this metal oxide cannot be conveniently cycled in combination with AILs, even if protonated. In a recent study, Lindberg et al. have shown that due to the different capability of PILs and AILs to form hydrogen bonds, only the acidic proton of PILs is able to induce reversible redox reactions in combination with MnO₂, while protons attached to AILs, e.g., in hydroxy groups do not display this ability [95]. In the last years several pseudocapacitive materials have been investigated and it

Table 2
Comparison of the properties of PIL-based supercapacitors.

Active Material	Electrolyte	Operative Voltage [V]	Specific Capacitance	Temperature of Use [°C]	Source
RuO ₂	[2-MetPyH][TFA]	2.5	83 F g ⁻¹ Half Cell	RT	[94]
RuO ₂	[1-Melm _H][HSO ₄]	1.5	44 F g ⁻¹ Full Cell	RT	[116]
RuO ₂	PEO-[1-Melm _H][HSO ₄]-[Im _H][HSO ₄]	1.5	39 F g ⁻¹ Full Cell	RT	[116]
RuO ₂	[Et ₂ MeN _H][TFO]	1	125 F g ⁻¹ Half Cell	25	[120]
MnO ₂	[2-MethoxyPyrH][TFA]	0.6	434 F g ⁻¹ Half Cell	RT	[87]
TiN	[2-MePyrH][TFA] (1:2)	2	300 F g ⁻¹ Half Cell	RT	[96]
VN	[2-MePyrH][TFA] (1:2)	1.7	291 F g ⁻¹ Half Cell	RT	[96]
PANI	[PyrH][HSO ₄]:H ₂ O (41:59)	0.8	380 F g ⁻¹ Half Cell	RT	[37]
Carbon Nanofiber	[1-EtIm _H][TFSI]	3	77 F g ⁻¹ Full Cell	RT	[111]
AC/POM	1 M [1-Bu-3-Melm][HSO ₄] _{aq}	1.1	233 F g ⁻¹ Half Cell	RT	[119]
AC	[Bu ₃ P _H][BF ₄]:ACN	3	200 F g ⁻¹ Half Cell	20	[34]
AC	[Pyr _H][NO ₃]	1.2	126 F g ⁻¹ Half Cell	RT	[97]
AC	[Pyr _H][HOOC]	1.2	130 F g ⁻¹ Full Cell	RT	[97]
AC	[Et ₃ N _H][TFSI]:PC (1:1)	2.5	120 F g ⁻¹ Full Cell	RT	[36]
AC	[Et ₃ N _H][TFSI]	2.5	115 F g ⁻¹ Full Cell	RT	[36]
AC	[Me ₃ N _H][TFSI]:(ACN/γ-BL/PC)	2.5	120–125 F g ⁻¹ Full Cell	25	[121]
AC	[Et ₃ N _H][TFSI]	2.4	14 F g ⁻¹ Full Cell ²	20	[35]
AC	[Me ₃ N _H][TFSI]:PC (1:1)	2.25	18 F g ⁻¹ Full Cell ²	20	[35]
AC	[Et ₃ N _H][TFSI] (0.3 M HQ)	2.5	72 F g ⁻¹ Full Cell	RT	[99]
AC	[Pyr _H][TFSI]:[Pyr _H][NO ₃] (0.28:0.72)	2	172 F g ⁻¹ Full Cell	25	[100]
AC	[Pyr _H][TFSI] (0.5 M NaTFSI)	2.2	22.5 F g ⁻¹ Full Cell ²	40	[102]
AC	[Pyr _H][TFSI]:2 G (8:2) (0.5 M NaTFSI)	2.5	30 F g ⁻¹ Full Cell ²	40	[102]
AC	[Pyr _H][TFSI]	2.2	25 F g ⁻¹ Full Cell ²	40	[80]
AC	[Pyr _H][TFSI] (1 wt.% H ₂ O)	2	30 F g ⁻¹ Full Cell ²	40	[80]
SiNW (Micro)	[Et ₃ N _H][TFSI]	4	1.9 mF cm ⁻² Full Cell	RT	[110]

² – Calculated for the full device [2-MetPyH][TFA] (2-methylpyridinium trifluoroacetic acid), [1-Melm_H][HSO₄] (1-methylimidazolium hydrogen sulfate), PEO-[1-Melm_H][HSO₄]-[Im_H][HSO₄] (poly(ethylene oxide)-1-methylimidazolium hydrogen sulfate-imidazolium hydrogen sulfate), [Et₂MeN_H][TFO] (diethylmethylammonium triflate), [2-MethoxyPyrH][TFA] (2-methoxypyrrrolidinium trifluoroacetic acid), [2-MePyrH][TFA] (2-methylpyrrolidinium trifluoroacetic acid), [Pyr_H][HSO₄] (pyrrolidinium hydrogen sulfate), [1-EtIm_H][TFSI] (1-ethylimidazolium bis(trifluoromethylsulfonyl)imide), [1-Bu-3-Melm][HSO₄] (1-butyl-3-methylimidazolium hydrogen sulfate), [Bu₃P_H][BF₄] (tributyl phosphonium tetrafluoroborate), ACN (acetonitrile), [Pyr_H][NO₃] (pyrrolidinium nitrate), [Pyr_H][HOOC] (pyrrolidinium formate), [Et₃N_H][TFSI] (triethylammonium bis(trifluoromethylsulfonyl)imide), PC (propylene carbonate), [Me₃N_H][TFSI] (trimethylammonium bis(trifluoromethylsulfonyl)imide), γ-BL (gamma-butyrolactone), HQ (hydroquinone), [Pyr_H][TFSI] (pyridinium bis(trifluoromethylsulfonyl)imide), [Pyr_H][NO₃] (pyridinium nitrate), NaTFSI (sodium bis(trifluoromethylsulfonyl)imide), 2 G (diglyme).

has been shown that besides metal oxides, also nitride and conducting polymers, e.g. PANI, can be successfully utilized in combination with PIL based electrolytes [37,96].

After the investigation dedicated to pseudocapacitors, the use of PILs in combination with AC has been considered. In 2010, Mysky et al. were the first to investigate the use of ACs in combination with PIL-based electrolytes, showing that these active materials can be cycled in a PIL, even at temperatures below 0 °C. [97] Demarcon et al. investigated the behavior of AC displaying different porosities and surface chemistries in combination with [Pyr_H][NO₃] and [Et₃N_H][TFSI].

[36] They showed that in these electrolytes, the influence of the porosity on the electrode capacitance is comparable to that observed in aqueous and organic electrolytes. Interestingly, they also observed that high amounts of oxygenated surface groups on the AC allow the occurrence of pseudocapacitive processes due to promoted proton hopping near the carbon surface. This effect can be amplified by attaching redox active functionalities on the carbon surface, which are further increasing the electrode's capacitance (Fig. 7) [98]. It should be mentioned here that Sathyamoorthi et al. demonstrated that PILs can also interact with redox active groups, e.g. hydroquinone, dispersed in the electrolyte [99].

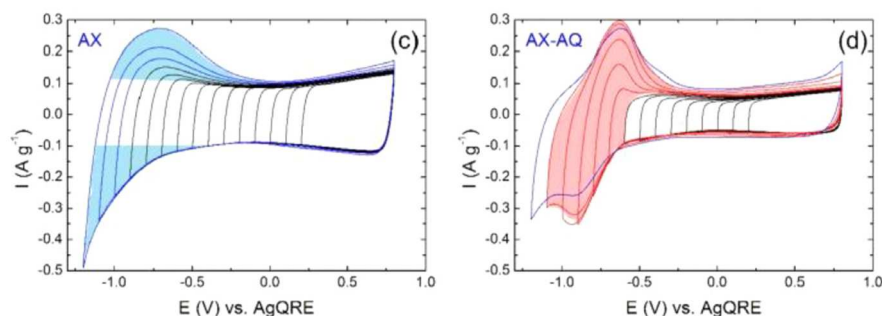


Fig. 7. Effect of redox active functionalities (AQ) attached to the electrodes surface (AXE) on the shape of CVs of a carbon based EDLC utilizing $[\text{Et}_3\text{N}_\text{H}][\text{TFSI}]$ as electrolyte. Figure taken with permission from [98].

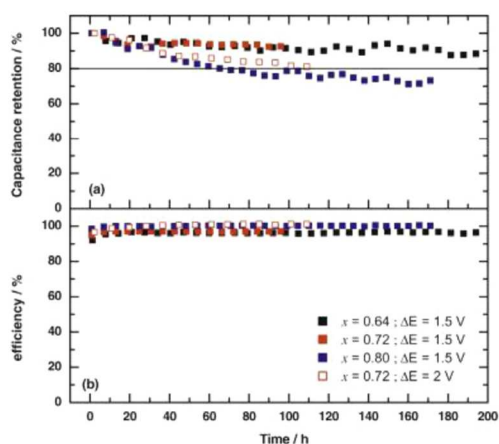


Fig. 8. Stability of AC-based EDLCs containing PIL based eutectic mixtures over prolonged floating at different operative voltages. Figure taken with permission from [100].

To further increase the operating temperature of PIL based electrolytes, Anouti et al. investigated the use of mixtures of phosphonium based PILs and organic solvents, in this case acetonitrile, as electrolyte for EDLCs [34]. They showed that EDLCs containing these electrolytes display good performances and that they can operate even at $-40\text{ }^\circ\text{C}$. Brand et al. investigated the cycling stability of EDLCs employing a mixture of a PIL and an organic solvent, illustrating that the use of these electrolytes guarantees a high cycling stability over prolonged cycling [35]. Timperman et al. investigated the use of eutectic mixtures of two PILs as electrolyte for EDLCs, demonstrating that these electrolytes allow the realization of EDLCs able to operate down to $-60\text{ }^\circ\text{C}$ due to the low melting point of such a mixture [100].

The results of these investigations indicate that PILs can be used in EDLCs. However, due to their limited electrochemical stability (compared to AILs), the operative voltage of PIL-based EDLCs (2–2.5 V) appears significantly lower compared to that of EDLCs based on AILs (3–3.5 V). The lower operative voltage is limiting the energy of PIL-based EDLCs, making it 30–40% lower than that of AIL-based EDLCs. [35,101] On the other hand, their use allows the possibility to develop protic electrolytes with a larger electrochemical stability compared to conventional aqueous electrolytes.

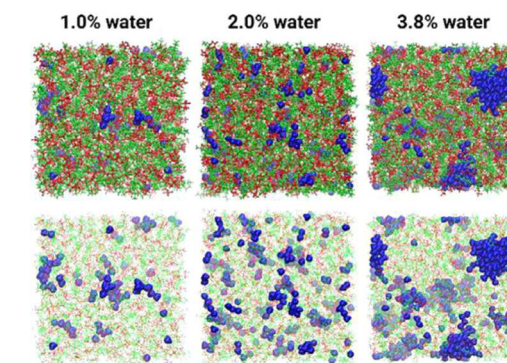


Fig. 9. Snapshots from classical molecular dynamics simulations at $30\text{ }^\circ\text{C}$ for $[\text{PyTfH}_4][\text{TFSI}]$ with different amounts of water. Left: 1 wt.% water, middle: 2 wt.% water, and right: 3.8 wt.% water. Enhanced clustering of water molecules upon increasing the concentration can be clearly observed. Water molecules are shown in blue whereas the ions of the liquid are shown with red and yellow lines. The top and bottom panels show opaque and translucent representations of the same snapshot. Figure taken with permission from [80].

The use of mixtures of PILs with organic solvents improves the transport properties of PIL-based electrolytes but is neither improving the electrode capacitance nor the EDLC operating voltage [102]. In these mixtures the PIL is acting as conducting salt, and the proton reactivity is partially smoothed by the presence of the organic solvent. It is important to notice that this is not the case when PILs are interacting with water. It is well known that the pH value of an electrolyte is significantly influencing the capacitances of carbonaceous electrodes, as it affects the mobility of protons and hydroxyl ions within the pores of the electrodes [103,104]. Demarconnay et al. successfully improved the capacitance of AC electrodes in a PIL by adding small amounts of a base to the electrolyte, which was effectively increasing the amount of hydroxyl ions within the water fraction [36]. This method is limited by the amount of water solved within the PIL, and it should be noted that the mixture can become saturated (the pH value remains constant). Nevertheless, this interesting study is demonstrating that the interplay between PIL and water (neat or containing a base or acid) can be utilized to modify the properties of a PIL and the behavior of carbonaceous electrodes cycled in such an electrolyte. In this context, mixtures of PILs and water appear rather interesting because, although they have a limited electrochemical stability due to the redox reactivity of water, they are able to

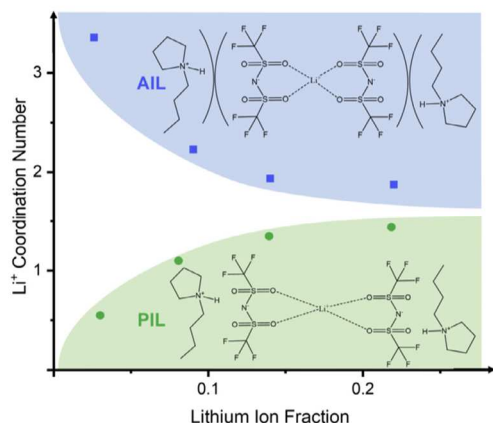


Fig. 10. Influence of the IL nature on the coordination of lithium ions in [TFSI]-based electrolytes. The Li coordination indicated in the figure refers to the number of TFSI anion around Li^+ . Figure taken with permission and modified from [123].

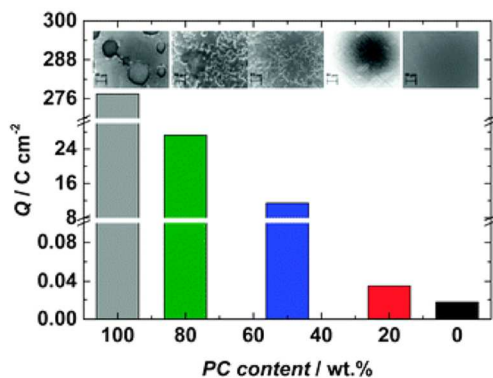


Fig. 11. Anodic dissolution of Al current collectors in mixture of PIL and PC. Higher amounts of IL decrease the dissolution of Al into the electrolyte. Figure taken with permission from [127].

maintain, or even improve, the ability of the PIL to act as proton-donor and -acceptor [105]. A recent study has shown that the properties of hydrophobic PILs, e.g., melting point and transport properties, are strongly influenced by the presence of already few weight percentages of water [80]. Utilizing classical molecular dynamics simulations (at 30 °C) it was observed that in hydrophilic PILs, water is distributed rather equally within the IL and, depending on the structure, binds stronger to the anion or cation. In presence of high fractions of water, the transport mechanisms of these PIL-water mixtures can even become governed by Grotthuss mechanisms, leading to increased proton hopping [106,107]. As a consequence, EDLCs containing these electrolytes display significantly higher power than EDLCs containing neat PILs and mixtures of PILs and organic solvents [108]. It is also worth to notice that the use of PIL-water mixtures increases the operating temperature of the EDLCs compared to aqueous systems, while keeping the electrolyte non-flammable. EDLCs

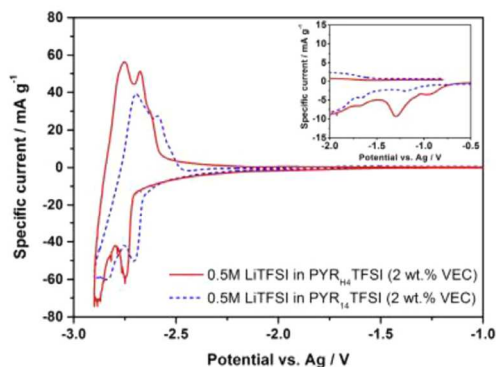


Fig. 12. Cyclic voltammograms of graphite in 0.5 M LiTFSI in [PYR₁₄][TFSI] with 2 wt.% VEC (red) and in 0.5 M LiTFSI in [PYR₁₄][TFSI] with 2 wt.% VEC (blue). The inset shows the VEC decomposition region during the first cycle. Figure taken with permission from [70].

containing mixtures of ILs and organic solvent are, on the other hand, flammable [109].

The results discussed above show that the use of PIL-based electrolytes in combination with pseudocapacitive materials or AC limit the operating voltages of supercapacitors to a maximum of 2.4–2.5 V. Aradilla et al. have shown, that by employing diamond-coated silicon nano wires (SiNWs) as electrode material in combination with [Et₃NH][TFSI], it is possible to operate a micro supercapacitor at 4 V with a stable performance [110]. More recently, Oyedotun et al. could cycle 1-EtIm₁TFSI in an oxygen-functionalized graphene based EDLCs up to 3 V with a good capacitance retention over prolonged time of cycling [111]. These results are indicating that the use of carbon with different properties compared to AC might increase the operating voltage of PIL-based supercapacitors. It is important to notice, however, that the mass loading of the electrodes utilized in the former study is significantly lower than that needed for industrial applications. Therefore, further investigations appear necessary to better understand the real performance and application of high voltage PIL-based EDLCs.

Recently also the confinement of PILs in a polymeric matrix has been considered, opening the field for PIL based solid electrolytes in EDLCs. This strategy has already been widely investigated in the application of AILs in LIBs and SCs, while PIL-based solid electrolytes were only used for fuel cells [112–115]. Ketabi et al. incorporated a eutectic mixture of a PIL in an PEO based polymer and used this innovative electrolyte in combination with RuO₂ and Ti electrodes [116]. They showed that, due to the good proton conduction, this PIL-based electrolyte could even be used at high current densities. In 2020, it was shown that EDLCs utilizing AC based electrodes with a PEO-based solid electrolyte incorporating [PyT₁₄][TFSI] display capacitances comparable to that of EDLCs containing neat (liquid) PILs at room temperature [117]. Although the devices were not optimized, the results of this study demonstrate that this approach is feasible and that its use could further improve the safety of PIL-based EDLCs by eliminating the risk of electrolyte leakage.

It is important to notice that all the PIL considered above display an acidic proton on the cation, being in an equilibrium state between ionic and neutral form. With the aim to reduce the corrosive potential of PILs, originating from the acid existing in the neutral state of a PIL, Treskow et al. introduced anion amphoteric ionic liquids (AAILs) [118]. These PILs bear their available proton on the anion, which is much less acidic compared to the conventional acids used for PILs, while being equilibrium free. Presented initially as possible electrolyte for fuel cells, the first use in an actual electrolyte for this specific type of PIL was as additive

in an aqueous supercapacitor. Hu et al. could drastically increase the cycle life of AC based electrodes with nanoconfined polyoxometalates in comparison to a regular aqueous electrolyte [119].

3.2. PILs in batteries

The introduction of a protic electrolyte with relatively low electrochemical stability and reactivity towards alkali metals was not seen as a feasible strategy for the realization of advanced and safer batteries. Thus, for long time, the use of PILs in these devices was not even considered.

In 2013, Böckenfeld et al. were the first to show that a mixture of $[\text{Pyr}_{\text{HH}}][\text{NO}_3]$ and PC can be successfully utilized in combination with lithium iron phosphate (LFP) electrodes [109]. Afterwards, Menne et al. reported the first example of a LIB containing a LFP cathode coupled with lithium titanate oxide (LTO) anode and having a neat PIL as electrolyte, in this case 1 M LiTFSI in $[\text{Et}_3\text{N}_{\text{H}}][\text{TFSI}]$ [122]. These works have shown that PILs can be successfully introduced in LIBs, and that their use allows the realization of stable devices with good performance, comparable to that achievable with AILs [123]. In the last years different electrode materials have been investigated with different types of PILs, and the results of these studies show that this class of IL can indeed be used in batteries [70,85,124]. Furthermore, they indicate that the use of PILs is particularly advantageous when high current densities (high C-rates) are applied. This latter finding is extremely interesting because one of the drawbacks associated to the use of AILs in LIBs is the limited power performance, which is related to the relatively high viscosity of AILs and, also, to the high coordination number of lithium ions within this electrolyte [125,126].

Utilizing Raman spectroscopy, Menne et al. demonstrated that the coordination of lithium ions in PIL-based electrolytes is markedly different compared to that in AIL-based electrolytes [123]. This difference is caused by the presence of the available proton, which is “competing” with the lithium ions for the coordination of the anion present in the electrolytic solution. Because of this competition, the coordination number of lithium ions in a PIL is lower than that in an AIL. The same group deepened this observation, revealing that the properties of the cation of the PIL, e.g., the size, influences the lithium coordination and that in order to improve the performance of PIL-based batteries, it is necessary to find an optimum between lithium coordination and viscosity [82]. When both parameters are optimized, as in the case of $[\text{Pyr}_{\text{HH}}][\text{FSI}]$, the employment of a PIL-based electrolyte in a LIB yields devices with performances comparable to that of conventional electrolytes up to 10 C at room temperature [81].

With the aim to further improve the performance of PIL-based batteries, also the use of mixtures of PC and $[\text{Pyr}_{\text{HH}}][\text{TFSI}]$ have been investigated [127]. As in the case of mixtures composed of AILs and PC, this approach allows the design of electrolytes with tunable properties which can display low flammability and good transport properties, leading to high performing systems [128]. It is worth to mention that high amounts of PIL within the electrolyte can reduce, or even suppress the occurrence of anodic dissolution of Al current collectors, a well known drawback of electrolytes containing the $[\text{TFSI}]^-$ anion. The same behavior was observed in mixtures of AIL and PC [128]. In order to enlarge the operating temperature of PIL-based electrolytes, which is limited by the relatively high m.p.s of these ILs (see previous section), eutectic mixtures of PILs have been investigated. It has been shown that the use of a mixture of $[\text{Pyr}_{\text{HH}}][\text{TFSI}]$ and $[\text{Pyr}_{\text{HH}}][\text{FSI}]$ and LiTFSI allows the realization of systems operating at 0 °C, thus a viable option to increase the operating temperature of PIL-based electrolytes [124].

The limited cathodic stability of PILs (ca. 2 V vs. Li/Li⁺) was initially considered as a limitation for the use of this class of ILs in combination with carbonaceous anodes, which are operating at potentials close to 0 V vs. Li/Li⁺. Menne et al. could successfully prevent the reduction of the protic cation at lower potentials by adding low amounts of an SEI forming additive to the electrolyte [70]. They have shown that the ad-

dition of 2 wt percent (wt.%) of vinyl ethylene carbonate (VEC) within a PIL-based electrolyte is enough to enable a reversible intercalation of lithium-ions in graphite and soft carbon electrodes. Interestingly, the performance of these anodic materials in PIL-based electrolytes is higher than that displayed in AIL-based electrolytes, despite the fact that the former are working almost 2 V outside the electrochemical stability of the electrolyte. More recently, Arnaiz et al. investigated the use of hard carbons in PIL-based electrolytes, demonstrating that also this type of carbonaceous anode can successfully be cycled in this class of IL. Contrary to graphite and soft carbon however, the electrode's performance in a PIL was not outperforming that achievable in an AIL based electrolyte [129].

For a long time, the use of PILs in lithium-metal batteries has not been investigated because the reactivity of PILs towards alkali and earth alkali metals was considered an obstacle for this application. Nevertheless, in 2020, Lingua et al. could show that the addition of a relatively high amount of SEI forming additive, e.g., 10 wt.% of vinylene carbonate (VC), enables the use of PILs in combination with metallic lithium. Utilizing an electrolyte composed of $[\text{Pyr}_{\text{HH}}][\text{TFSI}]$ and LiTFSI (4:1) and 10 wt.% of VC they could plate and strip lithium metal reversibly and realize high performance lithium-metal batteries containing LFP and NMC cathodes. It is interesting to observe that, as in the case of carbonaceous anodes, the use of PIL-based electrolytes allows higher performances compared to the use of AIL-based electrolytes [130].

As discussed in the introduction, the development of safe electrolytes is of crucial significance in the research for advanced batteries [5]. One of the most convenient approaches to reach this goal is the confinement of a liquid electrolyte in a solid matrix, e.g., polymeric electrolytes. In 2020 the first example of a lithium-metal battery containing a cross-linked polymer electrolyte (PEO based) encompassing a PIL ($[\text{Pyr}_{\text{HH}}][\text{TFSI}]/\text{LiTFSI}$) was developed. This innovative battery was displaying almost full specific capacity output and stable cycling at different current rates at RT. [117] In the same year also the confinement of a PIL within silica, resulting in an ionogel, was considered. Marie et al. showed that, due to the presence of the proton, PIL and AIL are behaving differently when confined in an ionogel and that the acidity of a PIL is a crucial parameter for the development of ionogels with a high lithium-ion mobility [132].

LIBs are certainly the most used electrochemical storage devices in our everyday life [133]. Nevertheless, due to concerns related to abundance and availability of lithium and metals like cobalt, in the last years many efforts have been directed towards the development of devices based on sodium, potassium or earth alkali metals like calcium [134–136]. AILs have been widely investigated in all these so-called post-lithium technologies, and interesting results have been reported [12,13,137,138]. Although only marginally, also the use of PIL-based electrolytes in these technologies has been investigated. Vogl et al. were the first group to successfully implement a PIL-based electrolyte into a sodium-ion hybrid device with a polyanionic cathode and an AC based anode [139]. As observed in LIBs, the performance displayed by the devices using the PIL-based electrolyte was higher than that observed in AIL-based electrolytes. However, it was not possible to cycle layered metal oxide electrodes in combination with PIL based electrolytes. Another PIL based electrolyte for sodium-ion batteries has been tested by Jankowski et al. They employed a distinct type of PIL, originally proposed for fuel cell applications, which has already been mentioned in the section about EDLCs (Chapter 3). The AAIL 1-ethyl-3-methylimidazolium trifluoromethylsulfoniylimide ($[\text{1-Et-3-Melm}][\text{TFSAm}]$) mixed with NaTFSI showed promising plating-stripping results for elemental sodium combined with suitable transport properties. Due to a broader ESW compared to conventional PILs, this AAIL is not dependent on additives to form an SEI [140].

Arnaiz et al. investigated the performance of hard carbon electrodes in combination with sodium as well as potassium PIL and AIL-based electrolytes [129,141]. They showed that, contrary to lithium-based batteries, the addition of VEC is not allowing a reversible insertion-

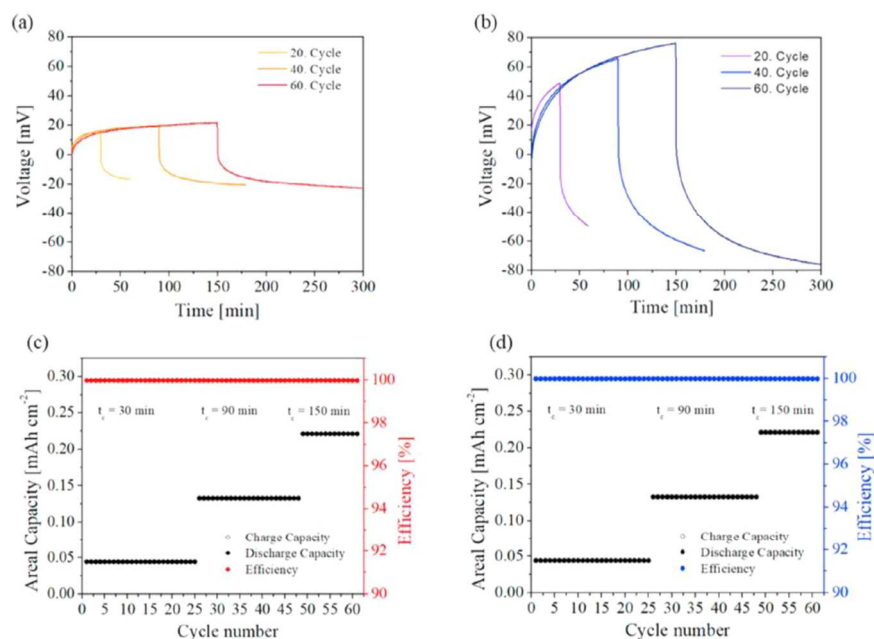


Fig. 13. Voltage profiles of symmetrical Li metal cells in combination with (a) $[\text{PyTf}_{14}][\text{FSl}]\text{-VC}$ and (b) $[\text{PyTf}_{14}][\text{TFSI}]\text{-VC}$ as electrolytes, as well as the results of charge-discharge measurements of (c) $[\text{PyTf}_{14}][\text{FSl}]\text{-VC/Li}$ and (d) $[\text{PyTf}_{14}][\text{TFSI}]\text{-VC/Li}$, all at different charge times. The experiment was conducted at 25 °C and with a current density of 0.088 mA cm⁻². Figure taken with permission from [131].

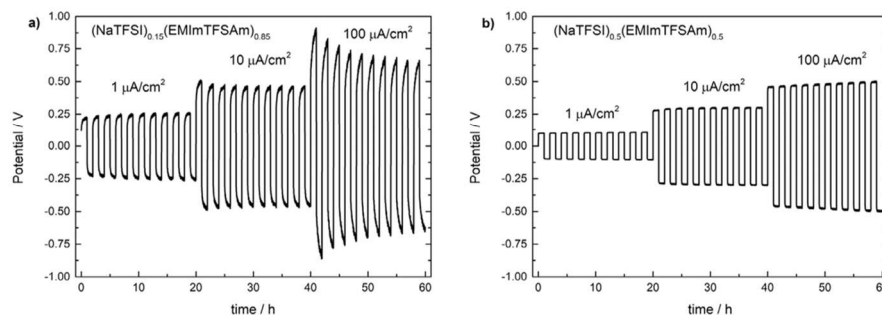


Fig. 14. Symmetrical Na-metal electrodes cycled in $[\text{1-Et-3-MeIm}][\text{TFSAm}]$ doped with different amounts of NaTFSI at 60 °C. Figure taken with permission from [140].

extraction of sodium and potassium ions within the hard carbon. In the case of these electrodes, the use of AILs appears presently more convenient. Finally, the use of PIL-based electrolytes containing CaTFSI has been recently reported. It has been shown that these electrolytes can be conveniently used in combination with AC-based electrodes, while the use in combination with battery electrodes appears more challenging [142].

4. Conclusion and future prospective

While considering the use of PIL in energy storage devices it is evident that this class of ILs, although less commonly used compared to

AILs, is certainly interesting. PILs display transport and thermal properties comparable to that of AILs, but the presence of the proton in their structure is strongly affecting their reactivity, electrochemical stability as well as their interplay with other chemical compounds, e.g., solvents and salts. These properties make PIL-based electrolytes unique and place them at the border between aqueous and aprotic electrolytes. In the future it will be necessary to further investigate the properties of PILs, e.g. their ionicity and/or super-ionicity, in order to design advanced PILs with properties tuned for a specific application. Particularly attention should be dedicated to the realization of highly conductive PILs with a “easily available” proton(s), which can be conveniently utilized

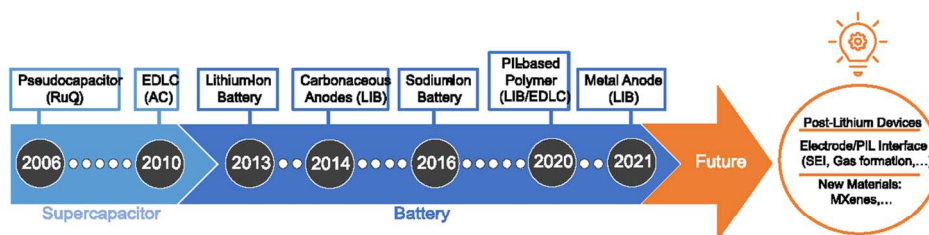


Fig. 15. Chronology of the use of PIL-based electrolytes in energy storage devices.

in electrochemical processes allowing a highly reversible and fast energy storage.

Fig. 15 depicts the progress of PILs-based electrolytes in SCs and batteries starting from their first application in 2006 until today and indicating technologies in which these electrolytes could be tested in the future.

The use of PILs in SCs has been investigated for 15 years. The results of these studies indicate that the use of PILs appears more advantageous in combination with pseudocapacitors rather than in EDLCs, as in these latter systems their narrow electrochemical stability is limiting the energy of the devices. In this regard, the understanding of the interplay between PILs and water appears as one of the most interesting aspects to investigate in the future. As a matter of fact, the possibility to control and tune the mobility of the proton in PILs would allow the realization of protic electrolytes with an enlarged electrochemical stability compared to aqueous electrolytes. These electrolytes could be extremely appealing for the full exploitation of pseudocapacitive materials and MXenes, which are nowadays considered of great importance for the future of high-power devices.

As discussed in the previous section (Chapter 3.2), PILs can be successfully employed in combination with a variety of anodic and cathodic materials for LIBs and, recently, it has also been shown that they can be used in combination with metallic lithium with the help of additives. The presence of the proton is modifying the lithium environment, rendering PIL-based electrolytes (neat or in combination with organic solvents) markedly different than the conventional AIL-based electrolytes. In the future it will be essential to better understand the SEI formation process in these electrolytes in order to further optimize their use in combination with anodic materials and metallic lithium. In parallel, it will be necessary to investigate their use with high voltage cathodes and, also, the gas evolution taking place in batteries containing these electrolytes. The understanding of these latter aspects appears of great importance to assess the real applicability on PILs-based electrolytes in lithium batteries. Furthermore, it will be very important to verify whether is possible to realize cheap and sustainable PIL, which can be produced in large scale.

To date only few studies have been dedicated to the use of PIL in post-lithium batteries. The results obtained with sodium-based systems although limited, are encouraging. Further investigations, however, are certainly needed to understand if the positive feature observed in lithium-based systems can be translated into sodium-based systems. More work is needed to understand the applicability of PIL in potassium and calcium-based systems. Yet unexplored applications for PILs in battery systems are e.g., lithium-air batteries where systems combined with protic electrolytes have already shown to yield good energy densities [143]. Two of the main problems of these metal-air batteries are the evaporation or/as well as flammability for either water or organic solvent-based electrolytes. The properties of PILs appear interesting in this context. Another possible future application could be sulfur-based lithium battery systems, in which AILs have already shown to be an effective method to inhibit the solvation of the sulfur electrode within the

electrolyte [144]. However, due to bad transport properties, the performance of such an IL based sulfur battery, especially at high current rates, needs improvement. This could be achieved by employing PILs instead of AILs, possibly displaying improved ion mobilities as they have shown already in more conventional lithium-ion battery systems.

Declaration of Competing Interest

No.

Acknowledgement

T.S. and A.B. wish to thank the Friedrich-Schiller University Jena for the support.

References

- [1] P. Hertzke, N. Müller, S. Schenk, Dynamics in the Global Electric-Vehicle market, McKinsey Center for Future Mobility, 2017.
- [2] J. Figgenger, et al., The development of stationary battery storage systems in Germany—a market review, *J. Energy Storage* 29 (2020) 101153.
- [3] C. Baum, et al., in: Future Energy Storage Systems for Mobility Applications, Fraunhofer Institute for Production Technology IPT, 2020, p. 48.
- [4] K. Liu, et al., Materials for lithium-ion battery safety, *Sci. Adv.* 4 (6) (2018) eaas9820.
- [5] Q. Wang, et al., Progress of enhancing the safety of lithium ion battery from the electrolyte aspect, *Nano Energy* 55 (2019) 93–114.
- [6] G. Walden, J. Stepan, C. Mikolajczak, Safety considerations when designing portable electronics with Electric Double-Layer Capacitors (Supercapacitors), in: 2011 IEEE Symposium on Product Compliance Engineering Proceedings, IEEE, 2011.
- [7] J. Zhang, et al., An overview on thermal safety issues of lithium-ion batteries for electric vehicle application, *IEEE Access* 6 (2018) 23848–23863.
- [8] K. Seddon, in: The International George Papatheodorou Symposium: Proceedings, Institute of Chemical Engineering and High Temperature Chemical Processes, Patras, 1999, p. 131.
- [9] J.S. Wilkes, A short history of ionic liquids—From molten salts to neoteric solvents, *Green Chem.* 4 (2) (2002) 73–80.
- [10] M. Freemantle, An Introduction to Ionic Liquids, Royal Society of chemistry, 2010.
- [11] S. Wilken, et al., *Ionic liquids in lithium battery electrolytes: composition versus safety and physical properties*, *J. Power Sources* 275 (2015) 935–942.
- [12] S. Biria, et al., Plating and stripping calcium at room temperature in an ionic-liquid electrolyte, *ACS Appl. Energy Mater.* 3 (3) (2020) 2310–2314.
- [13] M. Fiore, et al., Paving the way toward highly efficient, high-energy potassium-ion batteries with ionic liquid electrolytes, *Chem. Mater.* 32 (18) (2020) 7653–7661.
- [14] J.R. Nair, et al., Room temperature ionic liquid (RTIL)-based electrolyte cocktails for safe, high working potential Li-based polymer batteries, *J. Power Sources* 412 (2019) 398–407.
- [15] M. Moreno, et al., Ionic liquid electrolytes for safer lithium batteries I. investigation around optimal formulation, *J. Electrochem. Soc.* 164 (1) (2017) A6026–A6031.
- [16] I. Osada, et al., Ionic-liquid-based polymer electrolytes for battery applications, *Angew. Chem. Int. Ed.* 55 (2) (2016) 500–513.
- [17] A. González, et al., Review on supercapacitors: technologies and materials, *Renew. Sustain. Energy Rev.* 58 (2016) 1189–1206.
- [18] J.-W. Park, et al., Ionic liquid electrolytes for lithium–sulfur batteries, *J. Phys. Chem. C* 117 (40) (2013) 20531–20541.
- [19] C. Zhong, et al., A review of electrolyte materials and compositions for electrochemical supercapacitors, *Chem. Soc. Rev.* 44 (21) (2015) 7484–7539.
- [20] A. Balducci, Ionic liquids in lithium-ion batteries, in: *Ionic Liquids II*, Springer, 2017, pp. 1–27.
- [21] T.L. Greaves, C.J. Drummond, Protic ionic liquids: properties and applications, *Chem. Rev.* 108 (1) (2008) 206–237.

- [22] T.L. Greaves, C.J. Drummond, Protic ionic liquids: evolving structure–property relationships and expanding applications, *Chem. Rev.* 115 (20) (2015) 11379–11448.
- [23] A.S. Amarasekara, Acidic ionic liquids, *Chem. Rev.* 116 (10) (2016) 6133–6183.
- [24] M. Yoshizawa, W. Xu, C.A. Angell, Ionic liquids by proton transfer: vapor pressure, conductivity, and the relevance of ΔpK_a from aqueous solutions, *J. Am. Chem. Soc.* 125 (50) (2003) 15411–15419.
- [25] J.-P. Belieres, C.A. Angell, Protic ionic liquids: preparation, characterization, and proton free energy level representation, *J. Phys. Chem. B* 111 (18) (2007) 4926–4937.
- [26] K. Fumino, A. Wulf, R. Ludwig, The potential role of hydrogen bonding in aprotic and protic ionic liquids, *PCCP* 11 (39) (2009) 8790–8794.
- [27] R. Hayes, et al., The nature of hydrogen bonding in protic ionic liquids, *Angew. Chem. Int. Ed.* 52 (17) (2013) 4623–4627.
- [28] C. Zhao, et al., Electrochemistry of room temperature protic ionic liquids, *J. Phys. Chem. B* 112 (23) (2008) 6923–6936.
- [29] M.S. Miran, et al., Electrochemical properties of protic ionic liquids: correlation between open circuit potential for H_2/O_2 cells under non-humidified conditions and ΔpK_a , *RSC Adv.* 3 (13) (2013) 4141–4144.
- [30] P. Walden, Ueber die Molekulargröße und elektrische Leitfähigkeit einiger geschmolzenen Salze, *Bulletin de l'Académie Impériale des Sciences de St-Petersbourg* 8 (6) (1914) 405–422.
- [31] J.G. Huddleston, et al., Characterization and comparison of hydrophilic and hydrophobic room temperature ionic liquids incorporating the imidazolium cation, *Green Chem.* 3 (4) (2001) 156–164.
- [32] G.B. Appetecchi, et al., Synthesis of hydrophobic ionic liquids for electrochemical applications, *J. Electrochem. Soc.* 153 (9) (2006) A1685–A1691.
- [33] H. Ohno, M. Yoshizawa, Ion conductive characteristics of ionic liquids prepared by neutralization of alkylimidazoles, *Solid State Ion.* 154 (2002) 303–309.
- [34] I. Timperman, et al., Phosphonium-based protic ionic liquid as electrolyte for carbon-based supercapacitors, *Electrochem. Commun.* 13 (10) (2011) 1112–1115.
- [35] A. Brandt, et al., An investigation about the cycling stability of supercapacitors containing protic ionic liquids as electrolyte components, *Electrochim. Acta* 108 (2013) 226–231.
- [36] L. Demarconnay, et al., Optimizing the performance of supercapacitors based on carbon electrodes and protic ionic liquids as electrolytes, *Electrochim. Acta* 108 (2013) 361–368.
- [37] F. Al-Zohbi, et al., Impact of the aqueous pyrrolidinium hydrogen sulfate electrolyte formulation on transport properties and electrochemical performances for polyaniline-based supercapacitor, *J. Power Sources* 431 (2019) 162–169.
- [38] J.S. Wilkes, M.J. Zaworotko, Air and water stable 1-ethyl-3-methylimidazolium based ionic liquids, *J. Chem. Soc. Chem. Commun.* (13) (1992) 965–967.
- [39] G. Cravotto, et al., Preparation of second generation ionic liquids by efficient solvent-free alkylation of N-heterocycles with chloroalkanes, *Molecules* 13 (1) (2008) 149–156.
- [40] N. Yaghini, L. Nordstierna, A. Martinelli, Effect of water on the transport properties of protic and aprotic imidazolium ionic liquids—an analysis of self-diffusivity, conductivity, and proton exchange mechanism, *PCCP* 16 (20) (2014) 9266–9275.
- [41] H. Watanabe, et al., Hydrogen bond in imidazolium based protic and aprotic ionic liquids, *J. Mol. Liq.* 217 (2016) 35–42.
- [42] A. Noda, K. Hayamizu, M. Watanabe, Pulsed-gradient spin-echo 1H and 19F NMR ionic diffusion coefficient, viscosity, and ionic conductivity of non-chloroaluminate room-temperature ionic liquids, *J. Phys. Chem. B* 105 (20) (2001) 4603–4610.
- [43] Z. Wojnarowska, et al., High pressure as a key factor to identify the conductivity mechanism in protic ionic liquids, *Phys. Rev. Lett.* 111 (22) (2013) 225703.
- [44] W. Oghara, T. Aoyama, H. Ohno, Polarity measurement for ionic liquids containing dissociable protons, *Chem. Lett.* 33 (11) (2004) 1414–1415.
- [45] Z. Wojnarowska, et al., Observation of highly decoupled conductivity in protic ionic conductors, *PCCP* 16 (19) (2014) 9123–9127.
- [46] H. Watanabe, et al., Possible proton conduction mechanism in pseudo-protic ionic liquids: a concept of specific proton conduction, *J. Phys. Chem. B* 123 (29) (2019) 6244–6252.
- [47] H. Watanabe, et al., Effect of brønsted acidity on ion conduction in fluorinated acetic acid and n-methylimidazole equimolar mixtures as pseudo-protic ionic liquids, *J. Phys. Chem. B* 124 (49) (2020) 11157–11164.
- [48] C. Schreiner, et al., Fractional Walden rule for ionic liquids: examples from recent measurements and a critique of the so-called ideal KCl line for the Walden plot, *J. Chem. Eng. Data* 55 (5) (2010) 1784–1788.
- [49] K.R. Harris, On the use of the Angell–Walden equation to determine the “ionicity” of molten salts and ionic liquids, *J. Phys. Chem. B* 123 (32) (2019) 7014–7023.
- [50] A. Mariani, et al., The unseen evidence of reduced ionicity: the elephant in (the) room temperature ionic liquids, *J. Mol. Liq.* (2020) 115069.
- [51] C.A. Angell, Y. Ansari, Z. Zhao, Ionic liquids: past, present and future, *Faraday Discuss.* 154 (2012) 9–27.
- [52] M.A. Susan, et al., Brønsted acid–base ionic liquids and their use as new materials for anhydrous proton conductors, *Chem. Commun.* (8) (2003) 938–939.
- [53] M.A. Susan, et al., A novel Brønsted acid–base system as anhydrous proton conductors for fuel cell electrolytes, *Chem. Lett.* 32 (9) (2003) 836–837.
- [54] M. Yoshizawa, W. Xu, C.A. Angell, Ionic liquids by proton transfer: vapor pressure, conductivity, and the relevance of ΔpK_a from aqueous solutions, *J. Am. Chem. Soc.* 125 (50) (2003) 15411–15419.
- [55] Z.-B. Zhou, H. Matsumoto, K. Katsumi, Low-melting, low-viscous, hydrophobic ionic liquids: n-alkyl (alkyl ether)-N-methylpyrrolidinium perfluoroethyltrifluoroborate, *Chem. Lett.* 33 (12) (2004) 1636–1637.
- [56] Y. Dong, et al., Azeponium based protic ionic liquids: synthesis, thermophysical properties and COSMO-RS study, *J. Mol. Liq.* 264 (2018) 24–31.
- [57] J. Smith, et al., Rheology of protic ionic liquids and their mixtures, *J. Phys. Chem. B* 117 (44) (2013) 13930–13935.
- [58] V.V. Matveev, et al., NMR investigation of the structure and single-particle dynamics of inorganic salt solutions in a protic ionic liquid, *J. Mol. Liq.* 278 (2019) 239–246.
- [59] S.K. Shukla, N.D. Khupse, A. Kumar, Do anions influence the polarity of protic ionic liquids? *PCCP* 14 (8) (2012) 2754–2761.
- [60] M.E. Van Valkenburg, et al., Thermochemistry of ionic liquid heat-transfer fluids, *Thermochim. Acta* 425 (1–2) (2005) 181–188.
- [61] Y. Kohno, H. Ohno, Ionic liquid/water mixtures: from hostility to conciliation, *Chem. Commun.* 48 (57) (2012) 7119–7130.
- [62] X. Gao, et al., Concentrated ionic-liquid-based electrolytes for high-voltage lithium batteries with improved performance at room temperature, *ChemSusChem* 12 (18) (2019) 4185.
- [63] S. Brutti, et al., Ionic liquid electrolytes for high-voltage, lithium-ion batteries, *J. Power Sources* 479 (2020) 228791.
- [64] C. Arbizzani, et al., Safe, high-energy supercapacitors based on solvent-free ionic liquid electrolytes, *J. Power Sources* 185 (2) (2008) 1575–1579.
- [65] N. Handa, et al., A neat ionic liquid electrolyte based on FSI anion for electric double layer capacitor, *J. Power Sources* 185 (2) (2008) 1585–1588.
- [66] B. Pal, et al., Electrolyte selection for supercapacitive devices: a critical review, *Nanoscale Adv.* (2019).
- [67] P.A.Z. Suarez, et al., Electrochemical behavior of vitreous glass carbon and platinum electrodes in the ionic liquid 1-n-butyl-3-methylimidazolium trifluoroacetate, *J. Braz. Chem. Soc.* 13 (2002) 106–109.
- [68] G.H. Lane, Electrochemical reduction mechanisms and stabilities of some cation types used in ionic liquids and other organic salts, *Electrochim. Acta* 83 (2012) 513–528.
- [69] D.R. Macfarlane, et al., Pyrrolidinium imides: a new family of molten salts and conductive plastic crystal phases, *J. Phys. Chem. B* 103 (20) (1999) 4164–4170.
- [70] S. Menne, et al., Carbonaceous anodes for lithium-ion batteries in combination with protic ionic liquids-based electrolytes, *J. Power Sources* 266 (2014) 208–212.
- [71] H.L. Ngo, et al., Thermal properties of imidazolium ionic liquids, *Thermochim. Acta* 357 (2000) 97–102.
- [72] C. Nieto de Castro, et al., Thermal properties of ionic liquids and ionic liquids of imidazolium and pyrrolidinium liquids, *J. Chem. Eng. Data* 55 (2) (2010) 653–661.
- [73] V. Venkatraman, et al., Predicting ionic liquid melting points using machine learning, *J. Mol. Liq.* 264 (2018) 318–326.
- [74] M.T. Clough, et al., Thermal decomposition of carboxylate ionic liquids: trends and mechanisms, *PCCP* 15 (47) (2013) 20480–20495.
- [75] D.F. Evans, et al., Micelle formation in ethylammonium nitrate, a low-melting fused salt, *J. Colloid Interface Sci.* 88 (1) (1982) 89–96.
- [76] B.H. Suryanto, et al., Tuning the electrodeposition parameters of silver to yield micro/nano structures from room temperature protic ionic liquids, *Electrochim. Acta* 81 (2012) 98–105.
- [77] X. Lu, et al., Electrochemistry of room temperature protic ionic liquids: a critical assessment for use as electrolytes in electrochemical applications, *J. Phys. Chem. B* 116 (30) (2012) 9160–9170.
- [78] I. Timperman, et al., Triethylammonium bis (tetrafluoromethylsulfonate) amide protic ionic liquid as an electrolyte for electrical double-layer capacitors, *PCCP* 14 (22) (2012) 8199–8207.
- [79] M. Anouti, et al., Alkylammonium-based protic ionic liquids part I: preparation and physicochemical characterization, *J. Phys. Chem. B* 112 (31) (2008) 9406–9411.
- [80] T. Stettner, et al., Water in protic ionic liquids: properties and use of a new class of electrolytes for energy-storage devices, *ChemSusChem* 12 (16) (2019) 3827–3836.
- [81] S. Menne, T. Vogl, A. Balducci, The synthesis and electrochemical characterization of bis (fluorosulfonate) imide-based protic ionic liquids, *Chem. Commun.* 51 (17) (2015) 3656–3659.
- [82] T. Vogl, et al., The influence of cation structure on the chemical–physical properties of protic ionic liquids, *J. Phys. Chem. C* 110 (16) (2006) 8525–8533.
- [83] M. Anouti, et al., Synthesis and characterization of new pyrrolidinium based protic ionic liquids. Good and superionic liquids, *J. Phys. Chem. B* 112 (42) (2008) 13335–13343.
- [84] T. Wu, et al., Synthesis and characterization of protic ionic liquids containing cyclic amine cations and tetrafluoroborate anion, *J. Iran. Chem. Soc.* 8 (1) (2011) 149–165.
- [85] T. Stettner, F.C. Walter, A. Balducci, Imidazolium-based protic ionic liquids as electrolytes for lithium-ion batteries, *Batteries Supercaps* 2 (1) (2019) 55–59.
- [86] L. Mayrand-Provencher, et al., Pyrrolidinium-based protic ionic liquids as electrolytes for RuO₂ electrochemical capacitors, *J. Power Sources* 195 (15) (2010) 5114–5121.
- [87] C.A. Castro Ruiz, D. Bélanger, D. Rochefort, Electrochemical and spectroelectrochemical evidence of redox transitions involving protons in thin MnO₂ electrodes in protic ionic liquids, *J. Phys. Chem. C* 117 (40) (2013) 20397–20405.
- [88] H. Nakamoto, M. Watanabe, Brønsted acid–base ionic liquids for fuel cell electrolytes, *Chem. Commun.* (24) (2007) 2539–2541.
- [89] H.A. Elwan, M. Mamlouk, K. Scott, A review of proton exchange membranes based on protic ionic liquid/polymer blends for polymer electrolyte membrane fuel cells, *J. Power Sources* (2020) 229197.
- [90] W. Raza, et al., Recent advancements in supercapacitor technology, *Nano Energy* 52 (2018) 441–473.
- [91] M. Toupin, T. Brousse, D. Bélanger, Charge storage mechanism of MnO₂ electrode used in aqueous electrochemical capacitor, *Chem. Mater.* 16 (16) (2004) 3184–3190.
- [92] T. Brousse, D. Bélanger, J.W. Long, To be or not to be pseudocapacitive, *J. Electrochem. Soc.* 162 (5) (2015) A5185–A5189.

- [93] B.-O. Park, et al., Performance of supercapacitor with electrodeposited ruthenium oxide film electrodes—effect of film thickness, *J. Power Sources* 134 (1) (2004) 148–152.
- [94] D. Rochefort, A.-L. Pont, Pseudocapacitive behaviour of RuO₂ in a proton exchange ionic liquid, *Electrochem. Commun.* 8 (9) (2006) 1539–1543.
- [95] S. Lindberg, et al., Charge storage mechanism of α -MnO₂ in protic and aprotic ionic liquid electrolytes, *J. Power Sources* 460 (2020) 228111.
- [96] A. Djire, et al., Enhanced performance for early transition metal nitrides via pseudocapacitance in protic ionic liquid electrolytes, *Electrochem. Commun.* 77 (2017) 19–23.
- [97] R. Mysyk, et al., Pseudo-capacitance of nanoporous carbons in pyrrolidinium-based protic ionic liquids, *Electrochem. Commun.* 12 (3) (2010) 414–417.
- [98] B. Gorska, P. Ratajczak, F. Béguin, Faradaic processes on quinone-grafted carbons in protic ionic liquid electrolyte, *Electrochim. Acta* 328 (2019) 135090.
- [99] S. Sathyanoorathi, V. Suryanarayanan, D. Velayutham, Organo-redox shuttle promoted protic ionic liquid electrolyte for supercapacitor, *J. Power Sources* 274 (2015) 1135–1139.
- [100] L. Timperman, A. Vigeant, M. Anouti, Eutectic mixture of protic ionic liquids as an electrolyte for activated carbon-based supercapacitors, *Electrochim. Acta* 155 (2015) 164–173.
- [101] A. Balducci, et al., High temperature carbon-carbon supercapacitor using ionic liquid as electrolyte, *J. Power Sources* 165 (2) (2007) 922–927.
- [102] T. Stettner, et al., Mixtures of glyme and aprotic-protic ionic liquids as electrolytes for energy storage devices, *J. Chem. Phys.* 148 (19) (2018) 193825.
- [103] K. Babel, K. Jurewicz, KOH activated carbon fabrics as supercapacitor material, *J. Phys. Chem. Solids* 65 (2–3) (2004) 275–280.
- [104] V. Khomenko, E. Raymundo-Piñero, F. Béguin, A new type of high energy asymmetric capacitor with nanoporous carbon electrodes in aqueous electrolyte, *J. Power Sources* 195 (13) (2010) 4234–4241.
- [105] M. Anouti, et al., Aggregation behavior in water of new imidazolium and pyrrolidinium alkylcarboxylates protic ionic liquids, *J. Colloid Interface Sci.* 340 (1) (2009) 104–111.
- [106] M.r.m. Anouti, J. Jacquemin, P. Porion, Transport properties investigation of aqueous protic ionic liquid solutions through conductivity, viscosity, and NMR self-diffusion measurements, *J. Phys. Chem. B* 116 (14) (2012) 4228–4238.
- [107] J. Ingeny, S. Gehrke, B. Kirchner, How to harvest Grotthuss diffusion in protic ionic liquid electrolyte systems, *ChemSusChem* 11 (12) (2018) 1900–1910.
- [108] B. Gorska, et al., Effect of low water content in protic ionic liquid on ions electroadsorption in porous carbon: application to electrochemical capacitors, *PCCP* 19 (18) (2017) 11173–11186.
- [109] R.-S. Kühnel, et al., Mixtures of ionic liquid and organic carbonate as electrolyte with improved safety and performance for rechargeable lithium batteries, *Electrochim. Acta* 56 (11) (2011) 4092–4099.
- [110] D. Aradilla, et al., A step forward into hierarchically nanostructured materials for high performance micro-supercapacitors: diamond-coated SiNW electrodes in protic ionic liquid electrolyte, *Electrochem. Commun.* 63 (2016) 34–38.
- [111] K.O. Oyedotun, et al., Comparison of ionic liquid electrolyte to aqueous electrolytes on carbon nanofibres supercapacitor electrode derived from oxygen-functionalized graphene, *Chem. Eng. J.* 375 (2019) 121906.
- [112] Y.-S. Ye, J. Rick, B.-J. Hwang, Ionic liquid polymer electrolytes, *J. Mater. Chem. A* 1 (8) (2013) 2719–2743.
- [113] G.A. Tiruye, et al., All-solid state supercapacitors operating at 3.5 V by using ionic liquid based polymer electrolytes, *J. Power Sources* 279 (2015) 472–480.
- [114] V.M. Ortiz-Martínez, et al., Fuel cell electrolyte membranes based on copolymers of protic ionic liquid [HSO₃-BVI_m][TfO] with MMA and hPPSVE, *Polymer (Guildf)* 179 (2019) 121583.
- [115] D.E. Smith, D.A. Walsh, The nature of proton shuttling in protic ionic liquid fuel cells, *Adv. Energy Mater.* 9 (24) (2019) 1900744.
- [116] S. Ketabi, B. Decker, K. Lian, Proton conducting ionic liquid electrolytes for liquid and solid-state electrochemical pseudocapacitors, *Solid State Ion.* 298 (2016) 73–79.
- [117] T. Stettner, et al., Protic ionic liquids-based crosslinked polymer electrolytes: a new class of solid electrolytes for energy storage devices., *Energy Technol.* 8 (11) (2020) 2000742.
- [118] M. Treskow, et al., A new class of ionic liquids: anion amphiprotic ionic liquids, *J. Phys. Chem. Lett.* 3 (16) (2012) 2114–2119.
- [119] C. Hu, et al., Aqueous solutions of acidic ionic liquids for enhanced stability of polyoxometalate-carbon supercapacitor electrodes, *J. Power Sources* 326 (2016) 569–574.
- [120] N.L. Nguyen, D. Rochefort, Electrochemistry of ruthenium dioxide composite electrodes in diethylmethylammonium-triflate protic ionic liquid and its mixtures with acetonitrile, *Electrochim. Acta* 147 (2014) 96–103.
- [121] E. Coadou, et al., Comparative study on performances of trimethyl-sulfonium and trimethyl-ammonium based ionic liquids in molecular solvents as electrolyte for electrochemical double layer capacitors, *J. Phys. Chem. C* 117 (20) (2013) 10315–10325.
- [122] S. Menne, et al., Protic ionic liquids as electrolytes for lithium-ion batteries, *Electrochem. Commun.* 31 (2013) 39–41.
- [123] T. Vogl, et al., The beneficial effect of protic ionic liquids on the lithium environment in electrolytes for battery applications, *J. Mater. Chem. A* 2 (22) (2014) 8258–8265.
- [124] T. Vogl, S. Passerini, A. Balducci, The impact of mixtures of protic ionic liquids on the operative temperature range of use of battery systems, *Electrochem. Commun.* 78 (2017) 47–50.
- [125] P.M. Bayley, et al., The effect of coordinating and non-coordinating additives on the transport properties in ionic liquid electrolytes for lithium batteries, *PCCP* 13 (10) (2011) 4632–4640.
- [126] G.A. Giffin, et al., Connection between lithium coordination and lithium diffusion in [Pyr12O1][FTFSI] ionic liquid electrolytes, *ChemSusChem* 11 (12) (2018) 1981–1989.
- [127] T. Vogl, S. Menne, A. Balducci, Mixtures of protic ionic liquids and propylene carbonate as advanced electrolytes for lithium-ion batteries, *PCCP* 16 (45) (2014) 25014–25023.
- [128] S. Menne, R.-S. Kühnel, A. Balducci, The influence of the electrochemical and thermal stability of mixtures of ionic liquid and organic carbonate on the performance of high power lithium-ion batteries, *Electrochim. Acta* 90 (2013) 641–648.
- [129] M. Arnaiz, et al., Protic and aprotic ionic liquids in combination with hard carbon for lithium-ion and sodium-ion batteries, *Batteries Supercaps* 1 (6) (2018) 204–208.
- [130] G. Lingua, et al., Enabling safe and stable Li metal batteries with protic ionic liquid electrolytes and high voltage cathodes, *J. Power Sources* 481 (2021) 228979.
- [131] G. Lingua, et al., Enabling safe and stable Li metal batteries with protic ionic liquid electrolytes and high voltage cathodes, *J. Power Sources* 481 (2021) 228979.
- [132] A. Marie, et al., Silica based ionogels: interface effects with aprotic and protic ionic liquids with lithium, *PCCP* 22 (41) (2020) 24051–24058.
- [133] T. Ioannis, D. Tarvydas, N. Lebedeva, Li-ion Batteries for Mobility and Stationary Storage Applications, Publications Office of the European Union: Brussels, Belgium, 2018.
- [134] A. Ponrouch, M. Palacin, On the road toward calcium-based batteries, *Curr. Opin. Electrochem.* 9 (2018) 1–7.
- [135] C. Delmas, Sodium and sodium-ion batteries: 50 years of research, *Adv. Energy Mater.* 8 (17) (2018) 1703137.
- [136] R. Rajagopalan, et al., Advancements and challenges in potassium ion batteries: a comprehensive review, *Adv. Funct. Mater.* 30 (12) (2020) 1909486.
- [137] H. Sun, et al., A safe and non-flammable sodium metal battery based on an ionic liquid electrolyte, *Nat. Commun.* 10 (1) (2019) 1–11.
- [138] T. Shiga, et al., Insertion of calcium ion into prussian blue analogue in nonaqueous solutions and its application to a rechargeable battery with dual carriers, *J. Phys. Chem. C* 119 (50) (2015) 27946–27953.
- [139] T. Vogl, et al., The use of protic ionic liquids with cathodes for sodium ion batteries, *J. Mater. Chem. A* 4 (27) (2016) 10472–10478.
- [140] P. Jankowski, et al., Anion amphiprotic ionic liquids as protic electrolyte matrices allowing sodium metal plating, *Chem. Commun.* 55 (83) (2019) 12523–12526.
- [141] M. Arnaiz, et al., Aprotic and protic ionic liquids combined with olive pits derived hard carbon for potassium-ion batteries, *J. Electrochem. Soc.* 166 (14) (2019) A3504–A3510.
- [142] T. Stettner, et al., Ionic liquid-based electrolytes for calcium-based energy storage systems, *J. Electrochem. Soc.* (2020).
- [143] G. Girishkumar, et al., Lithium-air battery: promise and challenges, *J. Phys. Chem. Lett.* 1 (14) (2010) 2193–2203.
- [144] M.-K. Song, Y. Zhang, E.J. Cairns, A long-life, high-rate lithium/sulfur cell: a multifaceted approach to enhancing cell performance, *Nano Lett.* 13 (12) (2013) 5891–5899.

2. Results and Discussion

In this chapter, the work accomplished during the authors PhD, which resulted in eight different publications, will be presented in short summaries. They deal with the application of PILs in different areas of electrochemical energy storage topics and will be divided in three different parts.

The first and the second parts are about the implementation in EDLC as well as battery systems, respectively. Different approaches are used including synthesis, mixtures with different solvents and the employment of additives.

The third part covers work about the confinement of PILs in polymers, yielding solid electrolytes, and the differences associated by this change of environment compared to neat PILs.

2.1. PILs in EDLC systems

2.1.1. Publikation 2/Publikation 3: Water in Protic Ionic Liquids: Properties and Use of a New Class of Electrolytes for Energy-Storage Devices / Water in Protic Ionic Liquid Electrolytes: From Solvent Separated Ion Pairs to Water Clusters

As already explained, the implementation of PILs into EDLC systems is difficult due to slow ion transport properties of these electrolytes, mainly derived by high viscosities. This is drastically limiting the power capability of such devices; thus, adaptations of the electrolyte are necessary. Typically, this is done via mixtures with low viscous solvents typically of organic nature with broad ESWs (e.g., PC). Water is usually not considered as solvent due to its narrow ESW, in fact the electrolyte is carefully dried to ensure no residual water. In case of PILs, however, the ESW is limited anyway by the protic ions, which are prone to reduction.

In the past, it has already been shown that mixing PILs with water can drastically improve the transport properties of these compounds. Already few hundreds ppm of water have an impact on the chemical-physical properties of a PIL. This includes the ESW, and even though the impact on PILs is less drastic compared to other non-aqueous electrolytes, a broad ESW is still preferred to yield high specific energies. Thus, in this work mixtures only with 0.1, 1, 2 and

3.8 weight percent (wt%) water have been chosen. Higher amounts would limit the ESW, thus specific energy of an EDLC too much. On the other hand, these small amounts are enough to enhance the power potential considerably compared to an EDLC employing a neat PIL-based electrolyte.

The practical investigations focusing on the implementation of the electrolytes into AC-based EDLCs are complemented with molecular dynamic simulations, giving insight into the specific interactions on a molecular level. This is of particular interest, due to the special hydrogen-bond interactions present in a PIL, which can be even more pronounced in an aqueous environment.

[Pyr_{H4}][TFSI], an already established PIL, has been chosen as basis for the electrolyte, owing to its relatively good transport properties as well as ESW. While it is a hydrophobic IL, sufficient amounts of water can be solved to end up with an almost equimolar of H₂O : PIL ratio at 3.8 wt% of H₂O.

In Publication 2 and Publication 3 it could be shown that the chemical-physical properties of [Pyr_{H4}][TFSI] can be significantly influenced by the addition of H₂O. Viscosity and density are decreasing, while the conductivity is increasing with higher amounts of water. Additionally, the m.p. could be lowered even below RT, what is highly important for practical applications. In all mixtures the temperature dependence stays non-Arrhenius-like, a typical behavior of ILs.

While molecular dynamic simulations were carried out in both publications, giving insight about the molecules' coordination and alignment, Publication 3 focused much more on the interactions between ions and their mobilities. It was stated that, depending on the water content, water molecules are either isolated between ions or forming solvent shells of single ions composed of several water molecules or even larger clusters in the state of quasi-bulk water. In each state, the water is expected to show different physical properties, which have been further clarified: Firstly, the hydrogen bond decay rate becomes faster with higher amounts of water, correlating with higher conductivities of the electrolytes. Moreover, the hydrogen-bond-lifetime for H₂O-cation pairs is much higher compared to H₂O-anion pairs, due to the hydrophobic character of the latter. Interestingly, the highest hydrogen-bond-lifetime was found for H₂O-H₂O pairs in the 0.1 wt% electrolyte, simply because of the lower chance to form a new bond, since the water molecules are basically isolated from each other. The

alternatives are the energetically unfavorable free form or a bond with anions/cations of the IL.

It was also discovered that the dipole reorientation shows a similar trend compared to the hydrogen-bond-lifetime. The higher the water content, the faster the reorientation since the hydrogen bond-decay times becomes faster and more options for binding partners are available. An exception is the 0.1 wt% mixture, showing faster reorientation compared to the 1.0 wt% mixture, due to very few H₂O-H₂O bonds and otherwise weak H₂O-anion/cation bonds.

Lastly, the cation diffusion is faster than that of the anion, which is the same case in other PIL-water systems. Contrary to these systems, however, the cation mobility is stronger enhanced by increasing amounts of water than the anion mobility. On the other hand, the H₂O diffusion becomes lower at higher water contents since it behaves more and more like bulk water.

The implementation of the investigated mixtures into an AC-based EDLC was carried out in Publication 2. It was found that the ESW of the mixtures decreases with increasing water content. While the cathodic stability stays constant for all mixtures, due to the limitation of the available proton in the pyrrolidinium cation, the anodic stability is decreasing with increasing water content, related to the oxidation of H₂O. The lower ESW results in lower OPVs of AC-based electrodes when cycled in the mixtures. While the OPV of an EDLC employing neat [Pyr_{H4}][TFSI] reaches 2.2 V, it is reduced to 2.0, 1.9 or 1.8 V with 1, 2 or 3.8 wt% H₂O, respectively.

It was shown that the cycling of electrodes coated onto aluminum in the PIL-water electrolytes leads to anodic dissolution, even at the lowest water content. Additionally, it was assumed that the water-soluble binder carboxymethyl cellulose is not able to uphold complete mechanical functionality of the electrode. Thus, stainless steel current collectors as well as polyvinylidene fluoride binder were employed, resulting in a much higher stability of the systems, even when holding the maximal potential over several hundreds of hours.

Overall, the performance of AC-based EDLCs employing the water in PIL electrolyte could be increased most efficiently utilizing the PIL containing 2 wt% of H₂O, especially regarding the power capability. While the pure PIL [Pyr_{H4}][TFSI] is not able to operate at current densities higher than 2 to 5 A g⁻¹, the 2 wt% mixture is still delivering capacitances at 10 A g⁻¹. At 1 wt%, the improvement of transport properties is not significant enough to increase the power

capability, while at 3.8 wt% H₂O large faradic contributions at lower scan rates will lead to stronger capacitance fading.

Overall, it could be shown that the mixture of a PIL with water is a promising strategy to improve the power performance of a PIL-based EDLC. Nevertheless, the presence of water makes it necessary to change the design of the EDLC more to a water-based system. Furthermore, the properties of water molecules inside a hydrophobic PIL are drastically changing depending on the water content. Further investigations should explore the mixtures of a hydrophilic PIL with water, since stronger bonds between PIL and water molecules could lower the impact on the ESW, as in the case of water-in-salt electrolytes. Additionally, transport mechanisms related to proton-bonds (e.g., proton-hopping) should be more uniformly distributed within the electrolyte, since no water clusters should form.

Water in Protic Ionic Liquids: Properties and Use of a New Class of Electrolytes for Energy-Storage Devices

Timo Stettner,^[a, b] Sascha Gehrke,^[c] Promit Ray,^[c] Barbara Kirchner,^[c] and Andrea Balducci*^[a, b]

In this work, the properties of “water-in-PIL” (PIL = protic ionic liquid) electrolytes are reported based on 1-butylpyrrolidinium bis(trifluoromethanesulfonyl)imide (Pyr₄TFSI). Taking advantage of experimental and theoretical investigations, it is shown that the amount of water inside the electrolyte has a dramatic effect on the viscosity, conductivity, density, cation–anion interplay, and electrochemical stability of Pyr₄TFSI. The impact of water on the properties of this ionic liquid also affects its use as an electrolyte for electrochemical double-layer capacitors (EDLCs). It is shown that the presence of water improves the

transport properties of Pyr₄TFSI, with a beneficial effect on the capacitance retention of the devices in which these electrolytes are used. However, at the same time, water reduces the operative voltage of EDLCs containing this PIL as the electrolyte and, furthermore, it has a strong impact on the inactive components of these systems. To suppress this latter problem, and to realize EDLCs with high stability, the use of inactive components stable in aqueous environment appears necessary.

Introduction

In the last 15 years, ionic liquids (ILs) have been largely investigated as electrolytes for electrochemical energy-storage systems, such as batteries and supercapacitors.^[1] The interest in this application is related to the fact that ILs might display a set of properties (e.g., good transport properties, high thermal stability, low flammability, low vapor pressure, and high electrochemical stability) that match the properties required for the electrolyte of these systems very well.^[2]

Among the various subclasses of ILs, aprotic ionic liquids (AILs) have been certainly the most investigated.^[3] In the last few years, however, the interest in protic ionic liquids (PILs) has increased considerably.^[4] PILs display all the typical properties of ILs but hold one or more “free” protons in their structure. The presence of proton(s) makes the behavior of PILs markedly different to that of AILs, with important consequences for their use in energy-storage devices. It has been shown by our group that proton(s) might positively influence the lithi-

um environment, making PILs attractive for application in lithium-ion batteries (LIBs).^[5] However, because protons are easily reducible, their presence strongly limits the electrochemical stability of PILs. Consequently, the use of PILs in electrochemical double-layer capacitors (EDLCs), which is the most widespread class of supercapacitors, is not particularly appealing because it does not allow the realization of high-voltage devices.^[6]


Recently, solvent-in-salt electrolytes, electrolytic solutions in which the salt outnumbers the solvent in terms of volume and weight, have become extremely popular, and several works showed that these electrolytes display very interesting properties such as large electrochemical stabilities or an increased cycling stability.^[7] The realization of this kind of electrolyte is dependent on the solubility of a certain salt in a solvent, which can be either an organic solvent or water. In this latter case, “water-in-salt” is the term used to indicate these electrolytes.

Because ILs are salts, it is also possible to consider “solvent-in-ILs” electrolytes. The use of mixtures of IL and organic solvent has been widely investigated in the past, and among the various mixtures that have been considered, very highly concentrated electrolytes have also been used. It has been shown that these solvent-in-ILs electrolytes might display favorable features such as the ability to suppress anodic dissolution of Al current collectors.^[8] The use of water-in-ILs has been less investigated.^[9] Most likely, this is owing to the fact that one of the prerequisites for the use of ILs in energy-storage devices is, as for any type of non-aqueous electrolytic solutions, a very low water content. As a matter of fact, large amounts of water might have dramatic effects on the stability and cycle life of electrochemical devices.^[10] For this reason, the ILs used in LIBs and EDLCs typically contain less than 50–100 ppm of water.^[11]

[a] T. Stettner, Prof. Dr. A. Balducci
Institute for Technical Chemistry and Environmental Chemistry
Friedrich Schiller University
Philosophenweg 7a, 07743 Jena (Germany)
E-mail: andrea.balducci@uni-jena.de

[b] T. Stettner, Prof. Dr. A. Balducci
Center for Energy and Environmental Chemistry Jena (CEEC Jena)
Friedrich Schiller University
Philosophenweg 7a, 07743 Jena (Germany)

[c] S. Gehrke, P. Ray, Prof. Dr. B. Kirchner
Mulliken Center for Theoretical Chemistry
Rheinische Friedrich-Wilhelms-Universität
Berlingstr. 4 + 6, 53115 Bonn (Germany)

 Supporting Information and the ORCID identification number(s) for the author(s) of this article can be found under:
<https://doi.org/10.1002/cssc.201901283>.

In this sense, they can be considered as “dry” electrolytes. However, because in water-in-salt electrolytes the amount of water is extremely low, the realization of water-in-IL electrolytes could be an interesting approach to improve some properties of ILs (e.g., transport properties) without negative effects on the behavior of the electrochemical storage devices in which they are used as electrolytes.

Between AILs and PILs, this latter subgroup appears extremely appealing for the realization of highly concentrated water-based electrolytes, which could be classed as “water-in-PIL” electrolytes. The reasons are several. First of all, the mobility/reactivity of the proton(s) of the PIL could be tuned by the amount of water present in the electrolyte. This tunable proton mobility could be advantageous for the use of PILs in combination with materials suitable for energy storage, such as pseudocapacitive materials.^[12] Second, the use of highly concentrated electrolytes could have a favorable impact on the transport properties of PILs.^[13] Finally, the use of water-in-PIL electrolytes could also positively influence the operative temperature of PIL-based systems. As a matter of fact, several PILs proposed as electrolytes in energy-storage devices display melting points above 40 °C, making their use at room temperature quite challenging. It is well known that water can strongly affect the melting point of ILs, and the use of “water-in-PIL” could be helpful to increase the number of room-temperature applications of PIL-based devices.^[14] All these aspects could be advantageously utilized to permit a better use of this subclass of IL in energy-storage devices, including EDLCs.

In this manuscript, we investigate the influence of water content on the properties of PILs with the aim to verify the use of “water-in-PIL” electrolytes in EDLCs. In the first part of the work, the transport and electrochemical properties of the PIL 1-butylpyrrolidinium bis(trifluoromethanesulfonyl)imide (Pyr₁₄TFSI) containing different amounts of water are investigated in detail by utilizing several experimental techniques and classical molecular dynamics simulations. In the second part, the influence of these electrolytes on the operative voltage and stability of EDLCs based on activated carbon (AC) is reported. In the last part of the manuscript, the impact of the investigated electrolytes on the inactive components of EDLCs is considered.

Results and Discussion

Pyr₁₄TFSI is a hydrophobic PIL, not fully miscible with water, that has been investigated as an electrolyte for electrochemical energy-storage devices in several studies by our group.^[15] In large parts of these works, Pyr₁₄TFSI has been utilized dry, with a water content lower than 20 ppm. Subsequently, this dry PIL will be indicated as Pyr₁₄TFSI. The highest amount of water soluble in this PIL has been found to be equal to 38000 ppm, or 3.8 wt%. In the following, this solution will be indicated as 3.8% H₂O. To investigate the influence of water on the properties of Pyr₁₄TFSI, Pyr₁₄TFSI with 1 and 2 wt% water have also been considered. These latter solutions will be indicated as 1% H₂O and 2% H₂O. Knowing the density of the electrolyte at 30 °C (3.24 molL⁻¹ for Pyr₁₄TFSI, see Figure 2), it is possible to

calculate the molarity of Pyr₁₄TFSI in the investigated electrolytes at this temperature. As shown in Table 1, the consequence of an increased water content is a reduction of the Pyr₁₄TFSI molarity within the electrolyte, which decreases from

Water content [wt %]	Molarity (Pyr ₁₄ TFSI) [molL ⁻¹]	Molar fraction (H ₂ O) [mol %]
0	3.43	0
1	3.38	18.58
2	3.32	31.66
3	3.24	47.22

3.43 molL⁻¹ (Pyr₁₄TFSI) to 3.24 molL⁻¹ (3.8% H₂O). Another interesting parameter to be considered is the molar fraction of water within the investigated electrolytic solutions. In the dry Pyr₁₄TFSI, the molar fraction of water molecules is clearly 0 mol%. In 1% H₂O, the molar fraction of the water molecules is 18.58 mol%, and in the 3.8% H₂O this value increases to 47.22 mol%. These values give a clear indication about the considerable influence of a few percent of water on the ratio water/Pyr₁₄TFSI within the investigated electrolytes. The ratios of water/salt of these electrolytes are comparable with those of other water-in-salt systems published in the literature.^[7d] Thus, it appears reasonable to indicate the investigated electrolytic solutions as water-in-PIL.

Figure 1a shows the viscosity of the investigated electrolytes. At 30 °C, Pyr₁₄TFSI displays the highest viscosity with 43 MPas. This relatively high value is caused by the high inter-ionic bonding strength between the anions and cations, which limits their mobility.^[16] The addition of 1 wt% water decreases the viscosity to 37 MPas. This value drops to 31 MPas in the electrolyte 2% H₂O, and to 22 MPas in the electrolyte 3.8% H₂O. Compared with pure water, which at 30 °C displays a viscosity of approximately 8 MPas, these values are still rather high.^[17] However, it is important to remark that the presence of only 3.8 wt% of water is able to halve the viscosity of Pyr₁₄TFSI at 30 °C. This might have a significant impact on the performance of devices utilizing PIL-based electrolytes. A possible reason for this decrease in viscosity could be a worse coordination of Pyr₁₄⁺ cations and TFSI⁻ anions, and thus lower coulombic forces, owing to coordination with water molecules instead. Additionally, because water has a rather low viscosity compared with pure Pyr₁₄TFSI, it is clear that the overall viscosity shrinks with the addition of water, given that a large portion of the molecules in the mixture are water molecules. At higher temperatures, the viscosity of all investigated electrolytic solutions declines to approximately 10 MPas, and the differences between the various mixtures become less pronounced.

Figure 1b shows the influence of the temperature on the conductivity of the investigated electrolytes. At 30 °C, Pyr₁₄TFSI displays a conductivity of 3.6 mS cm⁻¹. With increasing water content, the conductivity rises from 4.3 to 5.1 and 5.6 mS cm⁻¹ for 1% H₂O, 2% H₂O, and 3.8% H₂O, respectively. In contrast to

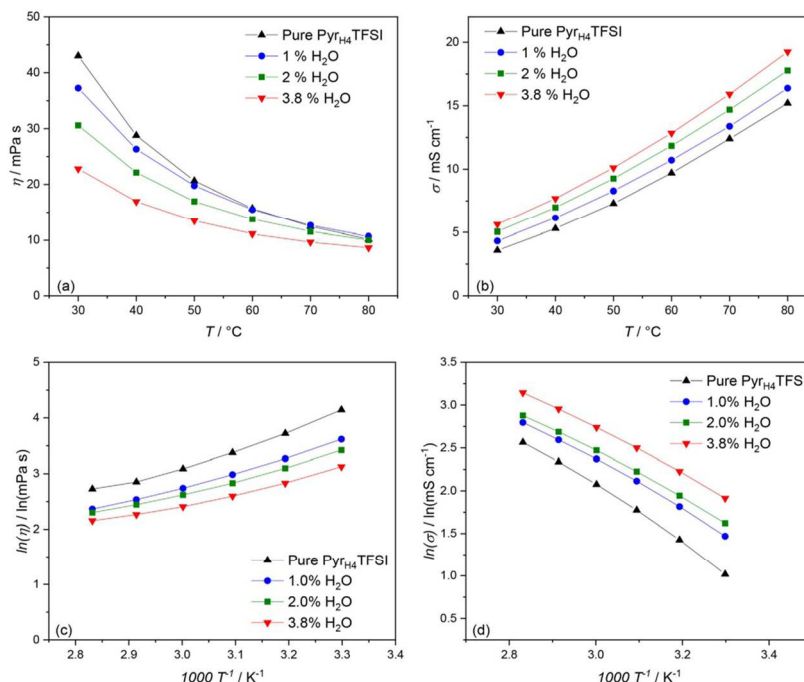


Figure 1. Influence of the temperature on the (a) viscosity and (b) conductivity of the investigated systems and corresponding Arrhenius plots for the (c) viscosity and (d) conductivity.

the viscosity, there is no convergence of the conductivity values at elevated temperatures. Instead, the differences between the mixtures even increase slightly. One reason for the higher conductivity of the mixtures with increased water content is of course the lower viscosity of these mixtures, and thus a higher ion mobility. Another important point to take into account is the fact that the conductivity is only limited by the ion mobility, which increases with temperature as long as the boiling point is reached. Another reason could be the assembly of water clusters, maybe even including Pyr_{14}^+ cations, with their protic nature, enhancing the overall conductivity, as seen in other protic ILs mixed with water.^[18]

Several studies reported that ILs, both AIL and PIL, do not follow the Arrhenius behavior of liquids.^[19] With the aim to verify if the presence of water changes this behavior, we considered the Arrhenius plot for conductivity as well as viscosity of the investigated electrolytic solutions. As shown in Figure 1 c, d, none of the electrolytes follows an Arrhenius behavior, indicating that the considered amount of water does not affect this typical behavior of ILs.

The influence of water on the density of the investigated electrolytic solutions is depicted in Figure 2. As shown, at 30 °C the highest density is measured for $\text{Pyr}_{14}\text{TFSI}$ (1.4 g cm^{-3}). The addition of water lowers the density to 1.392, 1.386, and 1.376 g cm^{-3} for 1% H_2O , 2% H_2O , and 3.8% H_2O , respectively.

It is interesting to notice that whereas the density of the $\text{Pyr}_{14}\text{TFSI}$ decreases linearly with increasing temperature, the electrolytes containing water display a drop of density after 60 °C, which could be related to the proximity to the boiling point of the water. As shown, the higher the water content, the greater the drop. As a consequence, at 80 °C $\text{Pyr}_{14}\text{TFSI}$ and 3.8% H_2O display a rather different density (almost 10%).

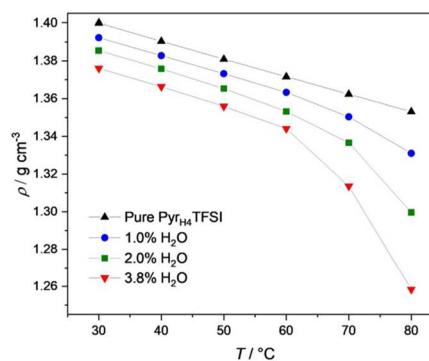


Figure 2. Influence of the temperature on the density of the investigated electrolytes.

Thermogravimetric analysis has shown that the behavior of the mixtures, up to the decomposition of $\text{Pyr}_{14}\text{TFSI}$, differs only slightly (Figure S1 in the Supporting Information). Although at 100 °C the evaporation of water can be observed (Figure S2 in the Supporting Information), not all water is removed from the mixtures, suggesting a strong interaction of water with the PIL.

To gain further insight into the properties of the investigated mixtures, we present results from the domain analysis performed by using classical molecular dynamics simulations at 30 °C. For the definition of the considered domains, the system was divided into polar, nonpolar, fluororous, and aqueous components; the water molecules constituted the aqueous phase whereas the terminal CF_3 groups of the anion constituted the fluororous phase. The terminal propyl fragment of the butyl chain of the cation was considered the nonpolar phase whereas the rest of the cation and the anion was considered as the polar phase. Table 2 shows the various domains and their re-

System	Polar	Nonpolar	Fluororous	Aqueous
$\text{Pyr}_{14}\text{TFSI}$	1.0, 500	36.70, 13.62	7.49, 66.76	–
1% H_2O	1.0, 407	33.65, 12.10	6.89, 59.07	30.82, 3.02
2% H_2O	1.0, 560	50.80, 11.02	9.28, 60.34	83.92, 3.05
3.8% H_2O	1.0, 560	55.52, 10.08	11.18, 50.09	33.11, 15.46

[a] Performed at 30 °C with the terminal CF_3 groups of the anion defined as the “fluororous” phase, the propyl fragment of the cation as the “nonpolar” phase, the water molecules as the “aqueous” phase, and the rest as the “polar” phase. The two comma-separated numbers represent the number of domains and the average size of the domains.

spective sizes formed in these liquids. Because the compositions of the various systems (ion pairs, water molecules) are different, the size of the domains is a more important consideration than the number of domains formed in the system. The polar domains form a single unit in all investigated systems. As far as the clustering of side chains is concerned, addition of water seems to favor the separation of domains in that the nonpolar domains become slightly smaller in size with increasing water concentration. The observation remains the same with the fluororous domains although the difference between the 1 and 2% water solutions are not pronounced. A decrease is, however, observed in the size of the fluororous domains in moving from the 2 to the 3.8% water solution. Concerning the size of the aqueous domains, approximately three water molecules are seen to aggregate on average in the 1 and 2% water solutions. The size of the aqueous domains, however, exhibits a drastic increase on increasing the water concentration beyond 2%. Approximately 15–16 water molecules are seen to cluster and form isolated units within the system. Figure 3 shows snapshots obtained from the simulations in which the enhanced clustering of water, at high water concentrations, can clearly be observed.

The combined distribution functions (CDFs) in Figure 4 illustrate the influence of the added water on the cation–anion interplay on a molecular level. We show here three-body CDFs

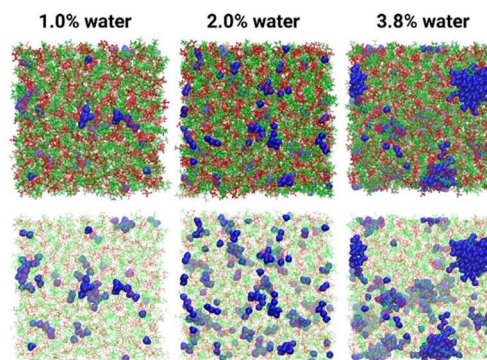


Figure 3. Snapshots from the classical molecular dynamics simulations at 30 °C. Left: 1% water, middle: 2% water, and right: 3.8% water. Enhanced clustering of water molecules upon increasing the concentration can be clearly observed. Water molecules are shown in blue whereas the ions of the liquid are shown with red and yellow lines. The top and bottom panels show opaque and translucent representations of the same snapshot.

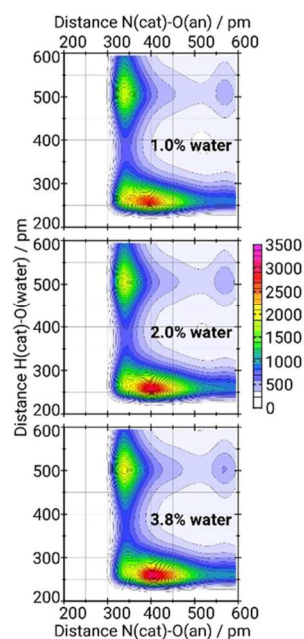


Figure 4. Combined distribution functions illustrating the interaction of water and ions. The x-axis represents the distance between the nitrogen atom of a certain cation and the oxygen atom of the nearest anion, whereas the y-axis represents the distance between the acidic hydrogen atom of the same cation to the nearest oxygen atom of a water molecule. The occurrence of the particular combinations is visualized by the color of the heat plot according to the scale shown on the right side.

that depict the cation–water distance on the *y*-axis versus the cation–anion distance on the *x*-axis each for the nearest neighbors. Thereby, the interaction between cation and anion is represented by the distance between the nitrogen atom of the cation and an oxygen atom of the anion. The hydrogen bond between the same cation's most acidic hydrogen and a water's oxygen atom displays the interaction with a water molecule. The most frequently appearing assembly is assigned by the red colored contour. The visible drift or broadening (≈ 20 pm) of this contour with increasing water content towards higher distances between the nitrogen and the oxygen indicates a weakening of the ionic network by the water.

Figure 5 compares the overall electrochemical stability windows (ESW) of the investigated electrolytes at 40 °C. Owing to the presence of a proton on the $\text{Pyr}_{\text{H}_4}^+$ cation, the cathodic limit of all electrolytes is comparable, and all mixtures are

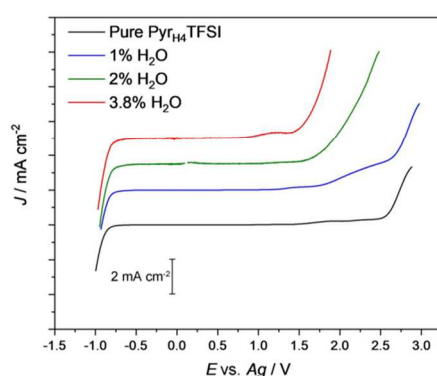


Figure 5. ESW of the investigated electrolytes measured at 40 °C (scan rate: 5 mV s^{-1}).

stable up to -0.8 V (vs. Ag) no matter what the water content is. However, the anodic limit is strongly affected by the water content. The electrolyte 3.8% H_2O is only stable up to approximately 1.5 V (vs. Ag), with minor currents already starting at 0.75 V (vs. Ag). In the electrolyte 2.0% H_2O , the stability increases to 1.75 V (vs. Ag), whereas the electrolyte 1.0% H_2O is stable up to 2 V (vs. Ag). $\text{Pyr}_{\text{H}_4}\text{TFSI}$ shows the highest anodic stability, and it is stable up to 2.6 V (vs. Ag). As a consequence of these differences, the overall ESW of the investigated electrolytes is very different and ranges between 3.4 ($\text{Pyr}_{\text{H}_4}\text{TFSI}$) and 2.3 V (3.8% H_2O). These results clearly show that the presence of water has a dramatic effect on the electrochemical stability of PILs and that small amounts of water drastically reduce the ESW of these ILs, owing to the reduction of the oxygen in the water molecule. However, it is interesting to note that these results could be also seen from a different perspective: that of the water-in-salt electrolytes. As mentioned above, the electrolyte 3.8% H_2O displays a ratio between water and PIL comparable to that of other water-in salts proposed in the literature.^[7d] Therefore, these results could be also

seen as an indication that hydrophobic PILs are suitable for the realization of water-based electrolytes with an overall ESW significantly higher than that of conventional aqueous electrolytes.

To understand the impact of the investigated electrolytes on the electrochemical behavior of energy-storage devices, we used them as model electrolytes for EDLCs. First, we evaluate the maximum operating voltage achievable with these electrolytic solutions. We observed that upon utilizing $\text{Pyr}_{\text{H}_4}\text{TFSI}$ it is possible to realize EDLCs with an operating voltage of 2.2 V. This value was the highest among the investigated systems. As a matter of fact, the operating voltages of EDLCs containing the electrolytes 1% H_2O , 2% H_2O , and 3.8% H_2O were equal to 2, 1.9, and 1.8 V, respectively (detailed information about the determination of the operating voltage and the mass balancing utilized for the EDLCs assembly is available in Figure S3 and Table S1 in the Supporting Information). These results, which are perfectly in line with the trend observed for the overall ESW, confirm that PILs are not especially suited for use as electrolytes in EDLCs. However, taking the previous considerations about water-in-salt electrolytes into account, these results also indicate that water-in-PIL electrolytes can be successfully utilized for the realization of EDLCs with higher operating voltage compared with conventional aqueous electrolytes.

Figure 6a compares the voltammetric profiles of the investigated EDLCs at 5 mV s^{-1} . As shown, the capacitance of the devices slightly increases in the electrolytes containing water.

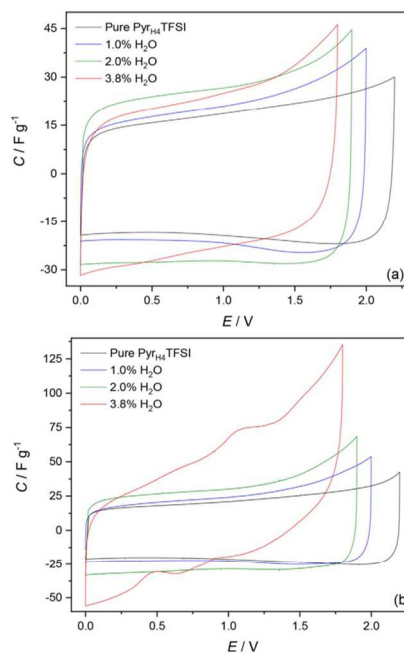


Figure 6. CV profiles of EDLCs containing the investigated electrolytes at 40 °C and (a) 5 mV s^{-1} and (b) 0.5 mV s^{-1} .

This increase is most likely owing to the better transport properties of the electrolytes compared with the neat PIL. At this scan rate, all devices display the typical rectangular shape of EDLCs. However, it is evident that the amount of water has an influence on the shape of the cyclic voltammograms, and that in the device containing the electrolyte 3.8% H₂O the occurrence of faradaic reactions at potentials higher than 1.5 V cannot be excluded. These reactions become evident if the scan rate of the cyclic voltammetry (CV) is reduced to 0.5 mV s⁻¹, as shown in Figure 6b. As can be seen, at this scan rate the CV of the EDLC containing 3.8% H₂O is completely distorted, and the occurrence of reversible redox reaction is clear. Under the same conditions, the EDLCs containing the other electrolytes do not show such a dramatic change, indicating that the amount of water they contain is not high enough to significantly alter the capacitive behavior of the EDLCs.

Figure 7 compares the capacitance retention of the investigated EDLCs with increasing current densities. As is shown, the amount of water within the electrolyte considerably affects the capacitance retention. The EDLC containing the electrolyte Pyr₁₄TFSI, which is the one displaying the lowest conductivity

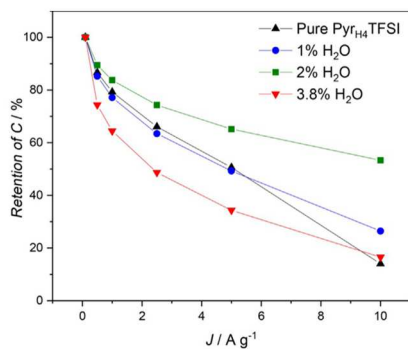


Figure 7. Capacitance retentions of EDLCs containing the investigated electrolytes at 40 °C.

and highest viscosity, retains the lowest charge at higher current densities. The addition of water to the electrolyte improved the capacitance retention at high current densities, for example, at 10 A g⁻¹. The EDLCs containing 2.0% H₂O retain 40% more charge than the device containing the dry PIL. However, a too-high water content appears detrimental, especially during tests at low current densities, as shown by the behavior of the EDLCs containing 3.8% H₂O.

It is worth noting that the presence of water also has a strong impact on the energy, power, and temperature behavior (in term of capacitance) of the investigated EDLCs. Details about these latter aspects are available in Figures S2 and S3 in the Supporting Information.

Taking these results into account, it appears that the water within the electrolyte affects the behavior of the EDLCs in several ways. On the one hand, it reduces the EDLCs' operating

voltage. On the other hand, it improves the transport properties of the PIL, with a beneficial effect on the capacitance retention of the devices containing these electrolytes. Nevertheless, when the water content becomes (too) high, as in the case of the electrolyte 3.8% H₂O, the use of these electrolytic solutions leads to the occurrence of faradaic reactions, which alter and reduce the stability of the devices.

To further investigate this latter point, we monitored the stability of the examined EDLCs over prolonged charge/discharge (CC) cycles as well as during float tests. Each device has been tested to its maximum operating voltage. The results of these tests are reported in Figure 8. As shown Figure 8a, after

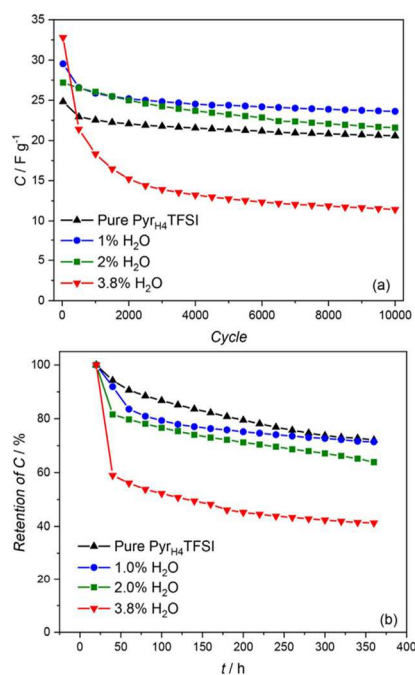


Figure 8. Variation of specific capacitance of EDLCs containing the investigated electrolytes during (a) galvanostatic CC performed at 0.5 A g⁻¹ and (b) float tests performed at the maximum operating voltage defined for each device. Both tests performed at 40 °C.

10000 cycles the EDLC containing the electrolyte 3.8% H₂O is the least stable, and the systems loses almost 50% of its initial capacitance during the first 1000 cycles. Although after this decay the capacitance stabilizes, at the end of the cycling the EDLC was able to retain only 35% of its initial capacitance. The stability of the EDLCs containing the electrolyte 2.0% H₂O was significantly higher, and after 10000 cycles this device was able to retain 80% of its initial capacitance. The capacitance retentions of the EDLCs containing the electrolytes 1.0% H₂O and Pyr₁₄TFSI were comparable, and at the end of the cycling both

devices retained approximately 85% of their initial capacitance. The differences observed during the galvanostatic cycling become more pronounced during the float tests. As shown in Figure 8b, after 350 h of float test, the EDLCs containing the electrolytes 1.0% H₂O and Pyr₁₄TFSI were able to retain approximately 70% of their initial capacitance. After the same amount of time, the EDLC containing 2.0% H₂O lost approximately 35% whereas the one containing 3.8% H₂O lost almost 60% of its initial capacitance.

The results of these tests clearly indicate that the amount of water present on the investigated electrolytes has a strong impact on the stability of the EDLCs in which they are used. The causes of this behavior could be several, for example, formation of gases (H₂ or O₂) and/or dissolution of electrode components such as current collectors and binder. To investigate this latter aspect, we took ex situ SEM images of the electrodes (positive and negative) of the EDLCs utilized for the float test reported above [energy-dispersive X-ray spectroscopy (EDX) measurements of the same electrodes are available in Figure S5 in the Supporting Information]. As shown in Figure 9a,b, the electrodes cycled in Pyr₁₄TFSI did not show significant signs of degradation, indicating that in this electrolyte the integrity of the electrodes was not altered by the float test. From the SEM images it is evident that the addition of water, to the contrary, strongly affected and reduced the electrode stability. Among the electrodes, the positive side appears as the most damaged one during the tests (Figure 9d,f, and h). The aluminium current collectors utilized for the preparation of the composite electrode used in the EDLCs show large holes, which likely originated from the anodic dissolution of this metal involving the complex Al(TFSI)₃ and/or the development of hydrofluoric acid from the TFSI⁻ anion.^[8] Furthermore, the active material seems to be removed either by the development of gases spalling it, or through the solvation of binder material. The electrodes utilized on the negative side (Figure 9c,e, and g), however, show changes of the surface resulting in “white” spots containing high amounts of oxygen (as determined by EDX measurements, see Figure S5 in the Supporting Information). It is important to note that the current collectors (Al) and the binder (sodium carboxymethyl cellulose) utilized in the investigated EDLCs are not stable in aqueous electrolytes. The use of the investigated electrolytes, which contain very low amounts of water, seems to reduce the stability of these inactive components and consequently that of the EDLCs.

Taking these points into account, for the optimization of water-in-PIL electrolytes the use of inactive components stable in water appears of importance. With the aim to investigate this aspect, AC-based electrodes containing stainless-steel (SS) current collectors and polyvinylidene fluoride (PVDF) as binder were prepared. These electrodes were utilized for the realization of EDLCs containing the investigated electrolytes. The stability of these devices was investigated through float tests, which were performed under identical conditions as those reported in Figure 8b. As shown in Figure 10, the use of inactive components stable in aqueous environments significantly increases the stability of EDLCs containing the investigated

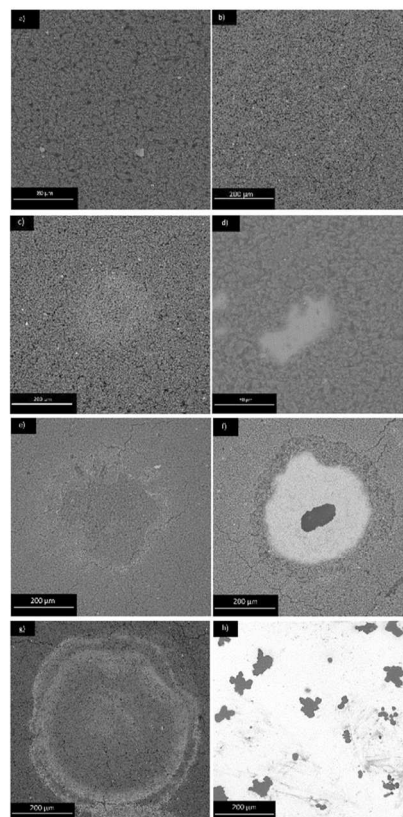


Figure 9. Ex situ SEM pictures of the electrodes of the EDLCs used for float testing. The sizes of the scale bars are 80 μm for a) and 200 μm for b)–h).

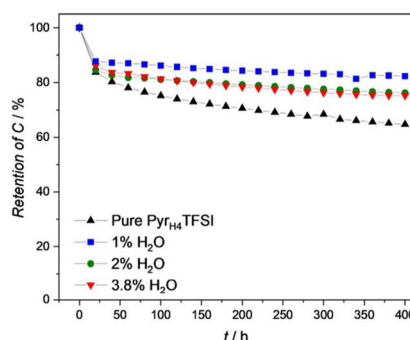


Figure 10. Capacitance retentions of EDLCs containing the investigated electrolytes at 40 °C during float tests at their maximum respective OPV. The inactive components of aluminum as the current collector and CMC as the binder have been exchanged with SS and PVDF, respectively.

water-in-PIL electrolytes. After 400 h, the EDLCs containing these electrolytes display a capacitance retention of approximately 80%, which is slightly higher than that displayed by the systems containing the pure PIL. These results clearly indicate the importance of the correct selection of cell components for an effective use of water-in-PIL electrolytes.

Conclusions

In this work, we investigated the impact of water on the chemical and physical properties of 1-butylpyrrolidinium bis(trifluoromethanesulfonyl)imide (Pyr_{H4}TFSI) and on its use as an electrolyte for electrochemical double-layer capacitors (EDLCs). We showed that the addition of a few wt% of water is enough to realize electrolytes with a water/protic ionic liquid (PIL) ratio comparable to that of water-in-salt electrolytes reported in the literature. Thus, these electrolytes can be classed as a “water-in-PIL” electrolyte.

The results of this study clearly indicate that the amount of water inside the electrolyte has a dramatic effect on the viscosity, conductivity, and density of this PIL; for example, the presence of 3.8 wt% water is able to halve the viscosity of Pyr_{H4}TFSI at 30 °C. The presence of water also strongly modifies the electrochemical stability window (ESW) of Pyr_{H4}TFSI, and the higher the amount of water, the lower is the ESW. Furthermore, the addition of water also impacts the state of aggregation of Pyr_{H4}TFSI at room temperature, making the use of EDLCs based on Pyr_{H4}TFSI possible at room temperature.

The impact of water on the properties of Pyr_{H4}TFSI also affects the use of this PIL as an electrolyte for EDLCs. We showed that the presence of a few wt% of water might reduce the operating voltage of Pyr_{H4}TFSI-based EDLCs by 400 mV. At the same time, however, the presence of water improves the transport properties of Pyr_{H4}TFSI, with a beneficial effect on the capacitance retention of EDLCs. However, if the water content within the PIL becomes (too) high, as for the electrolyte 3.8% H₂O, the use of “water-in-PIL” electrolytes might limit the long-term stability of the system. To suppress this problem and to realize EDLCs with high stability, the use of inactive components stable in aqueous environments appears necessary.

Experimental Section

Preparation of water/IL mixtures

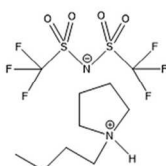


Figure 11. Structure of Pyr_{H4}TFSI.

To determine the maximum amount of water soluble in Pyr_{H4}TFSI (Figure 11), an excess amount of water was added to the dry Pyr_{H4}TFSI (H₂O < 10 ppm), thus forming two phases. After 24 h of stirring, the water phase was removed, and the amount of solvated water was determined by using a C20 Coulometric KF Titrator from Mettler Toledo. The other mixtures were prepared by adding a specific amount of water to Pyr_{H4}TFSI to gain a specific wt% (1 and 2) of water in

the resulting mixture, confirmed by Karl–Fischer titration. The obtained mixtures were stored in an MBraun LABmaster^{pro} ECO glovebox with < 1 ppm H₂O and < 1 ppm O₂ to ensure no further solvation of water in the mixtures. The evaporation of water was prevented by sealable bottles and using the prepared mixtures quickly after preparation.

Chemical and physical characterization

The conductivities of the electrolytes were measured by using a potentiostat ModuLabXM (Solartron analytical) in the temperature range 30–80 °C as described in [1d].

The viscosity of the electrolytes was determined by using a rheometer MCR 102 (Anton Paar) in the temperature range 30–80 °C as described in [1d].

The density of the electrolytes was determined in the temperature range 30–80 °C, by using a density meter DMA 4100M (Anton Paar).

Electrode preparation

AC-based electrodes were prepared following a procedure identical to that used by Krause et al.^[20] The dry composition of the electrodes was 90 wt% active material (AC, DLC Super, Norit), 5 wt% conducting agent (Super C65, Imerys), and 5 wt% binder (carboxymethyl cellulose, Dow). The mass loading of the electrodes was 2.6–3.5 mg cm⁻², and the electrode area was equal to 1.13 cm². The same procedure was also utilized for the realization of AC-based electrodes with identical characteristics but containing SS current collectors and PVDF binder.

As (oversized) counter electrodes, AC-based electrodes were used to determine the maximum operating voltage of the investigated EDLCs. The electrodes were prepared by following the procedure indicated in the literature.^[21] The electrode composition was 90 wt% AC (DLC Super, Norit), 5 wt% carbon black (Super C65, Imerys), and 5 wt% binder (polytetrafluoroethylene, Aldrich). The mass loading of these electrodes was approximately 40 mg cm⁻², and their area was 1.33 cm².

Electrochemical measurements

All electrochemical measurements were performed by using a three-electrode Swagelok cell setup. In every cell, Whatman glass microfiber filters (150 mm) were used as separators, drenched with 150 μL electrolyte. The cell assembly was done under argon atmosphere in an MBraun LABmaster^{pro} ECO glovebox with < 1 ppm H₂O and < 1 ppm O₂. All tests were performed at 40 °C to ensure that all electrolytes were liquid when employed in the cells.

The ESW of the electrolytes was measured by using a platinum electrode as working electrode, an oversized carbon electrode as counter electrode, and a silver electrode as pseudoreference electrode. After a 12 h open-circuit voltage (OCV) measurement to reach equilibrium, the cells were swept from OCV towards either the positive or negative direction at 1 mV s⁻¹ until a potential of -6 V (vs. OCV) or 6 V (vs. OCV) was reached, respectively.

For the determination of the operative voltage (OPV) of AC-based electrodes in the investigated electrolyte, an AC-based working electrode, an oversized carbon electrode as counter electrode, and a silver electrode as pseudoreference electrode were used. The operating voltage was determined by the method described in the literature.^[6]

The electrochemical behavior of the cells was investigated by using CVs performed at different scan rates (0.5, 1, 5, 2.5, 5, and 10 mVs^{-1}) and galvanostatic cycling experiments performed at different current densities (0.1, 0.5, 1, 2.5, 5, and 10 Ag^{-1}).

The stability tests were also performed by CC measurements with a scan rate of 0.5 Ag^{-1} . First, 10 000 simple CC cycles were executed. For the float tests, only 50 cycles were measured but with a 20 h period of holding the cell at its designated OPV afterwards. This was repeated until a period of roughly 400 h at the maximum voltage was reached, calculating the capacitance after each 50th cycle of the CC step.

Scanning electron microscopy

The SEM pictures were taken by using a pro X from Phenom™.

Thermogravimetric analysis

The thermogravimetric analysis (TGA) was performed with a PerkinElmer STA 6000 by using nitrogen as a carrier gas with a total flow rate of 20 mL min^{-1} . For each measurement, approximately 10 mg of electrolyte was put in a platinum crucible. For the TGA measurements, the samples were heated to 500 °C with a gradient of 10 °C min^{-1} . For isothermal measurements, a gradient of 50 °C min^{-1} was used to reach 100 °C, which was held for 100 min.

Computational details

All classical molecular dynamics simulations were performed with systems consisting of 400–600 ion pairs of $[\text{Pyr}_{14}][\text{TFSI}]$ with an appropriate number of water molecules to result in 1, 2, and 3.8 wt% “water-in-IL” solutions: the system sizes were chosen to allow for a sufficient number of water molecules for statistically significant results. The simulations were performed with the LAMMPS program package^[22] with initial configurations generated by PACKMOL.^[23] The Padua–Lopes force field^[24] was used for the IL with the SPC/E water model^[25] for the water molecules. We scaled down charges (determined from a restrained electrostatic potential fit^[26]) in the gas phase) to an absolute value of 0.8. Simulations were performed in the canonical ensemble for all analyses presented herein and in the isobaric-isothermal ensemble for the comparison of densities (see Table 2). For more details on the simulation methodologies, the reader is referred to our earlier work^[27] as well as an upcoming work on IL–water simulations. All systems were preequilibrated for at least 2 ns. The production run consisted of 15 ns for the pure liquid and the 1% water solution, 5 ns for the 2% water solution, and 1.5 ns for the 3.8% water solution. The production runs analyzed herein were performed at 3°.

Analysis of trajectories was performed by using our in-house code TRAVIS,^[28] we discuss herein radial distribution functions (RDFs) and results from domain analysis performed by using a radical Voronoi tessellation.^[29] Concerning the compositions of the simulations, 500 ion pairs of the pure liquid were simulated whereas the 1% water solution was composed of 407 ion pairs along with 93 water molecules. The 2 and 3.8% water solutions consisted of 560 ion pairs of the liquid with 256 and 512 water molecules, respectively.

Acknowledgements

T.S. and A.B. wish to thank the Friedrich Schiller University Jena and the Deutsche Forschungsgemeinschaft (DFG) within the project “Protic ionic liquids as electrolytes for lithium-ion batteries”.

Conflict of interest

The authors declare no conflict of interest.

Keywords: electrolyte · molecular dynamics · protic ionic liquids · supercapacitors · water in salt

- [1] a) P. C. Howlett, D. R. MacFarlane, A. F. Hollenkamp, *Electrochem. Solid-State Lett.* **2004**, *7*, A97–A101; b) M. Galiński, A. Lewandowski, I. Stepieniak, *Electrochim. Acta* **2006**, *51*, 5567–5580; c) A. Guerfi, M. Dontigny, P. Charest, M. Petitclerc, M. Lagacé, A. Vihj, K. Zaghib, *J. Power Sources* **2010**, *195*, 845–852; d) R.-S. Kühnel, N. Böckenfeld, S. Passerini, M. Winter, A. Balducci, *Electrochim. Acta* **2011**, *56*, 4092–4099; e) M. Lazhari, M. Mastragostino, A. Pandolfo, V. Ruiz, F. Soavi, *J. Electrochem. Soc.* **2011**, *158*, A22–A25; f) K. Francis, C.-W. Liew, S. Ramesh, K. Ramesh, *Ionics* **2016**, *22*, 919–925; g) J. Chapman Varela, K. Sankar, A. Hino, X. Lin, W.-S. Chang, D. Coker, M. Grinstaff, *Chem. Commun.* **2018**, *54*, 5590–5593.
- [2] a) A. Balducci, S. Jeong, G. Kim, S. Passerini, M. Winter, M. Schmuck, G. Appetecchi, R. Marcella, D. Mecerreyes, V. Barsukov, *J. Power Sources* **2011**, *196*, 9719–9730; b) J. Kalhoff, G. G. Eshetu, D. Bresser, S. Passerini, *ChemSusChem* **2015**, *8*, 2154–2175; c) S. Wilken, S. Xiong, J. Scheers, P. Jacobsson, P. Johansson, *J. Power Sources* **2015**, *275*, 935–942.
- [3] A. Balducci, *Top. Curr. Chem.* **2017**, *375*, 20.
- [4] a) T. L. Greaves, C. J. Drummond, *Chem. Rev.* **2015**, *115*, 11379–11448; b) A. Djire, J. Y. Ishimwe, S. Choi, L. T. Thompson, *Electrochem. Commun.* **2017**, *77*, 19–23; c) B. Gorska, J. Pernak, F. Béguin, *Electrochim. Acta* **2017**, *246*, 971–980; d) A. Kachmar, M. Carignano, T. Laino, M. Iannuzzi, J. Hutter, *ChemSusChem* **2017**, *10*, 3083–3090.
- [5] T. Vogl, S. Menne, R.-S. Kühnel, A. Balducci, *J. Mater. Chem. A* **2014**, *2*, 8258–8265.
- [6] A. Brandt, J. Pires, M. Anouti, A. Balducci, *Electrochim. Acta* **2013**, *108*, 226–231.
- [7] a) L. Suo, Y.-S. Hu, H. Li, M. Armand, L. Chen, *Nat. Commun.* **2013**, *4*, 1481; b) L. Suo, O. Borodin, T. Gao, M. Olguin, J. Ho, X. Fan, C. Luo, C. Wang, K. Xu, *Science* **2015**, *350*, 938–943; c) Y. Yamada, A. Yamada, *J. Electrochem. Soc.* **2015**, *162*, A2406–A2423; d) R.-S. Kühnel, D. Reber, A. Remhof, R. Figi, D. Bleiner, C. Battaglia, *Chem. Commun.* **2016**, *52*, 10435–10438; e) S. A. Ferdousi, M. Hilder, A. Basile, H. Zhu, L. A. O’Dell, D. Saurel, T. Rojo, M. Armand, M. Forsyth, P. Howlett, *ChemSusChem* **2019**, *12*, 1700–1711; f) H. Koshikawa, S. Matsuda, K. Kamiya, Y. Kubo, K. Uosaki, K. Hashimoto, S. Nakanishi, *J. Power Sources* **2017**, *350*, 73–79.
- [8] J. Krummacher, A. Balducci, *Chem. Mater.* **2018**, *30*, 4857–4863.
- [9] Y. Zhang, R. Ye, D. Henkensmeier, R. Hempelmann, R. Chen, *Electrochim. Acta* **2018**, *263*, 47–52.
- [10] D. Cericola, P. W. Ruch, A. Foelske-Schmitz, D. Weingarth, R. Kötz, *Int. J. Electrochem. Sci.* **2011**, *6*, 988–996.
- [11] a) A. González, E. Goikolea, J. A. Barrena, R. Mysyk, *Renewable Sustainable Energy Rev.* **2016**, *58*, 1189–1206; b) H. Srour, L. Chancelier, E. Bolimowska, T. Gutel, S. Mailley, H. Rouault, C. C. Santini, *J. Appl. Electrochem.* **2016**, *46*, 149–155.
- [12] B. Gorska, L. Timperman, M. Anouti, F. Béguin, *Phys. Chem. Chem. Phys.* **2017**, *19*, 11173–11186.
- [13] J. Ingenmey, S. Gehrke, B. Kirchner, *ChemSusChem* **2018**, *11*, 1900–1910.
- [14] K. R. Seddon, A. Stark, M.-J. Torres, *Pure Appl. Chem.* **2000**, *72*, 2275–2287.
- [15] a) S. Menne, M. Schroeder, T. Vogl, A. Balducci, *J. Power Sources* **2014**, *266*, 208–212; b) T. Vogl, C. Vaalma, D. Buchholz, M. Secchiarioli, R. Marassi, S. Passerini, A. Balducci, *J. Mater. Chem. A* **2016**, *4*, 10472–10478.

- [16] K. Ueno, H. Tokuda, M. Watanabe, *Phys. Chem. Chem. Phys.* **2010**, *12*, 1649–1658.
- [17] J. Kestin, M. Sokolov, W. A. Wakeham, *J. Phys. Chem. Ref. Data* **1978**, *7*, 941–948.
- [18] M. Anouti, J. Jones, A. Boisset, J. Jacquemin, M. Caillon-Caravancier, D. Lemordant, *J. Colloid Interface Sci.* **2009**, *340*, 104–111.
- [19] L. Timperman, P. Skowron, A. Boisset, H. Galiano, D. Lemordant, E. Frackowiak, F. Béguin, M. Anouti, *Phys. Chem. Chem. Phys.* **2012**, *14*, 8199–8207.
- [20] A. Krause, P. Kossyrev, M. Oljaca, S. Passerini, M. Winter, A. Balducci, *J. Power Sources* **2011**, *196*, 8836–8842.
- [21] S. Pohlmann, B. Lobato, T. A. Centeno, A. Balducci, *Phys. Chem. Chem. Phys.* **2013**, *15*, 17287–17294.
- [22] S. Plimpton, *J. Comput. Phys.* **1995**, *117*, 1–19.
- [23] L. Martínez, R. Andrade, E. G. Birgin, J. M. Martínez, *J. Comput. Chem.* **2009**, *30*, 2157–2164.
- [24] J. N. Canongia Lopes, A. A. Pádua, *J. Phys. Chem. B* **2004**, *108*, 16893–16898.
- [25] S. Chatterjee, P. G. Debenedetti, F. H. Stillinger, R. M. Lynden-Bell, *J. Chem. Phys.* **2008**, *128*, 124511.
- [26] U. C. Singh, P. A. Kollman, *J. Comput. Chem.* **1984**, *5*, 129–145.
- [27] P. Ray, R. Elfgren, B. Kirchner, *Phys. Chem. Chem. Phys.* **2019**, *21*, 4472–4486.
- [28] M. Brehm, B. Kirchner, *J. Chem. Inf. Model.* **2011**, *51*, 2007–2023.
- [29] M. Brehm, H. Weber, M. Thomas, O. Hollóczki, B. Kirchner, *ChemPhys-Chem* **2015**, *16*, 3271–3277.

Manuscript received: May 10, 2019

Accepted manuscript online: June 25, 2019

Version of record online: July 17, 2019

Water in Protic Ionic Liquid Electrolytes: From Solvent Separated Ion Pairs to Water Clusters

Sascha Gehrke,^[a, b] Promit Ray,^[a] Timo Stettner,^[c, d] Andrea Balducci,^[c, d] and Barbara Kirchner^{*[a]}

The large electrochemical and cycling stability of “water-in-salt” systems have rendered promising prospective electrolytes for batteries. The impact of addition of water on the properties of ionic liquids has already been addressed in several publications. In this contribution, we focus on the changes in the state of water. Therefore, we investigated the protic ionic liquid *N*-butylpyrrolidinium bis(trifluoromethanesulfonyl)imide with varying water content at different temperatures with the aid of molecular dynamics simulations. It is revealed that at very low

concentrations, the water is well dispersed and best characterized as shared solvent molecules. At higher concentrations, the water forms larger aggregates and is increasingly approaching a bulk-like state. While the librational and rotational dynamics of the water molecules become faster with increasing concentration, the translational dynamics are found to become slower. Further, all dynamics are found to be faster if the temperature increases. The trends of these findings are well in line with the experimental measured conductivities.

Introduction

Ionic liquids (ILs) have attracted great attention as alternative solvents for a wide variety of technological applications well beyond just the solvation of molecules.^[1–4] Their inherent ionic conductivity – a virtue of their ionic nature – renders ILs as promising candidates for potential electrolytes in a variety of electrochemical devices.^[5–9] However, some disadvantageous properties, their relatively high viscosity^[7,10] in particular, strongly limit their use. It has been shown, that one way to tackle this problem is the addition of molecular liquids.^[11–14] Thereby, water was revealed to be the most promising candidate to optimize the ILs properties in terms of the application as electrolytes by the enhancement of the diffusivity of the ions.^[12,15–19] Unfortunately, water has a low electrochemical window of 1.23 V which restricts the applicability of water-based electrolytes. However, it has been shown that the behavior of water differs significantly if the amount of ionic liquid clearly outnumbers the amount of water. The so-called water-in-salt systems are characterized by a large electro-

chemical and cycling stability.^[20–22] Moreover, extending studies based on aprotic ionic liquids^[7,23–26] to more protic ionic liquids (PILs)^[27–29] has shown to be an important preliminary step as PILs often exhibit enhanced conductivities on account of their water-like hydrogen bonding networks.^[30–33]

The impact of added water on the structure and properties of ILs has already been addressed in several studies^[13,34,35] highlighting differences between aprotic ILs and PILs. For the latter, the concept of contact ion pair, shared solvent ion pair, and separated ion pair^[36–39] could explain the change in the ions' state in dependence of the concentration of water.^[40] Furthermore, with the aid of spectroscopic methods supported by computer studies, it has been shown that water molecules tend to be isolated at lower concentration but form a nano-segregated continuous water network at higher concentrations.^[12,13,35,41–43] However, details about the changes of the water's state – especially according to the formation of water-in-salt systems – are still largely a mystery.

In recent works, we already investigated the protic ionic liquid *N*-butylpyrrolidinium bis(trifluoromethanesulfonyl)imide ([pyrH4][NTf₂]) as a promising potential electrolyte for lithium-ion batteries^[44–46] and characterized the impact of the addition of water on the properties of the ILs.^[47] This paper subsequently enhances the recent studies by giving closer attention to the changes in the water molecules' state. Therefore, systems with water contents of 0.1%, 1.0%, 2.0%, and 3.8% by weight are investigated at different temperatures at and above room temperature. First, the simulation methodologies and experimental measurements are introduced, followed by a detailed analysis of the structural aspects of these solutions which we round up with a thorough discussion of the dynamic properties.

[a] Dr. S. Gehrke, Dr. P. Ray, Prof. B. Kirchner
 Mulliken Center for Theoretical Chemistry, University of Bonn, Beringstr. 4 + 6, D-53115 Bonn, Germany
 E-mail: kirchner@thch.uni-bonn.de

[b] Dr. S. Gehrke
 Department of Physics and Astronomy, University College London, London WC1E 6BT, United Kingdom

[c] T. Stettner, Prof. A. Balducci
 Institute for Technical Chemistry and Environmental Chemistry, Friedrich-Schiller-University Jena, Philosophenweg 7a, D-07743 Jena, Germany

[d] T. Stettner, Prof. A. Balducci
 Center for Energy and Environmental Chemistry Jena (CEEC Jena), Friedrich-Schiller-University Jena, Philosophenweg 7a, D-07743 Jena, Germany

Supporting information for this article is available on the WWW under <https://doi.org/10.1002/cssc.202100660>

© 2021 The Authors. ChemSusChem published by Wiley-VCH GmbH. This is an open access article under the terms of the Creative Commons Attribution License, which permits use, distribution and reproduction in any medium, provided the original work is properly cited.

Computational Details

The [NTf₂]⁻ anion as well as the heterocyclic atoms of the cation were modeled using the specifically parametrized Canongia Lopes–Pádua force field.^[48] The remaining parameters for the cation were taken from the generalized OPLS force field for amines.^[49–51] Partial charges were calculated from a gas phase restrained electrostatic potential (RESP)^[52] fit of the isolated ions at the HF/6-31++G** level scaled down to an absolute value of 0.8.^[53] Charges are downscaled to account for the charge transfer and polarizability^[54–59] within ILs. However, the SPC/E^[60,61] model with unscaled charges was used for water in the IL-water mixtures. The finally applied charges, as well as other parameters, can be found in the ESI. The initial boxes were generated using the PACKMOL^[62] program with the compositions as listed in Table 1. The LAMMPS^[63] program was used to carry out the classical MD simulations detailed herein at temperatures of 30 °C (303 K), 50 °C (323 K), 60 °C (333 K), and 80 °C (353 K) respectively. Cut-offs for the Lennard-Jones interactions were taken at 15 Å with tail corrections. For the evaluation of long-range electrostatic interactions, we employed the standard Ewald sum technique^[64] with an accuracy of 10⁻⁵ Hartree beyond the cutoff distance. The timestep was set to 0.5 fs.

All boxes were first equilibrated in an *NpT* ensemble at the specified target temperature and 1 bar for 2 ns. Thereby, the temperature and the pressure were maintained using a Nosé–Hoover thermostat and a Nosé–Hoover barostat, respectively.^[65–68] Afterwards, the boxes were compressed to result in the average size of the last 1 ns of these equilibrations. The obtained densities are listed in Table 1. The fact, that the densities perfectly match with the experimental ones validates the applied model.

The systems were reequilibrated for another 5 ns in a canonical ensemble. Afterwards, the production runs were performed for 10 ns in the microcanonical ensemble to ensure the unperturbed calculation of the Newtonian equations. Trajectories and thermodynamic information were saved every 250 steps for later analysis.

Static calculations were performed by the ORCA 4.0.1 program,^[69,70] The electrostatic potential shown in Figure 1 was calculated using the PBEh-3c functional^[71–75] after previous geometry optimization with the same method.

The VMD^[76] program was used for structure visualization. Trajectory analysis was performed by TRAVIS^[77,78] which allows for a wide variety of analyses to be performed from trajectory files. In this work, we evaluated radial distribution functions (RDFs), combined distribution functions (CDFs), diffusion coefficients and lifetimes using the reactive flux approach.^[79,80]

Self-diffusion coefficients were calculated from the mean square displacements (MSDs) of the respective ions using the Einstein relation:

$$D = \lim_{t \rightarrow \infty} \frac{1}{6t} \left\langle \left| \vec{r}(t) - \vec{r}(0) \right|^2 \right\rangle \quad (1)$$

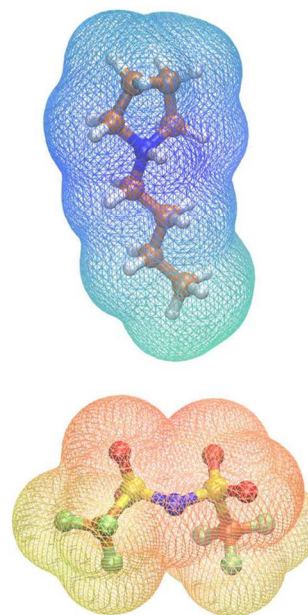


Figure 1. The ions of the investigated systems (top: cation, bottom: anion). The structures were optimized using the PBEh-3c functional after which the electrostatic potential was mapped on the electronic density (isosurface value 0.0004). The color scheme goes from -0.2 (red) over 0 (green) to 0.2 (blue).

with the positions $\vec{r}(t)$ at time t . Only the data points in the last half of the corresponding mean squared displacement functions (shown in the Supporting Information) are considered for the linear regression.

Subsequently, the diffusion coefficients were used to calculate ionic mobilities using the Nernst-Einstein relationship:

$$\mu = \frac{D_{\text{ions}} \cdot q}{k_B \cdot T} \quad (2)$$

with the self-diffusion coefficient D_{ions} , the charge q , the temperature T , and Boltzmann's constant k_B .

We also performed a radical Voronoi tessellation,^[81] using TRAVIS, to understand the formation of phases, clusters and microheteroge-

Table 1. The compositions and densities of the investigated systems. All densities are given in g mol^{-1} . The experimental densities are given in parenthesis if available. Ball-and-stick representations of the ions are shown in Figure 1 and in the Supporting Information.

water content:	pure IL	0.1%	1.0%	2.0%	3.8%
[pyrH ₄] ⁺ [NTf ₂] ⁻ pairs	300	489	407	560	560
water molecules	–	11	93	256	512
density at					
30 °C	1.40 (1.40)	1.40 (1.40)	1.39 (1.39)	1.39 (1.39)	1.38 (1.38)
50 °C	1.38 (1.38)	1.38 (1.38)	1.37 (1.37)	1.37 (1.37)	1.36 (1.37)
60 °C	1.37 (1.37)	1.37 (1.37)	1.36 (1.36)	1.36 (–)	1.34 (–)
80 °C	1.34 (1.35)	1.34 (1.34)	1.34 (1.33)	1.33 (–)	1.32 (–)

neous fragments. Herein, the liquid is formally dissected into its building blocks in order to define different subsets;^[81] the definition of these subsets is system-specific. All atoms are considered as Voronoi sites with the corresponding van der Waals radii being used to define borders, volumes and surfaces for each atom. The cells of each subset are formed from the atomic Voronoi cells and these initially defined subsets belong to the same domain if their cells share a common face. The average number of domains present in the liquid, N_{Dom} (domain count), can be obtained from such a formalism. Any value of N_{Dom} smaller than the total number of particular subsets that constitute it indicates a certain aggregation present in the system. If the domain count equals one, the subsets form a large, continuous microphase that stretches throughout the whole liquid.

Results and Discussion

Structure

The visualization of the trajectories, as illustrated by the representative snapshots in Figure 2, reveals an interesting distribution behavior of the added water. If the concentration of water is very low, the molecules are mostly found as single separated entities. With rising concentration, however, the water is increasingly clustering together to form big heterogeneous domains inside the liquid. It is justified to assume that a single water molecule clamped between ions shows a completely different behavior compared to a molecule in a small cluster or, even more extreme, to a molecule which is part of a bigger domain of quasi-bulk water. In general, there are three possible states the water can exist in:

- as a shared solvent molecule being part of the solvation shell of two ions simultaneously
- as part of a solvation shell of a single ion
- as quasi-bulk water.

In all these states, the physical properties of the water molecules should be significantly different. It should be noted here that the term “solvent” has to be taken with care. Especially for very low water content (see as an example the top panel of Figure 2), water is obviously not a solvent in the traditional sense of the term. More realistically spoken, water is a solute in the salt and should, therefore, be thought of something similar to crystal water in hydrate melts.

A robust way to quantify this cluster formation is the analysis of Voronoi domains.^[81] Therefore, we defined the following subsets based on the charge distribution of the electrostatic potentials shown in Figure 1:

- fluoruous subset: trifluoromethyl groups of the anions
- aqueous subset: the water molecules
- non-polar subset: the terminal propyl group of the cation
- polar subset: the rest of the cation and the anion

The resulting number of domains and the average respective domain sizes are shown in Table 2. Regardless of simulation temperature or concentration of water, the polar components are found to form a wide network detected as a single domain which is a well-known observation for ionic liquids.^[82,83] Interestingly, the non-polar as well as the fluoruous parts are both characterized by a slight increase of the domain size – the

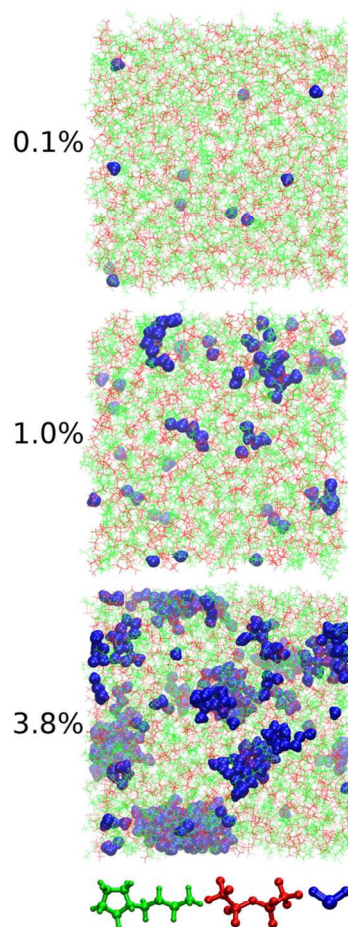


Figure 2. Snapshots from the simulations at 30 °C (303 K) for the 0.1%, 1.0% and 3.8% water solutions. The cations, anions and water molecules are shown in green, red and blue, respectively.

number of molecules in one domain – if small amounts of water are added. If the amount of water increases above 2.0%, however, the domain size increases rapidly which indicates the decomposition of the subset networks into smaller domains. Furthermore, for both subsets the domain numbers marginally decrease with increasing temperature. Meanwhile, for a water concentration of 0.1% the water is well dispersed as mostly single molecules over the simulation cell in well separated domains. With 1.0% water concentration, the average domain size increases to two molecules which indicates the appearance of small clusters. It has been shown that water clusters of small size form homodromic structures depending on their state.^[84,85] If the concentration of water is further increased, the clusters

Table 2. Results of the domain analysis performed with the three terminal carbon atoms (and the attached hydrogen atoms) of the butyl chain as the non-polar phase. The values give the number of respective separated domains. The average sizes of the respective domains are given in brackets since the simulations for different water concentrations were performed with varying numbers of ion pairs and water molecules.

<i>T</i>	pure IL			
	polar	non-polar	fluorous	aqueous
30°C	1.00 (300)	22.25 (13)	4.21 (71)	–
50°C	1.00 (300)	21.17 (14)	4.20 (71)	–
60°C	1.00 (300)	21.03 (14)	4.27 (70)	–
80°C	1.00 (300)	19.69 (15)	4.12 (73)	–
	0.1% water			
	polar	non-polar	fluorous	aqueous
30°C	1.00 (489)	35.06 (13)	6.46 (76)	10.52 (1)
50°C	1.00 (489)	33.38 (14)	6.31 (77)	10.53 (1)
60°C	1.00 (489)	32.43 (15)	6.30 (77)	10.33 (1)
80°C	1.00 (489)	32.81 (15)	6.38 (77)	10.34 (1)
	1.0% water			
	polar	non-polar	fluorous	aqueous
30°C	1.00 (407)	31.67 (13)	5.96 (68)	46.43 (2)
50°C	1.00 (407)	31.31 (13)	5.83 (69)	47.43 (2)
60°C	1.00 (407)	31.27 (13)	5.75 (70)	56.85 (2)
80°C	1.00 (407)	30.02 (14)	5.83 (70)	55.54 (2)
	2.0% water			
	polar	non-polar	fluorous	aqueous
30°C	1.00 (559)	44.60 (12)	8.61 (65)	41.61 (6)
50°C	1.00 (559)	45.10 (12)	8.63 (65)	64.92 (4)
60°C	1.00 (559)	45.75 (12)	8.57 (65)	76.27 (3)
80°C	1.00 (559)	44.23 (12)	8.35 (67)	85.22 (3)
	3.8% water			
	polar	non-polar	fluorous	aqueous
30°C	1.00 (559)	53.56 (10)	9.52 (58)	42.02 (12)
50°C	1.01 (557)	49.47 (11)	9.42 (59)	54.81 (9)
60°C	1.00 (557)	48.98 (11)	9.43 (59)	59.14 (9)
80°C	1.01 (556)	48.17 (11)	9.75 (57)	85.59 (6)

become bigger and increasingly dominating. A transition from small clusters (of two water molecules) to truly aggregated water molecules (with clusters of six and more molecules) is visible.

The combined distribution functions (CDFs) in Figure 3 reveal the molecular details of the ion-water interplay. Shown is the occurrence of assemblies of a water molecule at a certain distance from a cation and simultaneously at a given distance from an anion. For very low water concentrations, there is obviously only one prominent signal detected (named **A** in the following). The distances – about 185 pm for the water-anion distance and about 255 pm for the cation-water distance – are exactly those one would expect for the corresponding hydrogen bonds. Therefore, this peak can be assigned to the assembly illustrated in the top panel of Figure 4. The corresponding distances are marked by green lines. The two ions are separated by a water molecule in a way, that a hydrogen bond is formed between the cation and the water and another one between the same water and the anion. In other words, the water is in this case a shared solvent molecule.

With higher water content, two more signals become prominent:

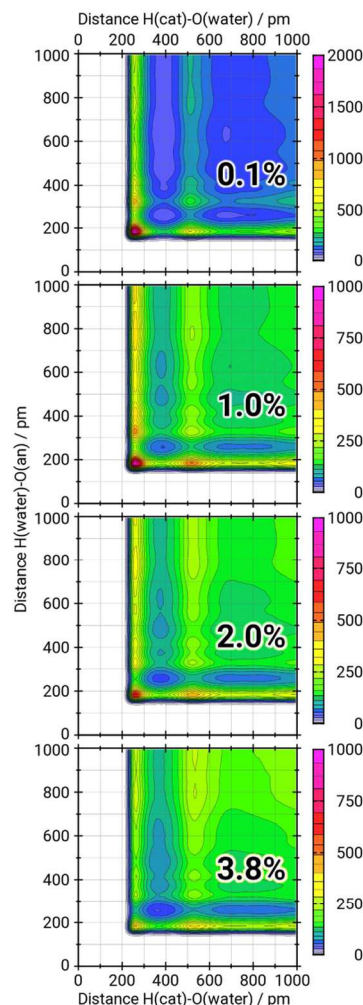


Figure 3. Combined distribution functions illustrating the occurrence of three body assemblies of a water molecule interaction with two ions simultaneously. The x-axis gives the distance between the acidic hydrogen atom of the cation and the oxygen of the water molecule. The y-axis gives the distance between the same water molecule's hydrogen atom and the oxygen atom of an anion. The heat plot represents the occurrence numbers of the certain assemblies. Note the different scaling in the top panel.

- The first one (named **B**) is characterized by the same distance between water and anion as in **A** but by a distance of 515 pm between cation and water. This signal can be explained by the assembly illustrated in the bottom panel of Figure 4 and the distances marked by the red lines. In this case the two ions are separated by a bridge of two water molecules. If each of the water molecule is assigned to the

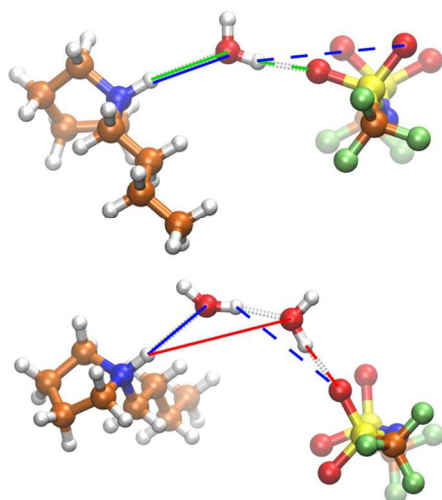


Figure 4. Most prominent assemblies found in the CDFs in Figure 3. The atoms are illustrated by the following color code: hydrogen (white), carbon (orange), nitrogen (blue), oxygen (red), fluorine (green), sulfur (yellow). Top: An anion and a cation separated by a single water molecule. Bottom: The two ions separated by a pair of water molecules. The relevant distances are marked with solid and dashed lines in blue, green, and red, respectively. See text for further explanation.

solvation shell of one ion, this state represents two solvation shells interacting with each other.

- The second prominent signal (named C) is at the same distance between cation and water as in A but at a distance of 335 pm between water and anion. Due to the fact that the anion contains four hydrogen bond interaction sites, there are two possible explanations for this signal: First, the water exists as a shared solvent molecule but the signal is not representing the water-anion distance of the interacting oxygen but, instead, of one of the other oxygen atoms (top panel of Figure 4, blue lines). Second, the water exists in two different interacting solvation spheres as in B (bottom panel of Figure 4, blue lines). Unfortunately, one has to act on the assumption that the signal contains contribution of both cases and is thereby degenerated.

Furthermore, in the CDF for the highest water content additional areas of high occurrence at higher distances in both dimensions are detected. These can be explained by the dominance of larger water clusters compared to the more distinct smaller clusters for the lower concentrations. Water molecules located in the inner region of larger clusters are not linked to any ion at all but only surrounded by other water molecules and thus comparable to molecules in a bulk water phase.

The qualitative interpretation of the CDFs in Figure 3 already reveals several interesting details. However, a quantitative interpretation is more challenging. Due to the different

number of ions and water molecules as well as the different size of the simulation boxes and the consequential different normalization of the occurrence numbers, the direct comparison of different CDFs is invalid. Nevertheless, it is feasible to compare the ratio of two or more values taken from a single CDF with the corresponding ratios from another CDF.

Due to the fact that the water can interact with the four oxygen atoms of the anion but only with the one acidic proton on the cation, even the comparison of the total numbers of the ratios A:B and A:C have to be handled with care. However, both ratios are clearly decreasing with increasing water concentration, as shown in Figure 5. Moreover, the slope of the A:C ratios is significantly less steep than for the A:B ratios. Another interesting observation is, that in the case of the A:C ratios the differences between different water concentrations are nearly the same for all temperatures, which becomes obvious if the eye-guiding lines in Figure 5 are compared. For the A:B ratios this clear order is not observed.

Ion pair and hydrogen bond dynamics

In Table 3 lifetimes of ion pairs and hydrogen bonds calculated using the reactive flux approach^[79,80] were summarized. As expected, all exchange rates increase with increasing temperature. Interestingly, the addition of water results in a similar effect.

Due to the fact, that the ion pair dynamics are directly related to the mobility of the ions the ion pair exchange rate can be correlated with the experimental conductivity,^[47] as visualized in Figure 6. A similar correlation can be observed for the exchange rate of the hydrogen bonds formed between cations and anions, demonstrating the importance of hydrogen bonding for the properties of ionic liquids. The revealed correlation between the calculated properties and the experimental data serves as a satisfying validation of the dynamical data.

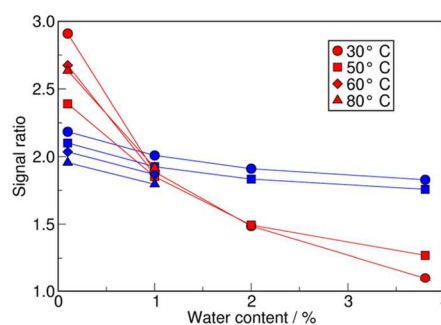


Figure 5. Evolution of the signal ratio with increasing water content. The ratio is given as the occurrence number of A divided by the occurrence number of B (red symbols) and C (blue symbols). The lines are a guide for the eye.

Water content	T	IP	H(cation)-O(anion)
pure	30°C	729.8	236.4
	50°C	372.3	124.6
	60°C	269.9	89.9
	80°C	176.7	60.4
0.1%	30°C	697.3	224.4
	50°C	361.0	119.8
	60°C	236.0	89.1
	80°C	172.5	59.1
1.0%	30°C	479.6	188.7
	50°C	304.4	108.3
	60°C	223.4	83.5
	80°C	152.5	56.4
2.0%	30°C	546.4	178.8
	50°C	276.4	101.4
	60°C	220.4	81.5
	80°C	136.6	52.5
3.8%	30°C	468.8	172.4
	50°C	263.8	97.5
	60°C	207.1	78.3
	80°C	133.1	51.2

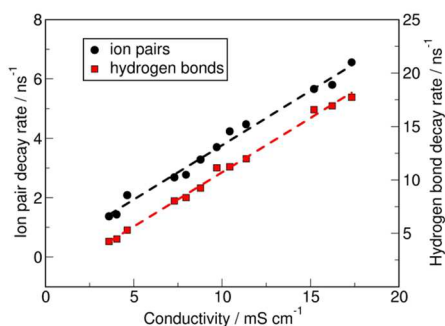


Figure 6. Relationship between the experimental conductivity^[47] and the inverse lifetimes (or decay rates) of hydrogen bonds and ion pairs.

The lifetimes of the water containing hydrogen bonds, listed in Table 4 reveal a similar behavior in terms of temperature dependence and water concentration as the ion pair dynamics. Interestingly, the lifetimes of the cation-water hydrogen bonds are even slightly higher than those of the water-water hydrogen bonds, except for the systems with 0.1% water content. In contrast, the lifetimes of the water-anion hydrogen bonds are significantly shorter. This observation renders the anion to be hydrophobic, while the cation's hydrophobic character is less pronounced.

The observation that the lifetimes of the water-water hydrogen bonds are longer than the corresponding cation-water hydrogen bond lifetimes in the systems with 0.1% water content can be understood if the underlying exchange process is taken into account: In the systems with a water concentration

of more than 0.1% clusters with more than two molecules are found. Therefore, it is possible that in the same step a water-water hydrogen bond is broken a new water-water hydrogen bond is formed. The high energetic stability of the new formed bond renders the barrier in this associative exchange mechanism to be smaller than a barrier towards a state of free partners in a dissociative mechanism.^[86] In contrast, the individual water molecules in the systems with 0.1% water content rarely get in contact with each other. In other words, the hydrogen bonds exist in seldomly occurring water dimers, surrounded by the ionic liquid. As a consequence, the state of the former bonding partners after the breaking event has to be either the energetically unfavored free form, or a hydrogen bond with the ionic liquid. In the first case, the process needs to overcome the higher barrier of the dissociative mechanism. In the second case, it can be assumed, that the influence of these energetically less favorable hydrogen bonds on the barrier is weaker than the impact of the water-water hydrogen bonds. Moreover, the concentration of the interaction sites in the IL is significantly lower than in water. Subsequently, the hydrogen bonds in the systems with 0.1% water content are found to be longer living.

Dipole reorientation

Figure 7 illustrates the dipole reorientation auto-correlation functions of the water molecules. Similar to the observed trend for the ion pair and hydrogen bond dynamics the reorientation becomes faster if the temperature increases.

For the systems with a water content of 1.0% and more a similar trend is observed if the concentration of water is increased. However, the systems with only 0.1% water content do not follow this trend, but show at all temperatures a much faster reorientation than the corresponding 1.0% systems. This is opposed to the trends in the hydrogen bond dynamics. Nonetheless, a similar line of argumentation can be used: The water is mostly found as single molecules in the systems with 0.1% and is therefore only relatively weakly bound by hydrogen bonds with the surrounding ions. At higher concentrations the water molecules are forming small clusters and subsequently they are fixed in optimal cluster arrangements. If the water concentration is only at 1.0% the found clusters consist of only 2–3 molecules, with strongly limited options to change the binding partner. Subsequently, the reorientation dynamics are slower. If the concentration increases the water's state changes more and more to that of bulk phase water, with a correspondingly rapid reorientation rate due to the fluctuating network of hydrogen bonds.

Diffusion and ionic conductivity

Self-diffusion coefficients are obtained from the Einstein relation using mean square displacements. Overall, the obtained diffusion coefficients are well comparable with diffusion

Table 4. Hydrogen bond lifetimes of hydrogen bonds in between water molecules as well as water molecules and ions calculated with the reactive flux approach. All values are given in ps.

Water content	T	H(cation)–O(water)	H(water)–O(anion)	H(water)–O(water)
0.1%	30 °C	338.5	37.4	590.7
0.1%	50 °C	139.9	18.5	242.3
0.1%	60 °C	98.9	13.4	141.2
0.1%	80 °C	47.8	7.8	86.5
1.0%	30 °C	174.0	28.0	87.2
1.0%	50 °C	80.3	16.1	50.6
1.0%	60 °C	73.2	11.0	39.9
1.0%	80 °C	47.5	7.7	29.4
2.0%	30 °C	132.4	23.9	41.1
2.0%	50 °C	79.2	13.5	38.0
2.0%	60 °C	57.3	9.1	35.9
2.0%	80 °C	43.8	5.9	25.4
3.8%	30 °C	103.3	19.2	28.2
3.8%	50 °C	59.9	12.5	26.3
3.8%	60 °C	42.8	9.0	24.4
3.8%	80 °C	41.7	4.7	22.3

coefficients (from both experiments and simulations) of several $[\text{NTf}_2]^-$ -based pure and doped ILs^[87–89] and IL-water systems.^[90]

The trends shown in Table 5 reveal that at all investigated temperatures and all concentrations of water the cation exhibits faster diffusion than the anion. This was already observed in several $[\text{NTf}_2]^-$ -based ILs.^[88,89] Diffusion coefficients of all investigated species show a marked increase with temperature. Moreover, the diffusion coefficients of the ions increase as well with increasing water content with a few exceptions. These exceptions are presumably due to the fact that calculations of diffusion constants based on relatively short simulation times are known to lead to considerable uncertainties.^[91]

The observation that the ionic diffusion is sped up by the addition of water was already reported for imidazolium based

PILs.^[92] However, the same work showed that the speed-up of the cation is larger than that of the anion. This is not the case for the pyrrolidinium based PIL investigated herein.

From the ionic mobility evaluated using the Nernst-Einstein relationship with the obtained diffusivity coefficients shown in Table 6, we observe that the average ionic mobility increases marginally with addition of water but more significantly with increase in temperature. Actually, the observed trends resemble those of the experimental conductivity^[47] as illustrated in Figure 8, which provides a good validation of the presented dynamical data.

Additionally, the data in Table 5 reveals, that water generally exhibits a much higher diffusion coefficient than the ions. Interestingly, the diffusion coefficient of the water is not increasing with higher water content, but in contrast decreasing. Before, it was shown that the dynamics of the hydrogen bonds become faster with increasing concentration. The same trends were observed for the rotations of the water molecules. These accelerations co-occur with an increase of the overall fluidity of the system in terms of the ion's diffusion coefficients and thus can be explained by a simple effect due to the dilution of the ionic liquid. This explanation is consistent with the recently published report, that the ion–ion interaction strength in PILs is not affected by the presence of water.^[93] Therefore, these observations alone do not allow an explicit statement about the state of the water.

The observed decrease of the translational mobility of the water molecules with increased concentration, however, shows an opposite trend compared to the system's fluidity. Hence, these findings clearly indicate that the water exists in different states within the ionic liquid depending on its concentration. While at low concentrations the water shows the typical behavior of a neutral molecule in an ionic liquid, the bulk water properties are more and more dominating if the concentration is increased. This is fully in line with the findings from the static analyses.

Table 5. Self diffusion constants for the different simulations. All values are given in $\text{pm}^2 \text{ps}^{-1}$ and in the order cation/anion/water.

	30 °C	50 °C	60 °C	80 °C
pure	13.2/8.5/-	30.2/24.5/-	47.3/38.9/-	100.8/93.9/-
0.1%	13.4/9.5/131.5	33.8/28.2/316.0	52.2/42.9/502.3	91.7/85.6/837.9
1.0%	21.0/17.5/109.9	35.5/33.3/256.1	60.3/43.6/496.7	100.2/91.8/631.0
2.0%	18.6/15.5/63.4	44.8/39.1/210.1	73.2/56.2/310.2	117.0/103.1/565.9
3.8%	24.1/18.5/52.2	49.9/41.2/134.0	70.3/60.2/139.2	124.8/113.5/345.8

Table 6. The ionic mobility for the different systems in $10^{-9} \text{m}^2 \text{s}^{-1} \text{V}^{-1}$ calculated according to the Nernst-Einstein relationship. All values are given as cation /anion/average ionic mobility.

	30 °C	50 °C	60 °C	80 °C
pure	4.1/2.6/3.4	5.6/4.5/5.1	7.3/6.0/6.7	11.7/10.9/11.3
0.1%	4.1/2.9/3.5	6.3/5.2/5.8	8.1/6.6/7.4	10.6/9.9/10.3
1.0%	6.5/5.4/6.0	6.6/6.2/6.4	9.3/6.7/8.0	11.6/10.7/11.1
2.0%	5.8/4.8/5.3	8.3/7.3/7.8	11.3/8.7/10.0	13.6/12.0/12.8
3.8%	7.5/5.7/6.6	9.3/7.6/8.5	10.9/9.3/10.1	14.5/13.2/13.8

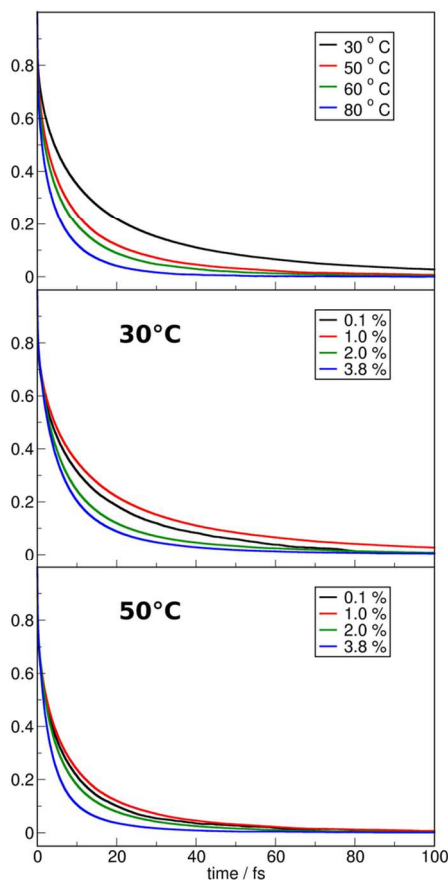


Figure 7. Water dipole reorientation dynamics in the water-in-IL solutions at different temperatures for the 1.0% water solution (top panel) and for the different concentrations at 30 °C (middle panel) and 50 °C (bottom panel).

Conclusions

The impact of water addition on the physical properties of the protic ionic liquid [pyrH4][NTf₂] was reported previously.^[47] In this contribution, we complete these investigations by focusing the point of view on the physical state of the added water with the aid of molecular dynamics simulations. To achieve this goal, ionic liquids with different amounts of water additives were simulated at varying temperatures. In the analysis, generally, three different states of the water are conceptually distinguished: First, water as a shared solvent molecule between two ions. Second, water as a member of a single solvent shell. And third, a state comparable to that in the bulk liquid.

Clear changes in the clustering behavior of the water molecules can already be identified by a simple visualization of

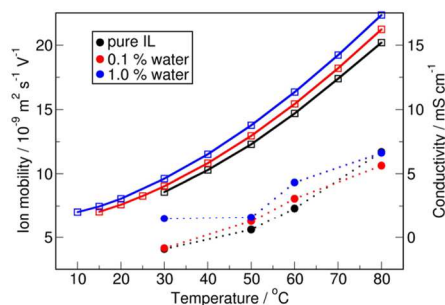


Figure 8. Ion mobility according to the Nernst-Einstein-relationship (circles and dotted lines) compared to the experimental conductivity^[47] (squares and solid lines). Both data sets show the same trends for the increasing temperature as well as for the increasing water content.

the obtained trajectories and are further quantified by a Voronoi-based domain analysis. Therein, it is found that for a water content of 0.1% the water is well dispersed as single molecules. With a content of 1.0% it is forming small clusters of two to three molecules. With higher contents, larger aggregates with average sizes of six and more molecules in averages are observed.

The molecular details of this clustering are illustrated with the aid of combined distribution functions. The simulations with 0.1% water content is dominated by one prominent signal, which can be explained with water molecules simultaneously bound in two hydrogen bonds – one with an anion and one with a cation. In the above described concept, these water molecules are identified as shared solvents. At higher concentrations two more peaks arise. One is explained with water molecules which are members in two interacting single solvent shells. The other can be assumed as degenerated and is most probably the result of overlying contributions of shared solvent molecules and interacting single solvent shell molecules. The ratio of shared solvent to interacting solvent shell molecules is found to clearly decrease with increasing water content. Finally, for the highest concentrations, the occurrence at larger distances become more dominating which can be explained by the presence of a quasi-bulk water microphase.

It is found that the decay rates of ion pairs and hydrogen bonds between cations and anions are correlated with the experimentally measured conductivities. Furthermore, the dynamics of both interactions become faster with increasing temperature as well as with increasing water content. Similar trends are observed for the reorientation of the water's dipoles. However, in this case an exception is found for the system with 0.1% water content, which shows a faster reorientation than what one would expect. At this concentration the water molecules are present individually and therefore, relatively free to rotate. At higher concentrations the water molecules are hindered by the emanating water–water interactions. If the concentration increases the size of the formed clusters increase and subsequently the water's state is more approaching the

state in the bulk phase and in consequence the dynamics become faster similar to the fluctuating hydrogen bond network.

Finally, the self diffusion coefficients calculated by the Einstein relation are analysed. It is shown, that all constants increase with increasing temperature. Furthermore, the coefficients of the ions increase with increasing water content. These trends are the same for the experimental conductivities.

Interestingly, the diffusion coefficients of the water molecules show the opposite trend corresponding the water content: The higher the water content is, the slower becomes the water's diffusion. The findings for the hydrogen bond dynamics and rotations of the water molecules can alternatively be explained as a side effect of the increase of the liquid's fluidity. However, the findings for the translations require a different explanation: For low concentrations the water behaves as a typical neutral solute in an ionic liquid. At higher concentrations this behavior is clearly due to a change in the water's state towards that in the bulk.

Acknowledgements

BK and PR would like to thank the support from the Deutsche Forschungsgemeinschaft under the SPP 1708 project KI768/15-1. BK and SG thank the BMBF under the LuCaMag project 03EK3051A for financial support. Open access funding enabled and organized by Projekt DEAL.

Conflict of Interest

The authors declare no conflict of interest.

Keywords: molecular dynamics · ionic liquids · water-in-salt · hydrogen bonds · electrolytes

- [1] H. Weingärtner, *Angew. Chem.* **2008**, *120*, 664–682; *Angew. Chem. Int. Ed.* **2008**, *47*, 654–670.
- [2] B. Kirchner, O. Hollóczki, J. N. Canongia Lopes, A. A. H. Pádua, *WIREs Comput. Mol. Sci.* **2014**, 202–214.
- [3] N. V. Plechkova, K. R. Seddon, *Chem. Soc. Rev.* **2008**, *37*, 123–150.
- [4] H. Olivier-Bourbigou, L. Magna, D. Morvan, *Appl. Catal. A* **2010**, *373*, 1–56.
- [5] T. Tsuda, C. L. Hussey, *Electrochem. Soc. Interface* **2007**, *16*, 42–49.
- [6] A. P. Abbott, K. J. McKenzie, *Phys. Chem. Chem. Phys.* **2006**, *8*, 4265–4279.
- [7] D. R. MacFarlane, N. Tachikawa, M. Forsyth, J. M. Pringle, P. C. Howlett, G. D. Elliott, J. H. Davis, M. Watanabe, P. Simon, C. A. Angell, *Energy Environ. Sci.* **2014**, *7*, 232–250.
- [8] A. Lewandowski, A. Świdwerska-Moczek, *J. Power Sources* **2009**, *194*, 601–609.
- [9] R. F. De Souza, J. C. Padilha, R. S. Gonçalves, J. Dupont, *Electrochem. Commun.* **2003**, *5*, 728–731.
- [10] A. Noda, K. Hayamizu, M. Watanabe, *J. Phys. Chem. B* **2001**, *105*, 4603–4610.
- [11] T. Takamuku, Y. Kyoshoin, T. Shimomura, S. Kittaka, T. Yamaguchi, *J. Phys. Chem. B* **2009**, *113*, 10817–10824.
- [12] B. Bhargava, Y. Yasaka, M. L. Klein, *Chem. Commun.* **2011**, *47*, 6228–6241.
- [13] C. E. Bernardes, M. E. Minas da Piedade, J. N. Canongia Lopes, *J. Phys. Chem. B* **2011**, *115*, 2067–2074.
- [14] V. V. Chaban, I. V. Voroshylova, O. N. Kalugin, O. V. Prezhdo, *J. Phys. Chem. B* **2012**, *116*, 7719–7727.
- [15] M. Kanakubo, T. Umeky, T. Aizawa, Y. Kurata, *Chem. Lett.* **2005**, *34*, 324–325.
- [16] K. R. Seddon, A. Stark, *Green Chem.* **2002**, *4*, 119–123.
- [17] R. E. Ramírez, L. C. Torres-González, A. Hernández, A. García, E. M. Sánchez, *J. Phys. Chem. B* **2010**, *114*, 4271–4275.
- [18] F. Castiglione, M. Moreno, G. Raos, A. Famulari, A. Mele, G. B. Appetecchi, S. Passerini, *J. Phys. Chem. B* **2009**, *113*, 10750–10759.
- [19] Q. Zhou, W. A. Henderson, G. B. Appetecchi, M. Montanino, S. Passerini, *J. Phys. Chem. B* **2008**, *112*, 13577–13580.
- [20] Y. Yamada, A. Yamada, *J. Electrochem. Soc.* **2015**, *162*, A2406–A2423.
- [21] L. Suo, O. Borodin, T. Gao, M. Olguin, J. Ho, X. Fan, C. Luo, C. Wang, K. Xu, *Science* **2015**, *350*, 938–943.
- [22] Y. Yamada, K. Usui, K. Sodeyama, S. Ko, Y. Tateyama, A. Yamada, *Nat. Energy* **2016**, *1*, 16129.
- [23] M. Armand, F. Endres, D. R. MacFarlane, H. Ohno, B. Scrosati, *Nat. Mater.* **2009**, *8*, 621–629.
- [24] M. Galiński, A. Lewandowski, I. Stepniak, *Electrochim. Acta* **2006**, *51*, 5567–5580.
- [25] J. F. Wishart, *Energy Environ. Sci.* **2009**, *2*, 956–961.
- [26] J. Kalhoff, G. G. Eshetu, D. Bresser, S. Passerini, *ChemSusChem* **2015**, *8*, 2154–2175.
- [27] N. Böckenfeld, M. Willeke, J. Pires, M. Anouti, A. Balducci, *J. Electrochem. Soc.* **2013**, *160*, A559–A563.
- [28] T. Vogl, S. Menne, R.-S. Kühnel, A. Balducci, *J. Mater. Chem.* **2014**, *2*, 8258–8265.
- [29] S. Menne, J. Pires, M. Anouti, A. Balducci, *Electrochem. Commun.* **2013**, *31*, 39–41.
- [30] H. Nakamoto, M. Watanabe, *Chem. Commun.* **2007**, 2539–2541.
- [31] L. Timperman, P. Skowron, A. Boisset, H. Galiano, D. Lemordant, E. Frackowiak, F. Béguin, M. Anouti, *Phys. Chem. Chem. Phys.* **2012**, *14*, 8199–8207.
- [32] W. Xu, C. A. Angell, *Science* **2003**, *302*, 422–425.
- [33] K. Fumino, A. Wulf, R. Ludwig, *Angew. Chem.* **2009**, *121*, 3230–3233; *Angew. Chem. Int. Ed.* **2009**, *48*, 3184–3186.
- [34] J. N. Canongia Lopes, M. F. Costa Gomes, A. A. Pádua, *J. Phys. Chem. B* **2006**, *110*, 16816–16818.
- [35] W. Jiang, Y. Wang, G. A. Voth, *J. Phys. Chem. B* **2007**, *111*, 4812–4818.
- [36] H. Sadek, R. M. Fuoss, *J. Am. Chem. Soc.* **1954**, *76*, 5897–5901.
- [37] E. Grunwald, *Anal. Chem.* **1954**, *26*, 1696–1701.
- [38] S. Winstein, E. Clippinger, A. Fainberg, G. Robinson, *J. Am. Chem. Soc.* **1954**, *76*, 2597–2598.
- [39] Y. Marcus, *Ion solvation*, Wiley, **1985**.
- [40] P. Stange, K. Fumino, R. Ludwig, *Angew. Chem.* **2013**, *125*, 3064–3068; *Angew. Chem. Int. Ed.* **2013**, *52*, 2990–2994.
- [41] S. Saha, H.-o. Hamaguchi, *J. Phys. Chem. B* **2006**, *110*, 2777–2781.
- [42] C. Hanke, R. Lynden-Bell, *J. Phys. Chem. B* **2003**, *107*, 10873–10878.
- [43] M. Del Popolo, C. Mullan, J. Holbrey, C. Hardacre, P. Ballone, *J. Am. Chem. Soc.* **2008**, *130*, 7032–7041.
- [44] P. Ray, T. Vogl, A. Balducci, B. Kirchner, *J. Phys. Chem. B* **2017**, *121*, 5279–5292.
- [45] P. Ray, A. Balducci, B. Kirchner, *J. Phys. Chem. B* **2018**, *122*, 10535–10547.
- [46] T. Vogl, P. Goodrich, J. Jacquemin, S. Passerini, A. Balducci, *J. Phys. Chem. C* **2016**, *120*, 8525–8533.
- [47] T. Stettner, S. Gehrke, P. Ray, B. Kirchner, A. Balducci, *ChemSusChem* **2019**, *12*, 3827–3836.
- [48] J. N. Canongia Lopes, A. A. Pádua, *J. Phys. Chem. B* **2004**, *108*, 16893–16898.
- [49] W. L. Jorgensen, D. S. Maxwell, J. Tirado-Rives, *J. Am. Chem. Soc.* **1996**, *118*, 11225–11236.
- [50] G. Kaminski, W. L. Jorgensen, *J. Phys. Chem.* **1996**, *100*, 18010–18013.
- [51] R. C. Rizzo, W. L. Jorgensen, *J. Am. Chem. Soc.* **1999**, *121*, 4827–4836.
- [52] U. C. Singh, P. A. Kollman, *J. Comb. Chem.* **1984**, *5*, 129–145.
- [53] W. J. Hehre, R. Ditchfield, J. A. Pople, *J. Chem. Phys.* **1972**, *56*, 2257–2261.
- [54] Y. Zhang, E. J. Maginn, *J. Phys. Chem. B* **2012**, *116*, 10036–10048.
- [55] T. Yan, C. J. Burnham, M. G. Del Popolo, G. A. Voth, *J. Phys. Chem. B* **2004**, *108*, 11877–11881.
- [56] T. I. Morrow, E. J. Maginn, *J. Phys. Chem. B* **2002**, *106*, 12807–12813.
- [57] V. V. Chaban, I. V. Voroshylova, O. N. Kalugin, *Phys. Chem. Chem. Phys.* **2011**, *13*, 7910–7920.
- [58] B. B. Hurisso, K. R. Lovelock, P. Licence, *Phys. Chem. Chem. Phys.* **2011**, *13*, 17737–17748.

- [59] S. Men, K. R. Lovelock, P. Licence, *Phys. Chem. Chem. Phys.* **2011**, *13*, 15244–15255.
- [60] H. Berendsen, J. Grigera, T. Straatsma, *J. Phys. Chem.* **1987**, *91*, 6269–6271.
- [61] S. Chatterjee, P. G. Debenedetti, F. H. Stillinger, R. M. Lynden-Bell, *J. Chem. Phys.* **2008**, *128*, 124511.
- [62] L. Martínez, R. Andrade, E. G. Birgin, J. M. Martínez, *J. Comput. Chem.* **2009**, *30*, 2157–2164.
- [63] S. Plimpton, *J. Comp. Physiol.* **1995**, *117*, 1–19.
- [64] T. Darden, D. York, L. Pedersen, *J. Chem. Phys.* **1993**, *98*, 10089–10092.
- [65] S. Nosé, *J. Chem. Phys.* **1984**, *81*, 511–519.
- [66] S. Nosé, *Mol. Phys.* **1984**, *52*, 255–268.
- [67] W. G. Hoover, *Phys. Rev. A* **1985**, *31*, 1695.
- [68] G. J. Martyna, M. L. Klein, M. Tuckerman, *J. Chem. Phys.* **1992**, *97*, 2635–2643.
- [69] F. Neese, *WIREs Comput. Mol. Sci.* **2012**, *2*, 73–78.
- [70] F. Neese, *WIREs Comput. Mol. Sci.* **2018**, *8*, e1327.
- [71] F. Weigend, *Phys. Chem. Chem. Phys.* **2006**, *8*, 1057–1065.
- [72] S. Grimme, J. Antony, S. Ehrlich, H. Krieg, *J. Chem. Phys.* **2010**, *132*, 154104.
- [73] S. Grimme, S. Ehrlich, L. Goerigk, *J. Comput. Chem.* **2011**, *32*, 1456–1465.
- [74] H. Kruse, S. Grimme, *J. Chem. Phys.* **2012**, *136*, 04B613.
- [75] S. Grimme, J. G. Brandenburg, C. Bannwarth, A. Hansen, *J. Chem. Phys.* **2015**, *143*, 054107.
- [76] W. Humphrey, A. Dalke, K. Schulten, *J. Mol. Graphics* **1996**, *14*, 33–38.
- [77] M. Brehm, B. Kirchner, *J. Chem. Inf. Model.* **2011**, *51*, 2007–2023.
- [78] M. Brehm, M. Thomas, S. Gehrke, B. Kirchner, *J. Chem. Phys.* **2020**, *152*, 164105.
- [79] S. Gehrke, M. von Domaros, R. Clark, O. Hollóczki, M. Brehm, T. Welton, A. Luzar, B. Kirchner, *Faraday Discuss.* **2018**, *206*, 219–245.
- [80] S. Gehrke, B. Kirchner, *J. Chem. Eng. Data* **2020**, *65*, 1146–1158.
- [81] M. Brehm, H. Weber, M. Thomas, O. Hollóczki, B. Kirchner, *ChemPhysChem* **2015**, *16*, 3271–3277.
- [82] O. Hollóczki, M. Macchiagodena, H. Weber, M. Thomas, M. Brehm, A. Stark, O. Russina, A. Triolo, B. Kirchner, *ChemPhysChem* **2015**, *16*, 3325–3333.
- [83] R. Elfgén, O. Hollóczki, B. Kirchner, *Acc. Chem. Res.* **2017**, *50*, 2949–2957.
- [84] E. Perlt, M. von Domaros, B. Kirchner, R. Ludwig, F. Weinhold, *Sci. Rep.* **2017**, *7*, 1–10.
- [85] J. Blasius, J. Ingenmey, E. Perlt, M. von Domaros, O. Hollóczki, B. Kirchner, *Angew. Chem.* **2019**, *131*, 3245–3249; *Angew. Chem. Int. Ed.* **2019**, *58*, 3212–3216.
- [86] S. Gehrke, O. Hollóczki, *Chem. Eur. J.* **2018**, *24*, 11594–11604.
- [87] H. Liu, E. Maginn, *J. Chem. Phys.* **2013**, *139*, 114508.
- [88] Z. Li, G. D. Smith, D. Bedrov, *J. Phys. Chem. B* **2012**, *116*, 12801–12809.
- [89] J. B. Haskins, W. R. Bennett, J. J. Wu, D. M. Hernández, O. Borodin, J. D. Monk, C. W. Bauschlicher Jr, J. W. Lawson, *J. Phys. Chem. B* **2014**, *118*, 11295–11309.
- [90] A.-L. Rollet, P. Porion, M. Vaultier, I. Billard, M. Deschamps, C. Bessada, L. Jouvencal, *J. Phys. Chem. B* **2007**, *111*, 11888–11891.
- [91] E. J. Maginn, R. A. Messerly, D. J. Carlson, D. R. Roe, J. R. Elliott, *LiveCoMS* **2018**, *1*, 6324.
- [92] N. Yaghini, L. Nordstierna, A. Martinelli, *Phys. Chem. Chem. Phys.* **2014**, *16*, 9266–9275.
- [93] J. E. Reid, R. J. Gammons, J. M. Slattery, A. J. Walker, S. Shimizu, *J. Phys. Chem. B* **2017**, *121*, 599–609.

Manuscript received: March 30, 2021
Revised manuscript received: June 21, 2021
Accepted manuscript online: June 24, 2021
Version of record online: July 12, 2021

2.1.2. Publikation 4: Mixtures of glyme and aprotic-protic ionic liquids as electrolytes for energy storage devices

The switch from lithium-ion based to alternative systems is an important but difficult task. As already mentioned, the application of PILs in post lithium devices has been rather scarce. One of the most promising and advanced alternatives is the sodium-ion system, in which graphite can only be charged reversibly via co-intercalation. Na-ions intercalate in a coordinated state, thus solvent molecules also enter the graphite. Therefore, it is necessary to tailor the electrolyte to be able to participate in this process. The benefits of graphite however, e.g., the high energy density, make this additional effort worthwhile. The most common solvent type employed for this purpose are glyme based. Hence, to introduce PILs into sodium-ion based system, a mixture with this solvent appears reasonable, offering the possibility to use an attractive anode material such as graphite.

The investigations were performed using five different electrolytes composed of varying amounts of $[\text{Pyr}_{\text{H4}}][\text{TFSI}]$ and bis(2-methoxyethyl) ether (diglyme, 2G) (0, 20, 50, 80 and 100 mol% of IL) all with 0.5 M NaTFSI. Their chemical-physical-properties were evaluated and, to give more insight regarding other IL-based systems, a comparison with an AIL, $[\text{Pyr}_{14}][\text{TFSI}]$ was carried out (same compositions with diglyme as $[\text{Pyr}_{\text{H4}}][\text{TFSI}]$).

Compared to the “pure” 2G (with 0.5 M NaTFSI), the “pure” ILs (with 0.5 M NaTFSI) display worse transport properties, owing to their high viscosities. $[\text{Pyr}_{\text{H4}}][\text{TFSI}]$ shows slightly better values compared to $[\text{Pyr}_{14}][\text{TFSI}]$, due to increased ion interactions in the latter. With increasing 2G content, the transport properties are improving, up to 80 mol% of 2G. Even though the 80 mol% 2G mixtures are still more viscous than the pure 2G, their conductivities are increased due to a higher concentration of charge carriers. The most crucial difference between AIL and PIL regarding the chemical-physical-properties lies in the presence of a “solvent-threshold” in the former. While the PIL mixtures are getting less viscous and more conductive in a linear behavior with increasing 2G content, the AIL mixtures show a large gap between 20 and 50 mol% of 2G, a behavior commonly observed in AIL-solvent mixtures.

More pronounced differences are visible in the electrochemical performances between the protic and aprotic mixtures. Due to the early reduction of the available proton in $[\text{Pyr}_{\text{H4}}][\text{TFSI}]$, the ESW of the protic mixtures is much lower, resulting in an overall ESW of around 3 V

compared to almost 4 V for the aprotic mixtures. Nevertheless, a trend of lower ESW for higher 2G content is visible in both protic and aprotic mixtures.

The lower ESW of the protic mixtures logically limit the OPV of AC-based electrodes cycled in these protic electrolytes. The highest OPV of 2.5 V was achieved with 20 mol% 2G, surprisingly decreasing with higher amounts of 2G, since the pure 2G mixture was able to withstand 3.4 V. Mixtures of [Pyr_{H4}][TFSI] and 2G higher than 20 mol% of 2G seem to result in unfavorable ion-solvent interactions leading to earlier electrolyte decomposition. For the aprotic mixtures, the OPVs did not show a direct correlation regarding their ESW either, displaying no linear increase of OPV with increasing AIL content. Nevertheless, the highest OPV was still displayed by the 20 mol% 2G electrolyte.

For full cell devices based on balanced AC-electrodes, the most obvious difference between protic and aprotic mixtures lies in the energy density, resulting from their higher OPVs. Additionally, the performance of devices based on electrolytes with higher IL content was limited by the high viscosity. This shows that depending on the requirements, higher solvent content can lead to higher power densities, while higher IL content can generate higher energy densities.

All in all, the proof of concept of a PIL-based sodium-ion capacitor was achieved. Unfortunately, it highlighted the drawbacks of such an IL-based high-power device, making high contents of solvent necessary to compensate high viscosities. Furthermore, as already anticipated, the energy density of the AIL-based EDLC systems was much higher compared to the protic system. Nevertheless, the ultimate idea of this project is the combination of only one AC-based electrode with a battery type electrode. In this case, the low cathodic stability of the protic system could be neglected due to an SEI, while the demands in power performance could be accomplished by higher content of solvent.



Mixtures of glyme and aprotic-protic ionic liquids as electrolytes for energy storage devices

T. Stettner,^{1,2} P. Huang,^{1,2} M. Goktas,^{1,2} P. Adelhelm,^{1,2} and A. Balducci^{1,2,a)}

¹Institute for Technical Chemistry and Environmental Chemistry, Friedrich-Schiller-University Jena, 07743 Jena, Germany

²Center for Energy and Environmental Chemistry Jena (CEEC Jena), Friedrich-Schiller-University Jena, 07743 Jena, Germany

(Received 10 November 2017; accepted 25 January 2018; published online 15 February 2018)

Ionic liquids (ILs) have been proven to be promising electrolytes for electrochemical energy storage devices such as supercapacitors and lithium ion batteries. In the last years, due to deficiency in storage of lithium on earth, innovative systems, such as sodium-based devices, attracted considerable attention. IL-based electrolytes have been proposed also as electrolytes for these devices. Nevertheless, in the case of these systems, the advantages and limits of IL-based electrolytes need to be further investigated. In this work we report an investigation about the chemical-physical properties of mixtures containing bis(2-methoxyethyl)ether diglyme (2G), which is presently considered as one of the most interesting solvents for sodium-based devices, and the ionic liquids 1-butyl-1-methylpyrrolidinium bis(trifluoromethanesulfonyl)imide (Py₁₄TFSI) and 1-butylpyrrolidinium bis(trifluoromethanesulfonyl)imide (Py_{H4}TFSI). The conductivities, viscosities, and densities of several mixtures of 2G and these ILs have been investigated. Furthermore, their impact on the electrochemical behaviour of activated carbon composite electrodes has been considered. The results of this investigation indicate that these mixtures are promising electrolytes for the realization of advanced sodium-based devices. *Published by AIP Publishing.* <https://doi.org/10.1063/1.5013117>

I. INTRODUCTION

Ionic liquids (ILs) are considered one of the most interesting classes of electrolytes for a large number of electrochemical storage devices. In the past, ILs have been successfully utilized in supercapacitors (SC)^{1–6} and lithium-ion batteries (LIBs).^{7–11} Several works showed that the use of IL-based electrolytes might have a beneficial impact on the safety as well as on the energy density of these devices.^{12–14} The favourable features displayed by IL-based devices are related to the unique chemical-physical properties of these molten salts and, especially, to their large electrochemical stability, low flammability, and low vapour pressure. So far, aprotic ionic liquids (AILs) have been the most investigated and utilized class of IL for the realization of IL based electrolytes for SC and LIBs. In both systems, AILs have been used as neat solvents as well as a co-solvent for a variety of organic solvents.^{4,13,15} It has been shown that the use of neat IL might have a positive impact on the safety of these devices, especially in the case of LIBs. On the other hand, the use of mixtures of IL and organic solvents offer the great advantage of making the tuning of the electrolyte properties possible, allowing the realization of high performance devices. More recently, protic ionic liquids (PILs) have also been proposed as electrolytes for SC and LIB. In the case of SC, the use of this class of IL does not appear particularly interesting.¹⁶ To the contrary, it has been shown

that PIL-based electrolytes are very promising electrolytes for LIBs.^{7,17,18} Thanks to the unique lithium environment present on these electrolytes, in neat IL as well as in mixtures with organic solvents, the use of PIL allows the realization of LIBs that are able to display high performances even at high current densities.^{8,19}

In the last years, due to the relative scarce storage of lithium on earth,²⁰ several efforts have been dedicated to the development of alternative alkaline metal-ion batteries. Among these systems, sodium-ion battery (SIB) are considered one of the most promising candidates, thanks to the high natural abundance of sodium and its low price, which make these devices ideal for stationary energy storage applications.²¹ In recent years, the research on SIBs followed the footsteps of LIBs' development by using similar electrode materials and electrolytes.²² Among the electrolytes proposed so far for SIBs, glyme-based electrolytes appear to be one of the most interesting. In fact, it has been shown that the use of glyme-based solvents allows the reversible formation of ternary intercalation compounds between the sodium or lithium ions, the glyme molecules, and the graphite and thus makes the use of graphite as an anode material for SIBs possible.^{23,24} ILs have also been considered for SIBs.²⁵ AILs have been utilized in combination with several materials and they have also been used for the realization of full cells.^{26,27} So far, PILs have only been used in combination with polyanionic or layered metal oxide cathodes.²⁸

As mentioned above, mixtures of ILs and organic solvents are presently considered as a very interesting class of electrolytes for many electrochemical devices. It is

^{a)}Author to whom correspondence should be addressed: andrea.balducci@uni-jena.de

important to notice that the investigation of these mixtures can also supply very helpful indications about the solvent-salt (which in these mixtures are the metal-salt and the ionic liquid) interactions. Information about these interactions is of crucial importance for the understanding of the chemical-physical and electrochemical properties of these electrolytes.

To the best of our knowledge, in the past, only few works have been dedicated to the investigation of mixtures of AIL and glyme-based solvents^{29,30} and none to mixtures of PIL and glyme-based solvents. Nevertheless, considering the interesting properties of these two classes of electrolytes, a deeper understanding of the properties of this kind of mixtures would be of importance for the realization of advanced sodium-based devices.

Taking this point into account, in this paper we investigated the chemical-physical properties of mixtures containing bis(2-methoxyethyl)ether diglyme (2G), the AIL 1-butyl-1-methylpyrrolidinium bis(trifluoromethanesulfonyl)imide (Pyr₁₄TFSI), and the PILs 1-butylpyrrolidinium bis(trifluoromethanesulfonyl)imide (Pyr_{H4}TFSI). In order to realize electrolytes suitable for sodium-based systems, sodium bis(trifluoromethanesulfonyl)imide (NaTFSI) has been used as conducting salt.

With the aim to have a better understanding of the properties of these mixtures, several ratios of 2G/IL have been considered. At the beginning of the manuscript, the conductivities, viscosities, and densities of the investigated electrolytes are considered. In the second part, the electrochemical stability of these mixtures is investigated. In the last part of the manuscript, the impact of these electrolytes on the operative voltage (OPV) of activated carbon is reported.

II. EXPERIMENTAL

A. Electrolyte preparation

The bis(2-methoxyethyl)ether diglyme (2G) (99.5%, obtained by Sigma-Aldrich) was used as received. The AIL 1-butyl-1-methylpyrrolidinium bis(trifluoromethanesulfonyl)imide (Pyr₁₄TFSI) (99%, obtained by Iolitech) was used as received. The PILs 1-butylpyrrolidinium bis(trifluoromethanesulfonyl)imide (Pyr_{H4}TFSI) was synthesized as previously reported.³¹ The sodium bis(trifluoromethanesulfonyl)imide (NaTFSI) (99.5%, obtained by Solvionic) was dried under vacuum at 60 °C for two days before its use.

Table I reports the composition of the investigated electrolytes. In all electrolytes, the concentration of NaTFSI was equal to 0.5M.

The electrolytes used for the investigations were prepared under an argon atmosphere in an *MBraun Labmaster^{pro} ECO* glovebox with <1 ppm H₂O and <1 ppm O₂. The water content of all electrolytes was lower than 30 ppm.

B. Chemical-physical-characterization

The conductivities of the electrolytes were measured using a potentiostat *ModuLabXM* (Solartron analytical) in the temperature range comprised between -30 and 80 °C following the procedure described in Ref. 13. The viscosity of the electrolytes was determined using a rheometer MCR 102

TABLE I. Compositions of the electrolytes investigated in this work. The ionic liquids Pyr₁₄TFSI and Pyr_{H4}TFSI were used for the realization of the electrolytes. NaTFSI (0.5M) was used as conductive salt.

2G (mol. %)	IL (mol. %)
0	100
20	80
50	50
80	20
100	0

(Anton Paar) in the temperature range comprised between -30 and 80 °C, following the protocol reported in Ref. 13. The density of electrolyte was determined in the temperature range comprised between 10 and 80 °C, using the density meter *DMA 4100M* (Anton Paar).

C. Electrode preparation

Activated carbon (AC) electrodes were prepared following the protocol developed by Krause *et al.*³² The dry composition of the electrodes was 90 wt. % of Norit DLC Super 30 (activated carbon), 5 wt. % Super C65 (conductive agent), and 5 wt. % carboxymethyl cellulose (CMC, binder). The mass loading of the electrodes varied between 2.6 mg/cm² and 3.5 mg/cm², the electrode area was equal to 1.13 cm².

For the evaluation of the operative voltage of the AC-based electrodes, an (oversized) counter electrode containing 85 wt. % of Norit DLC Super (activated carbon), 10 wt. % of Super C65 (carbon black), and 5 wt. % of polytetrafluoroethylene (PTFE, binder) were prepared following the procedure described in Ref. 33. The mass loading of these electrodes was about 40 mg/cm², while the area was 1.33 cm².

D. Electrochemical measurements

All electrochemical measurements have been carried out using a three-electrode *Swagelok* cell setup. In every cell, *Whatman* glass microfiber filters (150 mm) were used as separators, drenched with 150 μl electrolyte. The cell assembly was done under an argon atmosphere in an *MBraun Labmaster^{pro} ECO* glovebox with <1 ppm H₂O and <1 ppm O₂.

The electrochemical stability window (ESW) of the electrolytes were measured in a *Swagelok* cell using a platinum electrode as working electrode, an oversized carbon electrode as counter electrode, and a silver electrode as pseudoreference electrode. After a 12-h open circuit voltage (OCV) measurement to reach equilibrium, the cells were swept from OCV towards either positive or negative direction at 1 mV/s until a potential of -6 V vs. OCV and 6 V vs. OCV was reached respectively.

For the determination of the operative voltage (OPV) of AC-based electrodes on the investigated electrolyte, a *Swagelok* cell using an AC-based working electrode, an oversized carbon electrode as counter electrode, and a silver electrode as pseudoreference electrode were used.

The first step in the OPV measurements was an OCV measurement for 1 h, after which 50 cyclic voltammetry (CV) cycles at 20 mV/s, starting from the last recorded OCV value, ranging from 0.8 V vs. Ag to -0.8 V vs. Ag were carried

out to make sure the pores of the counter electrode were fully soaked. As next step, another OCV was measured for 12 h, giving the starting point for the actual OPV measurement, carried out via cyclic voltammetry (CV) with 5 mV/s scan rate. The working electrode was swept towards positive and negative directions, respectively, using a step of 0.1 V. The positive and negative limits were defined as the potential at which the Coulombic efficiency of the CV was dropping below 98%. The efficiency η was calculated using Eq. (1), with the sum of all positive currents I_+ and negative currents I_- ,

$$\eta_+ = \frac{\sum I_+}{\sum I_+ + \sum I_-} \text{ and } \eta_- = \frac{\sum I_-}{\sum I_+ + \sum I_-}. \quad (1)$$

The specific capacitance C was calculated with Eq. (2),

$$C = \frac{I}{a * m}, \quad (2)$$

in which I is either the average current over the respective voltage window on cyclic voltammogram or the constant current applied during galvanostatic cycling and a represents the slope of the voltage, in these cases the scan rate, while m is the mass of the electrode.

After the determination of the OPV, full cells were assembled and tested. Equation (3) was used for the electrode balancing,

$$m_1 * C_1 * U_1 = m_2 * C_2 * U_2. \quad (3)$$

m_1 and m_2 are the masses of the electrodes, C_1 and C_2 are the capacitances measured during the positive and negative OPV measurements, respectively, and U_1 and U_2 the positive and negative voltage range of the electrolyte, respectively.

The electrochemical behaviour of the cells was investigated using cyclic voltammograms carried out at different scan rates (1 mV/s, 2.5 mV/s, 5 mV/s, 10 mV/s, 25 mV/s, and 50 mV/s) and galvanostatic cycling experiments carried out at different current densities (0.5 A/g, 1 A/g, 2.5 A/g, 5 A/g, 10 A/g, and again 0.5 A/g). From these latter experiments, the specific capacitance was also calculated using Eq. (2).

III. RESULTS AND DISCUSSION

A. Chemical-physical properties

Figure 1 shows the conductivity evolution of the different mixtures upon increasing temperature. According to Fig. 1(a),

at 30 °C the 2G displays a conductivity of 5.4 mS/cm, which increases to 9.8 mS/cm at 80 °C.

Py₁₄TFSI displays a lower conductivity through all the investigated temperature range. At 30 °C this AIL displays a conductivity of 1.7 mS/cm, while at 80 °C its conductivity is equal to 9.3 mS/cm. It is interesting to notice that, with increasing temperature, the conductivity of the IL rises faster than that of the solution containing 2G. This different increase has been observed also in other mixtures containing organic solvent and IL, e.g., based on propylene carbonate.¹³ The conductivity of the mixtures of 2G and Py₁₄TFSI increases with the temperature following a trend similar to that of the pure Py₁₄TFSI, and at 80 °C all mixtures display higher conductivities compared to both the single components. The figure shows that the content of 2G inside the electrolytes has a strong influence on the values of conductivity. At 30 °C the mixture containing 20% 2G displays a conductivity of 2.9 mS/cm, which is a value lower than that of the pure 2G. At the same temperature, the mixtures containing 50% and 80% of 2G display a conductivity of 9.4 mS/cm and 10.1 mS/cm, respectively. These values are significantly higher (more than 30%) than those of the other investigated electrolytes. It is also interesting to notice that the conductivity of the mixtures containing 50% and 80% of 2G is very similar through all the investigated temperature range. Considering this behaviour, it is possible to assert that in the case of these mixtures there is a kind of 2G content threshold (in the order of 50%), above which an abrupt increase of conductivity is taking place.

Figure 1(b) shows the conductivity evolution of the electrolytes containing the Py_{H4}TFSI. This PIL has a melting point of 30 °C and, for this reason, the conductivity of the pure component is reported only up to this value. At this temperature, Py_{H4}TFSI displays a conductivity of 2.8 mS/cm, which rises to 13 mS/cm at 80 °C. These values are in agreement with those already reported in the literature for this PIL.³⁴ This figure shows that when the temperature increases, the conductivity of Py_{H4}TFSI rises faster than the one of 2G (as observed for the Py₁₄TFSI). At 80 °C, all investigated electrolytes, including the pure Py_{H4}TFSI, display higher conductivity than the 2G. In the case of these mixtures, the 2G amount in the electrolytes also has a strong influence on the conductivity and the higher the 2G content, the higher is the conductivity. Nevertheless, contrary to the 2G-AIL mixtures observed above, no 2G content threshold

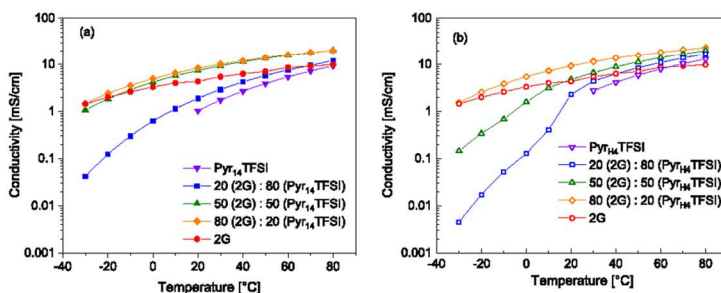


FIG. 1. Influence of the temperature on the conductivity of the (a) AIL-2G and (b) PIL-2G mixtures, all with 0.5M NaTFSI.

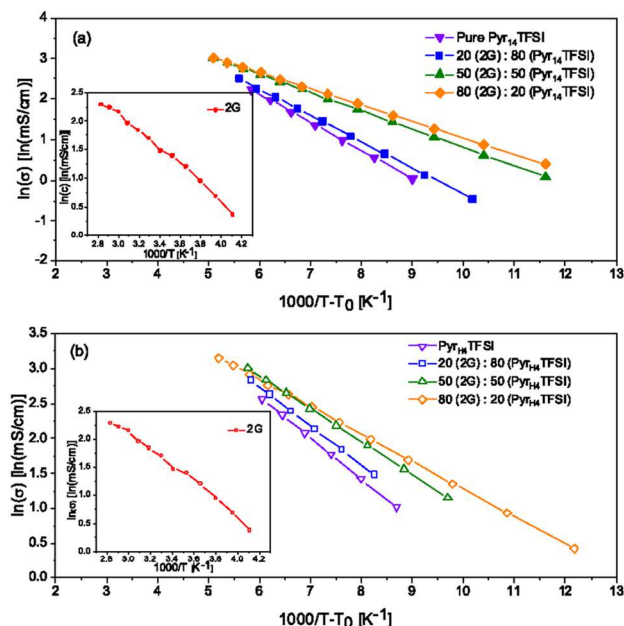


FIG. 2. VTF-plot of the conductivity curves of the (a) AIL-2G and (b) PIL-2G mixtures. The insets show the Arrhenius plot of the mixture based on pure 2G.

is observed, and the conductivity increases gradually with increasing solvent content. This latter behaviour has been observed for many other mixtures of organic solvents, e.g., PC, AIL and PIL.^{13,19} Overall, the mixtures containing the PIL display higher conductivity values compared to that containing the AIL.

Organic solution such as the 2G investigated in this work follow an Arrhenius behaviour. To the contrary, as reported already in the literature, ionic liquids (neat and in mixture with organic solvents) do not exhibit an Arrhenius behaviour.³¹ For this reason, the temperature dependence of the conductivity was determined using a Vogel-Tamman-Fulcher (VTF) equation.³⁵ The VTF parameters of the investigated mixtures are reported on the [supplementary material](#),

$$\sigma = \sigma_0 * \exp \left[\frac{-B_c}{T - T_0} \right]. \quad (4)$$

Figures 2(a) and 2(b) shows the VTF-plot for the investigated mixtures. In both figures, the Arrhenius plot of the 2G electrolyte is reported in the inset. As shown, all electrolytes containing ionic liquids display a linear behaviour. In all investigated electrolytes, the addition of 2G leads to an increase of conductivity. Nevertheless, as already discussed above, the changes in conductivity determined by the addition of 2G are markedly different in AIL, where a threshold is visible, compared to PIL-based electrolytes, where a gradual change is observed. This difference seems to indicate that the nature of the IL is influencing the ion-solvent interactions.

Figures 3(a) and 3(b) illustrate the influence of the temperature on the viscosity of the investigated electrolytes. According to Fig. 3(a), at 30 °C the Pyr₁₄TFSI displays a viscosity of 111 mPa s. This value is significantly higher than that displayed by the electrolyte containing the neat 2G, which at this

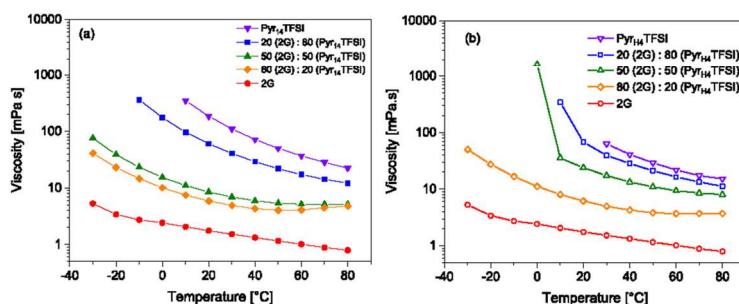


FIG. 3. Influence of the temperature on the viscosity of the (a) AIL-2G and (b) PIL-2G mixtures, all with 0.5M NaTFSI.

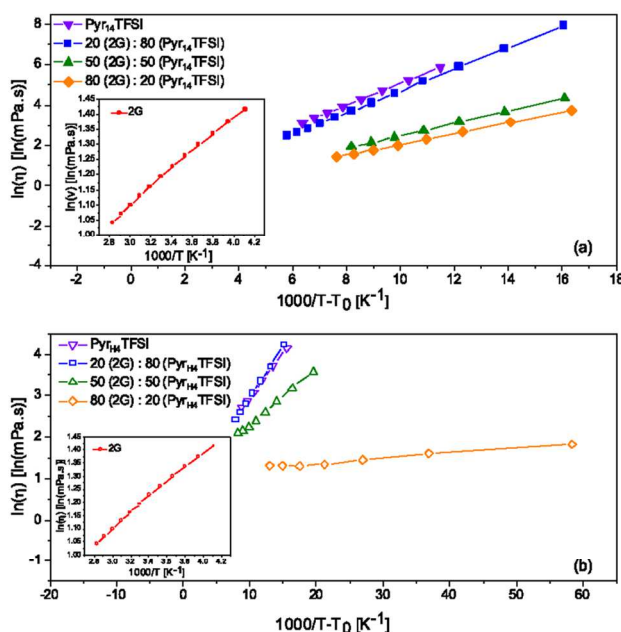


FIG. 4. VTF-plot of the viscosity curves of the (a) AIL-2G and (b) PIL-2G mixtures. The insets show the Arrhenius plot of the mixture based on pure 2G.

temperature displays a viscosity of 1.5 mPa s. The viscosity of the mixtures containing Pyr₁₄TFSI-2G is, at all investigated temperatures, lower than the one of the neat Pyr₁₄TFSI. The figure shows that the higher the amount of 2G in the electrolyte, the lower is the viscosity of the mixtures. As already observed for the conductivity measurement, a threshold of 2G concentration seems to be present. In the figure it is well visible that the mixtures containing 50% and 80% of 2G display from 80 °C till –10 °C, very similar values, which are significantly lower than that showed by the mixture containing 20% of 2G. Below –10 °C the viscosities of the two mixtures become different, but they are still an order of magnitude lower than those of the mixtures with 20% 2G. According to Fig. 3(b), in the case of the mixtures containing the Pyr_{H4}TFSI, a more gradual change of viscosity is observable, in agreement with the result observed for the conductivity. Pyr_{H4}TFSI has a melting point of 30 °C, which is higher than that of the Pyr₁₄TFSI. This higher melting point has a strong influence on the liquids range of the mixtures, which is dependent on the 2G content. The figure shows that the higher the 2G content, the lower are the viscosities and the larger the liquids range of the investigated mixtures.

As in the case of the conductivity measurements, the temperature dependence of the viscosity has also been determined via a VTF equation. The VTF parameters of the investigated mixtures are reported on the [supplementary material](#),

$$\eta = \eta_0 * \exp \left[\frac{-B_v}{T - T_0} \right]. \quad (5)$$

Figures 4(a) and 4(b) show the VTF plot for the two investigated classes of 2G-IL mixtures. As in the case of the

conductivity, the Arrhenius plot of the neat 2G based electrolytes is reported on the inset of the figure. Figure 4(a) shows that all the mixtures containing the Pyr₁₄TFSI display a linear behaviour and a marked difference between the electrolyte containing low and high amount of 2G is observed. Again, the electrolytes containing Pyr_{H4}TFSI show a more gradual change of viscosity over temperature. Nevertheless, it is interesting to notice that the mixture containing 80% 2G appears deviated from the ideal VTF behaviour. However, as it does not follow the Arrhenius behaviour, the VTF behaviour appears as the most appropriate to describe the variation of viscosity over temperature of this mixture.

Figure 5 shows a comparison of the densities of the investigated electrolytes. Overall, as visible, the higher the ionic liquid content in the mixtures, the higher their density. The density of the protic and aprotic mixtures are similar (except for the mixture containing 50% IL), due to the similar density of Pyr₁₄TFSI and Pyr_{H4}TFSI. All mixtures show a decreasing density with increasing temperature. The different behaviour between the protic and aprotic mixtures, when increasing the IL content higher than 20 mol. %, is visible here too.

B. Electrochemical characterization

1. Electrochemical stability window

Figure 6 reports the ESW of the investigated mixtures. Figure 6(a) shows that the mixture based on pure 2G and the AIL show electrochemical stabilities overall exceeding 4 V. The electrolyte containing the neat Pyr₁₄TFSI displays the larger ESW. The cathodic stability of this AIL appears

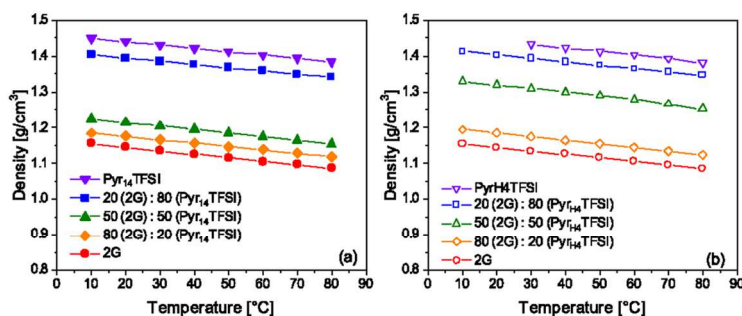


FIG. 5. Influence of the temperature on the density of the (a) AIL-2G and (b) PIL-2G mixtures, all with 0.5M NaTFSI.

to reach the Na plating potential, although a small peak at around -2 V vs. Ag is visible on the curve. On the other hand, the anodic stability of this electrolyte appears higher than 2.5 V vs. Ag, which is a value in line with those already observed for this AIL.⁷ The solution containing the neat 2G displays a marked peak at around -1.75 V vs. Ag, which might be originated by the occurrence of decomposition processes in the 2G solvent. At lower potentials, however, the current decreases and becomes more stable. The oxidation potential of this electrolyte results significantly lower than the one of the electrolyte containing the neat IL, indicating that the presence of 2G is limiting the stability of the TFSI anion. The mixtures containing 2G and Pyr₁₄TFSI display an ESW in between those of the two neat components. As shown, the mixture containing 20% of 2G shows a peak at -1.75 V vs. Ag and its cathodic limit appears to be at ca. -3 V vs. Ag. The presence of the solvent leads to a reduced anodic stability (ca. 1 V) compared to the neat AIL. When higher amounts of 2G (50% and 80%) are present in the mixtures, the intensity of the peak located at -1.75 V vs. Ag increases. At the same time, high amounts of solvent are also reducing the anodic stability of the mixtures.

The mixtures containing the protic ionic liquid Pyr_{H4}TFSI and 2G display a completely different behaviour. Figure 6(b) shows that the cathodic stability of all electrolyte containing the Pyr_{H4}TFSI is limited by the reduction of the proton of the PIL, which is occurring at ca. -1 V vs. Ag. Similar to the mixtures containing the AIL, the oxidation potential of all mixtures is decreasing with higher 2G content.

2. Operative voltage measurements

Figure 7 compares the maximum operative voltage (OPV) possible for AC-based electrodes on (a) 2G, (b) Pyr₁₄TFSI, and (c) Pyr_{H4}TFSI based electrolytes. In all cases, as for all following investigations, the OPV has been defined as the higher positive and the lowest negative potential limits, at which the efficiency of the charge-discharge was higher than 98%.

As shown, the use of these different electrolytes leads to different OPVs. As expected from the ESW results, the use of AC-based electrodes in combination with Pyr₁₄TFSI leads to the higher OPV (3.8 V). On the other hand, due to the limited cathodic stability of Pyr_{H4}TFSI, the use of this PIL in combination with AC-based electrodes leads to the smallest OPV (2.3 V). It is important to notice that the OPV observed in these two ILs are in agreement with values already reported in the literature.^{7,36} The OPV observed in 2G is equal to 3.4 V, which is a value in between those of the two IL-based electrolytes. This large OPV is somehow surprising considering the ESW of this neat solvent discussed above. Obviously, the peak observed at -1.7 V vs. Ag does not strongly affect the charge-discharge process, allowing the realization of high efficient storage process.

The nature of the electrolytes has also a strong influence on the shape of the CV curves as well as on the specific capacitance displayed by the AC-electrodes. As shown, when the Pyr₁₄TFSI is used, the AC electrodes display a capacitive behaviour, and they deliver a specific capacitance in the order of 50–60 F/g. This relative low value, which is in

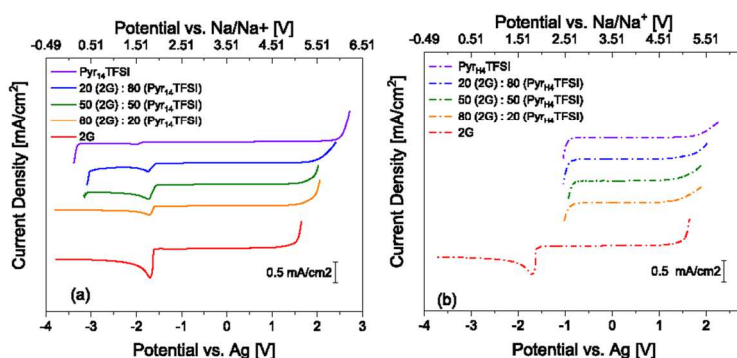


FIG. 6. ESW of the (a) AIL-2G and (b) PIL-2G mixtures, all with 0.5M NaTFSI (scan rate: 1 mV/s).

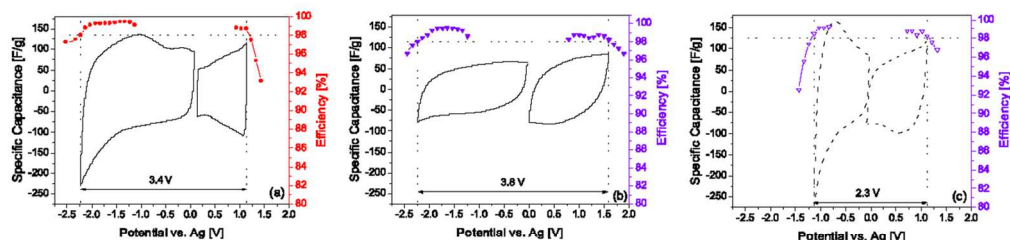


FIG. 7. Specific capacitance and Coulombic efficiency of an activated carbon electrode obtained from CV at 5 mV/s for the pure (a) 2G, (b) Py_{H4}TFSI, and (c) Py_{H4}TFSI based electrolyte, all with 0.5M NaTFSI.

agreement with those already reported for this type of carbon in similar IL-based electrolytes,³³ is obviously due to the high viscosity displayed by the electrolyte at room temperature. As shown, the use of Py_{H4}TFSI leads to the occurrence of faradic processes, evidenced by the presence of peaks on the CV, which are increasing the specific capacitance delivery by the AC electrodes (which reach values of more than 120 F/g). This behaviour and the values of specific capacitance delivered by the AC electrodes are in line with the previously reported result.³⁷ When the electrolyte containing the neat 2G is used, the AC electrode display specific capacitances of more than 100 F/g, which are possible, on the one hand, thanks to the relative high conductivity of the electrolyte (the highest among the three neat electrolytes) and, on the other hand, due to the occurrence of faradic processes, which are clearly visible in the CV profiles.

Figure 8 shows the OPVs displayed by the AC electrodes on the mixtures of Py_{H4}TFSI and 2G. In all mixtures OPVs higher than 3.5 V are possible. As visible, the oxidation potential is rather comparable in all three mixtures and in the order of 1.3–1.4 V vs. Ag. On the other hand, more marked differences can be seen for the cathodic limit. The mixture containing 20%, 50%, and 80% of 2G display an anodic limit of –2.5 V vs. Ag, –2.1 V vs. Ag and –2.3 V vs. Ag, respectively. These values indicate that there is no direct relationship between the ESW and the OPV shown by the AC electrodes. Nevertheless, the figure clearly shows that the shape of the CVs and the specific capacitance delivered by the electrode is affected by the ratio AIL/2G inside the electrolyte. Specifically, the higher the IL content, the more capacitive the CV shape. At the same time, high amounts of Py_{H4}TFSI in the mixture lead to a reduction of

the specific capacitance delivered by the AC electrodes. Obviously, this behaviour is caused by the fact that the presence of 2G improves the conductivities of the investigated mixtures but, at the same time, decreases their electrochemical stability.

Figure 9 shows the behaviour displayed by the AC electrodes in the electrolytes based on mixtures containing Py_{H4}TFSI and 2G. As shown, the OPV of the AC electrodes in these mixtures decreases with increasing solvent amount, from 2.5 V (20% 2G), over 2.1 V (50% 2G), to 1.9 V (80% 2G). This decrease of OPV is observable in both the positive and the negative limits. As visible in the figure, while the AC electrodes are stable up to –1.2 V vs. Ag in the mixture containing 20% 2G, the limit decreases to –1.0 V vs. Ag in the mixtures containing 50% and 80% of 2G. On the other hand, the positive limits for the AC electrodes in the mixtures containing 20% 2G are equal to 1.3 V vs. Ag and only 1.0 V vs. Ag for mixtures with higher solvent content. It is interesting to notice that the negative limits shown by the AC electrodes in these mixtures are smaller than those observed in neat 2G as well as in the neat Py_{H4}TFSI (see Fig. 8). Taking these results into account, it seems that the combination of these two components, especially in the case of high 2G contents, results in an unfavourable ion-solvent interaction, which is limiting both the negative and positive limits of AC-based electrodes.

As shown on the figure, the shape of the CVs shown by the AC electrodes is largely influenced by the 2G/PIL ratio. Large amounts of 2G lead to a shape similar to that observed in the neat 2G, while large amounts of PIL to those observed in the neat Py_{H4}TFSI. Different from the mixtures of 2G and

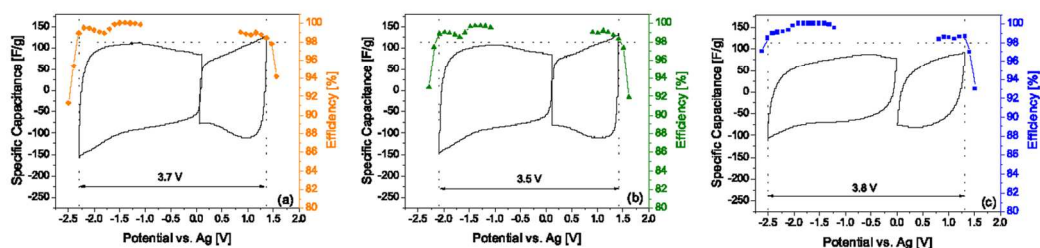


FIG. 8. Specific capacitance and Coulombic efficiency of an activated carbon electrode obtained from CV at 5 mV/s for the Py_{H4}TFSI based electrolytes with (a) 80 mol.% 2G, (b) 50 mol.% 2G, and (c) 20 mol.% 2G content, all with 0.5M NaTFSI.

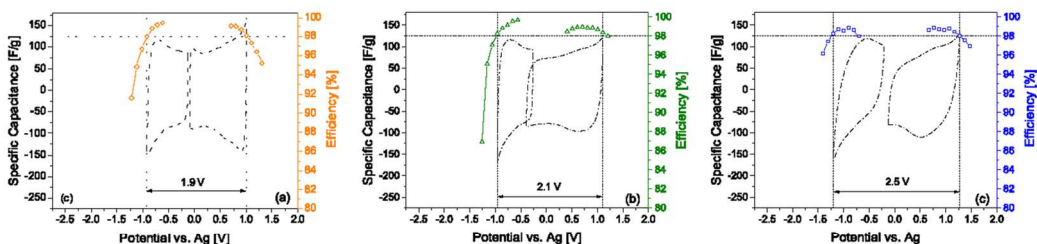


FIG. 9. Specific capacitance and Coulombic efficiency of an activated carbon electrode obtained from CV at 5 mV/s for the $\text{Pyr}_{14}\text{TFSI}$ based electrolytes with (a) 80 mol. % 2G, (b) 50 mol. % 2G, and (c) 20 mol. % 2G content, all with 0.5M NaTFSI.

AIL, the specific capacitance delivered by the AC electrodes is rather comparable on all three mixtures.

The results reported above indicated that mixtures of 2G and AIL and PIL display interesting chemical-physical properties and that they can be successfully tested in combination with AC-based electrodes. In order to investigate the use of these mixtures in electrochemical storage devices more in detail, electrochemical double layer capacitors (EDLCs) have been assembled and some preliminary test have been carried out. For this investigation, only selected mixtures, the one containing 80% 2G and 20% $\text{Pyr}_{14}\text{TFSI}$ and that containing 20% 2G and 80% $\text{Pyr}_{14}\text{TFSI}$, have been considered. The behaviour of EDLCs containing these two mixtures has been compared to that of devices containing the neat electrolytes.

Figure 10 shows the cyclic voltammograms, recorded at 5 mV/s, displayed by EDLCs containing the selected electrolytes. Figure 10(a) shows that the use of mixtures of 2G and $\text{Pyr}_{14}\text{TFSI}$ allows the realization of devices able to display

operative voltage similar to that of the neat IL, but capacitances comparable to that of the neat 2G. This behaviour, which has been already reported for mixtures of the same IL and other organic solvent, e.g., PC,¹³ confirms once more the advantage related to use of this type of electrolytes in view of the realization of high voltage IL based EDLCs. On the other hand, Fig. 10(b) shows that the use of PIL, either neat or in combination with organic solvent, does not allow the realization of high voltages. This result, which is line with those already reported in the literature, confirm that PILs are not the most promising IL for EDLC applications.

Figure 11 compares the capacitance retention shown by the EDLC containing the investigated electrolytes. As shown, due to the high viscosity of the neat ILs, the EDLC containing these electrolytes display, as expected, low capacitance retentions. On the other hand, the EDLC containing the neat 2G, due to the relative high conductivity of this electrolyte, displays good capacitance retentions toward higher current

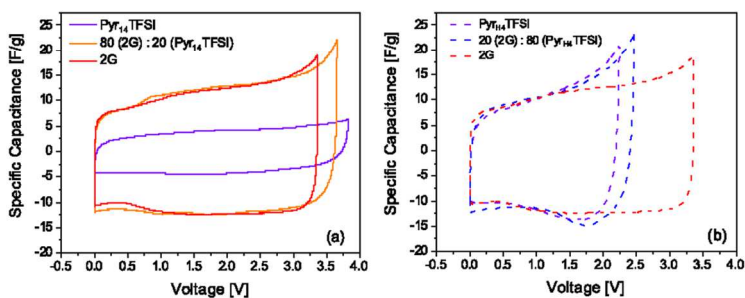


FIG. 10. Voltammetric profiles of EDLCs containing electrolytes based on (a) $\text{Pyr}_{14}\text{TFSI}$ and diglyme/(b) $\text{Pyr}_{14}\text{TFSI}$ and diglyme. Measured with 5 mV/s scan rate, all with 0.5M NaTFSI.

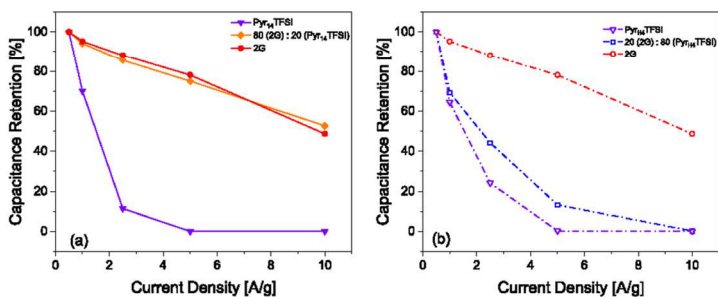


FIG. 11. Capacity retention of the capacitors containing electrolytes based on (a) $\text{Pyr}_{14}\text{TFSI}$ and diglyme/(b) $\text{Pyr}_{14}\text{TFSI}$ and diglyme, all with 0.5M NaTFSI.

densities, and at 10 A/g they are retaining 50% of their initial capacitance. When mixtures of IL and 2G are used, the capacitance retentions displayed by the EDLCs are depending on the amount of IL present in the mixture. As shown, the mixture containing the 80% IL (Py_{TH}4TFSI) displays a lower capacitance retention at 10 A/g compared to that containing only 20% IL (Py₁₄TFSI). These results, which are in agreement with those reported for other mixtures of organic solvents and ILs, clearly indicate that the ratio solvent/IL for these kind of mixtures has a strong impact on the capacitance retention and thus the power of EDLCs.

IV. CONCLUSION

In this work, we investigated the chemical physical properties of mixtures of diglyme and aprotic and protic ionic liquids having 0.5M NaTFSI as conducting salt. We showed that the conductivities and viscosities of all the investigated IL-based electrolytes fall into the typical range for electrochemical energy storage applications at room temperature and exhibit VTF behaviours. Interestingly, we observed that the nature of the IL strongly affected the properties of these mixtures. In the case of aprotic ionic liquids based mixtures, we could identify a concentration threshold for the solvent, beyond which a similar behaviour with pure 2G based electrolyte could be found. To the contrary, we found that the properties of mixtures of protic ionic liquids and 2G are changing gradually upon increased solvent concentration within the mixture. This behaviour, which might be related to the influence of the nature of the cation of the IL on the homogeneity of the mixtures, needs to be further investigated. Furthermore, in order to better understand the behaviour of these mixtures, other compositions, e.g., with high and low EG content, should also be addressed in the future. The results reported in this work show that the investigated mixtures can be successfully used in combination with AC based electrodes. We proved that the nature of the ionic liquid has a tremendous impact on the operative voltage as well as on the specific capacitance of the AC electrodes. While the use of PIL does not allow the realization of high voltage EDLCs, the use of mixtures of AIL and 2G allows the realization of high voltage EDLCs. When a proper ratio between IL/2G is used, these high voltage EDLCs can display capacitance retention comparable to the neat organic solvent up to current as high as 10 A/g.

Considering these results, mixtures of 2G and IL appear certainly as interesting electrolytes for Na-based electrochemical storage devices. Work is in progress to investigate the use of these mixtures in combination with SIB electrodes and to verify their feasibility for a use in Na-ion capacitors.

SUPPLEMENTARY MATERIAL

See [supplementary material](#) for VTF parameters of conductivity and viscosity of the different electrolytes.

ACKNOWLEDGMENTS

The authors wish to thank the Friedrich Schiller University Jena and the Deutsche Forschungsgemeinschaft (DFG) within

the project “Protic ionic liquids as electrolytes for lithium-ion batteries” for the financial support.

- ¹A. Brandt, S. Pohlmann, A. Varzi, A. Balducci, and S. Passerini, “Ionic liquids in supercapacitors,” *MRS Bull.* **38**, 554–559 (2013).
- ²M. Lazzari, M. Mastragostino, A. Pandolfo, V. Ruiz, and F. Soavi, “Role of carbon porosity and ion size in the development of ionic liquid based supercapacitors,” *J. Electrochem. Soc.* **158**, A22–A25 (2011).
- ³C. Largeot, P. Taberna, Y. Gogotsi, and P. Simon, “Microporous carbon-based electrical double layer capacitor operating at high temperature in ionic liquid electrolyte,” *Electrochem. Solid-State Lett.* **14**, A174–A176 (2011).
- ⁴V. Ruiz, T. Huynh, S. Sivakkumar, and A. Pandolfo, “Ionic liquid–solvent mixtures as supercapacitor electrolytes for extreme temperature operation,” *RSC Adv.* **2**, 5591–5598 (2012).
- ⁵J. Reiter, E. Paillard, L. Grande, M. Winter, and S. Passerini, “Physicochemical properties of *N*-methoxyethyl-*N*-methylpyrrolidinium ionic liquids with perfluorinated anions,” *Electrochim. Acta* **91**, 101–107 (2013).
- ⁶T. Tooming, T. Thornberg, L. Siinor, K. Tõnurist, A. Jänes, and E. Lust, “A type high capacitance supercapacitor based on mixed room temperature ionic liquids containing specifically adsorbed iodide anions,” *J. Electrochem. Soc.* **161**, A222–A227 (2014).
- ⁷S. Menne, M. Schroeder, T. Vogl, and A. Balducci, “Carbonaceous anodes for lithium-ion batteries in combination with protic ionic liquids-based electrolytes,” *J. Power Sources* **266**, 208–212 (2014).
- ⁸T. Vogl, S. Passerini, and A. Balducci, “The impact of mixtures of protic ionic liquids on the operative temperature range of use of battery systems,” *Electrochem. Commun.* **78**, 47–50 (2017).
- ⁹S. Menne, J. Pires, M. Anouti, and A. Balducci, “Protic ionic liquids as electrolytes for lithium-ion batteries,” *Electrochem. Commun.* **31**, 39–41 (2013).
- ¹⁰M. Ishikawa, T. Sugimoto, M. Kikuta, E. Ishiko, and M. Kono, “Pure ionic liquid electrolytes compatible with a graphitized carbon negative electrode in rechargeable lithium-ion batteries,” *J. Power Sources* **162**, 658–662 (2006).
- ¹¹A. Balducci, “Ionic liquids in lithium-ion batteries,” *Top. Curr. Chem.* **375**, 20 (2017).
- ¹²C. Arbizzani, G. Gabrielli, and M. Mastragostino, “Thermal stability and flammability of electrolytes for lithium-ion batteries,” *J. Power Sources* **196**, 4801–4805 (2011).
- ¹³R.-S. Kühnel, N. Böckenfeld, S. Passerini, M. Winter, and A. Balducci, “Mixtures of ionic liquid and organic carbonate as electrolyte with improved safety and performance for rechargeable lithium batteries,” *Electrochim. Acta* **56**, 4092–4099 (2011).
- ¹⁴S. Wilken, S. Xiong, J. Scheers, P. Jacobsson, and P. Johansson, “Ionic liquids in lithium battery electrolytes: Composition versus safety and physical properties,” *J. Power Sources* **275**, 935–942 (2015).
- ¹⁵A. Guerfi, M. Dontigny, P. Charest, M. Petitclerc, M. Lagacé, A. Vijn, and K. Zaghib, “Improved electrolytes for Li-ion batteries: Mixtures of ionic liquid and organic electrolyte with enhanced safety and electrochemical performance,” *J. Power Sources* **195**, 845–852 (2010).
- ¹⁶A. Brandt, J. Pires, M. Anouti, and A. Balducci, “An investigation about the cycling stability of supercapacitors containing protic ionic liquids as electrolyte components,” *Electrochim. Acta* **108**, 226–231 (2013).
- ¹⁷T. Vogl, S. Menne, R.-S. Kühnel, and A. Balducci, “The beneficial effect of protic ionic liquids on the lithium environment in electrolytes for battery applications,” *J. Mater. Chem. A* **2**, 8258–8265 (2014).
- ¹⁸S. Menne, T. Vogl, and A. Balducci, “Lithium coordination in protic ionic liquids,” *Phys. Chem. Chem. Phys.* **16**, 5485–5489 (2014).
- ¹⁹T. Vogl, S. Menne, and A. Balducci, “Mixtures of protic ionic liquids and propylene carbonate as advanced electrolytes for lithium-ion batteries,” *Phys. Chem. Chem. Phys.* **16**, 25014–25023 (2014).
- ²⁰U.S.-Geological-Survey; Mineral-Commodity-Summaries, Mineral-Commodity-Summaries, 2017.
- ²¹B. L. Ellis and L. F. Nazar, “Sodium and sodium-ion energy storage batteries,” *Curr. Opin. Solid State Mater. Sci.* **16**, 168–177 (2012).
- ²²M. D. Slater, D. Kim, E. Lee, and C. S. Johnson, “Sodium-ion batteries,” *Adv. Funct. Mater.* **23**, 947–958 (2013).
- ²³B. Jache and P. Adelhelm, “Use of graphite as a highly reversible electrode with superior cycle life for sodium-ion batteries by making use of co-intercalation phenomena,” *Angew. Chem., Int. Ed.* **53**, 10169–10173 (2014).
- ²⁴H. Moon, R. Tatara, T. Mandai, K. Ueno, K. Yoshida, N. Tachikawa, T. Yasuda, K. Dokko, and M. Watanabe, “Mechanism of Li ion desolvation

- at the interface of graphite electrode and glyme–Li salt solvate ionic liquids,” *J. Phys. Chem. C* **118**, 20246–20256 (2014).
- ²⁵A. Ponrouch, D. Monti, A. Boschini, B. Steen, P. Johansson, and M. Palacin, “Non-aqueous electrolytes for sodium-ion batteries,” *J. Mater. Chem. A* **3**, 22–42 (2015).
- ²⁶I. Hasa, S. Passerini, and J. Hassoun, “Characteristics of an ionic liquid electrolyte for sodium-ion batteries,” *J. Power Sources* **303**, 203–207 (2016).
- ²⁷L. Wu, A. Moretti, D. Buchholz, S. Passerini, and D. Bresser, “Combining ionic liquid-based electrolytes and nanostructured anatase TiO₂ anodes for intrinsically safer sodium-ion batteries,” *Electrochim. Acta* **203**, 109–116 (2016).
- ²⁸T. Vogl, C. Vaalma, D. Buchholz, M. Secchiarioli, R. Marassi, S. Passerini, and A. Balducci, “The use of protic ionic liquids with cathodes for sodium-ion batteries,” *J. Mater. Chem. A* **4**, 10472–10478 (2016).
- ²⁹K. Yoshida, M. Tsuchiya, N. Tachikawa, K. Dokko, and M. Watanabe, “Change from glyme solutions to quasi-ionic liquids for binary mixtures consisting of lithium bis(trifluoromethanesulfonyl) amide and glymes,” *J. Phys. Chem. C* **115**, 18384–18394 (2011).
- ³⁰M. Egashira, T. Asai, N. Yoshimoto, and M. Morita, “Ionic conductivity of ternary electrolyte containing sodium salt and ionic liquid,” *Electrochim. Acta* **58**, 95–98 (2011).
- ³¹L. Timperman, P. Skowron, A. Boisset, H. Galiano, D. Lemordant, E. Frackowiak, F. Béguin, and M. Anouti, “Triethylammonium bis(tetrafluoromethylsulfonyl) amide protic ionic liquid as an electrolyte for electrical double-layer capacitors,” *Phys. Chem. Chem. Phys.* **14**, 8199–8207 (2012).
- ³²A. Krause, P. Kossyrev, M. Oljaca, S. Passerini, M. Winter, and A. Balducci, “Electrochemical double layer capacitor and lithium-ion capacitor based on carbon black,” *J. Power Sources* **196**, 8836–8842 (2011).
- ³³S. Pohlmann, B. Lobato, T. A. Centeno, and A. Balducci, “The influence of pore size and surface area of activated carbons on the performance of ionic liquid based supercapacitors,” *Phys. Chem. Chem. Phys.* **15**, 17287–17294 (2013).
- ³⁴T. Vogl, *Chemical-Physical Investigation of Protic Ionic Liquid-Based Electrolytes* (Westfälische Wilhelms-Universität Münster, 2016).
- ³⁵J. Vila, P. Gines, J. Pico, C. Franjo, E. Jimenez, L. Varela, and O. Cabeza, “Temperature dependence of the electrical conductivity in emim-based ionic liquids: Evidence of Vogel–Tammann–Fulcher behavior,” *Fluid Phase Equilib.* **242**, 141–146 (2006).
- ³⁶P. Ruch, D. Cericola, A. Foelske-Schmitz, R. Kötz, and A. Wokaun, “Aging of electrochemical double layer capacitors with acetonitrile-based electrolyte at elevated voltages,” *Electrochim. Acta* **55**, 4412–4420 (2010).
- ³⁷S. Menne, T. Vogl, and A. Balducci, “The synthesis and electrochemical characterization of bis(fluorosulfonyl) imide-based protic ionic liquids,” *Chem. Commun.* **51**, 3656–3659 (2015).

2.2. PILs in Battery Systems

2.2.1. Publikation 5: Imidazolium-Based Protic Ionic Liquids as Electrolytes for Lithium-Ion Batteries

Besides improving the weak points of PILs by combining them with solvents, the identification of new and suitable PILs for application in electrochemical energy storage devices is of crucial importance for their development and use as electrolyte. In this work, we tried to find PILs applicable in LIBs, based on the imidazolium cation and the [TFSI]⁻ as well as [FSI]⁻ anions. This selection was based on data sets of PILs already synthesized in the past. While 1-methylimidazolium ([1-MeIm_H]) [TFSI]/[FSI], had been listed with low m.p.s below RT, the 1-2-dimethylimidazolium ([1-2-Me₂Im_H]) cation had only been synthesized with chloride and bromide anions, also with low m.p.s, indicating low ion-interactions for this cation. Since [Br]⁻ and [Cl]⁻ anions have very low ESWs, a switch to [TFSI]⁻ and [FSI]⁻ was necessary. Additionally, for [1-MeIm_H][TFSI]/[FSI], no further characterizations had been carried out, e.g., conductivity or ESW, thus no information for their application in electrochemical energy storage devices was present.

Ultimately, the four PILs, [1-MeIm_H][TFSI], [1-MeIm_H][FSI], [1-2-Me₂Im_H][TFSI] as well as [1-2-Me₂Im_H][FSI] were synthesized and fully characterized. The synthesis was carried out via the 2-step synthesis including a salt metathesis reaction as described in chapter 1.3 and the obtained PILs were confirmed via NMR spectroscopy. While both [FSI]⁻-based PILs are liquid below RT, the [TFSI]⁻-based ones are solid at RT, with [1-MeIm_H][TFSI] melting around 40 °C. Surprisingly this contradicts data available in the literature, which reports a m.p. of 9 °C, making it clear that appropriate drying of a PIL is of utter importance, since already few ppm of water will lower the m.p. drastically.

Afterwards, the chemical-physical properties of the PILs including viscosity, conductivity as well as density were evaluated. In addition to their lower m.p.s, both [FSI]⁻-based PILs show much lower viscosities compared to the [TFSI]⁻-based ones (see Figure 2 in Publikation 5). Nevertheless, [1-2-Me₂Im_H][TFSI] displays the same ionic conductivity as [1-2-Me₂Im_H][FSI], seemingly less depending on vehicular ion transport. On the other hand, [1-MeIm_H][TFSI] shows a much lower conductivity, in accordance with its high viscosity. Overall, it could be

shown that the [TFSI]⁻ anion will generally lead to higher viscosities and m.p.s, similar as the additional alkyl group in the imidazolium cation does. Nevertheless, the resulting conductivity is not only influenced by the pure ion mobility, but also ion-interactions leading to ion-pairing or possible hydrogen networks.

Regarding the electrochemical investigations, the ESW of all PILs was measured as the first step. While the cathodic limitation is nearly identical, owing to the reduction of the available proton on the imidazolium cation, the anodic stability differs slightly, depending on the employed anion. The [FSI]⁻ anion led to lower ESWs compared to the [TFSI]⁻ anion, which is in line with literature. As a next step, each PIL was employed as electrolyte in LFP half cells, using AC-based oversized counter electrodes and silver rods as quasi reference electrodes. In a preliminary C-rate test, [1-2-Me₂Im_H][FSI] and [1-2-Me₂Im_H][TFSI] were identified as most promising for this setup, being able to retain almost 50 % capacity even at 5 C. Surprisingly, [1-MeIm_H][FSI], displaying the best transport properties, was not able to deliver much capacity and capacity retention. Perhaps, the lithium-mobility within this PIL is restricted, due to an unfavorable lithium coordination.

In the last step, the stability of both [1-2-Me₂Im_H]⁺-based systems was investigated. While the [1-2-Me₂Im_H][TFSI] system was able to retain more than 80 % of the initial capacity, the [1-2-Me₂Im_H][FSI] system lost nearly all capacity after 25 cycles. Again, this could be related to a strong binding of the Li-ions within the PIL, since the insertion of the lithium into the LFP electrodes was deficient, as seen in the charge-discharge profile.

Overall, it could be shown that the identification of PILs suitable for electrochemical energy storage applications is a necessary but not trivial task. While literature data might give a first impression, it must be confirmed (especially regarding the water content) and, in most cases, completed for a full set of data regarding each PIL. Additionally, as already elaborated in the introduction, the combination of specific anions and cations leads to rather unpredictable chemical-physical-properties, due to individual interactions. While screening methods are a necessary tool in the future, trial and error methods like this study still appear as the most reliable approach for identifying new PILs.

Imidazolium-Based Protic Ionic Liquids as Electrolytes for Lithium-Ion Batteries

Timo Stettner,^[a] Florian C. Walter,^[a] and Andrea Balducci^{*[a]}

Protic ionic liquids (PILs) have been indicated as a promising class of ionic liquids (ILs) for the realization of high-performance lithium-ion batteries (LIBs). In this work we synthesize four different PILs containing the imidazolium-based cations 1,2-Dimethylimidazolium (1,2-DMim⁺) and 1-Methylimidazolium (1-Mim⁺), and the anions bis(trifluoromethanesulfonyl)imide (TFSI⁻) and bis(fluorosulfonyl)imide (FSI⁻). We show that these PILs display good conductivities and low viscosities and that they can be successfully used in combination with lithium iron phosphate (LFP) electrodes. Among the investigated electrolytes, 0.5 M LiTFSI in 1,2-DMImTFSI appears as the most promising candidate for the realization of systems with high capacity retentions at high C-rates and high cycling stabilities.

In the last decade ionic liquids (ILs) have been extensively investigated as electrolytes for electrochemical energy storage devices due to the favorable combination of properties like low viscosity, high conductivity, low flammability and low vapor pressure that these molten salts might display.^[1] Several studies showed that ILs could positively contribute to the safety of batteries, e.g. lithium-ion batteries (LIBs).^[2–5] Until now, however, the performance of IL-based systems do not match that of conventional devices containing organic liquid electrolytes.^[6] Furthermore, the cost of ILs is typically higher than that of conventional electrolytes. For this reason, further efforts are required to realize IL-based LIBs with performance and costs comparable with those of the state-of-the-art electrolytes. These efforts should be directed toward the realization of IL with designed properties for a specific device.

ILs can be divided in three subgroups: aprotic ionic liquids (AILs), protic ionic liquids (PILs) and zwitterionic ionic liquids. While the latter ones are often used in polymer gel electrolytes, in the field of batteries in general, AILs have been the most utilized subgroup.^[7–14] In the last years, however, the interest on the use of PILs as electrolytes for LIBs increased.^[6] It has been shown that PILs might display favorable transport and thermal properties, and that the presence of one or more proton(s) on the cation of these ILs, although limiting their cathodic stability, has a positive impact on the coordination of the lithium ions. This set of properties appears especially advantageous during tests at high current densities.^[15] PIL-based electrolytes have

been successfully used in combination with several cathodic materials, e.g. lithium iron phosphate (LFP), and anodic materials, e.g. graphite, used in LIBs.^[16–17] Nevertheless, many aspects related to the use of this subgroup of ILs in LIBs need to be further investigated.

So far, only a limited number of cations and anions have been utilized for the realization of PIL-based electrolytes.^[17–19] It is well known, however, that the chemical composition of the cation and the anion of ILs is dramatically affecting their properties.^[20] Therefore, investigations dedicated to the influence of the cation-anion combination on the properties of PIL-based electrolytes suitable for LIBs are of importance for the realization of devices containing these electrolytes.

Imidazolium based AILs have been intensively investigated as electrolytes for LIBs but, to the best of our knowledge, only a very limited number of studies reported the use of PIL based on this cation as electrolytes for LIBs. Nevertheless, taking into account the favorable properties of imidazolium-based ILs, their use could be of great interest for the realization of advanced LIBs. In this communication we report for the first time an investigation about a series of imidazolium-based PIL suitable for battery application containing the cations 1,2-Dimethylimidazolium (1,2-DMim⁺) and 1-Methylimidazolium (1-Mim⁺), and the anions bis(trifluoromethanesulfonyl)imide (TFSI⁻) and bis(fluorosulfonyl)imide (FSI⁻). In the first part of the manuscript, the chemical-physical properties of the electrolytes are investigated in detail. In the second part, the impact of these electrolytes on the chemical physical performance of LFP electrodes is reported.

Figure 1 shows the chemical structures of the PILs investigated in this work. For each PIL the used acronym as well as the state of aggregation at room temperature (RT) are also reported. As shown in the figure, the nature of the anion has a

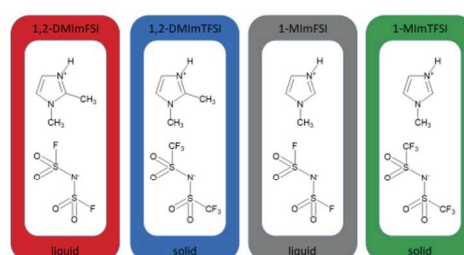


Figure 1. Overview of the synthesized and investigated PILs. The state of aggregation refers to RT.

[a] T. Stettner, F. C. Walter, Prof. A. Balducci
Institute for Technical Chemistry and Environmental Chemistry
Center for Energy and Environmental Chemistry Jena (CEEC Jena)
Friedrich-Schiller-University Jena
Philosophenweg 7 A, 07743 Jena, Germany
E-mail: andrea.balducci@uni-jena.de

strong influence on the aggregation state at room temperature. At RT the PILs containing TFSI⁻ as anion are solids, while those containing the FSI⁻ anion are liquids. A similar behavior has been also reported for pyrrolidinium based ILs and, therefore, is not surprising.¹¹⁷ It is important to notice that the state of aggregation at RT is strongly depending on the water content of the PIL. When large amounts of water (1% or more) are present in the PIL, the large majority of these compounds are liquids.^{19,21} When the content is reduced to only a few ppm, as in the case of this work, the difference in terms of aggregation state becomes visible. Unfortunately, this aspect has not been always carefully considered in the past and several PILs have been indicated as room temperature ILs even if they are not.

Figure 2 compares the conductivity, viscosity and density of the PILs investigated in this work. As shown in the figure, the nature of the anion has a strong influence on the chemical-physical properties of these ILs. Figure 2a shows that among the investigated PILs, the 1,2-DMImTFSI displays the highest viscosity over the whole investigated range of temperature (27.2 mPa s at 60 °C). The replacement of the cation 1,2-DMIm⁺ with the smaller cation 1-MIm⁺ reduces the viscosity of the PIL, but not dramatically: 1-MImTFSI displays a viscosity of 22.3 mPa s at 60 °C. To the contrary, a significant change in viscosity is observed when the smaller FSI⁻ replaces the TFSI⁻ anion. As indicated in the figure, 1,2-DMImFSI and 1-MImFSI display viscosities of 16.0 mPa s and of 15.6 mPa s, respectively, at 60 °C. These values are approx. 30% lower than those observed for the TFSI-based PILs. Considering these differences, it is reasonable to assume that the TFSI⁻ anion is responsible for higher ionic binding strengths, and thus higher viscosities, compared to the anion FSI⁻. This effect is most likely related to the bigger size of the TFSI⁻ anion, which facilitates the sterical matching between anion and cation.¹²² Figure 2b shows a comparison of the conductivities of the investigated PILs. As shown, 1-MImFSI displays the highest conductivity over the whole temperature range. At 60 °C, it displays a conductivity of 20.8 mS/cm. At 30 °C this PIL displays a conductivity of 9.5 mS/cm,

a value comparable to that of conventional electrolytes for LIBs.²³ On the other hand, 1-MImTFSI shows the lowest conductivity among all the PIL, with values of 3.1 mS/cm and 8.2 mS/cm at 30 °C and 60 °C, respectively. Taking these differences into account, the presence of the anion TFSI⁻ appears to have a rather strong (and negative) impact on the conductivity of PILs containing the cation 1-MIm⁺. It is interesting to notice, however, that this impact appears much less significant when the cation 1,2-DMIm⁺ is used. As shown in the figure, at 60 °C 1,2-DMImTFSI and 1,2-DMImFSI display conductivities of 14.9 mS/cm and 14.8 mS/cm, respectively. Taking these results into account it seems that the cation 1,2-DMIm⁺ influences the conductivity much more than the cation 1-MIm⁺. In order to confirm this assumption, however, a systematic investigation of the properties of PILs containing these cations and different anions would be necessary. This study, nevertheless, is out of the scope of the present work. Figure 2c compares the variation of the density over temperature of the investigated PILs. As shown, the 1-MIm⁺ based PILs display a higher density than the corresponding 1,2-DMIm⁺ PILs. Additionally, the PILs containing TFSI⁻ have a higher density compared to that containing the anion FSI⁻. This latter finding could be related to the higher viscosity of the TFSI⁻ anion.

Figure 3 shows a comparison of the electrochemical stability window (ESW) of the investigated PILs. As shown, in all PILs the cathodic limit is located around -0.6 to -0.65 V vs. Ag. This limit is obviously defined by the reduction of the proton in the cation of the PIL. From the results reported in the figure, it is evident that the different number of methyl groups present on the imidazolium cations used in this work does not seem to have an impact on the stability of the “free” proton. The anodic limit of the PIL is related to the nature of the anion and, as shown, the TFSI-based are slightly more stable than the FSI-based PILs. This result is in line with the results available in literature.¹¹⁷ 1,2-DMImFSI decomposes around 1.9 V vs. Ag, while all other PILs appear to be stable up to 2.0 V vs. Ag. Consequently, the overall ESW of this latter PIL is of approx. 2.55 V, while those of all the others amounts to approx. 2.75 V.

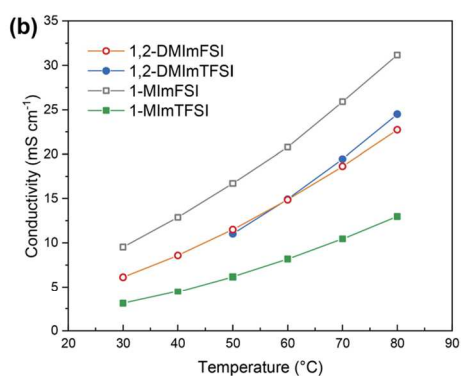


Figure 2. Influence of the temperature on the (a) viscosity, (b) conductivity, and (c) density of the PIL investigated in this work.

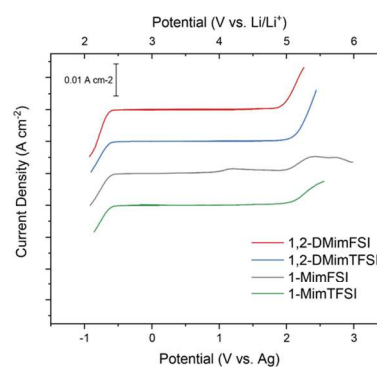


Figure 3. Electrochemical stability window of the pure synthesized PILs at 60 °C.

These values are slightly lower than those observed for pyrrolidinium based PIL.^[24] A similar trend has been also reported for AILs.^[25]

After the chemical-physical investigation described above, all the PIL have been mixed with 0.5 M LiTFSI to realize electrolytes suitable for a use in combination with LFP electrodes. After some initial test CVs which have been carried out to guarantee a good wetting of the LFP electrodes (results not shown), a C-rate test at 60 °C has been carried out. The results of these tests are reported in Figure 4. At 0.5 C the LFP

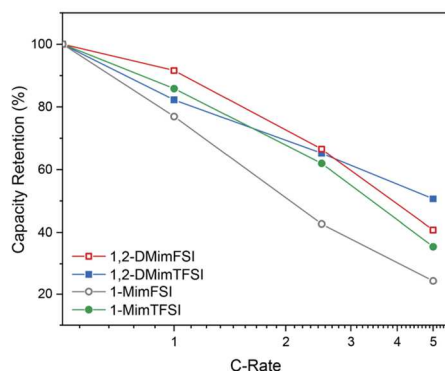


Figure 4. Capacity retention over increasing C-rate of LFP electrodes used in combination with electrolyte containing 0.5 M LiTFSI in PIL. The tests have been carried out at 60 °C.

electrodes display in 0.5 M LiTFSI in 1,2-DMImTFSI, 0.5 M LiTFSI in 1,2-DMImFSI, 0.5 M LiTFSI in 1-MImTFSI and 0.5 M LiTFSI in 1-MImFSI specific capacities of 158 mAh g⁻¹, 167 mAh g⁻¹, 113 mAh g⁻¹ and 143 mAh g⁻¹, respectively. These values indicate that in the investigated electrolyte the LFP electrodes can deliver good capacities, comparable or even higher of those observed in AILs or other PILs.^[17] When the C-rate is increased, the electrode capacity decreases, as expected. In spite of this, it is interesting to notice that overall the use of these PIL-based electrolytes allows a good retention capacity during tests carried out at high current densities. Among the investigated electrolytes, 0.5 M LiTFSI in 1,2-DMImTFSI appears as the most promising. The LFP electrode cycles in this electrolyte were able to retain more than 90% of their initial capacity at 1 C, and more than 50% at 5 C. For this reason, we decided to further investigate the behavior of the LFP electrodes in this electrolyte. In order to get information about the influence of the anion of the PIL on the electrochemical performance of LFP electrode, also the electrolyte 0.5 M LiTFSI in 1,2-DMImFSI has been considered.

Figure 5a shows a comparison of the capacity retention of LFP electrodes over 100 charge-discharge cycles carried out at 1 C and at 60 °C. As shown, the LFP electrode used in combination with 0.5 M LiTFSI in 1,2-DMImFSI was not displaying a good capacity retention, and after 25 cycles this electrode

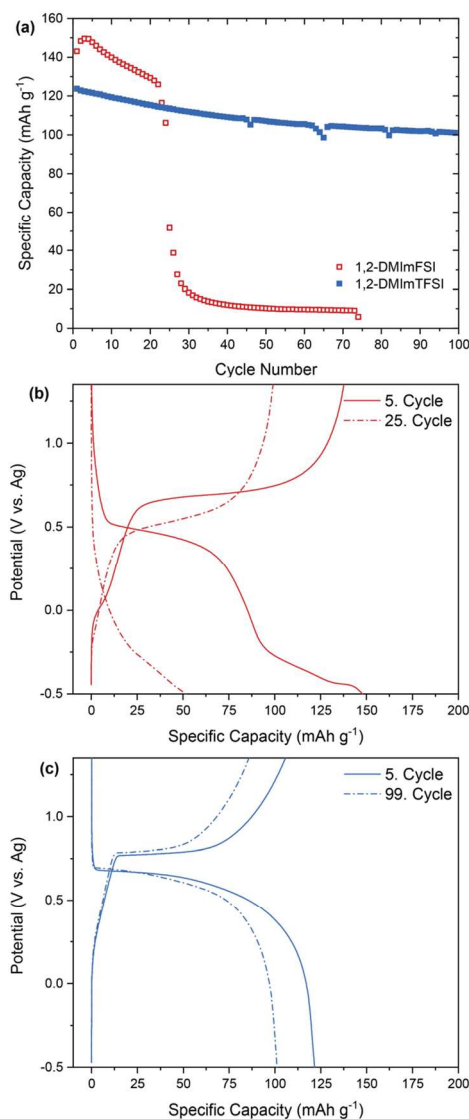


Figure 5. (a) Specific Capacity of LFP electrodes during test carried out at 60 °C and 1 C in combination with 0.5 M LiTFSI in 1,2-DMImFSI and 0.5 M LiTFSI in 1,2-DMImTFSI; (b) and (c) charge-discharge profiles of the LFP electrodes in the investigated electrolytes.

was not able to display a decent capacity. As shown in Figure 5b, this capacity fade was originated by the occurrence of (parasitic) reactions during the cycles, which were strongly reducing the efficiency of the charge-discharge process. To the contrary, the LFP electrode cycled in 0.5 M LiTFSI in 1,2-DMImTFSI was displaying a much more stable behavior, and it

was able to retain more than 80% of its initial capacity after 100 cycles. During the whole duration of the cycling process, no parasitic reactions were observed, and the efficiency of the charge-discharge was always close to 100% (Figure 5c). It has been shown that TFSI-based IL are typically displaying higher thermal stability compared to the FSI-based one⁶¹, and this difference could be one of the reasons of the better stability observed in 1,2-DMImTFSI. Study about this important point are currently in progress.

The realization of designed ILs is of crucial importance for the introduction of this class of electrolytes in electrochemical energy storage devices. In this manuscript we reported the chemical physical properties of four different imidazolium-based PILs, and we showed that these ILs display promising transport properties. Furthermore, we showed that despite their rather limited ESW, they can be successfully used as electrolytes for LIBs. Among the investigated PIL-based electrolytes 0.5 M LiTFSI in 1,2-DMImTFSI appears as the most promising. LFP electrodes utilized in combination with this electrolyte can deliver high capacity at low as well as at high C-rates and a good capacity retention during prolonged charge-discharge cycles carried out at 1 C and 60 °C. Further investigations are certainly needed to better understand the impact of imidazolium-based PILs on the electrochemical performance of other active cathodic and anodic active materials. Nevertheless, these results confirm that PILs can be seen as an interesting class of electrolyte for the realization of high-performance solvent-free LIBs.

Experimental

Synthesis of PILs

The PILs have been synthesized with a procedure similar to that reported in reference²⁶¹. The freshly distilled precursor, either 1,2-dimethylimidazole, or 1-methylimidazole (59.34 mmol, obtained by Aldrich) was put in a two-neck flask, topped by a reflux condenser and a dropping funnel. The latter one was filled with 5.35 ml HCl (35%, obtained by Merck). While dropping the HCl slowly to the precursor, the reaction mixture was stirred and cooled using an ice bath. After complete addition, the mixture was stirred at room temperature for 2 hours. Residual water was then evaporated using vacuum, to obtain a white salt, which was put into the two-necked flask for the next step. The flask was equipped with a reflux condenser and a dropping funnel. LiTFSI or LiFSI (59.34 mmol, obtained by Iolitec) was solved in 20 ml H₂O, filled into the dropping funnel and slowly dropped into the flask. Two phases were obtained during this metathesis, an aqueous on top and the PIL below. After complete addition and 2 h further stirring, the aqueous phase was removed using a separation funnel. To make sure no residual by-product LiCl was solved in the PIL, it was washed with water five times consecutively. The wash water was mixed with AgNO₃ to verify LiCl absence. As a last step, the PIL was dried under vacuum (10⁻³ mbar) and at 80 °C for three days. Following this procedure the PILs 1,2-dimethylimidazolium bis(trifluoromethanesulfonyl)imide (1,2-DMImTFSI), 1,2-dimethylimidazolium bis(fluorosulfonyl)imide (1,2-DMImFSI), 1-methylimidazolium bis(trifluoromethanesulfonyl)imide (1-MImTFSI) and 1-methylimidazolium bis(fluorosulfonyl)imide (1-MImFSI) were obtained. All PILs

display water contents lower than 30 ppm, as determined using Karl Fischer titration.

Electrolyte Preparation

Electrolytes containing the synthesized PILs and 0.5 M LiTFSI (Iolitec) have been prepared in an MBraun LABmaster^{pro} ECO glove box with <1 ppm H₂O and <1 ppm O₂. The water content of all electrolytes was lower than 30 ppm.

Chemical-Physical-Characterisation

The conductivities of the electrolytes were measured using a potentiostat ModuLabXM (Solartron analytical) in the temperature range comprised between -30 and 80 °C.²⁷¹ The viscosity of the electrolytes was determined using a rheometer MCR 102 (Anton Paar) in the temperature range comprised between -30 and 80 °C.²⁷¹ The density of the electrolytes was determined in the temperature range comprised between 10 and 80 °C, using a density meter DMA 4100 M (Anton Paar).

Electrode Preparation

LFP composite electrodes were prepared following a procedure identical to that used by Menne et al.²⁸¹ The dry composition of the electrodes is 85 wt% of active material (LFP, Südcemie) 10 wt% of conducting agent (Super C65, Imerys) and 5 wt% of binder (carboxymethyl cellulose, Dow). The mass loading of the electrodes is comprised between 2.5 mg/cm² and 3.2 mg/cm²; the electrode area was equal to 1.13 cm².

As (oversized) counter electrodes, activated carbon-based electrodes were used. The electrodes were prepared following the procedure indicated in reference²⁹¹. The electrodes composition is 90 wt% of activated carbon (DLC Super, Norit), 5 wt% of carbon Black (Super C65, Imerys) and 5 wt% of binder (polytetrafluoroethylene, Aldrich). The mass loading of these electrodes is about 40 mg/cm², and their area 1.33 cm².

Electrochemical Measurements

The ESWs of the electrolytes were measured in a Swagelok cell using a platinum electrode as working electrode, an oversized carbon electrode as counter electrode, and a silver electrode as pseudo reference electrode. 150 µl of the pure synthesized PILs have been utilized. After a 1.5-hour open circuit voltage (OCV) measurement (needed to reach an equilibrium), the cells were swept from OCV towards either positive or negative direction using a scan rate of 1 mV/s. Since one of the investigated electrolytes (1-MImTFSI) was liquid only above 60 °C, all the ESW measurements have been carried out in an oven at 60 °C, to make a fair comparison between the PILs possible.

The electrochemical behavior of the LFP electrodes in the PIL-based electrolytes has been investigated in a Swagelok cell. In the case of these measurements, the LFP working electrode was coupled with an oversized carbon counter electrode. As reference, a silver electrode was used. 150 µl of the prepared 0.5 M LiTFSI in PIL has been used as electrolyte. The first step of the measurements has been an OPV measurement for 8 hours. Afterwards, 10 cycles of cyclic voltammetry (CV) were carried out using a scan rate of 5 mV/s. Subsequently, the LFP electrodes were charged-discharged using C-rates ranging from 0.5 C to 5 C. For this test, the theoretical capacity of LFP (170 mAh g⁻¹) was used to define 1 C. Finally, tests at 1 C were carried out to investigate the electrode stability over

cycling. All the electrochemical tests have been carried out in an oven at 60 °C.

Acknowledgments

The authors wish to thank the Friedrich Schiller University Jena and the Deutsche Forschungsgemeinschaft (DFG) within the project "Protic ionic liquids as electrolytes for lithium-ion batteries" for the financial support.

Conflict of Interest

The authors declare no conflict of interest.

Keywords: electrolytes · imidazolium · lithium-ion batteries · lithium iron phosphate · protic ionic liquids

- [1] J. Kalhoff, G. G. Eshetu, D. Bresser, S. Passerini, *ChemSusChem* **2015**, *8*, 2154–2175.
- [2] M. Armand, F. Endres, D. R. MacFarlane, H. Ohno, B. Scrosati, in *Materials For Sustainable Energy: A Collection of Peer-Reviewed Research and Review Articles from Nature Publishing Group*, World Scientific, **2011**, pp. 129–137.
- [3] D. R. MacFarlane, N. Tachikawa, M. Forsyth, J. M. Pringle, P. C. Howlett, G. D. Elliott, J. H. Davis, M. Watanabe, P. Simon, C. A. Angell, *Energy Environ. Sci.* **2014**, *7*, 232–250.
- [4] C. Arbizzani, G. Gabrielli, M. Mastragostino, *J. Power Sources* **2011**, *196*, 4801–4805.
- [5] S. Wilken, S. Xiong, J. Scheers, P. Jacobsson, P. Johansson, *J. Power Sources* **2015**, *275*, 935–942.
- [6] A. Balducci, *Top. Curr. Chem.* **2017**, *375*, 20.
- [7] J.-H. Shin, W. A. Henderson, S. Passerini, *Electrochem. Commun.* **2003**, *5*, 1016–1020.
- [8] P. C. Howlett, D. R. MacFarlane, A. F. Hollenkamp, *Electrochem. Solid-State Lett.* **2004**, *7*, A97–A101.
- [9] A. Lewandowski, A. Świdwerska-Mocek, *J. Power Sources* **2009**, *194*, 601–609.
- [10] M. Ishikawa, T. Sugimoto, M. Kikuta, E. Ishiko, M. Kono, *J. Power Sources* **2006**, *162*, 658–662.
- [11] K. Francis, C.-W. Liew, S. Ramesh, K. Ramesh, *Ionics* **2016**, *22*, 919–925.
- [12] J. Vélez, L. Álvarez, C. del Río, B. Herradón, E. Mann, E. Morales, *Electrochim. Acta* **2017**, *241*, 517–525.
- [13] S. Tröger-Müller, J. Brandt, M. Antonietti, C. Liedel, *Chemistry–A European Journal* **2017**, *23*, 11810–11817.
- [14] S. Tröger-Müller, M. Antonietti, C. Liedel, *Phys. Chem. Chem. Phys.* **2018**, *20*, 11437–11443.
- [15] T. Vogl, S. Menne, R.-S. Kühnel, A. Balducci, *J. Mater. Chem. A* **2014**, *2*, 8258–8265.
- [16] S. Menne, M. Schroeder, T. Vogl, A. Balducci, *J. Power Sources* **2014**, *266*, 208–212.
- [17] S. Menne, T. Vogl, A. Balducci, *Chem. Commun.* **2015**, *51*, 3656–3659.
- [18] S. Menne, J. Pires, M. Anouti, A. Balducci, *Electrochem. Commun.* **2013**, *37*, 39–41.
- [19] A. Brandt, J. Pires, M. Anouti, A. Balducci, *Electrochim. Acta* **2013**, *108*, 226–231.
- [20] J. G. Huddleston, A. E. Visser, W. M. Reichert, H. D. Willauer, G. A. Broker, R. D. Rogers, *Green Chem.* **2001**, *3*, 156–164.
- [21] N. Böckenfeld, M. Willeke, J. Pires, M. Anouti, A. Balducci, *J. Electrochem. Soc.* **2013**, *160*, A559–A563.
- [22] O. Borodin, W. Gorecki, G. D. Smith, M. Armand, *J. Phys. Chem. B* **2010**, *114*, 6786–6798.
- [23] M. Ding, K. Xu, S. Zhang, K. Amine, G. Henriksen, T. Jow, *J. Electrochem. Soc.* **2001**, *148*, A1196–A1204.
- [24] T. Vogl, P. Goodrich, J. Jacquemin, S. Passerini, A. Balducci, *J. Phys. Chem. C* **2016**, *120*, 8525–8533.
- [25] M. Galiński, A. Lewandowski, I. Stepniak, *Electrochim. Acta* **2006**, *51*, 5567–5580.
- [26] L. Timperman, P. Skowron, A. Boisset, H. Galiano, D. Lemordant, E. Frackowiak, F. Béguin, M. Anouti, *Phys. Chem. Chem. Phys.* **2012**, *14*, 8199–8207.
- [27] R.-S. Kühnel, N. Böckenfeld, S. Passerini, M. Winter, A. Balducci, *Electrochim. Acta* **2011**, *56*, 4092–4099.
- [28] S. Menne, R.-S. Kühnel, A. Balducci, *Electrochim. Acta* **2013**, *90*, 641–648.
- [29] S. Pohlmann, B. Lobato, T. A. Centeno, A. Balducci, *Phys. Chem. Chem. Phys.* **2013**, *15*, 17287–17294.

Manuscript received: October 2, 2018
Revised manuscript received: November 5, 2018
Accepted manuscript online: November 5, 2018
Version of record online: November 29, 2018

2.2.2. Publikation 6: Enabling safe and stable Li metal batteries with protic ionic liquid electrolytes and high voltage cathodes

In the past, graphite and HC have been successfully employed in combination with PIL-based electrolytes, relying on the addition of VEC.[173] In this work we employ vinylene carbonate (VC) to reversibly cycle lithium-metal anodes in liquid PIL-based electrolytes in combination with a cathode based on NMC and LFP, respectively.

To find the optimal PIL based electrolyte for this setup, a comparison between $[\text{Pyr}_{\text{H4}}][\text{TFSI}]$ and $[\text{Pyr}_{\text{H4}}][\text{FSI}]$ has been carried out. The electrolyte is composed of a PIL:salt (LiTFSI/LiFSI) ratio of 4:1 with the addition of 10 wt% VC.

It has been observed that while the $[\text{FSI}]^-$ -based electrolyte displayed better transport properties and a lower m.p., the $[\text{TFSI}]^-$ -based electrolyte offers a slightly higher anodic stability. Usually, both electrolytes are limited to 2 V vs. Li^+/Li , however, with the addition of VC, lithium plating below 0 V vs. Li^+/Li is observed. Simple symmetrical lithium-metal cells were cycled using each electrolyte, showing reversible lithium-plating and -stripping in both cases. However, the cell using the $[\text{TFSI}]^-$ -based electrolyte is showing higher resistivities, which could hamper its performance in a LIB device.

This is confirmed in cells consisting of a Li-metal anode and a LFP cathode. While the cell cycled in the $[\text{TFSI}]^-$ -based electrolyte is not able to retain any capacity after only a few cycles, the cell cycled in the $[\text{FSI}]^-$ -based electrolyte is displaying a stable performance over prolonged cycling, even when increasing the C-rate.

After the LFP cathode material, NMC, working at even higher potentials, was tested in the $[\text{FSI}]^-$ -based electrolyte with the aim to increase the energy density. As in the case of the LFP cathode, the NMC electrode could be cycled with high stability but with even better power performance.

Finally, the protic $[\text{Pyr}_{\text{H4}}][\text{FSI}]$ -based electrolyte was compared to its aprotic “counterpart” $[\text{Pyr}_{14}][\text{FSI}]$ in combination with a lithium-metal/NMC cell. While both cells are stable over prolonged cycling, the former shows a higher rate capability. This may be due to the improved Li-ion mobility within PILs compared to AILs, as explained in chapter 1.7.2.



Contents lists available at ScienceDirect

Journal of Power Sources

journal homepage: www.elsevier.com/locate/jpowsour

Perspective

Enabling safe and stable Li metal batteries with protic ionic liquid electrolytes and high voltage cathodes

Gabriele Lingua^a, Marisa Falco^a, Timo Stettner^b, Claudio Gerbaldi^{a,*}, Andrea Balducci^{b,**}

^a GAME Lab, Department of Applied Science and Technology (DISAT), Politecnico di Torino, C.so Duca Degli Abruzzi 24, 10129, Torino, Italy

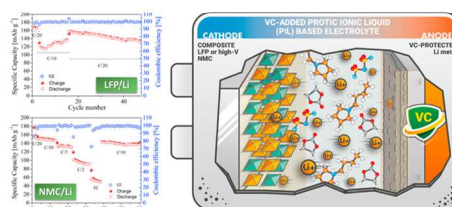
^b Friedrich-Schiller-University Jena, Institute for Technical Chemistry and Environmental Chemistry, Center for Energy and Environmental Chemistry Jena (CEEC Jena), Philosophenweg 7a, 07743, Jena, Germany



HIGHLIGHTS

- First ever example of lithium metal cell operated with protic ionic liquid (PIL).
- Vinylene carbonate (VC) electro-polymerised during cycling for Li metal protection.
- VC-added PIL-based electrolytes enable Li-metal cells with both LFP and 4-V class NMC.
- Stable cycling at high capacity of PIL-VC Li metal cells up to 1C at RT.
- High energy density, low-cost PIL-based Li metal batteries may turn into industrial reality.

GRAPHICAL ABSTRACT



ARTICLE INFO

Keywords:

Protic ionic liquid
Vinylene carbonate
Lithium battery
Lithium metal protection
High voltage cathode

ABSTRACT

Here, we present first examples of lithium metal cells stable and safely operating with $\text{PYR}_{44}(\text{TFSI}^-/\text{FSI}^-)$ -based protic ionic liquid (PIL) electrolytes, which is accomplished by encompassing vinylene carbonate (VC) in the PIL-salt solution. VC not only enhances the stability window of PIL electrolytes; it also undergoes electrochemical decomposition during initial cycling, thus creating a protective barrier at the electrolyte/electrode interface. The protective film prevents degradation at the Li metal anode due to hydrogen release, as well as at the cathode side at anodic potential. Materials and related devices are investigated in terms of their main physico-chemical characteristics, ionic conductivity, compatibility with the Li metal electrode, and electrochemical behavior by impedance spectroscopy, cyclic voltammetry and galvanostatic cycling. Newly designed electrolyte formulations enable direct cycling of Li-metal cells with PILs to achieve excellent stability with both standard LFP and 4-V class NMC-based cathodes, almost full capacity ($\geq 160 \text{ mAh g}^{-1}$) and highly reversible operation at ambient temperature and different current rates up to 1C. The PIL-VC based cell outperforms the corresponding bare PIL electrolyte as well as the aprotic $\text{PYR}_{14}\text{TFSI}$ based cells, thus enlightening a feasible strategy to suppress the high reactivity of PILs towards alkali metals; along with the use of appropriate materials, this may turn high energy density, low-cost PIL-based Li-metal batteries into industrial reality in the coming years.

* Corresponding author.

** Corresponding author.

E-mail addresses: claudio.gerbaldi@polito.it (C. Gerbaldi), andrea.balducci@uni-jena.de (A. Balducci).

<https://doi.org/10.1016/j.jpowsour.2020.228979>

Received 16 July 2020; Received in revised form 16 September 2020; Accepted 22 September 2020

Available online 30 September 2020

0378-7753/© 2020 Elsevier B.V. All rights reserved.

1. Introduction

In the forthcoming decade, the growth in electrification of modern society will mainly be driven by the irreversible deployment towards decarbonization in many critical sectors: large investments for the exploitation of renewable energy resources are increasing worldwide, with particular attention to wind and solar power energy plants, which are the most mature technologies [1]. In this scenario, batteries are identified as high-performance systems that can efficiently store and deliver energy on demand along with reducing the carbon footprint of the transportation sector, stabilize the power grid and support a wide range of strategic industries [2]. Lithium-ion batteries (LIBs) are nowadays one of the most important energy storage devices. LIBs are already dominating the portable consumer electronic market and have been indicated as the most promising electrochemical devices for the realization of hybrid-electric, plug-in and full electric vehicles, as well as for advanced delocalized energy storage units [3]. The commercially available LIBs contain electrolytes based on organic carbonate mixtures (e.g., ethylene carbonate - EC, and diethyl or dimethyl carbonate - DEC/DMC). These electrolytes show high ionic conductivity, excellent wetting properties and low charge-transfer resistance at the interface with the active materials [4]. However, the presence of flammable and volatile organic solvents accounts for serious safety hazards, including leakage, auto-combustion and/or explosion in abusive conditions [5]; these features are also accompanied by serious environmental issues, such as pollution of soil/water sources and human health, especially at the end of the battery life without proper recycling/remanufacturing [6].

These issues are prompting research on the development of new electrolyte materials. In this scenario, ionic liquids (ILs) are considered amongst the most promising candidates to replace conventional organic liquid electrolytes [7]. ILs are an interesting class of salts having melting points lower than 100 °C, with major advantages over organic solvents, which include negligible vapour pressure at low/moderate temperature, high chemical and thermal stability, and, in some cases, hydrophobicity; as a result, they are considered safe due to non-flammability, and they have also attracted great attention for use as “green” solvents in chemical reactions [8–10].

Synthesis procedures of several families of aprotic ILs (AILs) have already been deeply studied and optimized [11–13], as well as their energy application as electrolytes or electrolyte components for electrochemical devices - including rechargeable batteries, fuel cells, double-layer capacitors and hybrid supercapacitors - due to their high ionic conductivity and electrochemical stability [14–19]. Nevertheless, a subset family of ILs, called protic ionic liquids (PILs), is receiving increasing attention in recent years, as they possess all the attractive features of AILs, but, in addition, they are typically cheaper and easier to prepare, thus more sustainable [20,21]. PILs are synthesized via direct neutralization reactions of a Brønsted acid (proton donor) and a Brønsted base (proton acceptor) [14], resulting in most cases in a nitrogen-containing organic cation singly or doubly protonated with a corresponding counter anion. The main advantage of PILs over AILs is the presence of less shielded cations in the former ones, intrinsically responsible for the “cation competition effect”, which, in a mixture of PIL-Li salts, results in loosely coordinated Li⁺ ions along with improved mobility [22,23].

The use of PILs as electrolytes in LIBs is rather recent [24], and their use in high-energy Li metal battery has never been considered so far because of the presence of acidic protons, which are strongly reactive towards the Li metal electrode. It is well known that Li metal is the ultimate choice for the anode amongst all possible candidates, because it has the highest theoretical capacity (3860 mAh g⁻¹) and lowest electrochemical potential (-3.04 V vs. the standard hydrogen electrode) [3, 25–27]. Furthermore, the Li metal anode is the core of Li-S and Li-air systems, both of which are being intensively studied for next-generation energy-storage applications [28], and it allows the

intriguing opportunity of reaching the maximum energy density achievable by Li metal cells operating with high voltage cathodes (e.g., LMNO, LiCoPO₄, NMC at very low Co content or Li-rich NMC) [29,30]. Therefore, the combination of PILs as electrolyte components with the Li metal anode is still a great challenge, possibly leading to high-energy density devices, with improved performances compared to the systems with AILs, mostly due to the enhanced mobility of Li⁺. Considering all the above mentioned attractive features of PILs, the introduction of this (these) innovative electrolyte(s) could be of importance for the development of safe and cheaper IL-based Li-metal batteries, thus establishing new market opportunities.

In this work, we report for the first time the use of pyrrolidinium-based PILs with Li metal as anode in two different lithium metal battery configurations, using either lithium iron phosphate (LFP) or lithium nickel manganese cobalt oxide (NMC) as cathodes. The electrolytes consist of solutions of *N*-butylpyrrolidinium-bis(trifluoromethanesulfonyl)imide (PYR_{H4}TFSI) or *N*-butylpyrrolidinium-bis(fluorosulfonyl)imide (PYR_{H4}FSI) in combination with lithium bis(trifluoromethanesulfonyl)imide (LiTFSI) or lithium bis(fluorosulfonyl)imide (LiFSI), respectively. The electrolyte solutions are combined with vinylene carbonate (VC) that has the fundamental purpose of promoting the formation of a stable protective layer on the Li metal anode, preventing detrimental reactions due to the protic ILs, by means of electrochemically induced reductive decomposition upon initial cycling [31, 32]. Within this work, remarkably stable ambient temperature cycling at different current regimes is firstly demonstrated even with >4 V class NMC composite cathodes, as well as in comparison with the corresponding AIL-based cells.

2. Experimental

2.1. Synthesis of protic ionic liquids (PILs) and PIL-based electrolyte solutions

N-butylpyrrolidinium-bis(trifluoromethanesulfonyl)imide (PYR_{H4}TFSI) and *N*-butylpyrrolidinium-bis(fluorosulfonyl)imide (PYR_{H4}FSI) were synthesized following similar procedures described elsewhere [14,33]. In a first step, the yellowish precursor 1-butylpyrrolidine (98%, obtained by Aldrich) was distilled at 60 °C and 20 mbar. After the distillation, the resulting colorless 1-butylpyrrolidine (25 mmol) was put in a two-neck flask equipped with a magnetic stirrer and a dropping funnel filled with 5.35 ml of HCl (35%), topped by a reflux condenser. The reaction flask was placed in an ice bath and HCl (in molar excess) was added dropwise under continuous stirring. After the addition, the ice bath was removed and the solution was stirred for 2 h at ambient temperature. Residual water and reactants were removed under reduced pressure, leaving 1-butylpyrrolidine-chloride as a solid.

The 1-butylpyrrolidine chloride (25 mmol) was dissolved in 8 ml of H₂O and then put into a two-neck flask equipped with the same setup used for the first synthesis step. In order to get the final TFSI and FSI PILs, equimolar amounts of LiTFSI (99.95%, from Aldrich, now Merck) or LiFSI (99.95%, from Aldrich, now Merck), respectively, were dissolved in 18 ml of H₂O and filled into the dropping funnel. In both cases, the lithium salt solution was added dropwise to the 1-butylpyrrolidine chloride solution while keeping stirring. The solution was stirred for 3 h to ensure complete anion exchange. At the end of the reaction, a separating funnel was used to remove the aqueous phase from the organic one. Subsequently, the protic ionic liquids were washed six times with water, to remove residual LiCl. To test on complete removal, AgNO₃ was added to the washing water. LiCl reacts with AgNO₃ to AgCl, which is poorly soluble, so the absence of a precipitation confirms the complete removal of LiCl. As a last step, residual water was removed by reduced pressure and heating (60 °C, 3.0 × 10⁻³ mbar).

In an Ar-filled dry glove box (MBraun UniLab, O₂ and H₂O < 1 ppm), two liquid electrolyte solutions were prepared, hereafter named H₄TFSI and H₄FSI, consisting in LiTFSI or LiFSI (both battery-grade, from

Solvionic, vacuum-dried at 150 °C for 48 h, and at 70 °C for 24 h before use, respectively) dissolved in Py₁H₄TFSI or Py₁H₄FSI PILs (vacuum-dried at 60 °C for 48 h) to obtain one fully TFSI⁻ and one fully FSI⁻ anion based solution, respectively. In both cases, the molar ratio between the PIL and the corresponding Li salt is 4:1, which was selected, being the one with highest lithium salt concentration without crystalline phase formation, avoiding detrimental effect to battery cycling [34].

The solutions were stirred for several hours at 30 °C until complete salt dissolution. A portion of each of the above mentioned solutions was added with 10 wt% of vinylene carbonate - VC (battery grade, *Solvionic*, used as received), followed by stirring to ensure homogeneity of the resulting solutions, hereafter named H₄TFSI-VC and H₄FSI-VC. The four PIL-based electrolyte solutions were safely stored in the dry glove box.

2.2. Characterisation techniques

The ionic conductivity of the electrolytes was measured using a potentiostat *ModuLabXM (Solartron analytical)* in the temperature range between -30 and 80 °C. The samples were placed in sealed cells with Pt plated electrodes. The conductivity values were calculated from the dielectric measurements following the method reported by Leys et al. [35]. Cells for conductivity tests feature platinum plated electrodes and were filled with the electrolyte under argon atmosphere. Impedance spectroscopy was carried out in the frequency range of 300 KHz to 1 Hz, with an alternating current of 5 mV, to measure the resistance. The viscosity of the electrolytes was determined using a rheometer *MCR 102 (Anton Paar)*, starting with shear rate of 500 s⁻¹ for the analysis at 10 °C and progressively increasing it by 250 s⁻¹ for each 10 °C step in the temperature range between 10 and 80 °C. The density of the electrolytes was determined in the temperature range between 20 and 80 °C, using the density meter *DMA 4100 M (Anton Paar)*.

The electrochemical stability window (ESW) was measured in a three-electrode cell with a Pt working electrode (WE), an oversized carbon counter electrode (CE), and an Ag quasireference electrode (QRE). After 12 h of equilibration at the open circuit voltage (OCV), the potential was linearly varied to -3 V or 3 V vs. Ag QRE with a scan rate of 1 mV s⁻¹. The ESW was also evaluated in Li-metal cells, with lithium metal as both CE and QRE, using a stainless steel (SS-316) *ECC-Ref test cell (EL-Cell GmbH, Germany)*. A *Whatman* glass wool disk, previously soaked with PIL electrolyte solution, was sandwiched between the two electrodes, namely copper foil and a lithium metal disk. The potential was linearly swept from OCV to -0.3 V vs. Li⁺/Li with a scan rate of 0.1 mV s⁻¹. Fresh electrolyte was used for the anodic and the cathodic sweeps, respectively.

The Li plating/stripping experiments were carried out using two-electrode *Swagelok* cells equipped with Li metal electrodes. *Whatman* glass microfiber filters (150 μm) were used as separators drenched with 150 μL of electrolyte. The cells were assembled under Ar-atmosphere in a *MBraun LABmasterpro ECO glove box* (O₂ and H₂O < 1 ppm). Galvanostatic cycling (GC) tests were performed at 25 °C at a fixed current density of 0.088 mA cm⁻² (0.1 mA current, 1.13 cm² electrode area), with plating or stripping steps lasting for different times (i.e., 30, 90 and 150 min).

2.3. Electrode/cell preparation and electrochemical testing

The electrochemical performance of the liquid electrolytes in lab-scale Li metal cells was evaluated by means of charge/discharge GC with both LiFePO₄ (LFP) and LiNiMnCoO₂ (NMC) based electrodes. *Whatman* GF/A glass wool disks were used as separators drenched with 200 μL of electrolyte. The composition of the LFP composite electrodes was 80 wt% of the active material LFP (LiFePO₄+C, Life Power® P2, BASF), 12 wt% of the electrically conductive agent (carbon black C-ENERGY™ Super C65) and 8 wt% of poly(vinylidene fluoride) - PVdF (*Solvay Solef 2010*) as the binder, while the composition of the NMC composite electrodes was 94% of the active material NMC (Ni:Mn:Co =

6:2:2, BASF), 3% of the electrically conductive agent C65 and 3 wt% of PVdF as the binder. The following procedure was adopted for all the electrode preparations. First, powders of active material and C65 were gently mixed in a hand mortar. Successively, the mixture was added to a solution of PVdF in ≈1 ml of *N*-methyl pyrrolidone (NMP, *Aldrich*, now *Merck*) under constant stirring, which was continued for 3–4 h at ambient laboratory temperature (i.e., ≈21 °C). The resulting dense, homogeneous slurry was casted onto an Al current collector using a doctor-blade. NMP solvent was removed by evaporation at ambient temperature and further drying at 120 °C/vacuum for 24 h prior to utilization. The average active material mass loadings were 5 and 6 mg cm⁻² for the LFP- and the NMC-based electrodes, respectively, with thickness values in the range of 50–60 μm. The lab-scale cells were cycled at ambient laboratory temperature at different current-rates, where the rate denoted as C/n corresponds to a full discharge (or a full charge) in n hours, based on the theoretical cathode capacity (C) of the corresponding electrode material. The lab-scale Li/PIL-based electrolyte/LFP cells were cycled between 2.7 and 3.7 V vs. Li⁺/Li, while the Li/PIL-based electrolyte/NMC cells between 3.0 and 4.3 V vs. Li⁺/Li, where the Li metal was used as both CE and reference electrodes. The electrochemical tests described above were performed using a *VMP3* electrochemical workstation (20 V, ±400 mA) by *BioLogic Science Instruments (France)* using *ECC-Std test cells (EL-Cell GmbH, Germany)*. Test cells were assembled inside the Ar-filled glove box to avoid moisture contamination.

3. Results and discussion

Fig. 1 shows the comparison of viscosity (1a) and ionic conductivity (1b) of the two PIL-based electrolytes investigated in this work: H₄TFSI-VC and H₄FSI-VC. At 30 °C, the TFSI-based electrolyte displays a viscosity of 38 mPa s, while the viscosity of the FSI-based electrolytes is 27 mPa s. Just for comparison, these values are lower than those displayed by the neat PILs at the same temperature (43 mPa s for Py₁H₄TFSI and 30 mPa s for Py₁H₄FSI) [36,37], which is most likely due to the presence of VC. The significant difference between the viscosity of H₄FSI-VC (39 mPa s) and that of H₄TFSI-VC (60 mPa s) at 20 °C might be related to the proximity of the melting point of crystalline Py₁H₄TFSI [38]. At higher temperature (80 °C), the two electrolytes display comparable viscosity values (9 and 11 mPa s for H₄FSI-VC and H₄TFSI-VC, respectively). As shown in **Fig. 1b**, the ionic conductivity of the H₄FSI-VC is higher than that of the H₄TFSI-VC over the entire temperature range investigated. This trend is not surprising considering that H₄FSI-VC displays viscosity values lower than those of H₄TFSI-VC in the same temperature range. This is commonly observed when comparing ILs with TFSI⁻ vs. their counterparts with FSI⁻, due to the anion size [37]. Accordingly, the difference in conductivity is more marked at lower temperature: at 20 °C the FSI-based electrolyte is displaying a conductivity of 5.5 mS cm⁻¹, while the TFSI-based one a value of 1.9 mS cm⁻¹. It is also noticed that although the viscosities of the investigated PIL-based electrolytes are lower compared to their neat counterparts, the conductivity of the former ones is lower (e.g., at 30 °C, 8.6 mS cm⁻¹ for Py₁H₄FSI vs. 7.7 mS cm⁻¹ for H₄FSI-VC and 4.0 mS cm⁻¹ for Py₁H₄TFSI vs. 3.0 mS cm⁻¹ for H₄TFSI-VC) [39]. This observation can be explained considering that the introduction of lithium salt increases the amount of charge carriers, thus increasing the recombination of ions in the system and lowering the overall conductivity. Nevertheless, it has already been shown, that the mobility of Li⁺-ions is rather high in protic ionic liquids, especially compared to that in their aprotic counterparts [22]. Lastly, an important part of the charge transport in these electrolytes is performed by the protons of the PILs. It has been demonstrated that PILs might be able to form a hydrogen-bonded network, which allows H⁺ migration through structural diffusion (the "Grotthuss mechanism") [40,41]. However, since the conductivity of the electrolytes under study is not increasing drastically compared to their viscosities, in this case, conventional vehicular charge transport is likely to be the dominant process.

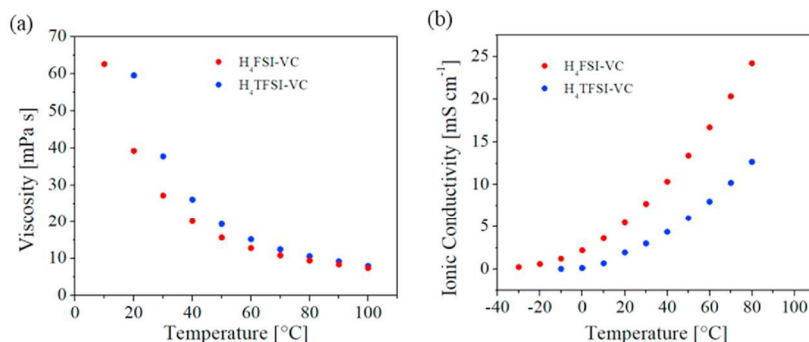


Fig. 1. Influence of the temperature on the (a) viscosity and (b) ionic conductivity of the investigated PIL-based electrolytes.

As shown in Fig. S1 (Supplementary Data), the variation of density over temperature displays a comparable linear trend for both H₄TFSI-VC and H₄FSI-VC. Also in this case, the difference between the two electrolytes is related to the nature of the anion counterpart. At 30 °C, the FSI-based electrolyte shows a density of 1.37 g cm⁻³, while the density of the TFSI-based electrolyte is 1.45 g cm⁻³; moreover, both electrolytes are denser compared to their pure counterparts.

As mentioned in the introduction, the electrochemical stability window (ESW) of PILs is limited by the presence of the labile proton(s) in the cation structure. Specifically, the cathodic potential limit is considerably reduced compared to that of their aprotic counterparts.

On the other hand, it has been already shown that the anodic stability window (ASW) of PILs is almost analogous to that of AILs having the same anion [42]. Neat Pyr_{H4}TFSI and Pyr_{H4}FSI show comparable cathodic potential limits, close to -1 V vs. Ag QRE while, in terms of anodic potential limit, the FSI-based PIL results to be less stable towards oxidation due to the higher chemical and electrochemical reactivity of the former compared to the latter anion. Similar behavior has been observed before [43]. The comparison of Fig. 2a,b clearly shows that the addition of VC leads to a variation of ASW of the two PIL electrolytes. It seems that the oxidation process of VC, at ca. 4.6 V vs. Li⁺/Li [44], prevails over the other oxidation mechanisms, defining the oxidation potential limits for H₄TFSI-VC and H₄FSI-VC. In addition, the presence of VC leads to a notable improvement of the cathodic stability window (CSW) in both electrolytes. As shown in Fig. 2b (and in the magnification reported in Fig. S2 in Supplementary Data), both of them are stable till -2.9 V vs. Ag QRE (corresponding to ca. 0 V vs. Li⁺/Li, which is the potential at which lithium plating takes place). The cathodic potential limit results to be ca. 2 V higher compared to the neat PIL one, indicating clearly that the presence of VC, through a polymerization/decomposition process, leads to obtain a protective layer on the Li metal surface, likely preventing the direct contact between Li metal and PIL [31,44]. In order to get further information about the electrochemical reduction of VC, the CSW was also evaluated in a Li/H₄FSI-VC/Cu cell with a Li metal electrode as the reference. The easily detectable reduction process occurring in the voltage range between 1.5 and 2 V vs. Li QRE (inset of Fig. S3 in Supplementary Data) can be assigned to the electrochemical reduction (polymerization) of VC.

In general, this process occurs at relatively high potential values as compared to the other components in the common electrolytes [31,45], promoting the formation of a passivation layer, which prevents detrimental reactions due to [Pyr_{H4}]⁺ at the Li-metal anode.

To further investigate the compatibility of the PIL-based electrolytes with the Li metal electrode, Li plating/stripping experiments were also carried out. Fig. 3a,b show the voltage profiles of Li metal symmetrical cells, using H₄FSI-VC and H₄TFSI-VC solutions as electrolytes.

The plating/stripping profile of the H₄FSI-VC sample is characterized

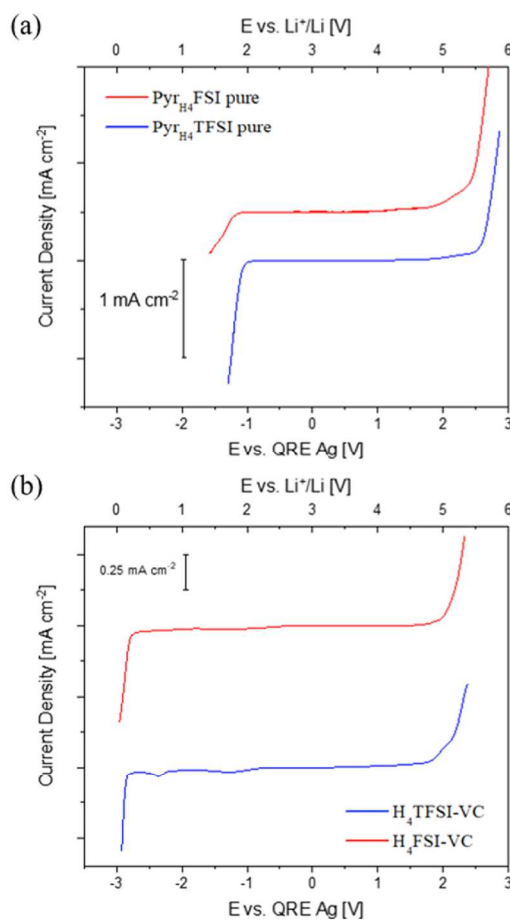


Fig. 2. Electrochemical stability window of: (a) pure Pyr_{H4}FSI and Pyr_{H4}TFSI; (b) H₄TFSI-VC and H₄FSI-VC electrolytes.

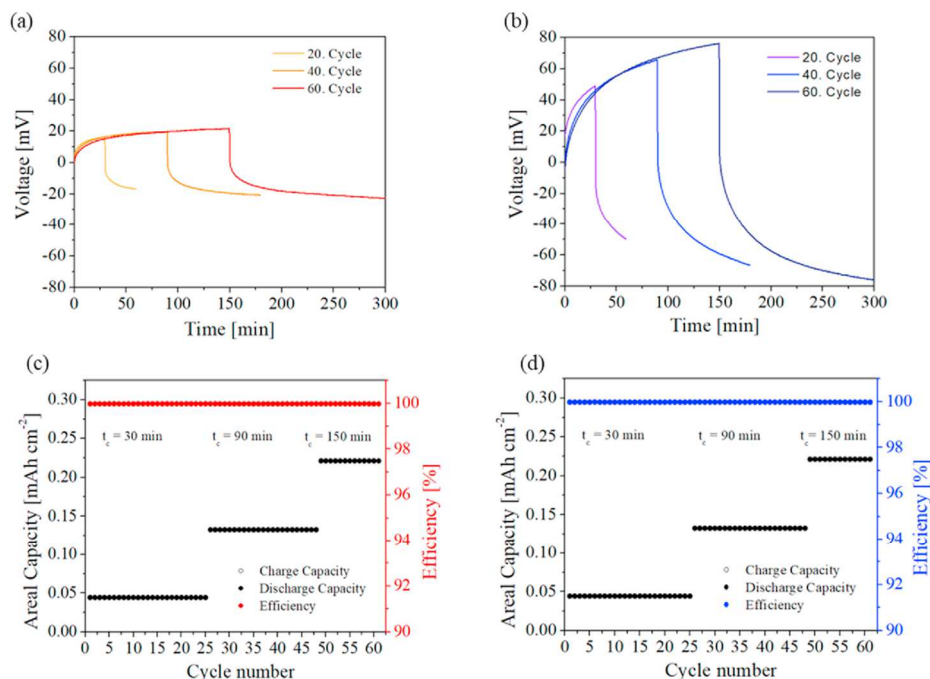


Fig. 3. Voltage profiles of symmetrical Li metal cells in combination with (a) H_4 FSI-VC and (b) H_4 TFSI-VC as electrolytes, as well as the results of charge-discharge measurements of (c) H_4 FSI-VC/Li and (d) H_4 TFSI-VC/Li, all at different charge times. The experiment was conducted at 25 °C and the current density of 0.088 mA cm⁻².

by relatively limited overpotential ($\pm \approx 15$ –20 mV) and flatter outline when compared with the TFSI counterpart ($\pm \approx 50$ –80 mV). This behavior could be imputed to the intrinsic properties of FSI-based electrolytes. Fig. S4 shows the poor reversibility of the lithium plating/stripping process without VC addition, corresponding to a severe increase of cell overpotential and capacity fade from the early cycles.

The lower viscosity, higher conductivity and the capacity of forming a more stable solid electrolyte interface (SEI) make lithium ion diffusion and plating/stripping processes easier with FSI anion [46]. Fig. S5 in supplementary data clearly demonstrates the better film forming ability of FSI-based electrolytes, limiting the increase of the electrolyte bulk resistance during the plating/stripping process, which could be directly correlated to the reduced overpotential. Nevertheless, both cells appear to be stable even during prolonged constant-current plating/stripping steps; in fact, no sign of severe electrolyte degradation was observed, both in terms of overpotential (cell resistance) and coulombic efficiency (reversibility). Fig. 3c,d show stable cycling up to 60 cycles with each step lasting for 150 min, along with high (>99.9%) efficiency during the whole measurement. The plating/stripping analysis underlines the beneficial effect of VC when added into the electrolyte solution, effectively limiting decomposition reactions of the PILs after prolonged contact with Li metal, and accounting for the excellent lithium plating/stripping ability in PIL-based electrolytes.

Fig. 4a,b clearly show the difference in the galvanostatic behavior of Li/PIL-based electrolyte/LFP cells with and without VC. As evident in Fig. 4a, the use of PIL-based electrolyte in direct contact with the Li metal electrode leads to rapid cell failure in about five cycles. Actually, the acidic proton strongly affects the reactivity of PILs towards alkali metal electrodes, making them extremely more reactive than their

aprotic counterparts [47]. This reactivity is presently hindering the use of PIL-based electrolytes in alkali metal batteries, limiting the field of application of this family of electrolytes. The high irreversible capacity of the first cycle clearly accounts for side reactions, including the deprotonation of the pyrrolidinium cation resulting in H₂ evolution and PIL degradation. The presence of VC was found to be fundamental to allow cycling with Li metal anode, as shown in Fig. 4b. The Li/ H_4 TFSI-VC/LFP cell shows the typical flat plateaus of LFP cathode material for the first cycles, corresponding to Li⁺ ion deinsertion (charge) and insertion (discharge) from/in the LiFePO₄/FePO₄. The Li metal cell assembled with H_4 TFSI-VC is able to deliver 170 mAh g⁻¹ during the first cycle at C/20 and 120 mAh g⁻¹ at C/10, with high reversibility (Coulombic efficiency - CE approaching 100% during the whole cycling test) and a remarkably improved capacity retention ($\approx 75\%$ after 50 cycles) as compared to the VC-free cell. To our knowledge, in addition of being remarkable, this is the first result of this kind with a liquid PIL-based electrolyte.

These excellent results can only be explained considering the decomposition/polymerization of vinylene carbonate occurring during the first charge, resulting in the formation of a protective film onto the Li metal electrode. Similar to other alkyl carbonates, VC is also reduced to species containing $-OCO_2Li$ groups, part of which may also have C=C double bonds. However, in contrast to the commonly used alkyl carbonate solvents the reduction of VC probably forms polymeric chains by reactions of the double bond through radical polymerization [31]. The polymerization of VC at the surface of the Li metal electrode during the first reduction process occurring at the Li metal anode affects the surface chemistry of the electrode, reducing the irreversible capacity and suppressing the rapid electrolyte degradation, making the use of PILs with

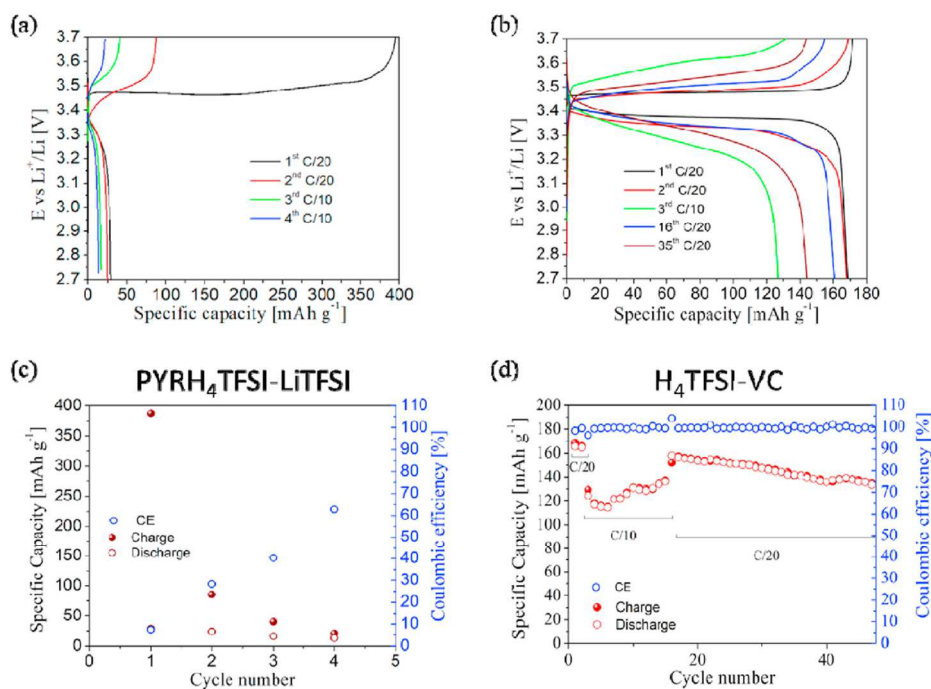


Fig. 4. Galvanostatic charge/discharge cycling behavior of [Li metal/PIL-based electrolyte/LFP] cells assembled with PYRH₄TFSI-LiTFSI and H₄TFSI-VC PIL-based electrolytes, respectively: voltage vs. specific capacity profiles at different C rates and evolution of the specific capacity (a,b) and specific charge/discharge capacity and coulombic efficiency vs. cycle number at C/10 and C/20 rates (c,d). All of the measurements were performed at ambient laboratory temperature ($\approx 21^\circ\text{C}$), setting the same C rate for both the charge and discharge steps.

Li metal anode possible. It also accounts for a very stable passivation film onto the Li metal electrode; actually, it can constantly sustain the volumetric variation of the lithium electrodes, which normally induces significant mechanical stress on the SEI leading to the formation of cracks and exposing fresh-lithium directly to the electrolyte.

In our system, we can even assume that the bare new, free, exposed lithium metal surface that might form upon cycling almost completely reacts again with the excess of VC, to form a new SEI in equilibrium with the peculiar polarization conditions that the electrode is experiencing [48,49], thus accounting for the limited capacity fade upon cycling. The stability and robustness of the protective layer upon cycling at higher current regimes was confirmed by reducing the current rate again to C/20 after the 15th cycle: the cell recovered almost 95% of the initial discharge specific capacity. The rather consistent capacity drop while doubling the current rate to C/10 likely accounts for the rather low Li^+ ion diffusion/mobility throughout the VC-based protective film formed; further optimization is needed in this respect, in particular considering the effect of the PIL anion and electrolyte formulation.

Motivated by the promising results discussed above, obtained with standard LFP-based electrodes operating at moderate voltages and well in the stability range of common LIB electrolytes, the performance of H₄TFSI-VC was assessed in lab-scale Li metal cell using high voltage NMC-based composite cathodes. Primary advantages of NMC-based LIBs are their high energy density and stability, allowing devices to be lighter and more compact, more durable and better to manage. Actually, the upper voltage limit for NMC is around 4.2 V vs. Li^+/Li , much higher than the LFP, which is around 3.5 V vs. Li^+/Li . If the capacities of the batteries remain constant, the energy content is defined by the voltage, which

turns NMC to be a material suitable to build much higher energy density batteries compared to LFP, particularly when combined with the lithium metal anode.

Similarly to the LFP-based cell operating with the fully TFSI-based PIL/VC-based mixture, the discharge voltage profile is stable and reproducible upon initial cycling, but the Coulombic efficiency decreases quickly from the 9th cycle (see Fig. S6 in Supplementary Data). These drawbacks, probably related to the TFSI⁻ anion, can be improved to a large extent by employing a solution based on the FSI⁻ anion, considering the remarkable performance in terms of anodic stability and more stable SEI formation [50]. Future work is needed to confirm whether this poor cycling ability is to be attributed to the TFSI⁻ anion or to the quantity of VC in the system.

Taking these results into account, and in order to enhance the electrochemical performance of the NMC/Li cell with PIL-based electrolyte, we investigated its behavior in combination with H₄TFSI-VC. Fig. 5a shows the typical charge/discharge profiles of an NMC cathode in a Li metal cell with the configuration Li/H₄TFSI-VC/NMC at different charge/discharge rates up to 1C in the voltage range of 3.0–4.3 V vs. Li^+/Li . The specific capacity delivered by the cell exceeded 155 mAh g^{-1} during the initial cycles at C/20 rate, which is fundamental for proper initial activation of this cathode material. The capacity drop while doubling the current rate to C/10 was actually very limited and the cell still delivered more than 145 mAh g^{-1} (15th cycle), 130 mAh g^{-1} (20th cycle) at C/5, 85 mAh g^{-1} (30th cycle) at C/2 and about 50 mAh g^{-1} (38th cycle) even at 1C. In addition, reversible charge discharge behavior was observed throughout 60 cycles, suggesting that the FSI-based electrolyte solution allows relatively stable operation with NMC cathodes, as shown in

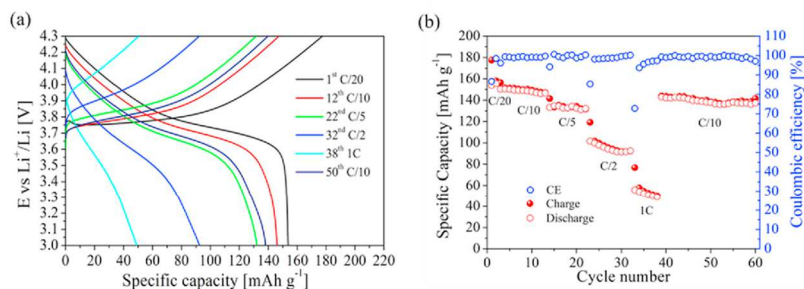


Fig. 5. Galvanostatic charge/discharge cycling behavior of [Li metal/ H_4 FSI-VC/NMC] cells: voltage vs specific capacity profiles at different C rates (a) and evolution of the specific capacity and the Coulombic efficiency with the cycle number (b). All of the measurements were performed at ambient laboratory temperature ($\approx 21^\circ\text{C}$), setting the same C rate for both the charge and discharge steps.

Fig. 5b. Except for cycling at a high current rate of 1C, the coulombic efficiency was stable above 99% during the whole test. The specific capacity was almost completely restored when the current rate was lowered back to C/10 (capacity retention of 95%), with no straightforward ($\approx 8\%$) fading even after 60 cycles. At present, we may ascribe what we observed to a better (improved compared to TFSI) and stable passivating layer at the interface of Li metal to effectively prevent its contact with the electrolyte solution that may cause the deterioration of the performance upon prolonged cycling.

In our case, with sufficiently high concentration of VC present in the electrolyte, residual VC likely remains in the electrolyte after anode SEI formation, which may undergo oxidation at the interface with the high-voltage cathode, resulting in increased overall cell impedance. As already suggested in previous studies [51], the formation of a poly(VC) film on the NMC cathode at high anodic potential values is the most likely explanation for the large improvement in capacity retention (or lifetime) as well as the slight increase of resistance, which may compromise the cell performance at higher discharge rates. Therefore, future studies should be focused on the investigation and optimization of the content of VC. The impact of VC on the parasitic reactions occurring at the cathode could be summarized in a decrease of detrimental electrolyte oxidation reactions at the positive electrode, mainly responsible for the limited lifetime.

Furthermore, we compared the performance of PIL/VC-based electrolytes with the corresponding AIL-based electrolytes (either bare or added with VC) in a Li/PYR₁₄FSI-LiFSI/NMCLi metal cell configuration. Fig. S7 in supplementary data shows comparable electrochemical performance of the PIL/VC and bare AIL based electrolytes at low C/20 and C/10 rates upon initial cycling, while the difference in performance becomes more pronounced moving towards higher C rates: actually, the specific capacity of H_4 FSI-VC starts to gradually drop. The corresponding bare AIL-based cell does not show the same drop in discharge capacity at higher current rates of C/2 and 1C. However, the CE trend and capacity retention upon decreasing the current back to C/10 is extremely improved for the PIL/VC-based electrolyte. This likely accounts for a more stable SEI layer formed by this latter electrolyte compared to the bare AIL-based one. On the other hand, the presence of the protecting layer arising from VC reduction increases the internal resistance and, correspondingly, decreases the rate capability: optimization in this regard is required. This is demonstrated by the comparison in Fig. 6, where it can be clearly seen that the addition of VC, particularly at high amounts (10% by weight in the present work), to the AIL-based electrolyte leads to a remarkable drop in the rate capability of the Li/PYR₁₄FSI-LiFSI-VC/NMC cell. Indeed, Fig. 6 shows the electrochemical performance of the electrolyte solutions based on PIL and AIL,

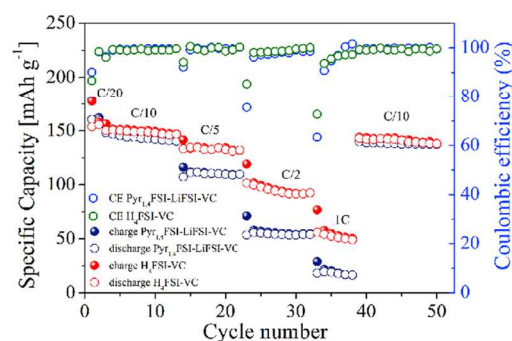


Fig. 6. Comparison of the constant-current (galvanostatic) charge/discharge cycling behavior of different [Li metal/IL solution/NMC] cells assembled with H_4 FSI-VC electrolyte and the corresponding one with the aprotic PYR₁₄FSI-LiFSI-VC: evolution of the specific capacity and the Coulombic efficiency at different C rates with the cycle number.

both comprising VC additive. The PIL-VC cell actually outperforms the AIL-VC based counterpart at each of the tested current regimes (enhancement of specific capacity output of the PIL-VC based cell compared to the AIL-VC based counterpart: 4, 15, >40% at C/20-C/10, C/5, C/2-1C rates, respectively). The results of Fig. 6 clearly demonstrate that, at the same conditions of temperature, current rates, active material loading and amount of VC, PIL-based electrolytes allow superior cycling in lithium metal batteries compared to AILs, particularly at high C-rates. This enlightens how the intrinsic properties of PILs and their lower viscosity affect positively the lithium ion mobility and the corresponding cell behavior. Nonetheless, one should consider that the target of this work is not to compare the performance of PILs and AILs, but demonstrate the positive effects of VC additive when combined with the former. Here, VC was demonstrated to be fundamental to achieve stable cycling in Li metal cells with PILs, remarkably limiting the surface reactivity of PIL-based electrolytes vs. the Li metal electrode and, concurrently, enhancing the electrode stability during electrochemical tests, thus foreseeing a bright future for high energy density Li metal and post-Li batteries.

4. Conclusions

In this work, we presented the first examples of lab-scale lithium metal cells stable and safely operating with $\text{PYR}_{\text{H}_4}^+(\text{TFSI}^-/\text{FSI}^-)$ -based protic ionic liquid (PIL) electrolytes. This is accomplished by the use of vinylene carbonate (VC) encompassed in the PIL-salt solution, and resulted in steady prolonged cycling performance at ambient temperature with standard LFP and, even more remarkably, with 4 V class NMC-based cathodes. All the beneficial properties of PILs, in terms of ease of synthesis and cost with respect to AILs, have been matched, with the remarkable outcome of enabling the safe use of the Li metal anode, which is characterized by the highest theoretical capacity and lowest electrochemical potential. The electrolytes under investigation, comprised of *N*-butylpyrrolidinium-(TFSI⁻/FSI⁻) based PILs, (TFSI⁻/FSI⁻) based lithium salts and vinylene carbonate (VC) additive, have been tested in Li metal lab-scale cells assembled with LFP and NMC cathodes. The use of VC ensured the formation of a protective layer at the interface between Li metal and the PIL-based electrolytes as well as on the cathode at high anodic potentials, allowing the cells to deliver capacities comparable to those achieved with their AIL-based counterparts.

For sure, to properly engineer the use of PILs with Li metal anode, improvements and optimization are needed, as well as the thorough understanding of several mechanisms occurring within the cell. The protective layer formation and surface chemistry of the Li metal anode before and after cycling, the specific role of FSI⁻ or TFSI⁻ anions as well as the interface with high-voltage cathodes, all need to be clarified. Nonetheless, in this work we are demonstrating for the first time that it is possible to successfully utilize PIL-based electrolytes also in lithium-metal batteries, and such an initial proof-of-concept represents an important contribution for the realization of cutting-edge, safer, high energy density lithium metal batteries to power next generation electric devices to face the global energy/environmental challenge.

CRedit authorship contribution statement

Gabriele Lingua: Investigation, Data curation, Visualization, Formal analysis, Writing - original draft. **Marisa Falco:** Conceptualization, Methodology, Investigation, Validation, Writing - original draft. **Timo Stettner:** Investigation, Validation, Data curation, Formal analysis, Writing - original draft. **Claudio Gerbaldi:** Conceptualization, Visualization, Supervision, Writing - review & editing, Project administration, Funding acquisition. **Andrea Balducci:** Resources, Supervision, Project administration, Funding acquisition, Writing - review & editing.

Declaration of competing interest

The authors declare that they have no known competing financial interests or personal relationships that could have appeared to influence the work reported in this paper.

Acknowledgements

M.F. and C.G. acknowledge financial support by the Si-DRIVE Project (<http://sidrive2020.eu/>), which received funding from the European Union's Horizon 2020 research and innovation program under Grant Agreement no. 814464. The ENABLES project (<http://www.enable-project.eu/>) received funding from the European Union's Horizon 2020 research and innovation program under Grant Agreement no. 730957. T.S. and A.B. wish to thank the Friedrich-Schiller University of Jena for the financial support.

Appendix A. Supplementary data

Supplementary data to this article can be found online at <https://doi.org/10.1016/j.jpowsour.2020.228979>.

[org/10.1016/j.jpowsour.2020.228979](https://doi.org/10.1016/j.jpowsour.2020.228979).

References

- [1] M.Z. Jacobson, M.A. Delucchi, Providing all global energy with wind, water, and solar power, Part I: technologies, energy resources, quantities and areas of infrastructure, and materials, *Energy Pol.* 39 (2011) 1154–1169, <https://doi.org/10.1016/j.enpol.2010.11.040>.
- [2] P.J. Loftus, A.M. Cohen, J.C.S. Long, J.D. Jenkins, A critical review of global decarbonization scenarios: what do they tell us about feasibility? *Wiley Interdiscip. Rev. Clim. Chang.* 6 (2015) 93–112, <https://doi.org/10.1002/wcc.324>.
- [3] B. Scrosati, J. Garche, Lithium batteries: status, prospects and future, *J. Power Sources* 195 (2010) 2419–2430, <https://doi.org/10.1016/j.jpowsour.2009.11.048>.
- [4] K. Hayashi, Y. Nemoto, S.I. Tobishima, J.I. Yamaki, Mixed solvent electrolyte for high voltage lithium metal secondary cells, *Electrochim. Acta* 44 (1999) 2337–2344, [https://doi.org/10.1016/S0013-4686\(98\)00374-0](https://doi.org/10.1016/S0013-4686(98)00374-0).
- [5] Q. Wang, P. Ping, X. Zhao, G. Chu, J. Sun, C. Chen, Thermal runaway caused fire and explosion of lithium ion battery, *J. Power Sources* 208 (2012) 210–224, <https://doi.org/10.1016/j.jpowsour.2012.02.038>.
- [6] M. Contestabile, S. Panero, B. Scrosati, Laboratory-scale lithium-ion battery recycling process, *J. Power Sources* 92 (2001) 65–69, [https://doi.org/10.1016/S0378-7753\(00\)00523-1](https://doi.org/10.1016/S0378-7753(00)00523-1).
- [7] A. Balducci, S.S. Jeong, G.T. Kim, S. Passerini, M. Winter, M. Schmueck, G. B. Appetecchi, R. Marcella, D. Mecerreyes, V. Barsukov, V. Khomenko, I. Cantero, I. De Meazza, M. Holzapfel, N. Tran, Development of safe, green and high performance ionic liquids-based batteries (ILIBATT project), *J. Power Sources* 196 (2011) 9719–9730, <https://doi.org/10.1016/j.jpowsour.2011.07.058>.
- [8] D.R. Macfarlane, N. Tachikawa, M. Forsyth, J.M. Pringle, P.C. Howlett, G.D. Elliott, J.H. Davis, M. Watanabe, P. Simon, C.A. Angell, Energy applications of ionic liquids, *Energy Environ. Sci.* 7 (2014) 232–250, <https://doi.org/10.1039/c3ee42099j>.
- [9] Y. Pu, N. Jiang, A.J. Ragauskas, Ionic liquid as a green solvent for lignin, *J. Wood Chem. Technol.* 27 (2007) 23–33, <https://doi.org/10.1080/02773810701282330>.
- [10] P. Kubisa, Ionic liquids as solvents for polymerization processes—Progress and challenges, *Prog. Polym. Sci.* 34 (2009) 1333–1347, <https://doi.org/10.1016/j.progpolymsci.2009.09.001>.
- [11] M. Watanabe, M.L. Thomas, S. Zhang, K. Ueno, T. Yasuda, K. Dokko, Application of ionic liquids to energy storage and conversion materials and devices, *Chem. Rev.* 117 (2017) 7190–7239, <https://doi.org/10.1021/acs.chemrev.6b00504>.
- [12] G.B. Appetecchi, M. Montanino, S. Passerini, Ionic liquid-based electrolytes for high energy, safer lithium batteries, *ACS Symp. Ser.* 1117 (2012) 67–128, <https://doi.org/10.1021/bk-2012-1117.ch004>.
- [13] M. Moreno, E. Simonetti, G.B. Appetecchi, M. Carewska, M. Montanino, G.-T. Kim, N. Loeffler, S. Passerini, Ionic liquid electrolytes for safer lithium batteries, *J. Electrochem. Soc.* 164 (2017) A6026–A6031, <https://doi.org/10.1149/2.0051701jes>.
- [14] M. Anouti, M. Caillon-Caravani, Y. Dridi, H. Galiano, D. Lemordant, Synthesis and characterization of new pyrrolidinium based protic ionic liquids. Good and superionic liquids, *J. Phys. Chem. B* 112 (2008) 13335–13343, <https://doi.org/10.1021/jp805992b>.
- [15] J. Fuller, A.C. Breda, R.T. Carlin, Ionic liquid-polymer gel electrolytes from hydrophilic and hydrophobic ionic liquids, *J. Electroanal. Chem.* 459 (1998) 29–34, [https://doi.org/10.1016/S0022-0728\(98\)00285-X](https://doi.org/10.1016/S0022-0728(98)00285-X).
- [16] J.-H. Shin, W.A. Henderson, S. Passerini, PEO-based polymer electrolytes with ionic liquids and their use in lithium metal-polymer electrolyte batteries, *J. Electrochem. Soc.* 152 (2005) A978, <https://doi.org/10.1149/1.1890701>.
- [17] A. Balducci, R. Dugas, P.L. Taberna, P. Simon, D. Pflé, M. Mastragostino, S. Passerini, High temperature carbon-carbon supercapacitor using ionic liquid as electrolyte, *J. Power Sources* 165 (2007) 922–927, <https://doi.org/10.1016/j.jpowsour.2006.12.048>.
- [18] R.F. De Souza, J.C. Padilha, R.S. Gonçalves, J. Dupont, Room temperature dialkylimidazolium ionic liquid-based fuel cells, *Electrochem. Commun.* 5 (2003) 728–731, [https://doi.org/10.1016/S1388-2481\(03\)00173-5](https://doi.org/10.1016/S1388-2481(03)00173-5).
- [19] S. Ferrari, E. Quartarone, P. Mustarelli, A. Magistris, M. Fagnoni, S. Protti, C. Gerbaldi, A. Spinella, Lithium ion conducting PVdF-HFP composite gel electrolytes based on *N*-methoxyethyl-*N*-methylpyrrolidinium bis(trifluoromethanesulfonyl)-imide ionic liquid, *J. Power Sources* 195 (2010) 559–566, <https://doi.org/10.1016/j.jpowsour.2009.08.015>.
- [20] T.L. Greaves, C.J. Drummond, Protic ionic liquids: properties and applications, *Chem. Rev.* 108 (2008) 206–237, <https://doi.org/10.1021/cr068040u>.
- [21] K. Ghandi, A review of ionic liquids, their limits and applications, *Green Sustain. Chem.* 4 (2014) 44–53, <https://doi.org/10.4236/gsc.2014.41008>.
- [22] T. Vogl, S. Menne, R.S. Kühnel, A. Balducci, The beneficial effect of protic ionic liquids on the lithium environment in electrolytes for battery applications, *J. Mater. Chem. A* 2 (2014) 8258–8265, <https://doi.org/10.1039/c3ta15224c>.
- [23] S. Menne, T. Vogl, A. Balducci, Lithium coordination in protic ionic liquids, *Phys. Chem. Chem. Phys.* 16 (2014) 5485–5489, <https://doi.org/10.1039/c3cp55183k>.
- [24] S. Menne, J. Pires, M. Anouti, A. Balducci, Protic ionic liquids as electrolytes for lithium-ion batteries, *Electrochem. Commun.* 31 (2013) 39–41, <https://doi.org/10.1016/j.echem.2013.02.026>.
- [25] D. Lin, Y. Liu, Y. Cai, Reviving the lithium metal anode for high-energy batteries, *Nat. Nanotechnol.* 12 (2017) 194–206, <https://doi.org/10.1038/nnano.2017.16>.
- [26] W. Xu, J. Wang, F. Ding, X. Chen, E. Nasrulin, Y. Zhang, J.-G. Zhang, Lithium metal anodes for rechargeable batteries, *Energy Environ. Sci.* 7 (2014) 513–537, <https://doi.org/10.1039/C3EE40795K>.

- [27] M. Forsyth, G.M.A. Girard, A. Basile, M. Hilder, D.R. MacFarlane, F. Chen, P. C. Howlett, Inorganic-organic ionic liquid electrolytes enabling high energy-density metal electrodes for energy storage, *Electrochim. Acta* 220 (2016) 609–617, <https://doi.org/10.1016/j.electacta.2016.10.134>.
- [28] P.G. Bruce, S.A. Freunberger, L.J. Hardwick, J.M. Tarascon, Li₂O₂ and Li₂S batteries with high energy storage, *Nat. Mater.* 11 (2012) 19–29, <https://doi.org/10.1038/nmat3191>.
- [29] J. Yan, X. Liu, B. Li, Recent progress in Li-rich layered oxides as cathode materials for Li-ion batteries, *RSC Adv.* 4 (2014) 63268–63284, <https://doi.org/10.1039/c4ra12454e>.
- [30] Christian Julien, Comparative issues of cathode materials for Li-ions batteries, *INORGA* 2 (2014) 132–154, <https://doi.org/10.3390/inorganics2020132>.
- [31] D. Aurbach, K. Gamolsky, B. Markovsky, Y. Gofer, M. Schmidt, U. Heider, On the use of vinylene carbonate (VC) as an additive to electrolyte solutions for Li-ion batteries, *Electrochim. Acta* 47 (2002) 1423–1439, [https://doi.org/10.1016/S0013-4686\(01\)00858-1](https://doi.org/10.1016/S0013-4686(01)00858-1).
- [32] H. Ota, Y. Sakata, A. Inoue, S. Yamaguchi, Analysis of vinylene carbonate derived SEI layers on graphite anode, *J. Electrochem. Soc.* 151 (2004) A1659, <https://doi.org/10.1149/1.1785795>.
- [33] L. Timperman, P. Skowron, A. Boisset, H. Galiano, D. Lemordant, E. Frackowiak, F. Béguin, M. Anouti, Triethylammonium bis(tetrafluoromethylsulfonyl)amide protic ionic liquid as an electrolyte for electrical double-layer capacitors, *Phys. Chem. Chem. Phys.* 14 (2012) 8199–8207, <https://doi.org/10.1039/c2cp40315c>.
- [34] W.A. Henderson, S. Passerini, Phase behavior of ionic liquid-LiX mixtures: pyrrolidinium cations and TFSI- anions, *Chem. Mater.* 16 (2004) 2881–2885, <https://doi.org/10.1021/cm049942j>.
- [35] J. Leys, M. Wübbenhoist, C. Preethy Menon, R. Rajesh, J. Thoen, C. Glorieux, P. Nockemann, B. Thijs, K. Binnemans, S. Longuemart, Temperature dependence of the electrical conductivity of imidazolium ionic liquids, *J. Chem. Phys.* 128 (2008), <https://doi.org/10.1063/1.2827462>.
- [36] T. Vogl, S. Menne, A. Balducci, Mixtures of protic ionic liquids and propylene carbonate as advanced electrolytes for lithium-ion batteries, *Phys. Chem. Chem. Phys.* 16 (2014) 25014–25023, <https://doi.org/10.1039/c4cp03830d>.
- [37] S. Menne, T. Vogl, A. Balducci, The synthesis and electrochemical characterization of bis(fluorosulfonyl)imide-based protic ionic liquids, *Chem. Commun.* 51 (2015) 3656–3659, <https://doi.org/10.1039/c4cc09665g>.
- [38] T. Vogl, S. Passerini, A. Balducci, The impact of mixtures of protic ionic liquids on the operative temperature range of use of battery systems, *Electrochem. Commun.* 78 (2017) 47–50, <https://doi.org/10.1016/j.echem.2017.04.002>.
- [39] T. Stettner, S. Gehrke, P. Ray, B. Kirchner, A. Balducci, Water in protic ionic liquids: properties and use of a new class of electrolytes for energy-storage devices, *ChemSusChem* 12 (2019) 3827–3836, <https://doi.org/10.1002/cssc.201901283>.
- [40] J. Ingenmey, S. Gehrke, B. Kirchner, How to harvest grothuss diffusion in protic ionic liquid electrolyte systems, *ChemSusChem* 11 (2018) 1900–1910, <https://doi.org/10.1002/cssc.201800436>.
- [41] U.A. Rana, M. Forsyth, D.R. MacFarlane, J.M. Pringle, Toward protic ionic liquid and organic ionic plastic crystal electrolytes for fuel cells, *Electrochim. Acta* 84 (2012) 213–222, <https://doi.org/10.1016/j.electacta.2012.03.058>.
- [42] T. Stettner, P. Huang, M. Goktas, P. Adelhelm, A. Balducci, Mixtures of glyme and aprotic-protic ionic liquids as electrolytes for energy storage devices, *J. Chem. Phys.* 148 (2018), <https://doi.org/10.1063/1.5013117>.
- [43] M. Kerner, N. Pylahan, J. Scheers, P. Johansson, Ionic liquid based lithium battery electrolytes: fundamental benefits of utilising both TFSI and FSI anions? *Phys. Chem. Chem. Phys.* 17 (2015) 19569–19581, <https://doi.org/10.1039/C5CP01891A>.
- [44] Y. Dong, J. Demeaux, B.L. Lucht, Investigation of the effect of added methylene ethylene carbonate (MEC) and vinylene carbonate (VC) on LiNi_{0.5}Mn_{1.5}O₄/graphite cell performance, *J. Electrochem. Soc.* 163 (2016) A2413–A2417, <https://doi.org/10.1149/2.1341610jes>.
- [45] D. Pritzl, S. Solchenbach, M. Wetjen, H.A. Gasteiger, Analysis of vinylene carbonate (VC) as additive in graphite/LiNi_{0.5}Mn_{1.5}O₄ cells, *J. Electrochem. Soc.* 164 (2017) A2625–A2635, <https://doi.org/10.1149/2.1441712jes>.
- [46] D.M. Piper, T. Evans, K. Leung, T. Watkins, J. Olson, S.C. Kim, S.S. Han, V. Bhat, K. H. Oh, D.A. Buttry, S.H. Lee, Stable silicon-ionic liquid interface for next-generation lithium-ion batteries, *Nat. Commun.* 6 (2015) 1–10, <https://doi.org/10.1038/ncomms7230>.
- [47] J.R. Nair, F. Colò, A. Kazzazi, M. Moreno, D. Bresser, R. Lin, F. Bella, G. Meligrana, S. Fantini, E. Simonetti, G.B. Appetecchi, S. Passerini, C. Gerbaldi, Room temperature ionic liquid (RTIL)-based electrolyte cocktails for safe, high working potential Li-based polymer batteries, *J. Power Sources* 412 (2019) 398–407, <https://doi.org/10.1016/j.jpowsour.2018.11.061>.
- [48] C. Naudin, J.L. Bruneel, M. Chami, B. Desbat, J. Grondin, J.C. Lassègues, L. Servant, Characterization of the lithium surface by infrared and Raman spectroscopies, *J. Power Sources* 124 (2003) 518–525, [https://doi.org/10.1016/S0378-7753\(03\)00798-5](https://doi.org/10.1016/S0378-7753(03)00798-5).
- [49] R. Schmitz, R. Ansgar Müller, R. Wilhelm Schmitz, C. Schreiner, M. Kunze, A. Lex-Balducci, S. Passerini, M. Winter, SEI investigations on copper electrodes after lithium plating with Raman spectroscopy and mass spectrometry, *J. Power Sources* 233 (2013) 110–114, <https://doi.org/10.1016/j.jpowsour.2013.01.105>.
- [50] M. Kerner, Pyrrolidinium FSI and TFSI-based polymerized ionic liquids as electrolytes for high-temperature lithium-ion batteries, *Batteries* 4 (2018) 10, <https://doi.org/10.3390/batteries4010010>.
- [51] J.C. Burns, N.N. Sinha, D.J. Coyle, G. Jain, C.M. VanElzen, W.M. Lamanna, A. Xiao, E. Scott, J.P. Gardner, J.R. Dahn, The impact of varying the concentration of vinylene carbonate electrolyte additive in wound Li-ion cells, *J. Electrochem. Soc.* 159 (2011) A85–A90, <https://doi.org/10.1149/2.028202jes>.

2.2.3. Publikation 7: Ionic Liquid-Based Electrolytes for Calcium-Based Energy Storage Systems

As mentioned in the previous chapter, in the last years the investigations dedicated to post-lithium batteries increased significantly. Among the various technologies, calcium-based systems are considered with high attention, due to the high theoretical energy density of calcium-metal anodes as well as its low cost and sustainability.[181]

Calcium-based systems are still in their infancy and only recently the successful use of conventional electrolytes like EC or PC could be achieved. Since this was done above 75 °C, the employment of highly flammable or volatile solvents seems rather risky, making ILs an attractive alternative. Nevertheless, little progress has been done and only limited to AILs. Thus, as a proof of concept, [Pyr_{H4}][TFSI] mixed with PC (8:2 molar ratio) and 0.1 M Ca(TFSI)₂ as calcium salt was investigated in terms of its chemical-physical-properties as well as its electrochemical performance in combination with AC-based electrodes in an EDLC setup. This protic electrolyte has been compared to the aprotic counterpart, using [Pyr₁₄][TFSI] with the same PC and Ca(TFSI)₂ amount.

The transport properties of both electrolytes have been found to be relatively comparable, owing to the similar characteristics of both ILs. The biggest difference lies in the m.p. of the ILs, resulting in a broader temperature window for the aprotic electrolyte compared to the protic one. Furthermore, the impact on the transport properties by mixing each IL with PC is more pronounced in case of [Pyr₁₄][TFSI], simply because it has a higher viscosity compared to [Pyr_{H4}][TFSI]. Overall, both electrolytes display acceptable transport properties, especially considering the use in a battery device.

A more pronounced difference between the two electrolytes is visible in the ESW, as expected. While the aprotic electrolyte can withstand an overall potential window of 5.1 V, the ESW of the protic electrolyte is only 3.2 V. As explained before, this is due to the small cathodic stability due to hydrogen evolution by reduction of the protic cation. The anodic stability is on the other hand almost identical, since in both cases the [TFSI]⁻ anion is oxidized.

In a next step, the OPV of AC-based electrodes in each electrolyte were investigated. Like the ESW, the electrodes within the aprotic electrolyte were able to be charged up to 3.3 V, while

the ones in the protic electrolyte could only be charged up to 2.4 V. Additionally, balanced AC-based EDLCs employing the aprotic electrolyte displayed slightly higher capacitances compared to EDCLs employing the protic version, combined with better power performance, despite almost similar transport properties at 30 °C.

Finally, both electrolytes were employed in a Ca-ion battery half-cell using TiS_2 as active material for the working electrode. However, only the electrolyte based on $[\text{Pyr}_{14}][\text{TFSI}]$ was able to achieve calcium insertion into the TiS_2 at 100 °C. During the cycling of $[\text{Pyr}_{\text{H4}}][\text{TFSI}]$ decomposition of the electrolyte was taking place, making it impossible to reach calcium insertion potentials.

For the half-cell employing the aprotic electrolyte, it was found that in addition to insertion of Ca-ions into TiS_2 , also co-intercalation of $[\text{Pyr}_{14}]^+$ cations takes place. This has been already observed in PC-based electrolytes, in which case the PC molecules are co-intercalating. This leads to amorphization and increase in interlayer distances, which is more pronounced in the IL-based electrolyte. While this process is somewhat reversible and Ca-ions seem preferably inserted, it still damages the electrode.

Overall, this proof-of-concept for IL-based electrolytes in Ca-ion systems has shown the difficulties linked to this yet rather unexplored system. While the operating temperature at 100 °C makes an IL-based electrolyte the perfect candidate, there is still very much work left to implement it successfully. Considering these results, this is even more true for PIL-based electrolytes. While for AIL-based electrolytes the right combination of cation and active material can already lead to improvements, it seems that an efficient SEI will be necessary for the introduction of PIL-based electrolytes in these devices.



Ionic Liquid-Based Electrolytes for Calcium-Based Energy Storage Systems

T. Stettner,^{1,=} R. Dugas,^{2,=} A. Ponrouch,^{2,3,*,#,z} and A. Balducci^{1,3,*,#,z}

¹Institute for Technical Chemistry and Environmental Chemistry Center for Energy and Environmental Chemistry Jena (CEEC Jena) Philosophenweg 7a, 07743 Jena, Germany

²Institut de Ciència de Materials de Barcelona (ICMAB-CSIC), Campus UAB, 08193 Bellaterra, Catalonia, Spain

³ALISTORE—European Research Institute, CNRS FR 3104, Hub de l'Energie, 80039 Amiens, France

In this work, aprotic and protic ionic liquid (IL)-based electrolytes designed for calcium-based energy storage systems are investigated. We have shown that these electrolytes display good transport properties and electrochemical stabilities comparable with those of IL-based electrolytes proposed for lithium and sodium-based systems. The use of these electrolytes in electrochemical double layer capacitors (EDLCs) leads to the realization of devices displaying good capacitances paired with a high reversibility and stability. Their use in combination with TiS_2 cathode appears more problematic as the cation of the ILs is inserting in the layered structure of this material during the charge process. In this latter case a careful design of the cation appears necessary to guarantee selective insertion of Ca^{2+} and reversible charge-discharge process.

© 2020 The Author(s). Published on behalf of The Electrochemical Society by IOP Publishing Limited. This is an open access article distributed under the terms of the Creative Commons Attribution Non-Commercial No Derivatives 4.0 License (CC BY-NC-ND, <http://creativecommons.org/licenses/by-nc-nd/4.0/>), which permits non-commercial reuse, distribution, and reproduction in any medium, provided the original work is not changed in any way and is properly cited. For permission for commercial reuse, please email: permissions@iopublishing.org. [DOI: [10.1149/1945-7111/ab9c89](https://doi.org/10.1149/1945-7111/ab9c89)]



Manuscript submitted May 14, 2020; revised manuscript received June 8, 2020. Published June 23, 2020.

Supplementary material for this article is available [online](#)

Calcium-based energy storage devices are more and more considered as an attractive alternative to state-of-the-art storage systems such as the lithium-ion battery (LIB). A Ca-ion system relying on an insertion type anode such as graphite would fall short in terms of performance when compared with the state-of-the-art LIBs. However, the use of Ca metal as anode material (1.34 Ah g⁻¹ and 2.06 Ah cm⁻³) can lead to a leap-frog in energy density in addition of being advantageous in terms of cost and sustainability, Ca being the 5th most abundant element on the Earth's crust.¹ The development of Ca-based systems, however, is in an early stage and very few, if any, full-cell studies exist,² by contrast with the more advanced technology based on magnesium (8th most abundant element).^{3,4} Nevertheless, the lower polarizing character of Ca^{2+} when compared with Mg^{2+} holds promise for faster reaction kinetics and hence better power performances for Ca batteries.

One severe obstacle on the road towards calcium-based systems has been the successful deposition and stripping of calcium in inorganic electrolytes. While Mg metal plating can be traced back to the early 1920s, using an electrolyte based on Grignard reagents (R-MgX , X = Br, Cl),⁵ reversible Ca plating and stripping was demonstrated recently in a carbonate solvent based electrolyte (ethylene carbonate (EC) and propylene carbonate (PC)) at temperatures above 75 °C or at room temperature in ether and glyme based electrolytes.⁶⁻⁹ Although these solvents are relatively cheap and largely used, they are highly flammable and toxic.¹⁰ For this reason, the use of safer alternative appears of importance in view of the development of Ca-based systems. Ionic liquids (ILs) have been shown to be a promising alternative in a vast amount of devices, such as batteries, electrochemical capacitors and hybrid, high power devices.¹¹⁻¹⁵ So far, the use of ILs in Ca-based systems has been scarcely investigated.^{16,17} Nevertheless, considering the favorable properties of ILs, the investigation of their use in Ca-based system appears of importance.

In this work we report about the use of IL-based electrolytes in combination with electrode materials suitable for the realization of Ca-based systems. The ionic liquids 1-butyl-1-methylpyrrolidinium bis(trifluoromethylsulfonyl)imide ($\text{PyT}_{14}\text{TFSI}$) and 1-butylpyrrolidinium bis(trifluoromethylsulfonyl)imide ($\text{PyT}_{14}\text{TFSI}$) have been

utilized. $\text{PyT}_{14}\text{TFSI}$ is an aprotic IL (AIL), which has been used in a large number of storage systems during the last 10 years. $\text{PyT}_{14}\text{TFSI}$ is a protic IL (PIL), which holds a “free” proton on the cation.¹⁸⁻²¹ This latter category of IL is attracting an increasing interest in the field of batteries, due to distinct interactions of the protic ions within the electrolyte, leading e.g. to an increased lithium-ion mobility compared to AILs.^{20,22-26} To the best of our knowledge, PILs have never been used for Ca-based systems. Thus, both AIL and PIL have been employed in combination with calcium bis(trifluoromethylsulfonyl)imide ($\text{Ca}(\text{TFSI})_2$) to obtain electrolytes suitable for Ca-based systems. In order to achieve a satisfactory solubility of this salt (0.1 mol l⁻¹), 20 mol% of PC have been added in all considered electrolytic solutions. In the first part of the manuscript, the chemical-physical properties of the selected electrolytes have been investigated. Afterwards, their use in combination with activated carbon (AC) has been considered with the aim to verify if these electrolytes can be utilized for the realization of electrical double layer capacitors (EDLC) and, eventually, of hybrid devices based on Ca chemistry. In the last part of the manuscript the intercalation of calcium ions into layered TiS_2 has been addressed, being one of the very few cathode material for which a fully reversible intercalation of Ca^{2+} was demonstrated.²⁷

Experimental

Preparation of the electrolyte.— $\text{PyT}_{14}\text{TFSI}$ was synthesized using the same procedure described in Ref. 28. 1-butylpyrrolidin has been used as precursor, LiTFSI for the anion exchange. $\text{PyT}_{14}\text{TFSI}$ as well as $\text{PyT}_{14}\text{TFSI}$ (obtained from *Iolitech*) and PC (obtained from *Sigma Aldrich*, 99.7%) were mixed in a 8:2 molar ratio, respectively. Subsequently $\text{Ca}(\text{TFSI})_2$ was added to achieve a molarity of 0.1 mol l⁻¹. Before preparation the water amount in the used liquids has been determined to be below 20 ppm using a *C20 Coulometric KF Titrator* from *Mettler Toledo*. The electrolyte was prepared in an *MBraun LABmasterpro ECO* glove box under argon atmosphere with <1 ppm H₂O and <1 ppm O₂.

Chemical-physical-characterisation.—The conductivity of the electrolyte was measured using a potentiostat *ModuLabXM (Solartron analytical)* in the temperature range comprised between 30 and 80 °C as described in Ref. 29. The viscosity of the electrolytes was determined using a rheometer *MCR 102 (Anton*

⁼These authors contributed equally to the work.

^{*}Electrochemical Society Member.

^zE-mail: aponrouch@icmab.es; andrea.balducci@uni-jena.de

Paar) in the temperature range comprised between 30 and 80 °C as described in Ref. 29.

Electrode preparation.—AC-based electrodes were prepared following a procedure identical to that used by Krause et al.³⁰ The dry composition of the electrodes was 90 wt % of active material (AC, *DLC Super, Norit*) 5 wt % of conducting agent (*Super C65, Imerys*) and 5 wt % of binder (carboxymethyl cellulose, *Dow*). The mass loading of the electrodes was comprised between 2.6 mg cm⁻² and 3.5 mg cm⁻², the electrode area was equal to 1.13 cm². As (oversized) counter electrodes, AC-based electrodes were used to determine the maximum operative voltage (OPV) of the investigated EDLCs. The electrodes were prepared following the procedure indicated in Ref. 31. The electrode composition was 90 wt % of AC (*DLC Super, Norit*), 5 wt % of carbon black (*Super C65, Imerys*) and 5 wt % of binder (polytetrafluoroethylene, *Aldrich*). The mass loading of these electrodes was about 40 mg cm⁻², and their area was 1.33 cm².

TiS₂ (99.995%, *Aldrich*) electrodes were prepared by tape casting with 10% polyvinylidenefluorid binder and 10% carbon black (*Super P, Timcal*) as conductive additive, as described in Ref. 32. An aluminium foil was used as current collector. 11 mm diameter electrodes were employed with a loading of 0.8 mg cm⁻².

Electrochemical measurements.—All electrochemical measurements in the EDLC setup have been carried out using a three-electrode *Swagelok* cell setup. In every cell, *Whatman* glass microfiber filters (150 mm) were used as separators, drenched with

150 µl electrolyte. The cell assembly was done under argon atmosphere in an *MBraun LABmasterpro ECO glove box* with <1 ppm H₂O and <1 ppm O₂. All tests were carried out at 30 °C to ensure that all electrolytes were liquid when employed in the cells.

The electrochemical stability window (ESW) of the electrolytes was measured using a platinum electrode as working electrode, an oversized carbon electrode as counter electrode, and a silver electrode as quasireference electrode (QRE). After a 12-hour open circuit voltage (OCV) measurement to reach equilibrium, the cells were swept from OCV towards either positive or negative direction at 1 mV s⁻¹ until a potential of -6 V vs OCV and 6 V vs OCV was reached, respectively. For each direction, fresh electrolyte was used.

For the determination of the OPV of AC-based electrodes in the investigated electrolyte an AC-based working electrode, an oversized carbon electrode as counter electrode, and a silver electrode as QRE were used. The OPV was determined via the method described in Ref. 33.

The electrochemical behavior of the cells was investigated using cyclic voltammetry (CV) carried out at different scan rates (1 mV s⁻¹, 5 mV s⁻¹, 10 mV s⁻¹, 25 mV s⁻¹, 50 mV s⁻¹ and 100 mV s⁻¹) and galvanostatic cycling (CC) experiments carried out at different current densities (0.1 A g⁻¹, 0.25 A g⁻¹, 0.5 A g⁻¹, 1 A g⁻¹ and 2.5 A g⁻¹).

TiS₂ electrodes were cycled in *Swagelok* cells at 100 °C in three electrodes configuration with Ag QRE and activated carbon CE (*YP17, Kuraray*). Four layers of glass fiber separators (*Whatman GF/D*) were employed, with the reference electrode placed in the middle. The separators were soaked in PC at 100 °C for 5 d then

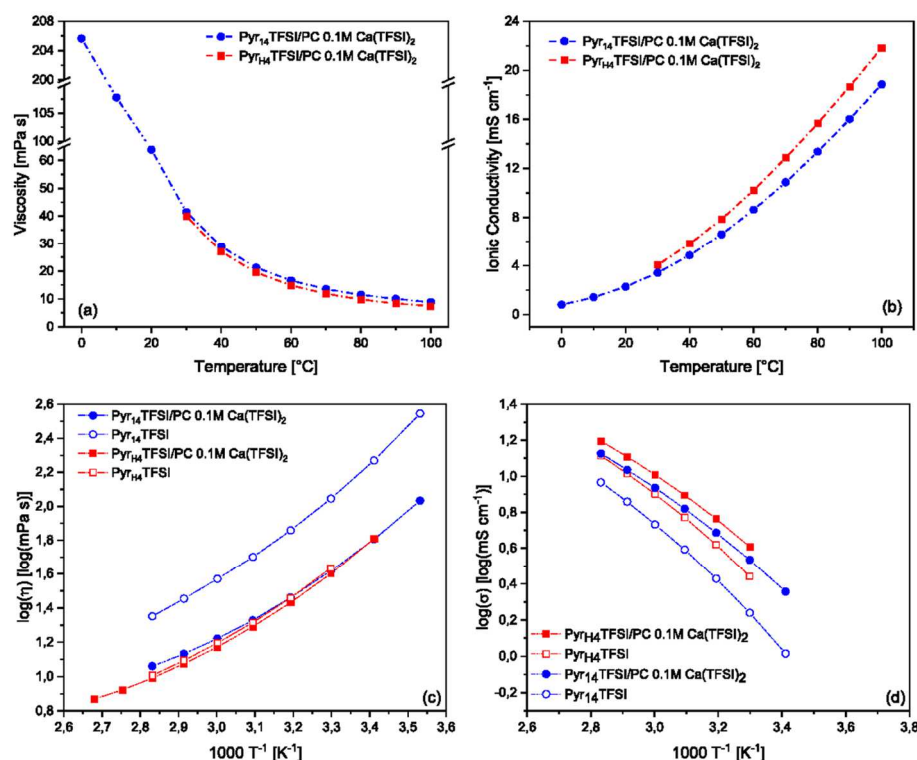


Figure 1. Influence of the temperature on the (a) viscosity and (b) conductivity of the electrolytes based on Pyr₁₄TFSI:PC (blue) and Pyr_{Tf4}TFSI:PC (red), both with 0.1 mol l⁻¹ Ca(TFSI)₂. (c) and (d) show Arrhenius plots of the viscosity and conductivity of the electrolytes based on Pyr₁₄TFSI and Pyr_{Tf4}TFSI with Ca(TFSI)₂ as well as pure Pyr_{Tf4}TFSI and pure Pyr₁₄TFSI.

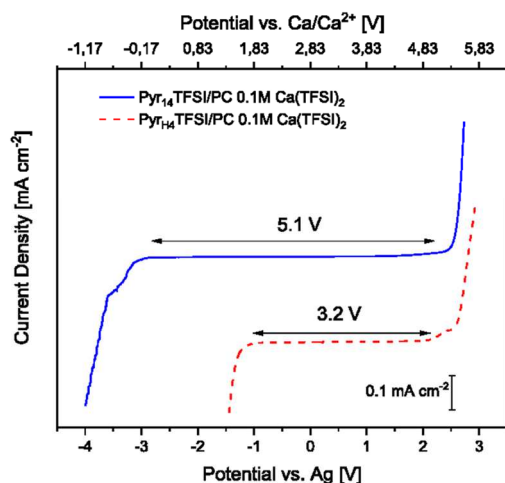


Figure 2. Electrochemical stability of the investigated electrolytes at room temperature (scan rate of 1 mV s^{-1}).

rinsed with dimethyl carbonate and dried before use. The CE were pre-charged in symmetric cells at room temperature to ensure that they remain in a safe voltage window with respect to electrolyte oxidation during cycling of TiS_2 and suppress electrolyte dilution effects. For cycling of TiS_2 in $\text{Pyr}_{14}\text{TFSI}:\text{PC}$ (0.1 M Ca(TFSI)_2), the CE were pre-charged in PC (0.1 M Ca(TFSI)_2) to ensure Ca^{2+} is the ion released by the CE at first reduction of TiS_2 ; for cycling in $\text{Pyr}_{14}\text{TFSI}:\text{PC}$, the CE were pre-charged in the same electrolyte to avoid the presence of Ca^{2+} in the cell.

TiS_2 was discharged and charged galvanostatically at $C/50$ ($C \Leftrightarrow 1$ divalent cation inserted in TiS_2 in 1 h) between -2.4 and -0.25 V vs Ag , with each step limited to 40 h, using an *MPG-2 potentiostat (Bio-Logic)*. In case of complete reoxidation of TiS_2 , the charge was limited in capacity rather than when reaching the higher cut-off potential.

Ex situ X-ray diffractometry.—After cycling, the cells were disassembled in the glove box; the active material was recovered, rinsed with dimethyl carbonate and embedded in glass capillaries to record X-ray diffraction patterns in θ - θ configuration using a *Bruker D8 Advance A25 diffractometer* equipped with a $\text{Mo K}\alpha 1$ radiation source ($\lambda = 0.7093 \text{ \AA}$) and Johansson monochromator.

Results and Discussion

At first, the chemical-physical properties of the considered mixtures of PC and AIL and PIL have been investigated. Since the melting point of $\text{Pyr}_{14}\text{TFSI}$ is $-3 \text{ }^\circ\text{C}$ and that of $\text{Pyr}_{\text{H4}}\text{TFSI}$ is higher than $30 \text{ }^\circ\text{C}$ the operating temperature range of the former is wider. Figure 1a shows the influence of the temperature on the viscosity of both electrolytes. Until $30 \text{ }^\circ\text{C}$, the viscosity of the electrolyte containing $\text{Pyr}_{14}\text{TFSI}$ is rather high, starting with 206 mPa s at $0 \text{ }^\circ\text{C}$, and decreasing to 42 mPa s at $30 \text{ }^\circ\text{C}$. At this temperature, the electrolyte containing $\text{Pyr}_{\text{H4}}\text{TFSI}$ displays a comparable viscosity (39 mPa s). With increasing temperature, the viscosity of both electrolytes is decreasing in a similar way. At $100 \text{ }^\circ\text{C}$ the viscosity is reduced to 9 mPa s and 7 mPa s for the electrolyte containing the AIL and the PIL, respectively. From $30 \text{ }^\circ\text{C}$ on, the electrolyte containing $\text{Pyr}_{\text{H4}}\text{TFSI}$ is showing an overall lower viscosity compared to the one containing the AIL. This is due to the additional alkyl chain in the $[\text{Pyr}_{14}]^+$ cation, which is impeding the movement of ions.³⁴ Since the ILs are diluted with PC, this effect

is less pronounced. Compared with the viscosity of 0.1 M Ca(TFSI)_2 in PC ($\sim 3.5 \text{ mPa s}$ at $25 \text{ }^\circ\text{C}$) the neat IL-based electrolytes display an increased viscosity.³⁵ This is not surprising due to the strong interionic bonds between cations and anions of the IL. Nevertheless, the viscosities displayed by both electrolytes appear suitable for the use in energy storage devices.

The influence of the temperature on the ionic conductivity of the electrolytes is displayed in Fig. 1b. Starting at $0 \text{ }^\circ\text{C}$ the electrolyte containing $\text{Pyr}_{14}\text{TFSI}$ is exhibiting a conductivity of 0.8 mS cm^{-1} , which is rising to 3.4 mS cm^{-1} at $30 \text{ }^\circ\text{C}$ and to 18.9 mS cm^{-1} at $100 \text{ }^\circ\text{C}$. Analogous, the ionic conductivity of the electrolyte containing $\text{Pyr}_{\text{H4}}\text{TFSI}$ is increasing from 4 mS cm^{-1} at $30 \text{ }^\circ\text{C}$ to 21.8 mS cm^{-1} at $100 \text{ }^\circ\text{C}$, which is slightly higher than the aprotic one, due to the higher viscosity of the latter one. Additionally, in PILs the ion transport is not only governed by vehicular mechanisms but also by ion, or more specific, proton hopping. This latter transport is independent of the viscosity, which may explain the stronger increase in conductivity of the PIL.³⁶⁻³⁹

Near room temperature the IL containing electrolytes display similar ionic conductivity compared to 0.1 M Ca(TFSI)_2 in PC with approximately 3 mS cm^{-1} at $30 \text{ }^\circ\text{C}$.³⁵ Figures 1c–1d depict the Arrhenius plots of the viscosity and conductivity of the investigated electrolytes and, for comparison, the pure $\text{Pyr}_{14}\text{TFSI}$ and $\text{Pyr}_{\text{H4}}\text{TFSI}$. The mixtures with PC and Ca(TFSI)_2 are showing the typical “non-Arrhenius” behavior of ILs. Among the two electrolytes, the $\text{Pyr}_{14}\text{TFSI}$ and PC mixture appears to deviate more from the behavior of the pure IL than that containing the $\text{Pyr}_{\text{H4}}\text{TFSI}$. This is especially true when the viscosities are considered. Very likely, this is due to the general higher viscosity of the $\text{Pyr}_{14}\text{TFSI}$, which is more easily reduced when mixed with a low viscosity solvent.

Figure 2 shows the ESW of the investigated electrolytes. The electrolyte containing $\text{Pyr}_{14}\text{TFSI}$ displays an overall potential window of about 5.1 V , which is the result of a large cathodic ($\sim -3 \text{ V vs Ag}$) as well as anodic ($\sim 2.1 \text{ V vs Ag}$) stability. The ESW of the electrolyte containing $\text{Pyr}_{\text{H4}}\text{TFSI}$ is significantly lower, and equal to 3.2 V . The cathodic stability appears therefore limited by the cation $[\text{Pyr}_{14}]^+$ or $[\text{Pyr}_{\text{H4}}]^+$ decomposition, rather than the calcium plating, the lower stability in the latter case being due to the presence of the “free” proton which is getting reduced at -1.1 V vs Ag .¹⁸ The anodic stability of both electrolytes, on the other hand, is comparable, suggesting that it is dictated by the reduction of the $[\text{TFSI}]^-$ anion. It is important to notice that the ESWs of both electrolytes are comparable with those of the pure ILs.⁴⁰

In order to effectively utilize the investigated electrolytes in combination with AC-based electrodes, the OPV of these electrolytes need to be assessed.⁴¹ Obviously, the maximum OPV achievable with AC-based electrodes is lower than the ESW measurement. This is due to the higher reactivity of the AC surface compared to that of the inert Pt electrode utilized for the determination of the ESW.⁴² Figure 3 compares the maximum OPV possible for AC-based electrodes in the two investigated electrolytes, as obtained by CV measurements. The positive and negative limits have been defined considering the Coulombic efficiency of the process (threshold 98%). It has to be noted that calcium has not been used as electrolyte component for EDLC in the past, partly because the electroadsorption of large bivalent ions can be problematic at a given pore size and because of superior transport properties of conventional ions like quaternary ammonium cations.⁴³ As shown in Fig. 3a, the use of the electrolyte containing $\text{Pyr}_{14}\text{TFSI}$ allows a maximum OPV of 3.3 V , which is resulting from a negative and positive limit of -1.91 V vs Ag and 1.39 V vs Ag , respectively. This OPV is smaller compared to that reported for the pure $\text{Pyr}_{14}\text{TFSI}$ in combination with the same electrodes (3.8 V), but is comparable with that observed for other mixtures of $\text{Pyr}_{14}\text{TFSI}$ and alkali metals, e.g. Li and Na, based salts.⁴⁰ This difference is mainly caused by a shortening of the cathodic stability, suggesting a possible parasitic contribution due to the reduction of the solvent molecules present in the calcium cation complex. By contrast, the cathodic stability of the electrolyte containing $\text{Pyr}_{\text{H4}}\text{TFSI}$ is only slightly modified by the use

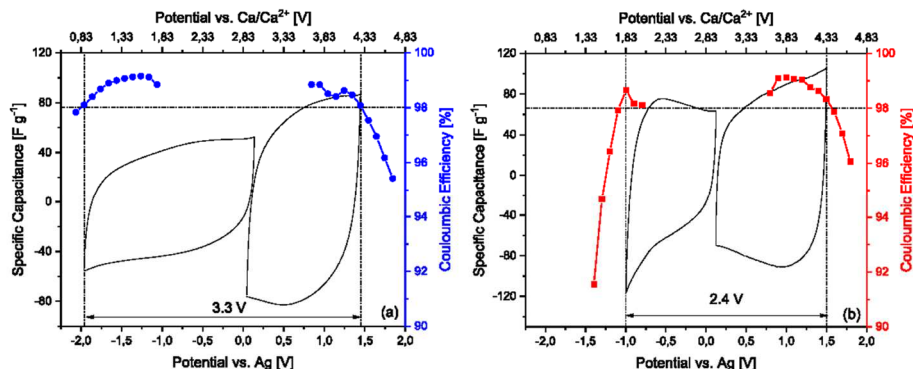


Figure 3. Specific capacitance and Coulombic efficiency obtained by CV at 5 mV s^{-1} using an AC electrode and the aprotic (a) and protic (b) IL-based electrolytes. The horizontal line represents a 98% threshold in efficiency, the vertical lines mark the potential at which the efficiency falls below 98%.

of AC (-0.95 V vs Ag) when compared with Pt electrode (-1.1 V vs Ag) and an ESW of 2.4 V is obtained. The reduction of the free proton of the $[\text{PyT}_{\text{H}_4}]^+$ cation thus appears to be only slightly affected by the nature of the electrode used. As for the anodic stability recorded with AC electrodes, both electrolytes present similar values (about 1.5 V vs Ag) dictated by the TFSI anion oxidation, about 1 V earlier than with the Pt electrode. These results are comparable to those reported for AC-based electrodes used in combination with neat $\text{PyT}_{\text{H}_4}\text{TFSI}$ (Figure S1).⁴⁰

After these measurements, EDLCs containing the AC-based electrodes and the two investigated electrolytes have been assembled and tested. The tests have been carried out utilizing the maximum OPV determined in the previous experiments. Figure 4 shows the CVs of the EDLCs containing the two electrolytes. Both EDLCs display the typical rectangular shape characteristic of these devices, and no significant faradic peaks are visible. Overall, the EDLC containing $\text{PyT}_{14}\text{TFSI}$ appears to display a better performance than the one containing $\text{PyT}_{\text{H}_4}\text{TFSI}$. The former displays a higher OPV ($3.3 \text{ V vs } 2.4 \text{ V}$) and capacitance (25 F g^{-1} vs 20 F g^{-1}) than the latter.

Afterwards, CC measurements carried out at different current densities were performed. As shown in Fig. 4, also during these tests the EDLC containing $\text{PyT}_{14}\text{TFSI}$ appears to display a better performance than the one containing $\text{PyT}_{\text{H}_4}\text{TFSI}$. At 0.1 A g^{-1} the device capacitance was equal to 18 F g^{-1} and 16 F g^{-1} for the system containing the AIL and the PIL, respectively. Both systems

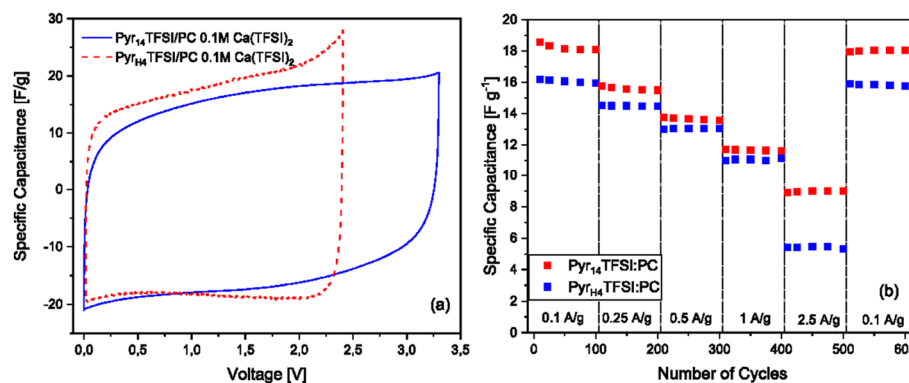


Figure 4. (a) Cyclic Voltammetry (scan rate 1 mV s^{-1}) and (b) capacitance retention at different current densities of EDLCs containing the investigated electrolytes. The test have been carried out at $30 \text{ }^\circ\text{C}$.

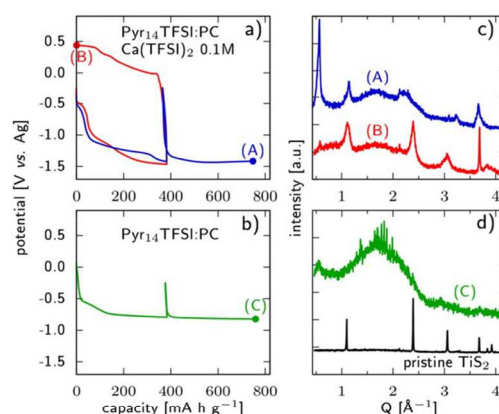


Figure 5. Galvanostatic charge/discharge profiles of TiS_2 electrodes at $C/50$ in $\text{PyT}_{14}\text{TFSI:PC}$ (0.1 M Ca(TFSI)_2) (a) and $\text{PyT}_{\text{H}_4}\text{TFSI:PC}$ (b) and $100 \text{ }^\circ\text{C}$; X-ray diffraction patterns of the active material after extended reduction or one complete cycle in $\text{PyT}_{14}\text{TFSI:PC}$ (0.1 M Ca(TFSI)_2) (c) and after extended reduction in $\text{PyT}_{\text{H}_4}\text{TFSI:PC}$ (d). The diffraction pattern of pristine TiS_2 is reported in Ref. 32 as well in (d).

display good capacitance retention up to 1 A g^{-1} . At 2.5 A g^{-1} however, the device containing the electrolyte based on $\text{Py}_{14}\text{TFSI}$ shows a low capacitance retention, compared to the one based on $\text{Py}_{14}\text{TFSI}$. This difference could be partially caused by the operative temperature of the experiment (30°C), which is in proximity of the melting point of the PIL.

Taking these results into account, the use of the investigated IL-based electrolytes in combination with battery materials, we performed CC measurements of TiS_2 in $\text{Py}_{14}\text{TFSI:PC}$ (0.1 M Ca(TFSI)_2) electrolyte, which displays the highest cathodic stability limit (Fig. 2). A pre-calculated AC CE and a Ag QRE were used, to prevent the cell to be limited by a Ca anode.⁴⁴

In order to investigate the impact of the investigated electrolytes when used in combination with battery materials, we performed CC measurements of TiS_2 in $\text{Py}_{14}\text{TFSI:PC}$ (0.1 M Ca(TFSI)_2) electrolyte, which displays the highest cathodic stability limit (Fig. 2). A pre-calculated AC CE and a Ag QRE were used, to prevent the cell to be limited by a Ca anode.⁴⁴

The voltage of the TiS_2 electrode for one galvanostatic cycle or prolonged reduction at $C/50$ in $\text{Py}_{14}\text{TFSI:PC}$ (0.1 M Ca(TFSI)_2) at 100°C is reported in Fig. 5. After an initial decrease from -0.5 to about -1.2 V vs Ag , the voltage nearly stabilizes and the discharge is limited in capacity to 0.8 Ca^{2+} per formula unit (i.e., 383 mAh g^{-1} (TiS_2) in 40 h). This response differs from that of the same electrode in 0.3 M Ca(TFSI)_2 in PC, where the voltage gradually decreases and no plateau is reached.³²

As the current is reversed, the voltage quickly reaches the value of the initial rest potential, showing a high hysteresis. At this point, the current was reversed again in the case of the prolonged reduction and a capacity corresponding to another 0.8 Ca^{2+} could be passed through the cell (reaching point (A)). In a second cell, the first oxidation was pursued until annulling the net capacity passed through the cell reaching point (B) at 450 mV vs Ag .

To better understand the role of the $[\text{Py}_{14}]^+$ cation, a prolonged reduction of TiS_2 was performed in an electrolyte which does not contain calcium cations (in $\text{Py}_{14}\text{TFSI:PC}$, Fig. 5b). The voltage response appears very similar to the one obtained in $\text{Py}_{14}\text{TFSI:PC}$ (0.1 M Ca(TFSI)_2), though shifted by $\approx 400 \text{ mV}$ towards positive values. This shift can be attributed to a difference in potential of the QRE between the two electrolytes, since a comparable difference is observed for the CE: $-600 \text{ mV vs Ag QRE}$ in $\text{Py}_{14}\text{TFSI:PC}$ (0.1 M Ca(TFSI)_2) and -150 mV in $\text{Py}_{14}\text{TFSI:PC}$ after 15 h rest (not shown). As the current is reversed after a specific capacity of 383 mAh g^{-1} has been reached, the voltage increases by more than 500 mV , reaching the cut-off limit, which shows that the hysteresis is important in this electrolyte as well. As in the case of the electrolyte containing Ca(TFSI)_2 salt, the reduction could subsequently be extended by a capacity value equivalent to 0.8 Ca^{2+} in TiS_2 , reaching point (C).

Ex-situ X-ray diffraction (XRD) patterns are reported in Figs. 5c and 5d for TiS_2 tested in $\text{Py}_{14}\text{TFSI:PC}$ (0.1 M Ca(TFSI)_2) and $\text{Py}_{14}\text{TFSI:PC}$, respectively. The diffraction pattern of pristine TiS_2 powder is also reported in Fig. 5d for comparison. After extended reduction in $\text{Py}_{14}\text{TFSI:PC}$ (0.1 M Ca(TFSI)_2) (pattern (A)), peaks of TiS_2 can still be identified at wavenumbers of 1.1 , 2.4 , and 3.7 \AA^{-1} , despite their important broadening. The most intense peak, at a value of 0.57 \AA^{-1} corresponding to an interlayer distance of 11.1 \AA , is a consequence of the intercalation of cations in the structure, possibly with concomitant intercalation of PC molecules. It is worth mentioning that using 0.3 M Ca(TFSI)_2 in PC electrolyte, a similar peak related to solvent co-intercalation was observed.³² However, the latter was recorded at a higher Q value of 0.68 \AA^{-1} and suggests that $[\text{Py}_{14}]^+$ cation (larger than PC) can be inserted in TiS_2 .

After a complete cycle in $\text{Py}_{14}\text{TFSI:PC}$ (0.1 M Ca(TFSI)_2) (pattern (B)), the characteristic peaks of TiS_2 are still clearly identified despite significant broadening, indicative of reduced crystallite size after discharge and charge. The peak at 0.57 \AA^{-1} is also observed, indicating that the processes occurring in reduction were not fully reversed at oxidation. These results suggest that insertion and de-insertion of cations inside the structure of TiS_2 is

possible in this electrolyte, as it was shown to occur in PC (0.3 M Ca(TFSI)_2).²⁹ However, by contrast with the IL free electrolyte, cycling in $\text{Py}_{14}\text{TFSI:PC}$ (0.1 M Ca(TFSI)_2) lead to a higher degree of amorphization of the host structure and only partial removal of the intercalated species upon oxidation (the peak at 0.57 \AA^{-1} being still observed in point (B), Fig. 5c). The XRD data in Fig. 5d reveals quasi total amorphization of TiS_2 after extended reduction in $\text{Py}_{14}\text{TFSI:PC}$. A low intensity peak is still present at 0.55 \AA^{-1} as a remaining of the largest ordering range in the intercalated phase.

Overall, it appears that intercalation of $[\text{Py}_{14}]^+$ into TiS_2 can take place leading to the formation of significant interlayer distances and amorphization. A lower degree of amorphization being reached after reduction in $\text{Py}_{14}\text{TFSI:PC}$ (0.1 M Ca(TFSI)_2) than in $\text{Py}_{14}\text{TFSI:PC}$ suggests preferential insertion of Ca^{2+} with respect to $[\text{Py}_{14}]^+$. Nevertheless, the insertion is not fully selective since the same voltage trend is observed in both electrolytes and similar interlayer distances are obtained upon reduction. These results also differ from the one obtained in $\text{Py}_{14}\text{TFSI}$ free electrolyte, in which the capacity and degree of amorphization reached in reduction are lower than in the electrolytes employed in the present work.

Conclusions

The development of innovative electrolytes is of great importance for the development of advanced Ca batteries. In this work we showed that electrolytes based on mixtures of PC and AIL/PIL containing the salt Ca(TFSI)_2 display good transport properties and ESWs comparable with those of electrolytes with similar composition, but suitable for Li- or Na-based systems. The use of these electrolytes in EDLCs with AC electrodes showed to be a viable strategy to obtain devices displaying good capacitances paired with a high reversibility and stability. When AIL-based electrolytes are used, also high voltage devices can be realized. Considering these results, AC appears therefore as suitable material for the realization of Ca-based devices. The use of IL-based electrolytes in combination with TiS_2 , on the other hand, appears more challenging. In order to build a reliable Ca-based battery device, the active material should either insert Ca^{2+} selectively, or accommodate the large cation of the IL without damage. We showed that this is not the case for the combination of $[\text{Py}_{14}]^+$ with TiS_2 , which is known for having the ability to host a broad variety of species in its structure but gets amorphized upon insertion of the $[\text{Py}_{14}]^+$ cation. In order to overcome this problem, the use of different IL, e.g. with different cations, and the investigation of other active materials should be considered in the future.

Acknowledgments

AB and TS wish to thank the Friedrich Schiller University of Jena for the financial support. Funding from the European Research Council (ERC) under the European Union's Horizon 2020 research and innovation programme (ERC-2016-STG, CMBAT grant agreement No 715087) is acknowledged. RD acknowledges support of the Beatriu de Pinós postdoctoral programme of the Government of Catalonia's Secretariat for Universities and Research of the Ministry of Economy and Knowledge (2017 BP 00187). A. Ponrouch is grateful to the Spanish Ministry for Economy, Industry and Competitiveness Severo Ochoa Programme for Centres of Excellence in R&D (SEV-2015-0496). We thank Dr. R. Verrelli for providing us with TiS_2 electrodes and for helpful discussion.

ORCID

A. Ponrouch  <https://orcid.org/0000-0002-8232-6324>
A. Balducci  <https://orcid.org/0000-0002-2887-8312>

References

1. D. Monti, A. Ponrouch, R. B. Araujo, F. Bardé, P. Johansson, and M. R. Palacín, "Multivalent batteries—prospects for high energy density: Ca batteries." *Frontiers in Chemistry*, **7**, 79 (2019).
2. M. E. Arroyo-de Dompablo, A. Ponrouch, P. Johansson, and M. Palacín, "Achievements, challenges, and prospects of calcium batteries." *Chem. Rev.* (2019).
3. C. Vaalma, D. Buchholz, M. Weil, and S. Passerini, "A cost and resource analysis of sodium-ion batteries." *Nature Reviews Materials*, **3**, 18013 (2018).
4. R. Deivanayagam, B. J. Ingram, and R. Shabazzian-Yassar, "Progress in development of electrolytes for magnesium batteries." *Energy Storage Materials*, **21**, 136 (2019).
5. L. Gaddum and H. French, "The electrolysis of grignard solutions1." *JACS*, **49**, 1295 (1927).
6. A. Ponrouch, C. Frontera, F. Bardé, and M. R. Palacín, "Towards a calcium-based rechargeable battery." *Nat. Mater.*, **15**, 169 (2016).
7. D. Wang, X. Gao, Y. Chen, L. Jin, C. Kuss, and P. G. Bruce, "Plating and stripping calcium in an organic electrolyte." *Nat. Mater.*, **17**, 16 (2018).
8. Z. Li, O. Fuhr, M. Fichtner, and Z. Zhao-Karger, "Towards stable and efficient electrolytes for room-temperature rechargeable calcium batteries." *Energy & Environmental Science*, **12**, 3496 (2019).
9. A. Shyamsunder, L. E. Blanc, A. Assoud, and L. F. Nazar, "Reversible calcium plating and stripping at room temperature using a borate salt." *ACS Energy Lett.*, **4**, 2271 (2019).
10. EuropeanChemicalsAgency. Community rolling action plan: Ethylene Carbonate. 2019 05.07.2019 23.10.
11. M. Ishikawa, T. Sugimoto, M. Kikuta, E. Ishiko, and M. Kono, "Pure ionic liquid electrolytes compatible with a graphitized carbon negative electrode in rechargeable lithium-ion batteries." *J. Power Sources*, **162**, 658 (2006).
12. K. L. Van Aken, M. Beidaghi, and Y. Gogotsi, "Formulation of ionic-liquid electrolyte to expand the voltage window of supercapacitors." *Angew. Chem. Int. Ed.*, **54**, 4806 (2015).
13. Z. Lin, D. Barbara, P.-L. Taberna, K. L. Van Aken, B. Anasori, Y. Gogotsi, and P. Simon, "Capacitance of Ti3C2Tx MXene in ionic liquid electrolyte." *J. Power Sources*, **326**, 575 (2016).
14. M. Moreno, E. Simonetti, G. Appetecchi, M. Carewska, M. Montanino, G.-T. Kim, N. Loeffler, and S. Passerini, "Ionic liquid electrolytes for safer lithium batteries I. investigation around optimal formulation." *J. Electrochem. Soc.*, **164**, A6026 (2017).
15. H. Sun, G. Zhu, X. Xu, M. Liao, Y.-Y. Li, M. Angell, M. Gu, Y. Zhu, W. H. Hung, and J. Li, "A safe and non-flammable sodium metal battery based on an ionic liquid electrolyte." *Nat. Commun.*, **10**, 3302 (2019).
16. T. Shiga, H. Kondo, Y. Kato, and M. Inoue, "Insertion of calcium ion into prussian blue analogue in nonaqueous solutions and its application to a rechargeable battery with dual carriers." *The Journal of Physical Chemistry C*, **119**, 27946 (2015).
17. S. Biria, S. Pathreker, F. S. Genier, H. Li, and I. D. Hosein, "Plating and stripping calcium at room temperature in an ionic-liquid electrolyte." *ACS Appl. Energy Mater.*, **3**, 2310 (2020).
18. P. A. Z. Suarez, C. S. Consorti, R. F. D. Souza, J. Dupont, and R. S. Gonçalves, "Electrochemical behavior of vitreous glass carbon and platinum electrodes in the ionic liquid 1-n-Butyl-3-Methylimidazolium trifluoroacetate." *J. Braz. Chem. Soc.*, **13**, 106 (2002).
19. L. Demarconnay, E. G. Calvo, L. Timperman, M. Anouti, D. Lemordant, E. Raymundo-Piñero, A. Arenillas, J. Menéndez, and F. Béguin, "Optimizing the performance of supercapacitors based on carbon electrodes and protic ionic liquids as electrolytes." *Electrochim. Acta*, **108**, 361 (2013).
20. S. Menne, T. Vogl, and A. Balducci, "Lithium coordination in protic ionic liquids." *Phys. Chem. Chem. Phys.*, **16**, 5485 (2014).
21. M. Hasani, J. L. Yarger, and C. A. Angell, "On the use of a protic ionic liquid with a novel cation to study anion basicity." *Chemistry-A European Journal*, **22**, 13312 (2016).
22. T. Vogl, C. Vaalma, D. Buchholz, M. Secchiaroli, R. Marassi, S. Passerini, and A. Balducci, "The use of protic ionic liquids with cathodes for sodium-ion batteries." *Journal of Materials Chemistry A*, **4**, 10472 (2016).
23. T. Vogl, S. Passerini, and A. Balducci, "The impact of mixtures of protic ionic liquids on the operative temperature range of use of battery systems." *Electrochem. Commun.*, **78**, 47 (2017).
24. M. Arnaiz, A. Bothe, S. Dsoke, A. Balducci, and J. Ajuria, "Aprotic and protic ionic liquids combined with olive pits derived hard carbon for potassium-ion batteries." *J. Electrochem. Soc.*, **166**, A3504 (2019).
25. P. Jankowski, K. Matuszek, M. Treskow, M. Armand, D. MacFarlane, and P. Johansson, "Anion amphiprotic ionic liquids as protic electrolyte matrices allowing sodium metal plating." *Chem. Commun.*, **55**, 12523 (2019).
26. S. Lindberg, S. Jeschke, P. Jankowski, M. Abdelhamid, T. Brousse, L. Bideau, P. Johansson, and A. Matic, "Charge storage mechanism of α -MnO₂ in protic and aprotic ionic liquid electrolytes." *J. Power Sources*, **460**, 228111 (2020).
27. D. S. Tchitchekova, A. Ponrouch, R. Verrelli, T. Broux, C. Frontera, A. Sorrentino, F. Bardé, N. Biskup, M. E. Arroyo-de Dompablo, and M. R. Palacín, "Electrochemical intercalation of calcium and magnesium in TiS₂: fundamental studies related to multivalent battery applications." *Chem. Mater.*, **30**, 847 (2018).
28. T. Stettner, F. C. Walter, and A. Balducci, "Imidazolium-based protic ionic liquids as electrolytes for lithium-ion batteries." *Batteries & Supercaps*, **2**, 55 (2019).
29. R.-S. Kühnel, N. Böckenfeld, S. Passerini, M. Winter, and A. Balducci, "Mixtures of ionic liquid and organic carbonate as electrolyte with improved safety and performance for rechargeable lithium batteries." *Electrochim. Acta*, **56**, 4092 (2011).
30. A. Krause, P. Kossyrev, M. Oljaca, S. Passerini, M. Winter, and A. Balducci, "Electrochemical double layer capacitor and lithium-ion capacitor based on carbon black." *J. Power Sources*, **196**, 8836 (2011).
31. S. Pohlmann, B. Lobato, T. A. Centeno, and A. Balducci, "The influence of pore size and surface area of activated carbons on the performance of ionic liquid based supercapacitors." *Phys. Chem. Chem. Phys.*, **15**, 17287 (2013).
32. R. Verrelli, A. Black, R. Dugas, D. Tchitchekova, A. Ponrouch, and M. Palacín, "Steps towards the use of TiS₂ electrodes in Ca batteries." *J. Electrochem. Soc.*, **167**, 070532 (2020).
33. A. Brandt, J. Pires, M. Anouti, and A. Balducci, "An investigation about the cycling stability of supercapacitors containing protic ionic liquids as electrolyte components." *Electrochim. Acta*, **108**, 226 (2013).
34. T. Vogl, S. Menne, R.-S. Kühnel, and A. Balducci, "The beneficial effect of protic ionic liquids on the lithium environment in electrolytes for battery applications." *Journal of Materials Chemistry A*, **2**, 8258 (2014).
35. J. D. Forero-Saboya, E. Marchante, R. Araujo, D. Monti, P. Johansson, and A. Ponrouch, "Cation solvation and physicochemical properties of Ca battery electrolytes." *The Journal of Physical Chemistry C*, **123**, 29524 (2019).
36. Z. Wojnarowska, Y. Wang, J. Pionteck, K. Grzybowska, A. P. Sokolov, and M. Paluch, "High pressure as a key factor to identify the conductivity mechanism in protic ionic liquids." *Phys. Rev. Lett.*, **111**, 225703 (2013).
37. Z. Wojnarowska, K. Kolodziejczyk, K. J. Paluch, L. Tajber, K. Grzybowska, K. L. Ngai, and M. Paluch, "Decoupling of conductivity relaxation from structural relaxation in protic ionic liquids and general properties." *Phys. Chem. Chem. Phys.*, **15**, 9205 (2013).
38. Z. Wojnarowska, Y. Wang, K. J. Paluch, A. P. Sokolov, and M. Paluch, "Observation of highly decoupled conductivity in protic ionic conductors." *Phys. Chem. Chem. Phys.*, **16**, 9123 (2014).
39. J. Ingenmey, S. Gehrke, and B. Kirchner, "How to harvest Grothuss diffusion in protic ionic liquid electrolyte systems." *Chem. Sus. Chem.*, **11**, 1900 (2018).
40. T. Stettner, P. Huang, M. Goktas, P. Adelhelm, and A. Balducci, "Mixtures of glyme and aprotic-protic ionic liquids as electrolytes for energy storage devices." *J. Chem. Phys.*, **148**, 193825 (2018).
41. S. Vaquero, J. Palma, M. Anderson, and R. Marcella, "Mass-balancing of electrodes as a strategy to widen the operating voltage window of carbon/carbon supercapacitors in neutral aqueous electrolytes." *Int. J. Electrochem. Sci.*, **8**, 10293 (2013).
42. K. Xu, S. P. Ding, and T. R. Jow, "Toward reliable values of electrochemical stability limits for electrolytes." *J. Electrochem. Soc.*, **146**, 4172 (1999).
43. E. Avraham, B. Yaniv, A. Soffer, and D. Aurbach, "Developing ion electroadsorption stereoselectivity, by pore size adjustment with chemical vapor deposition onto active carbon fiber electrodes. Case of Ca²⁺/Na⁺ separation in water capacitive desalination." *The Journal of Physical Chemistry C*, **112**, 7385 (2008).
44. R. Dugas, J. D. Forero-Saboya, and A. Ponrouch, "Methods and Protocols for Reliable Electrochemical Testing in Post-Li Batteries (Na, K, Mg, and Ca)." *Chem. Mater.*, **31**, 8613 (2019).

2.3. Confinement of PILs

2.3.1. Publikation 8: Silica based ionogels: interface effects with aprotic and protic ionic liquids with lithium

In this work, we investigated the effect of confining ILs ([Pyr₁₄][TFSI] and [Pyr_{H4}][TFSI]) within a meso- and microporous silica monolith material, with the aim to develop a highly conductive ionogel. This solid electrolyte prevents leakage of electrolyte and is combined with the low flammability of ILs, making it a very safe and attractive alternative electrolyte system.

Of very high interest is the behavior of the different types of ILs, either protic or aprotic, when confined (e.g., in very small pores). In general, this confinement has an influence on the thermal properties like m.p. or T_g, transport properties and on the interactions on a molecular scale in general, which can be analyzed via Raman spectroscopy. These influences also depend on the pore sizes of the silica, thus by changing the structure of the host material the resulting properties of the ionogel can be adjusted to some extent. Furthermore, the influence caused by the addition of a lithium salt, necessary for the application in LIB application, was also investigated.

First, the thermal properties were investigated. It could be shown, that the m.p. of [Pyr₁₄][TFSI] is increased when confined in the silica, contrary to [Pyr_{H4}][TFSI] where the m.p. is decreased when confined. This suggests a higher affinity of the more polar liquid [Pyr_{H4}][TFSI] for the host network compared to the less polar liquid [Pyr₁₄][TFSI]. Interestingly, when the lithium salt LiTFSI is added the behavior only changes for [Pyr_{H4}][TFSI]. The lithium-ions appear to change the interaction between the silica pore walls and the [Pyr_{H4}]⁺ cation, owing to the high affinity of Li-ions towards silica, competing with the H-bonding of the PIL and the silica surface groups.

Depending on the pore size, the heat capacity of all systems changed similarly. With increasing pore size, the surface to volume ratio decreased, thus less IL is constrained at the pore walls, allowing an increase in macroscopic entropy.

A pore size dependency was also observed for the conductivity of the different systems. When increasing the pore size, the conductivity does so too. Overall, however, the conductivity of

the confined ILs is decreased compared to the bulk ILs. This is simply because of a restricted ion mobility within the host structure.

Lastly, the coordination of Li-ions was investigated by employing Raman spectroscopy. Using the ratio between the signal from coordinated $[\text{TFSI}]^-$ and the total signal of $[\text{TFSI}]^-$, the coordination number of Li^+ was calculated for each system. In $[\text{Pyr}_{14}][\text{TFSI}]$ the coordination of Li^+ by $[\text{TFSI}]^-$ decreased when confined, as the interaction between Li^+ and silanolates is preferred compared to the interaction of Li^+ and $[\text{TFSI}]^-$. On the other hand, there was no clear change visible for the protic system. We assume that this is due to stronger interactions between silanolates and $[\text{Pyr}_{\text{H}4}]^+$, competing with the Li^+ .

This study has shown that the confinement of ILs has significant effects on their properties and affects the intermolecular interactions. Furthermore, the presence of the proton in PILs seems to play a very important role in these interactions, depending also on the surface properties of the host matrix. In the future, it will be necessary to investigate the role of the ΔpK_a of a PIL on the changes in properties, especially the coordination of Li^+ . Of course, the application of these ionogels in electrochemical energy storage devices should also be considered.

Cite this: *Phys. Chem. Chem. Phys.*, 2020, **22**, 24051

Silica based ionogels: interface effects with aprotic and protic ionic liquids with lithium†

Angélique Marie,^a Bilel Said,^b Anne Galarneau,^b Timo Stettner,^c Andrea Balducci,^{b,c} Maxime Bayle,^a Bernard Humbert^b and Jean Le Bideau^b *^a

In the frame of the development of solid ionogel electrolytes with enhanced ion transport properties, this paper investigates ionogel systems constituted by ~80 wt% of ionic liquids (ILs) confined in meso-/macroporous silica monolith materials. The anion–cation coordination for two closely related ILs, either aprotic (AIL) butyl-methylpyrrolidinium or protic (PIL) butylpyrrolidinium, both with bis(trifluoromethylsulfonyl)imide (TFSI) anions, with and without lithium cations, is studied in depth. The ILs are confined within silica with well-defined mesoporosities (8 to 16 nm). The effects of this confinement, onto melting points, onto conductivity followed by impedance spectroscopy, and onto lithium–TFSI coordination followed by Raman spectroscopy, are presented. Opposite effects have been observed on the melting temperature: it increased for the AIL (+2 °C) upon confinement, while it decreased for the PIL (–2 °C). With lithium, the confinement led to an increase of the melting temperature (+1 °C) for the PIL and AIL. Regarding ionic conductivities, a relative maximum was observed at 40 °C for a mesopore diameter of 10 nm for the AIL with 0.5 M lithium, while it was not clearly visible for the PIL. These differences are discussed in view of the charge balance at the interface between silanols and ILs: the presence of a PIL, contrary to an AIL, is expected to modify the acidity of the silica. Raman data showed that the coordination number of lithium by TFSI is reduced upon AIL confinement, although this was not observed for PILs. At last, this work highlights the impact of the acidity of a PIL on the chemistry occurring at the interface of the host network within ionogels.

Received 6th July 2020.
Accepted 29th September 2020
DOI: 10.1039/d0cp03599h

rsc.li/pccp

Introduction

Ionic liquids (ILs) have been studied intensively for different purposes, from catalysts to sensors, energy storage devices, optical devices, *etc.* One of the key features of ILs is to be composed solely of ions, and to be at a liquid state below 100 °C. This results in good dynamics and transport properties,¹ very low flammability and low vapour pressures, making them highly attractive alternatives for conventional electrolytes for electrochemical storage devices.² Different classes of ILs are of interest, owing to specific properties. Besides broadly studied aprotic ILs (AILs), protic ILs (PILs) represent a subclass of ILs displaying interesting properties originating from a possible “free” proton. Unlike AILs, charge conduction in PILs can be enhanced due to the association of Grotthuss (proton hopping) and vehicular (proton remain linked to a carrier) mechanisms.^{3,4} Although the largest field of application for PILs this far has been fuel cells, they still have been employed as electrolytes in several other energy storage devices.⁵

Another general advantage of PILs is their synthesis, which is simpler as well as cheaper compared to the synthesis of AILs.⁶ They are obtained by proton transfer between a Brønsted acid and a Brønsted base. Theoretically, a full conversion of Brønsted molecules to ions is expected for a high pK_a difference, based on aqueous measurements, between an acid and a base. Nevertheless, a high pK_a difference in turn results in a high coulombic interaction between cations and anions,⁷ thus leading to strong interactions within cation–anion pairs or aggregates. Such strong interactions result in a decrease of the ionicity, *i.e.* an unintended decrease of the effective concentration of “free” ions.⁸ This affects the viscosity and the conductivity of the ILs.^{9,10} Nevertheless, when associated with lithium, the free proton of PILs was shown to improve the lithium-ion mobility.¹¹ Also, aggregated areas are commonly found in ILs,¹² and confining the ILs allows breaking down of the aggregated regions, thus increasing the ionicity and favoring lithium conduction.¹³

The present study aims at comparing the anion–cation coordination of two closely related ILs, based on bis(trifluoromethylsulfonyl)imide (TFSI) anions and either *N*-butyl-*N*-methylpyrrolidinium (AIL) or *N*-butylpyrrolidinium (PIL), with and without lithium–TFSI salt. These ILs are confined within meso-/macroporous silica monoliths with 2 μm macropores and various mesopore diameters ranging from 8 to 16 nm. The effects

^a Université de Nantes, CNRS, Institut des Matériaux Jean Rouxel, IMN, F-44000 Nantes, France. E-mail: jean.lebideau@cnrs-imn.fr^b ICGM, Univ. Montpellier, CNRS, ENSCM, Montpellier, France^c Institute for Technical Chemistry and Environmental Chemistry, Friedrich-Schiller-University, Jena, Philosophenweg 7a, 07743 Jena, Germany

† Electronic supplementary information (ESI) available. See DOI: 10.1039/d0cp03599h

Paper

of this confinement onto the melting temperature, conductivity, and lithium-TFSI coordination, followed by Raman spectroscopy, are presented.

Experimental

Ionic liquids

The pyrrolidinium-based AIL *N*-butyl-*N*-methylpyrrolidinium bis(trifluoromethanesulfonyl)imide (Pyr14 TFSI) has been purchased from Iolitech (99%), LiTFSI from Aldrich (99.95%). The pyrrolidinium-based PIL *N*-butyl-pyrrolidinium bis(trifluoromethanesulfonyl)imide (PyrH4 TFSI) was synthesized following a procedure similar to that described elsewhere.^{14,15} Two solutions at 0.5 M LiTFSI were prepared in Pyr14 TFSI and PyrH4 TFSI. The water content of the ILs is lower than 40 ppm, as measured by Karl Fisher titration before DSC and conductivity measurements.

Silica synthesis

Hierarchical meso-/macroporous silica monoliths (6 mm diameter and 10 cm length) with around 90% total porosity were synthesized accordingly to already published methods,^{16–18} which combines silica sol-gel synthesis in acidic medium (HNO₃) with spinodal decomposition, due to the addition of polymers (polyethylene oxide, 20 kDa) at 40 °C. Hence, monoliths with macropores of 2.5 μm diameter and a skeleton thickness of 3 μm are obtained. By applying post-treatments in NH₄OH 0.1 M at different temperatures (from 40 to 80 °C) and durations (6 to 24 h) the mesopore diameters are adjusted from 8 to 16 nm (Table 1). All monoliths are calcined under air at 550 °C for 8 h to remove remaining polymers.

The macropore volumes, diameters and surface areas were measured by Hg porosimetry after outgassing the samples at room temperature. The mesopore volumes, diameters and surface areas were determined using nitrogen sorption isotherms at 77 K after outgassing the samples at 250 °C.

Ionogel preparation

Silica monoliths were cut into pellets of around 3 mm high and 6 mm diameter. Before impregnation of ILs within silica, silica monoliths, ILs and ionogels were dehydrated overnight under 0.5 mbar at 50 °C. Pellets were immersed in ILs for one week in closed vials. The same dehydration process was carried out prior to any characterization experiment.

Calorimetry

Phase transitions of bulk and confined ILs were studied by differential scanning calorimetry.

Few mg of ILs and ionogels were hermetically sealed in aluminium pans. After initial heating at 100 °C, the samples were quenched down to –100 °C at a cooling rate of ~30 °C min⁻¹. A first heating, up to 100 °C, at 10 °C min⁻¹ is applied and allows a simple observation of the heat capacity increase corresponding to the glass transition temperature, which is measured at the inflexion point. The samples were then cooled again to –100 °C (~30 °C min⁻¹) and heated at 2 °C min⁻¹ to measure the temperature and the enthalpy of the cold crystallisation and melting. The melting temperature is taken at the maximum of the transition. For each sample (ILs and ionogels), the heat flow is given per mass unit of IL.

Ionic conductivity

The ionic conductivity of samples was studied by complex impedance spectroscopy (CIS) between –20 °C and 90 °C using a VMP 3, Biologic. The amplitude voltage used was 7 mV and the frequency range was 184–100 mHz.

Raman spectroscopy

Raman spectra were recorded with a standard Fourier-transform spectrometer (Bruker) using a 1064 nm Nd:YAG laser line. The laser power was set to 300 mW, the spectral resolution to 2 cm⁻¹ and each presented spectrum was an average of 400 scans.

Results and discussion

Thermal behaviour

The macroporosity of the hierarchical meso-/macroporous silica monolith supports was studied by SEM and Hg porosimetry and the mesoporosity using N₂ adsorption/desorption isotherms at 77 K (Table 1). A typical SEM image is presented in Fig. S1 (ESI†). Macropore diameters of the silica monoliths are around 2.5 μm with a skeleton thickness of 3 μm, the macropore volume is around 2 mL g⁻¹ and the macropore surface area is around 4 m² g⁻¹. The mesopore volume is around 1 mL g⁻¹, which represents around one third of the total pore volume. The mesopore diameters increase from 8 to 16 nm, with the increase of NH₄OH post-treatment duration and temperature (Table 1), leading to a decrease in the surface area from 600 to 300 m² g⁻¹. All monoliths feature a silanol density of 5–6 SiOH per nm² (calculated from Raman spectroscopy). The impregnated IL weight in silica is obtained from the difference between the weight of silica after IL impregnation and the weight of pristine dried silica. For each case, the IL weight represents more than 82% of the total weight of ionogels (Table S1, ESI†) in accordance with a total pore filling.

The confinement of ILs in these hierarchical macroporous silica monolithic matrices with different mesoporosities leads to variations in their change-of-state temperatures, which can be studied by DSC. Heat rates at 10 °C min⁻¹ and 2 °C min⁻¹ are used in order to measure precisely (i) the heat capacity at the glass transition, and (ii) the cold crystallization and melting temperature, respectively. DSC scans for unconfined and confined Pyr14 TFSI are shown in Fig. 1. For the other studied ILs (Pyr14 Li-TFSI, PyrH4 TFSI, PyrH4 Li-TFSI) DSC scans are

Table 1 Structural characteristics of silica monoliths before impregnation

Silica monolith	$\phi_{\text{meso}}(\text{N}_2)$ (nm)	$S_{\text{BET}}(\text{N}_2)$ (m ² g ⁻¹)	$V_{\text{meso}}(\text{N}_2)$ (cm ³ g ⁻¹)	$V_{\text{macro}}(\text{Hg})$ (cm ³ g ⁻¹)	V_{total} (cm ³ g ⁻¹)
40 °C – 8 h	8.1	636	0.97	1.99	2.96
40 °C – 13 h	8.5	584	0.97	2.09	3.06
40 °C – 24 h	9.8	546	1.03	2.22	3.25
50 °C – 24 h	11.2	540	1.06	2.29	3.35
60 °C – 24 h	12.6	437	1.03	2.23	3.26
80 °C – 24 h	16.2	336	1.19	2.47	3.66

PCCP

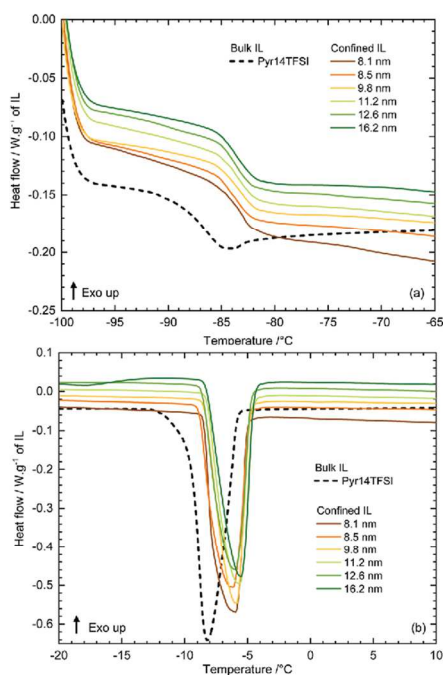


Fig. 1 DSC measurements for Pyr14 TFSI bulk and confined: (a) glass and (b) melting transitions. The heat flow is reported in relation to the mass of ILs. Curves are offset for visibility.

shown in Fig. S2 (ESI[†]). Table 2 summarizes the IL phase transitions (bulk and confined).¹⁹ Fig. 2 presents the evolution of the glass transition temperature, the calorific capacity variation during the glass transition, the melting transition temperatures, and the melting enthalpy, vs. the mesopore diameter. The glass transition temperatures T_g of Pyr14 TFSI, Pyr14-Li-TFSI, and PyrH4-Li-TFSI increase when the IL is confined in silica matrices, as shown in Fig. 1a and 2a. For confined and unconfined PyrH4 TFSI, the glass transition was not observed in the temperature range studied. The heat capacity modification ΔC_p (Fig. 2b) of Pyr14 TFSI, either pure or containing Li, is not

significantly modified by confinement, whereas the heat capacity of PyrH4 Li TFSI shows a larger increase. Nevertheless, the heat capacity of these three ILs seems to increase with the increase of mesopore diameter of the silica matrices. This appeared to be consistent with a decrease of surface to volume ratio, relatively less IL being constrained at the interface, thus allowing a macroscopic increase in entropy and thus an increase in heat capacity.

The variation in melting temperature T_m as a function of mesopore diameter is shown in Fig. 2c. The melting temperatures are -8.2 °C and $+31.2$ °C for Pyr14 TFSI and PyrH4 TFSI, respectively. Confinement effects in opposite manners for Pyr14 TFSI and PyrH4 TFSI were observed: confinement of Pyr14 TFSI resulted in an increased T_m of 1.9 °C ($T_m^c = -6.3$ °C), whereas for PyrH4 TFSI confinement resulted in a decrease in melting temperature of about 1.5 °C ($T_m^c = 29.7$ °C). Upon addition of Li salt, confinement of Pyr14-Li-TFSI showed an increase of T_m of 1.1 °C ($T_m^c = -9.4$ °C); the confinement of PyrH4-Li-TFSI caused a very small T_m increase of about 0.8 °C ($T_m^c = 25.7$ °C), unlike for neat PyrH4 TFSI, which showed a decrease of 1.5 °C.

Sign of ΔT_m upon confinement	Pyr14 TFSI	PyrH4 TFSI
Without Li	$T_m^c > T_m$	$T_m^c < T_m$
With Li	$T_m^c > T_m$	$T_m^c > T_m$

Upon addition of lithium, there is only a small difference between Pyr14 and PyrH4, with an increase of T_m of around 1 °C with confinement. However, it is without lithium that the difference is larger between the two ILs, with a T_m increase of 1.9 °C for Pyr14 and a decrease of -1.5 °C for PyrH4 with confinement. Even if these differences are not decisive in terms of devices performances, the study of T_m variation allows us to better analyse and understand the interactions of the ILs with the silica surface. The interactions between the IL and the silica pore wall with the given chemistry is thus different between Pyr14 TFSI and PyrH4 TFSI. Moreover, these interactions at the IL-silica interface are modified in the presence of Li cations. The Gibbs-Thomson model allows a rationalization of the melting/solidification temperature of confined ILs:

$$\frac{T_m^c - T_m}{T_m} = 2 \frac{(\gamma_{L-I} - \gamma_{S-I})\nu}{r_{\text{meso}} \Delta_m H} \quad (1)$$

Table 2 Thermal properties of non-confined ILs and of values averaged over all pores size for confined ILs

ILs	T_g^a /°C	ΔC_p /J g ⁻¹ K ⁻¹	T_m^a /°C	$\Delta_m H$ /J g ⁻¹
Pyr14TFSI	-86.59	0.244	-8.18	45.56
Confined Pyr14TFSI	-83.4 ± 0.1	0.26 ± 0.01	-6.3 ± 0.6	35.8 ± 0.9
Pyr14TFSI + 0.5 M LiTFSI	-76.05	0.274	-10.53 (-7.53)	40.59
Confined Pyr14TFSI + 0.5 M LiTFSI	-74.5 ± 0.6	0.28 ± 0.02	-9.4 ± 0.3	29.8 ± 0.8
PyrH4TFSI	—	—	31.36	59.95
Confined PyrH4TFSI	—	—	29.9 ± 0.9	51 ± 2
PyrH4TFSI + 0.5 M LiTFSI	-72.19	0.0276	(8.20) 24.9	41.19
Confined PyrH4TFSI + 0.5 M LiTFSI	-70.9 ± 0.7	0.13 ± 0.05	25.7 ± 0.1	36 ± 1

^a Minor melting events are given in parenthesis, taken at the peak maximum. They are comprised of $\Delta_m H$ values.

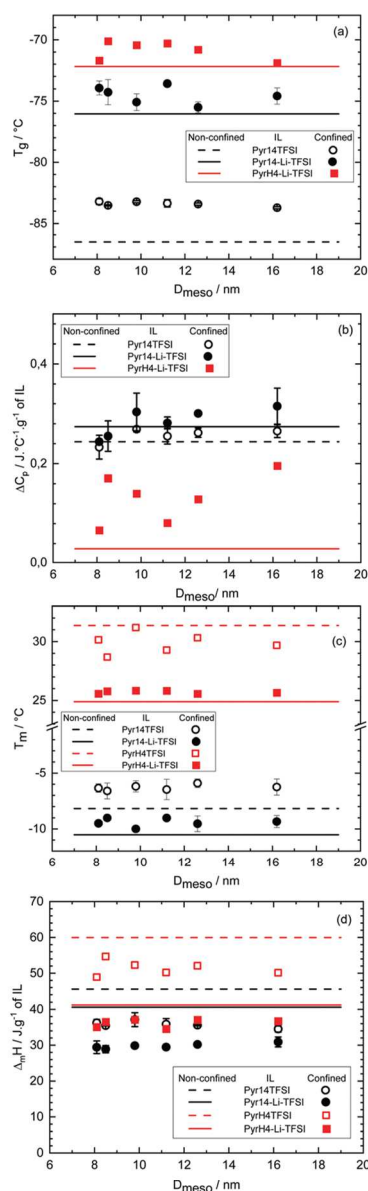


Fig. 2 DSC results for (a) glass transition, (b) calorific capacity variations during the glass transition, (c) melting temperature and (d) enthalpy of fusion for bulk and confined ILs. The heat flow is reported in relation to the mass of IL in the studied samples. Horizontal solid and dotted lines are eye guides referencing to non-confined ILs.

with T_m^c and T_m as the melting temperature of the confined and unconfined IL, γ_{S-1} and γ_{L-1} as the interface energies between the silica wall and the IL depending on whether it is in the solid or liquid state, ν as the molar volume of the IL ($\Delta\nu$ during phase change is neglected), $\Delta_m H$ as the melting enthalpy of the unconfined IL and r_{meso} as the pore radius. The interface energies γ_{S-1} and γ_{L-1} are taken positive and are homogeneous at chemical potentials, the system spontaneously evolves towards a chemical potential decrease. If $\gamma_{S-1} < \gamma_{L-1}$, then $T_m^c > T_m$: the liquid state of the confined IL is favored. These are the situations of Li-free Pyr14 TFSI, and those of Pyr14 and PyrH4 with Li. If $\gamma_{S-1} > \gamma_{L-1}$, then $T_m^c < T_m$: the liquid state of the confined IL is favored. This is the situation of Li-free PyrH4 TFSI. The decrease of melting point upon confinement is classically observed for liquids with high affinity for the surface matrix as water in hydrophilic silica.^{20,21} It was also observed for IL, such as hydrophilic 1-butyl-3-methylimidazolium $[\text{CF}_3\text{SO}_3]^-$ IL, in silica.²² Confinement can preserve the original liquid nature of some ILs at a much lower temperature than bulk T_m . For water, a thin non freezable layer between the core ice and the pore walls exists at very low temperature and has been recently observed for silica and carbon supports.²¹

In other words, the physico-chemical affinity between the host network and the confined IL at liquid state is lower when $T_m^c > T_m$ compared to when $T_m^c < T_m$. For Pyr14 TFSI, the T_m increase indicates an attracting effect between Pyr14 TFSI at solid state and silica pores. In contrast, for PyrH4 TFSI, the T_m decrease upon confinement shows an attractive effect between PyrH4 TFSI at liquid state and the silica pores. The behaviors of Pyr14 and PyrH4 are similar to what is observed for a non-ionic and polarizable liquid, such as CCl_4 confined, in graphite and in silica, respectively.²³

For Pyr14-Li-TFSI and PyrH4-Li-TFSI, the melting temperature increased upon confinement (Fig. 2 and 3), as observed in a previous study.¹⁶ The presence of Li cations at the interface appears to decrease the interaction between the pyrrolidinium and TFSI ions with the silica pore walls. Thus, this is consistent

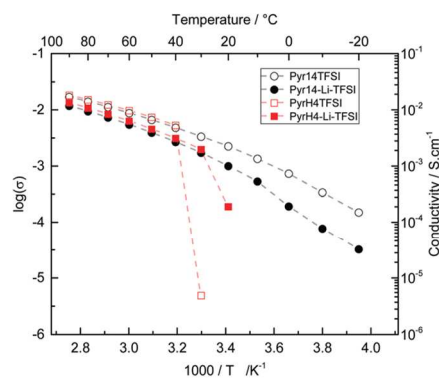


Fig. 3 Ionic conductivity of bulk ILs. Breaks on conductivity are due to melting transition of PyrH4 TFSI and PyrH4-Li-TFSI (around 30°C).

with a high affinity of Li cations towards silica for both ILs. It is therefore no longer Pyr14 or PyrH4 which interacts with the silica wall, but a layer involving Li cations. This is consistent with previous studies, showing that Li cations preferentially move towards the interface between the IL and the pore wall.¹³ It is also worth pointing out that confinement in silica shows stronger effects in the case of PyrH4, which might be due to the larger importance of H-bonding within the IL and SiO-H surface groups of silica, which disturbance is in turn compensated upon lithium addition by SiO-H-SiO-Li exchange. No dependency of melting temperature on the mesopore size was observed as expected by the Gibbs-Thompson model as the presence of the macropores averages the effect of the mesopores.

Conductivity

The ionic conductivity of bulk ILs is shown in Fig. 3. Above 40 °C, the conductivities of Pyr14 TFSI and PyrH4 TFSI were very similar, with and without Li. As expected, the addition of Li TFSI decreased the conductivity. Upon cooling, a slope break appeared for PyrH4 based ILs due to the solid-to-liquid transition (at about 30 °C). For Pyr14-based ILs, this slope break is smaller and appeared at lower temperature (lower T_m). The conductivity values of ILs are comparable with those obtained previously.^{10,24}

Fig. 4 shows the conductivity of Pyr14 TFSI ionogels compared to that of the neat IL. For each ionogel, the conductivity was lower but showed the same behavior as that of the non-confined IL (Fig. S3, ESI†). It is worth pointing out that the conductivity of the ionogels does not correspond to the intrinsic conductivity of confined ILs, since for a given form factor, the amount of IL in ionogels (~80 wt%) is lower than in unconfined ILs (100 wt%).¹⁶ In order to study the conductivity independent of the volume of confined ILs, the molar conductivity is calculated for each non-confined and confined IL. For confined ILs, the ionic conductivity ($\sigma_{\text{confined IL}}$) is calculated such as:

$$\sigma_{\text{confined IL}} = \frac{\sigma_{\text{ionogel}}}{V_{\text{IL}}/V_{\text{ionogel}}} \frac{M}{\rho} \quad (2)$$

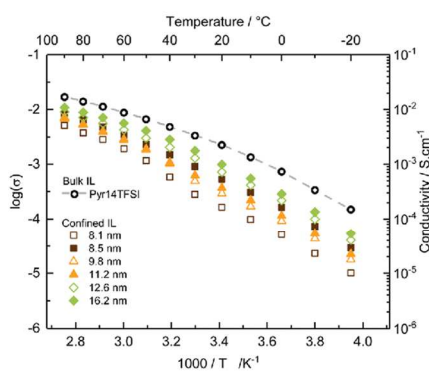


Fig. 4 Ionic conductivity of Pyr14TFSI ionogels, compared to the IL Pyr14TFSI.

here, σ_{ionogel} is the conductivity of the whole ionogel, V_{IL} and V_{ionogel} are the volumes of IL confined and the ionogel, M is the molar mass and ρ is the specific weight of the IL.

The molar conductivity vs. mesopore diameter at 40 °C is presented in Fig. 5. A similar pore size dependency was observed at the other temperatures. For AIL Pyr14 without lithium, the conductivity increases with mesopore diameter. A slight relative maximum occurs at around 10 nm for Pyr14-Li-TFSI, as already reported in a previous study with Pyr13-Li-TFSI confined in similar silica.⁵ The PIL PyrH4 with lithium does not show clearly any extremum at this temperature. In a previous work, we concluded that the dynamics of the silanol groups could help to create a diffusion path at the interface for the Li cation, and that the optimum mesopore diameter might indicate that the best diffusion of ions should occur when (i) the silica interface was saturated by lithium ions and when (ii) an almost equal ratio of ions was present at the surface of the pore and in the volume of the pore. This assumption was also proposed in catalysis, where the best compromise between the highest reactivity and the highest diffusion was estimated for an equal amount of molecules on the surface of the pore and in the volume of the pore (leading to an optimal mesopore diameter equal to 5–7 times the size of the molecule, calculated from the

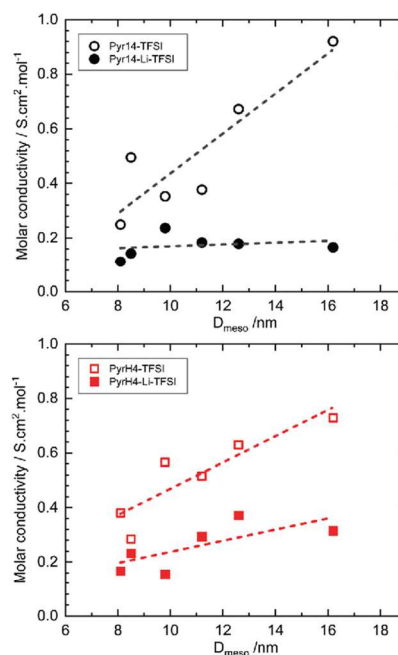


Fig. 5 Evolution of the molar conductivity of Pyr14 TFSI, PyrH4 TFSI, Pyr14-Li-TFSI and PyrH4-Li-TFSI with the confinement at 40 °C. The molar conductivity is calculated as the conductivity normalized by the volume of IL confined in the silica matrices. Horizontal solid and dotted lines are eye guides showing the conductivities of non-confined ILs.

Paper

Ruckenstein law).¹⁶ In the present study, carried out with the same silica and the same Li salt amount, we obtained the same result for the AIL Pyr14–Li–TFSI, showing sizes similar to that of Pyr13–Li–TFSI. For PIL PyrH4–Li–TFSI, the absence of clear extremum at 40 °C could be due to the drastic different effects of the AIL vs. PIL on the acidity of the silica. This was recently shown for drastic different effects of the AIL and PIL on a series of *para*-substituted benzoic acids; there, the Hammett ρ values for the acidic dissociation in some PILs were about the same as that in water but significantly smaller than that in the AIL.²⁵ Consequently, in the present study, the PIL should create an impactful amount of silanolate on the surface, thus decreasing drastically the ratio between the amount of Li cations and silanolate. An excessively large number of silanolate sites vs. the given amount of Li cations might turn into traps for part of the Li cations, or to strong interactions between PIL cations with the interface, at the expense of the release of the Li⁺ from its coordination by TFSI. This is investigated below by means of Raman spectroscopy.

Raman spectroscopy study

The interactions on a molecular scale at the interfaces can be investigated using Raman spectroscopy, through the study of the vibrational eigenmodes of our compounds. More specifically, the *cis* and *trans* conformations of the TFSI anion (noted *cis* and *trans* hereafter): these are sensitive to the chemical environment and to the confinement, presenting different signatures. In this work, we focus our attention on the 720–765 cm⁻¹ range of the Raman spectra.

In non-confined Pyr14 TFSI (inset in Fig. 6a), the symmetric elongation mode of the whole TFSI anion appears through the band located at 742 cm⁻¹.^{16,26,27} It should be noted that both *cis* and *trans* conformations participate in this contribution.^{28,29} This band shifts at about 744 cm⁻¹ in the case of PyrH4 TFSI (inset in Fig. 6b), indicating an increase of the interactions between TFSI and the pyrrolidinium cations, which may be due to the presence of a hydrogen atom bonded to the nitrogen.^{11,24}

Addition of lithium to the Pyr14 TFSI leads to the appearance of a shoulder on the previous band at about 748 cm⁻¹, accounting for the coordination of Li⁺ to TFSI.^{24,28,30} For PyrH4–Li–TFSI, this additional contribution merges with the band at 744 cm⁻¹, giving an asymmetrical band shifted toward the higher wavenumbers.

The number of TFSI anions coordinating a Li⁺ cation can be estimated using the ratio of the integrated intensity of the 748 cm⁻¹ band (A_{coord}) over the integrated intensity of the whole band (A_{tot}).^{11,31} If we consider that all the Li⁺ are coordinated by TFSI, its coordination number CN can be calculated

$$\text{CN} = \frac{A_{\text{coord}}}{A_{\text{tot}}} \times \frac{1}{x} \quad (3)$$

with x as the molar fraction of Li⁺ in the IL (0.132 in Pyr14 TFSI and 0.125 in PyrH4 TFSI). To calculate these integrated intensities, the signal can be decomposed into two (one non-coordinated and one coordinated) or three (*cis*, *trans* and coordinated) components. This latter decomposition gives more precise results and is

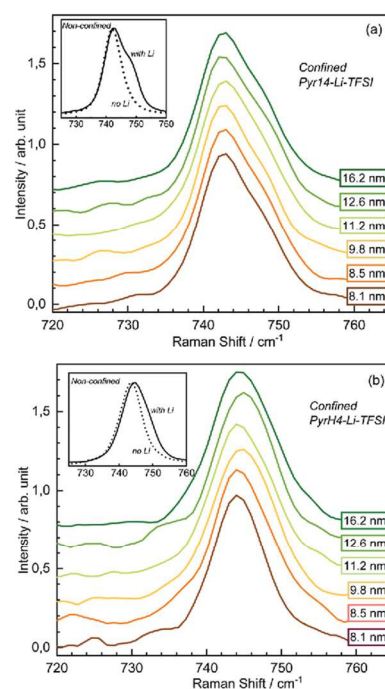


Fig. 6 Raman spectra of non-confined and confined ILs: (a) Pyr14–Li–TFSI and (b) PyrH4–Li–TFSI. Raman spectra of neat ILs are added for comparison in dashed lines. Silica pore sizes are indicated in front of corresponding confined IL spectra. Spectra normalised on intensity maximum and shifted for visibility.

presented in Fig. 7. To support and confirm the choice of this method, a decomposition of the signal has also been performed using a Bayesian positive source separation algorithm (BPSS, Fig. S4, ESI†). This unsupervised numerical approach gave the same results presented here, and thus are not detailed in this paper with a view to greater clarity and concision. For more information, one can find details in ref. 32. It is to be noted that both approaches show only one band for the vibration mode of the coordinated species. This point does not allow further conclusion on the possible position difference between *cis* and *trans* configurations in the coordinated complexes.

For the Pyr14–Li–TFSI and PyrH4–Li–TFSI-based ionogels and ILs, the best fits of the Raman spectra were obtained using three pseudo-Voigt functions, named C1, C2 and Ccoord (details on the method and obtained parameters are available in Tables S2 and S3, ESI†). For each non-confined IL spectrum, Ccoord parameters (relative intensities and positions) were in good agreement with the already reported results.^{11,24,33} For Pyr14–Li–TFSI, the positions of *cis* and *trans* components have been reported to be separated by 2 cm⁻¹, which is in agreement with the 1.3 cm⁻¹ measured on our spectra between C1 and C2.

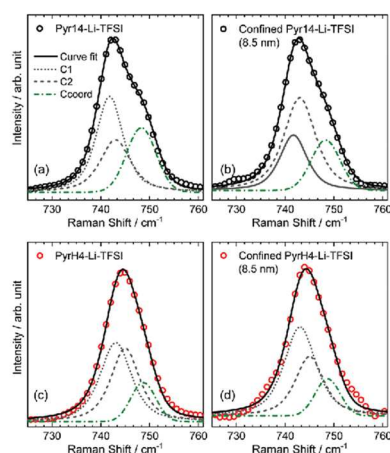


Fig. 7 Decomposition of Raman spectra of Pyr14-Li-TFSI and PyrH4-Li-TFSI (a and c) non-confined and (b and d) confined in 8.5 nm silica pore. The C1 and C2 components represent SI conformations non-coordinating Li^+ , while Ccoord represent the TFSI conformations coordinating Li^+ .

The positions of *cis* and *trans* components in the above study were not reported for PyrH4 TFSI or PyrH4-Li-TFSI. Thus, the C1 and C2 fitted peaks could not be surely attributed to the *cis* and *trans* conformations. However, the sum of their integrated intensity remained a good representation of the non-coordinated conformations of TFSI.

The CN was evaluated with this method at 2.1 TFSI per Li^+ for Pyr14-Li-TFSI and 1.1 TFSI per Li^+ for PyrH4-Li-TFSI (Fig. 8). For the same lithium-salt concentration (0.5 M LiTFSI), previous studies estimated a CN at 2 TFSI in Pyr14-Li-TFSI, and at 1.2 TFSI for PyrH4-Li-TFSI.^{11,24,33}

For ILs confined in silica, two different behaviors emerged. For confined Pyr14-Li-TFSI, the CN decreased to ~ 1.5 . On the other hand, the CN remained unchanged for PyrH4-Li-TFSI (~ 1.2). The confinement of Pyr14-Li-TFSI lowered the interactions between TFSI and Li^+ due to a preferential interaction of Li^+ with silanols.^{13,16} For confined PyrH4-Li-TFSI, it was not possible to observe clearly such an effect, maybe due to PIL

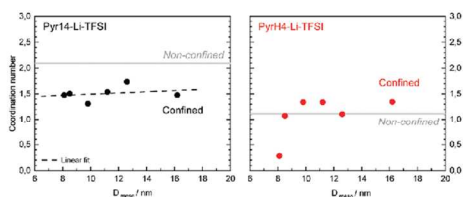


Fig. 8 Coordination number of Li^+ by TFSI in confined Pyr14-Li-TFSI (left) and PyrH4-Li-TFSI (right) compared to non-confined ILs (horizontal gray lines). In confinement, the coordination number of Pyr14-Li-TFSI decreases. There is no clear modification of the coordination number in confinement for PyrH4-Li-TFSI.

interactions with silanols, and to an average coordination of TFSI not only by lithium but also by protons.

Conclusions

Aprotic butylmethylpyrrolidinium bis(trifluoromethylsulfonyl)imide (AIL) and protic butylpyrrolidinium bis(trifluoromethylsulfonyl)imide (PIL) ionic liquids have been confined within a silica host network. Opposite effects on the melting temperatures have been observed; upon confinement, without lithium, it increased for the AIL, while it decreased for the PIL. With lithium, confinement still led to an increase of the melting temperature for the AIL, and in this case even for the PIL. Regarding ionic conductivities, at 40 °C, a small relative maximum was found around pore sizes of 10 nm for the AIL with lithium. This might be due to the charge balance at the interface between silanols/silanolates and the ionic liquid: the presence of a PIL, contrary to an AIL, is expected to modify the acidity of the silica rather strongly. Thus the charge balance between ILs with a given amount of lithium salt and host network is modified. Raman data showed that the coordination number of lithium by bis(trifluoromethylsulfonyl)imide is reduced upon confinement of the AIL, although this was not observed when confining a PIL. This study also highlights the real impact of the acidity of a PIL on the chemistry occurring at the interface of the host network within ionogels, and gives knowledge for a better choice of host network for confined species adaptation in perspective of all solid devices.

Conflicts of interest

There are no conflicts to declare.

References

- 1 K. Hayamizu, S. Tsuzuki and S. Seki, *J. Phys. Chem. A*, 2008, **112**, 12027–12036.
- 2 S. Wilken, S. Xiong, J. Scheers, P. Jacobsson and P. Johansson, *J. Power Sources*, 2015, **275**, 935–942.
- 3 H. Watanabe, T. Umecky, N. Arai, A. Nazet, T. Takamuku, K. R. Harris, Y. Kameda, R. Buchner and Y. Umabayashi, *J. Phys. Chem. B*, 2019, **123**, 6244–6252.
- 4 J. Ingenmey, S. Gehrke and B. Kirchner, *ChemSusChem*, 2018, **11**, 1900–1910.
- 5 T. L. Greaves and C. J. Drummond, *Chem. Rev.*, 2015, **115**, 11379–11448.
- 6 M. Hirao, H. Sugimoto and H. Ohno, *J. Electrochem. Soc.*, 2000, **147**, 4168.
- 7 K. Ueno, Z. Zhao, M. Watanabe and C. A. Angell, *J. Phys. Chem. B*, 2012, **116**, 63–70.
- 8 K. Ueno, H. Tokuda and M. Watanabe, *Phys. Chem. Chem. Phys.*, 2010, **12**, 1649–1658.
- 9 L.-M. Wang, C. A. Angell and R. Richert, *J. Chem. Phys.*, 2006, **125**, 074505.
- 10 T. Vogl, P. Goodrich, J. Jacquemin, S. Passerini and A. Balducci, *J. Phys. Chem. C*, 2016, **120**, 8525–8533.

Paper

PCCP

- 11 S. Menne, T. Vogl and A. Balducci, *Phys. Chem. Chem. Phys.*, 2014, **16**, 5485–5489.
- 12 C. D'Agostino, M. D. Mantle, C. L. Mullan, C. Hardacre and L. F. Gladden, *ChemPhysChem*, 2018, **19**, 1081–1088.
- 13 A. Guyomard-Lack, P.-E. Delannoy, N. Dupré, C. V. Cerclier, B. Humbert and J. Le Bideau, *Phys. Chem. Chem. Phys.*, 2014, **16**, 23639–23645.
- 14 T. Stettner, F. C. Walter and A. Balducci, *Batteries Supercaps*, 2019, **2**, 55–59.
- 15 L. Timperman, P. Skowron, A. Boisset, H. Galiano, D. Lemordant, E. Frackowiak, F. Béguin and M. Anouti, *Phys. Chem. Chem. Phys.*, 2012, **14**, 8199–8207.
- 16 A. Guyomard-Lack, B. Said, N. Dupré, A. Galarneau and J. Le Bideau, *New J. Chem.*, 2016, **40**, 4269–4276.
- 17 A. Galarneau, Z. Abid, B. Said, Y. Didi, K. Szymanska, A. Jarzębski, F. Tancret, H. Hamaizi, A. Bengueddach, F. Di Renzo and F. Fajula, *Inorganics*, 2016, **4**, 9.
- 18 A. Galarneau, A. Sachse, B. Said, C.-H. Pelisson, P. Boscaro, N. Brun, L. Courtheoux, N. Olivi-Tran, B. Coasne and F. Fajula, *C. R. Chim.*, 2016, **19**, 231–247.
- 19 M. Kunze, S. Jeong, E. Paillard, M. Winter and S. Passerini, *J. Phys. Chem. C*, 2010, **114**, 12364–12369.
- 20 K. Morishige, H. Yasunaga and Y. Matsutani, *J. Phys. Chem. C*, 2010, **114**, 4028–4035.
- 21 K. Morishige, *J. Phys. Chem. C*, 2018, **122**, 5013–5019.
- 22 M. Kanakubo, Y. Hiejima, K. Minami, T. Aizawa and H. Nanjo, *Chem. Commun.*, 2006, 1828–1830.
- 23 L. D. Gelb, K. E. Gubbins, R. Radhakrishnan and M. Sliwinski-Bartkowiak, *Rep. Prog. Phys.*, 1999, **62**, 1573–1659.
- 24 T. Vogl, S. Menne, R.-S. Kühnel and A. Balducci, *J. Mater. Chem. A*, 2014, **2**, 8258–8265.
- 25 F. Gao, P. Ji and J.-P. Cheng, *J. Org. Chem.*, 2020, **85**, 3041–3049.
- 26 Y. Umebayashi, T. Mitsugi, K. Fujii, S. Seki, K. Chiba, H. Yamamoto, J. N. Canongia Lopes, A. A. H. Pádua, M. Takeuchi, R. Kanzaki and S. Ishiguro, *J. Phys. Chem. B*, 2009, **113**, 4338–4346.
- 27 M. Herstedt, W. A. Henderson, M. Smirnov, L. Ducasse, L. Servant, D. Talaga and J. C. Lassègues, *J. Mol. Struct.*, 2006, **783**, 145–156.
- 28 J. C. Lassègues, J. Grondin, R. Holomb and P. Johansson, *J. Raman Spectrosc.*, 2007, **38**, 551–558.
- 29 A. Martinelli, *Eur. J. Inorg. Chem.*, 2015, 1300–1308.
- 30 M. Kunze, S. Jeong, E. Paillard, M. Schönhoff, M. Winter and S. Passerini, *Adv. Energy Mater.*, 2011, **1**, 274–281.
- 31 J.-C. Lassègues, J. Grondin and D. Talaga, *Phys. Chem. Chem. Phys.*, 2006, **8**, 5629–5632.
- 32 C. Carteret, A. Dandeu, S. Moussaoui, H. Muhr, B. Humbert and E. Plasari, *Cryst. Growth Des.*, 2009, **9**, 807–812.
- 33 J. Pitawala, A. Martinelli, P. Johansson, P. Jacobsson and A. Matic, *J. Non-Cryst. Solids*, 2015, **407**, 318–323.

2.3.2. Publikation 9: Protic Ionic Liquids-Based Crosslinked Polymer Electrolytes: A New Class of Solid Electrolytes for Energy Storage Devices

This publication considered the confinement of PILs in another polymeric host matrix, specifically amorphous poly(ethyleneoxide) (PEO), a very popular polymer for solid electrolyte applications. Whereas the combination of AILs and polymers has been intensively investigated in the past, the confinement of PILs in polymers has only been applied in conductive membranes for fuel cells. This work is split in three parts, with the first dedicated to the characterization of the solid electrolyte. The second part is dedicated to the implementation of the PIL-PEO solid electrolyte in AC-based EDLCs, and the last to the implementation in LIBs.

Initially, the morphology of the polymer electrolyte (PEO_HPyr) is investigated via a scanning electron microscope (SEM), revealing homogenous and wrinkled textures. The crosslinking, induced via UV light and benzophenone (2 %) enables high uptake of PIL without leakage while ensuring robustness and flexibility. Next, the thermal stability of the PEO_HPyr was evaluated, showing only slight deviation from the pure [Pyr_{H4}][TFSI] at temperatures higher than 300 °C combined with very stable mass retention at 60 °C under N₂ or O₂ atmosphere over a long time period. Furthermore, the conductivity of the electrolyte was investigated, which is in most cases the weak point of a solid electrolyte. Although the conduction is obviously lower compared to the pure [Pyr_{H4}][TFSI] or [Pyr_{H4}][TFSI] with 0.5 M LiTFSI (HPyr), it is reasonably high compared to other solid electrolytes, especially at RT. Finally, the ESW of PEO_HPyr was measured, showing an almost identical result to the pure [Pyr_{H4}][TFSI]. The latter points highlight the suitability as electrolyte in electrochemical energy storage devices.

For the implementation in an AC-based EDLC the first step was to select an OPV, which was set at 2.0 V, slightly lower than the maximum OPV achievable for pure [Pyr_{H4}][TFSI] (2.2 V), to ensure a safe and stable cycling of the device. While the system was able to achieve capacitances comparable to an EDLC employing neat [Pyr_{H4}][TFSI] as electrolyte over a very large period of cycling and even floating, the power performance is rather limited. This is due to several factors, including foremost the unoptimized interface between polymer electrolyte and electrode surface. In these investigations, a simple sandwich composition was employed, impairing the charge transfer between electrolyte and electrode. Certainly, this can drastically be improved by a, e.g., a drop-down synthesis of the polymer onto the electrodes.

Additionally, the system was operating at RT, a temperature where EDLCs employing pure [Pyr_{H4}][TFSI] do not even work since the electrolyte is solid without any ion mobility, contrary to PEO_HPyr.

The work dedicated to the use of PEO_HPyr in LIBs was novel not only because it was the first example of implementing a PIL-based solid electrolyte in this system. We also reported, for the first time, the use of an PIL-based electrolyte in combination with metallic lithium. Considering the reactivity of [Pyr_{H4}][TFSI] towards elemental lithium, this latter aspect appears of great interest.

To enable this reversible cycling of Li-metal electrodes in PEO_HPyr, the addition of vinylene carbonate (VC) is necessary, seemingly responsible for the formation of an SEI, protecting the electrolyte from decomposition. With the combination of Li-metal electrodes and LFP electrodes, we were, for the first time, able to build a LIB metal cell based on a solid electrolyte encompassing a PIL, with high efficiencies and high energy densities, close to the theoretical value of LFP.

This work gave novel and important information about the use of PIL-based electrolytes in electrochemical energy storage devices in several aspects. First, PILs are suitable to be employed in polymers as solid electrolytes to further enhance the safety of these devices. Furthermore, the combination of lithium metal with a protic electrolyte has been enabled, suppressing decomposition through the addition of VC. This opens the possibility to employ lithium-metal anodes as well as lithium-metal references electrodes in combination with PIL-based electrolytes.

Protic Ionic Liquids-Based Crosslinked Polymer Electrolytes: A New Class of Solid Electrolytes for Energy Storage Devices

Timo Stettner, Gabriele Lingua, Marisa Falco, Andrea Balducci,* and Claudio Gerbaldi*

Herein, the preparation of an innovative crosslinked polymer electrolyte (PEO_HPyr) encompassing protic ionic liquids (PILs) displaying high ionic conductivity, wide thermal, and electrochemical stability is reported, thus suitable for use in safe energy storage devices. The first example of an all-solid-state electrochemical double layer capacitor (EDLC) containing a PEO_HPyr-based electrolyte is presented, which shows high performance at ambient temperature and exceptional stability. Furthermore, the first example of a PIL-based lab-scale lithium-metal cell with lithium iron phosphate cathodes is also presented, which provides almost full capacity (i.e., 150 mAh g⁻¹ at C/20) and highly reversible cycling at ambient conditions and different current rates. The excellent results obtained clearly demonstrate that PIL-based crosslinked polymer electrolytes represent a new and very interesting class of solid electrolytes for energy storage devices.

1. Introduction

Protic ionic liquids (PILs) are a subgroup of ionic liquids (ILs) characterized by the presence of an acidic proton in their structure. PILs display the typical properties of ILs, including high thermal stability and low flammability, with the advantage of being easily synthesized through simple acid-base reactions.^[1] Although less popular than aprotic ionic liquids (AILs), PIL-based electrolytes have been considered in energy applications for many years. Initially, PILs have been mainly used as

electrolytes for fuel cells.^[2] Afterward, their use as electrolytes in electrochemical capacitors has been investigated, and, only recently, they have been proposed as electrolytes for Li-ion batteries (LIBs).^[3] In the last couple of years, their use in Na ion as well as K-ion batteries has also been considered.^[1c,4] The results of these studies indicate that PIL-based electrolytes allow the realization of alkali metal-ion batteries with promising performances. Furthermore, they showed that the acidic proton in the structure of PILs could be advantageously used to tune the ion environment and the storage process dynamics taking place in these devices. It has been shown, for example, that the presence of this proton is favorably influencing the coordination of Li⁺ ions in LIBs, making PILs suitable for high-power applications.^[5]


Finally, it has also been shown that aqueous solutions containing high concentration of PILs, which can be indicated as “water-in-PIL” electrolytes, display unique properties and are acting like aprotic and protic electrolytes at the same time.^[6]

It is evident that the properties of PILs and PIL-based electrolytes are strongly influenced by the acidic proton and by the environment in which the proton is present. Dry PILs (with a water content lower than 50 ppm) display transport and thermal properties comparable to that of AILs. However, the presence of the acidic proton limits the electrochemical stability window (ESW) of PILs, making it significantly lower compared with that of AILs.^[7] In spite of this, it has been shown that the use of film forming additives decomposing within the ESW of PILs enables the use of carbonaceous anodes, e.g., graphite and hard/soft carbon, in combination with PIL-based electrolytes.^[8]

To date, a large number of investigations have been dedicated to polymer electrolytes based on room temperature (RT) ILs, suitable for electrochemical double layer capacitors (EDLCs) and LIBs, but all of them have been realized utilizing AILs.^[9] Polymer electrolytes based on PILs have been used as proton conductive membranes in fuel cells.^[10] Trivedi et al. successfully implemented a mixture of protic and aprotic polymeric electrolytes in an activated carbon-based EDLC, whereas Mishra et al. used a PIL-based gel polymer in a proton battery.^[11] To the best of our knowledge, however, safe, self-standing, and robust polymer electrolytes encompassing PILs, which are suitable for stable operation in EDLCs and LIBs, have not been reported. Nevertheless, the development of these polymer electrolytes could be interesting for several reasons. First of all,

T. Stettner, Prof. A. Balducci
 Institute for Technical Chemistry and Environmental Chemistry
 Center for Energy and Environmental Chemistry Jena (CEEC Jena)
 Friedrich Schiller University Jena
 Philosophenweg 7a, 07743 Jena, Germany
 E-mail: andrea.balducci@uni-jena.de

G. Lingua, M. Falco, Prof. C. Gerbaldi
 GAME Lab
 Department of Applied Science and Technology (DISAT)
 Politecnico di Torino
 C.so Duca degli Abruzzi, 24-10129 Torino, Italy
 E-mail: claudio.gerbaldi@polito.it

 The ORCID identification number(s) for the author(s) of this article can be found under <https://doi.org/10.1002/ente.202000742>.

© 2020 The Authors. Published by Wiley-VCH GmbH. This is an open access article under the terms of the Creative Commons Attribution License, which permits use, distribution and reproduction in any medium, provided the original work is properly cited.

DOI: 10.1002/ente.202000742

the immobilization of PILs inside of a polymer network would reduce the risk of leakage typical for other liquid electrolytes, thus further improving the safety of systems and their cycle life. In addition, the use of polymer electrolyte membranes could enable the use of PILs in flexible and/or shapeable storage systems. Finally, the use of a solid electrolyte incorporating a PIL could also be a strategy to overcome the limitation related to the high reactivity of these ILs toward alkali metals, which is presently hindering the practical use of PIL-based electrolytes in high energy/power density alkali metal batteries, thus limiting the field of application of this family of electrolyte. This latter aspect appears particularly interesting, because the direct use of lithium metal would make the use of PIL in the next generation of high-energy density batteries possible, e.g., Li-S and Li-air.

In this work, we propose the use of PIL-based polymer electrolytes suitable for application in energy storage devices. In particular, we studied a novel polymer electrolyte based on UV-crosslinked poly(ethylenoxide) (PEO), encompassing the PIL 1-butylpyrrolidinium bis(trifluoromethanesulfonyl)imide (Pyr_{TH4}TFSI) and lithium bis(trifluoromethanesulfonyl)imide (LiTFSI). In the first part of the manuscript, the ionic conductivity, thermal properties, and electrochemical stability of this novel polymeric electrolyte are investigated. In the second part of this study, we demonstrate, for the first time, that the PIL-based crosslinked polymer electrolytes can be successfully used for the realization of solid EDLCs and solid lithium-metal batteries, able to display high performance at RT.

2. Results and Discussion

2.1. Chemical-Physical Characterization

The crosslinked PEO-based polymer electrolyte encompassing Pyr_{TH4}TFSI, namely PEO_HPyr, was prepared by a simple, green, solvent-free procedure. It includes a hot-pressing step (15 min) for film formation and a rapid (6 min) free-radical reaction induced by UV light (UV curing) to crosslink the network. This results in an easy-to-handle, ready-to-use electrolyte membrane. The polymer electrolyte contains equal amounts by weight of PEO and Pyr_{TH4}TFSI (i.e., 41%), 16% of LiTFSI, and 2% of benzophenone (BP) as the hydrogen abstraction photoinitiator.

The crosslinking step, which is sketched in **Figure 1A**, allows obtaining a transparent, self-standing film, which is elastic and shape retaining, as shown in **Figure 1B**. As previously demonstrated, the crosslinking step is fundamental to obtain amorphous, highly ionic conductive PEO-based electrolytes encompassing high amount of IL without any leakage, while keeping good mechanical properties and integrity.^[10a,12]

The scanning electron microscope (SEM) images, energy-dispersive X-ray spectroscopy (EDX) mapping and surface profile analysis indicate that these membranes are highly homogeneous (**Figure S1** and **S2**, Supporting Information). More in-depth field emission scanning electron microscopy analysis was performed to characterize the morphology of the photocured polymer electrolytes. Representative microscopy images are shown in **Figure 2**, which were taken from a cross-sectional view to better show the morphology of the crosslinked samples. As already reported in previous studies,^[13] the surface of the

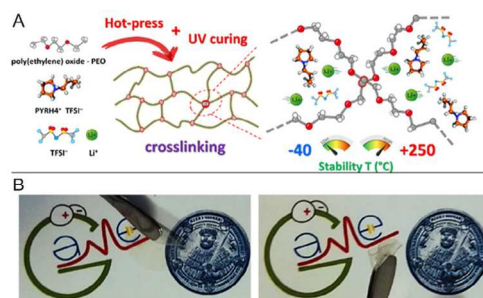


Figure 1. A) Schematics of materials, polymer electrolyte preparation, and crosslinking at different magnifications with indication of the temperature range of stability. B) Digital photographs of the PEO_HPyr polymer electrolyte membrane under investigation, showing excellent robustness and elasticity even well above the melting temperature of PEO.

polymer electrolyte shows uniform wrinkled textural features, due to crosslinking of the PEO chains under UV light in the presence of BP. Within these, amorphous PEO domains are alternated to some residual-ordered (semi-crystalline) domains. In case the same precursor mixture is processed without final UV irradiation, the resulting sample shows nonuniform and hardly homogeneous texture (inset of **Figure 2b**). Conversely, UV-induced crosslinking allows encompassing high amount of PIL and salt, leading to a material with dramatically different morphological characteristics in terms of homogeneity and robustness. Here, the amorphous UV-cured PEO-based network is able to efficiently hold the PIL without any leakage (see, in particular, the previous study^[12]).

The prepared PEO_HPyr displays a flash point higher than 300 °C, and when exposed to an open flame, they do not catch fire (**Figure S3**, Supporting Information).

Figure 3 compares the thermal stability of the neat Pyr_{TH4}TFSI of the binary mixture LiTFSI:Pyr_{TH4}TFSI (1:4 molar ratio, indicated as HPyr) and PEO_HPyr. As shown in **Figure 3A**, the thermal stability of the three electrolytes is very similar, and all of them start to decompose around 300 °C. Above this temperature, the liquids are steadily decomposing, whereas HPyr shows an increased stability compared with pure Pyr_{TH4}TFSI. This can be attributed to the presence of LiTFSI, a salt with a higher thermal stability, in the former. The polymer electrolyte membrane behaves differently. As shown in **Figure 3A**, it displays a distinct decomposition between 300 and 330 °C. The weight loss in this temperature range can be attributed to the decomposition of Pyr_{TH4}TFSI, which is accounting for roughly 40% of the total mass of PEO_HPyr. Above 330 °C, PEO starts to decompose, and at 460 °C, only lithium compounds, e.g., lithium oxide and other non-volatile residues, are left. **Figure 3B** shows the thermal stability of PEO_HPyr during isothermal measurements carried out at 60 °C for 24 h under nitrogen (blue) and oxygen (black) atmosphere. In these conditions, the polymer electrolyte membrane is extremely stable, and it only loses 1–2% of its initial weight. This minor loss, however, is due to the residual water, which was absorbed prior

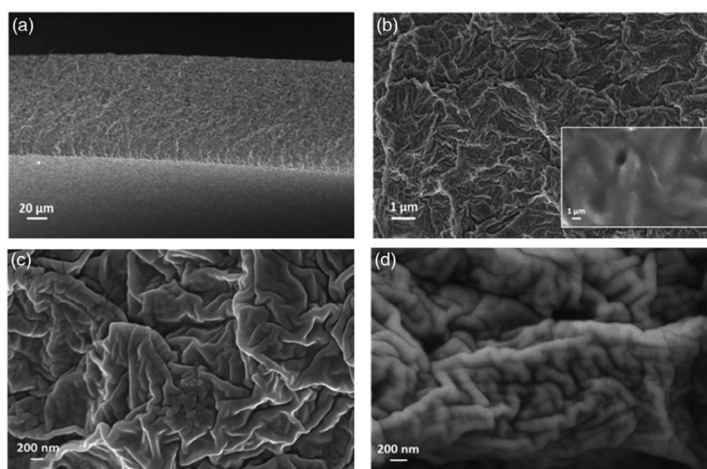


Figure 2. a–d) SEM images of the crosslinked PEO_HPy polymer electrolyte, showing its microstructure at increasing magnification; the inset of (b) show the appearance of a non UV-crosslinked polymer electrolyte obtained with the same precursor mixture.

to the test, as the different preparation steps are carried out under controlled atmosphere and using only battery grade and/or carefully dried materials.

Figure 4 shows a comparison of the variation of conductivities at different temperatures of neat $\text{Py}_{\text{T}14}\text{TFSI}$, HPy, and PEO_HPy. As shown, neat $\text{Py}_{\text{T}14}\text{TFSI}$ displays a conductivity of 3.5 mS cm^{-1} at 30°C . Below this temperature, however, this PIL does not display any practical conductivity due to its crystallization. HPy, which is a binary mixture of $\text{Py}_{\text{T}14}\text{TFSI}$ and LiTFSI, displays a lower conductivity compared with the neat PIL (1.3 mS cm^{-1} at 30°C) but, at the same time, a larger temperature range in which the electrolyte is displaying a decent conductivity (0.03 mS cm^{-1} at 10°C), due to the melting point decrease induced by LiTFSI. The ionic conductivity of PEO_HPy at 30°C is 0.14 mS cm^{-1} , which is a high value for a solid polymer electrolyte, especially near RT.^[10c] Considering these results, the practicable temperature window of PEO_HPy is wider compared with the liquid electrolytes, which represents a substantial advantage offered by the polymer electrolyte. The fully amorphous character of the film obtained by the UV-induced crosslinking of the macromolecular chains is demonstrated by the lack of a clear change in an activation energy at $40\text{--}60^\circ\text{C}$, which is generally observed with typical semi-crystalline PEO-based electrolytes, obtained by standard solvent casting and/or hot-pressing. due to the phase transition of crystalline PEO.^[10a,10b] This result is consistent with the differential scanning calorimetry (DSC) measurement (Figure S4A, Supporting Information), where no obvious melting or crystallization peaks are observed. Similarly, other literature reports about crosslinked PEO-LiTFSI-ILs films show that the crystallization of PEO and $\text{P}(\text{EO})_n\text{LiTFSI}$ complexes can be hindered in these ternary electrolytes.^[14] Nevertheless, in these systems, the crystallization of excess IL may occur depending on the

composition.^[14c] In the present work, this latter phenomenon was not observed by either SEM or DSC analyses. The ionic conductivity shows a Vogel–Tamman–Fulcher (VTF) dependence typical of fully amorphous polymer electrolytes.^[14b,14c] The VTF plot of the logarithm of conductivity versus $(T-T_0)^{-1}$ for PEO_HPy is shown in Figure S4B, Supporting Information. Figure S5, Supporting Information, shows the VTF plot of the ionic conductivity of $\text{Py}_{\text{T}14}\text{TFSI}$ and HPy. The apparent activation energy (E_a) can be extracted from the linear interpolation of the ionic conductivity data according to Equation (1)^[15]

$$\ln \sigma = A + \frac{E_a}{R(T - T_0)} \quad (1)$$

Here, A is a factor depending on the ionic conductivity at infinite temperature, R is the universal gas constant, and T_0 is a parameter customarily located 30 K below the glass transition temperature (T_g), which is related to the zero configurational entropy of the system.^[15] On the basis of the first DSC heating scan, T_g is located at -50.7°C . From the linear fit, apparent E_a values of 4.8, 5.4, and 7.0 kJ mol^{-1} have been calculated for $\text{Py}_{\text{T}14}\text{TFSI}$, HPy, and PEO_HPy, respectively. These values indicate that the E_a of PEO_HPy is rather comparable to that of the liquid PIL, and it is also similar to that of $\text{Py}_{\text{T}14}\text{TFSI}/\text{LiTFSI}$ solutions.^[15]

Figure 5 shows the ESW of the PEO_HPy at RT (scan rate of 0.1 mV s^{-1}). The crosslinked PEO_HPy electrolyte displays an overall ESW of $\approx 3.5 \text{ V}$ (with cathodic and anodic limits of -0.9 and 2.6 V versus Ag, respectively). This value is lower than that observed for many AIL-based polymeric electrolytes, but is comparable to that of the liquid PIL (see Figure S6, Supporting Information), indicating that the immobilization of $\text{Py}_{\text{T}14}\text{TFSI}$ in

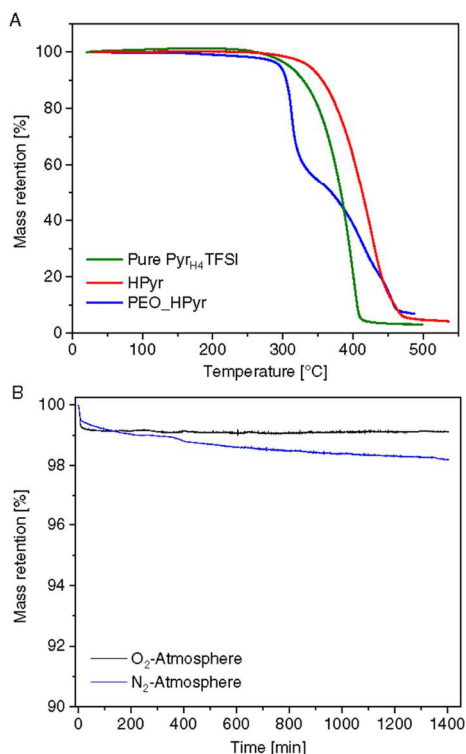


Figure 3. A) TGA of pure Pyr₁₄TFSI, HPyr, and PEO_HPyr heated at 10 °C min⁻¹. B) Isothermal (60 °C) mass loss of PEO_HPyr under O₂ and N₂ atmosphere, respectively.

a PEO matrix is not significantly affecting the electrochemical stability of this PIL.

Considering these results, the PEO_HPyr appears as an electrolyte with an interesting set of transport, thermal, and electrochemical properties. These properties are making this cross-linked PIL-based solid polymer electrolyte suitable for the realization of electrochemical energy storage devices operating at RT.

2.2. All-Solid PEO_HPyr-Based EDLCs

At first, the PEO_HPyr was used for the realization of a proof-of-concept lab-scale all-solid EDLC containing activated carbon-based electrodes and having an operating voltage of 2 V. This operating voltage was selected, because it is safely achievable with the liquid HPyr.^[6] As shown in the cyclic voltammogram (CV) in Figure 6A, this all-solid EDLC displays a capacitive-like behavior without any signs of irreversible redox reactions. Clearly, due to the limited electrolyte conductivity, the system shows a rather high resistance, as visible in the constant current

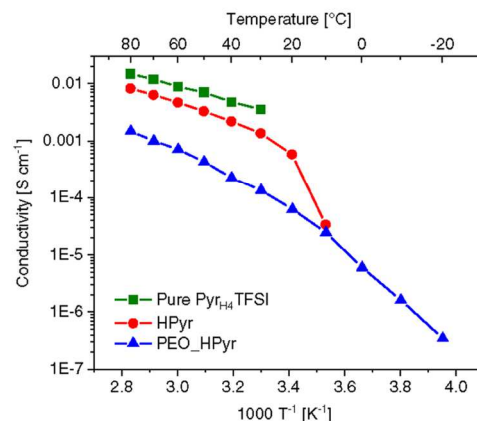


Figure 4. Arrhenius plot of the ionic conductivity in the range of -20 to 80 °C of the crosslinked PEO_HPyr polymer electrolyte compared with HPyr liquid electrolyte and neat Pyr₁₄TFSI.

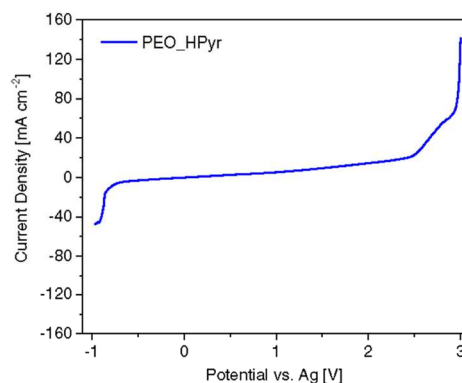


Figure 5. ESW of the polymer electrolyte (PEO_HPyr), measured via linear sweep voltammetry with a platinum working electrode, silver reference electrode, and an oversized carbon counter electrode at 40 °C and 0.1 mV s⁻¹.

(CC) (galvanostatic) charge/discharge voltage profiles versus time in Figure 6B. Nevertheless, this resistance appears comparable with that observed with other ILs (both protic and aprotic), and it is certainly acceptable for a lab-scale device, especially considering that the EDLC under study is solid state and has been tested at RT.^[16]

With the aim to investigate the overall performance of the all-solid EDLC, also CC tests at different current density rates and float tests at different voltages have been carried out. Figure 7A shows the behavior of the EDLC under study during 1200 CC cycles carried out at different current densities. During the initial 100 cycles at 1 mA g⁻¹, the capacitance of the device is constantly

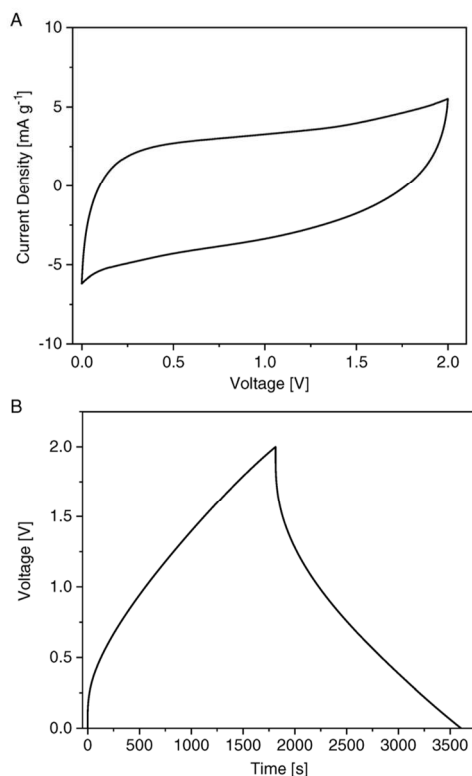


Figure 6. A) CV at 0.5 mV s^{-1} and B) CC curve at 1 mA g^{-1} of an activated carbon-based EDLC using PEO_HPyR.

increasing, and this increase becomes more marked when the current density is reduced to 0.5 mA g^{-1} (cycles 100–200). This behavior is typical for highly viscous electrolytes, e.g., ILs, and it has been reported in the literature several times.^[16d,17] An optimization of the electrode/electrolyte interface, as well as of the charge protocol/conditions, could reduce the time needed for this activation process. Nevertheless, this kind of optimization is out of the scope of this work and, therefore, was not carried out.^[17,18] It is very important to notice that the all-solid EDLC is able to deliver a capacitance of 12 F g^{-1} . By comparison, a device with the same electrodes used in combination with a PIL-based liquid electrolyte is able to deliver a capacitance of $18\text{--}20 \text{ F g}^{-1}$.^[6,16b] Considering the fact that the investigated system was not optimized (see below) and it was an all-solid EDLC, the capacitance delivered by the investigated devices under the applied operative conditions can certainly be considered as very promising. Due to the limited electrolyte conductivity, the capacitance retention of the investigated EDLC during tests at higher current densities is limited, and the system is able to deliver a moderate capacitance of 6 F g^{-1}

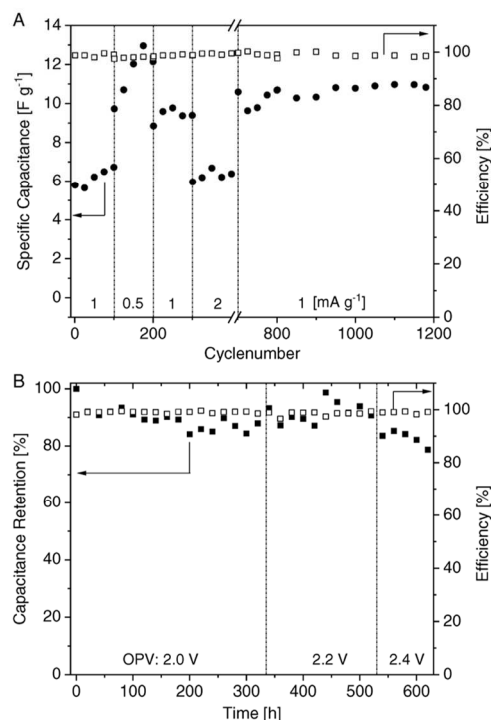


Figure 7. A) Rate capability test performed via CC measurements at different current densities and B) float test at different operative voltages of an activated carbon-based EDLC using PEO_HPyR at 1 mA g^{-1} .

only up to 2 mA g^{-1} . Above this latter value, the capacitance drops significantly, although the system provides a stable behavior (cycles 400–700, not shown). After the rate capability test at different current densities, the all-solid EDLC was cycled for over 500 cycles at 1 mA g^{-1} , and it showed a very good cycling stability, with a constant capacitance of $\approx 10 \text{ F g}^{-1}$. To gain a better understanding of the stability of this innovative EDLC, after the CC tests, also float tests were carried out (Figure 7B). Initially, the voltage of the EDLC was held at 2 V. As shown in the figure, after 340 h at this voltage, the all-solid EDLC device was able to keep 90% of its initial capacitance. Afterward, the cell voltage was increased to 2.2 V, which is the maximal operative voltage possible using liquid HPyr. Even at this voltage, the all-solid EDLC displays a very high stability for 240 h with a capacitance retention of 90%. Finally, the cell voltage was increased to 2.4 V. At this voltage, the device with PEO_HPyR is less stable, and its capacitance decreases faster, dropping already after 50 h below 80% of its initial capacitance. The same behavior is observed with liquid HPyr.^[6] It is important to remark that at an industrial level, one of the stability targets of EDLCs is to display a capacitance retention of 80% after

500 h of float at the maximum operative voltage.^[16a] Considering the results of the float test, the investigated all-solid EDLC, although not optimized, appears to display a very remarkable stability. It is also worth mentioning that the Nyquist plots of the device are not drastically changing during the float test (see Figure S7, Supporting Information).

Overall, the results reported earlier are very interesting, as the all-solid-state EDLC displays good capacitance and high cycling stability, the latter even higher compared with an EDLC operating with liquid HPyr.^[6] Combined with the general advantages of an all-solid-state EDLC, such as no risk of leakage, compactness, and the possibility for the design and realization of flexible devices, they appear even more attractive. It is also important to remark that these results were obtained using electrodes with a rather high mass loading ($2.6\text{--}3.5\text{ mg cm}^{-2}$) for a solid-state system, that the investigated devices were not optimized (e.g., in terms of electrode balancing and electrode–electrolyte surface), and that all the tests were carried out at RT. Considering these points, it is reasonable to suppose that the performance of the investigated systems can be significantly improved in the near future. Work is in progress to realize an optimized all-solid EDLC.

2.3. All-Solid PEO_HPyr-Based Lithium-Metal Cell

As expected, considering the ESW of liquid HPyr, deprotonation of the $[\text{PyT}_{\text{H}4}]^+$ cation, followed by the electrolyte degradation and hydrogen evolution upon reduction at the Li-metal anode, results in an irregular voltage profile during the first charge and cell failure in four CC cycles in a Li/PEO_HPyr/lithium iron phosphate (LFP) cell at C/10 rate and RT (Figure S8, Supporting Information).^[10d] Preventing the direct contact of the anode with the PIL is fundamental to avoid hydrogen evolution. The confinement of the PIL in the crosslinked polymer matrix is not 100% sufficient to avoid this phenomenon; therefore, an effective protective layer on Li metal is fundamental to enable cycling with PILs. In this regard, vinylene carbonate (VC) was, herein, experimented as an additive to allow the formation of the Li-metal protective layer.

The use of VC as an additive is widespread in LIB electrolytes.^[10d] This cyclic carbonate bears a double bond, allowing the formation of a protective layer on the anode upon electrochemical reduction during the first charge. This process occurs at relatively high potentials versus Li^+/Li as compared with the other components in the common electrolytes, promoting the formation of a passivation layer, which avoids further undesired decomposition reactions.^[10d]

As a preliminary test to check the effectiveness of a VC-based layer to prevent the decomposition of the PIL, a film of poly(vinylene carbonate) was obtained from VC upon a free radical-induced polymerization triggered by azobisisobutyronitrile (AIBN). The film was weighed and then swelled in the PIL overnight. No weight change could be detected after swelling, confirming that the uptake of the liquid phase was negligible. Thus, VC-based films qualitatively proved to be good candidates for preventing the diffusion of $[\text{PyT}_{\text{H}4}]^+$ toward the Li-metal anode. As PEO_HPyr is obtained by a free radical crosslinking process, the simple addition of VC in the PIL-based polymer

electrolyte mixture would result in the grafting/polymerization of VC, thus preventing the formation of an effective VC-based protective film on lithium metal.^[11b]

Therefore, here, we prepared a proof-of-concept lab-scale solid-like Li-metal cell in which the surface of the lithium-metal electrode was wetted with few drops of a solution of $\text{PyT}_{\text{H}4}\text{TFSI}$ and LiTFSI (having a PIL:salt molar ratio equal to 4:1) added with 10% by weight of VC prior to contacting the crosslinked PEO_HPyr polymer electrolyte and stacking the cell components in a standard sandwiched Li/PEO_HPyr-VC/LFP configuration. The cell was cycled at C/20 and C/10 rate (i.e., ≈ 0.01 and 0.02 mA cm^{-2} , respectively), based on the content of LFP active material (AC) and its theoretical capacity (170 mAh g^{-1}) at RT (Figure 8A). Differently from the cell with the PEO_HPyr alone, flat voltage profiles typical for LFP are observed, with a rather limited overpotential (below 100 mV at C/20 rate), considering the amount of VC used to prepare the swelling solution, the

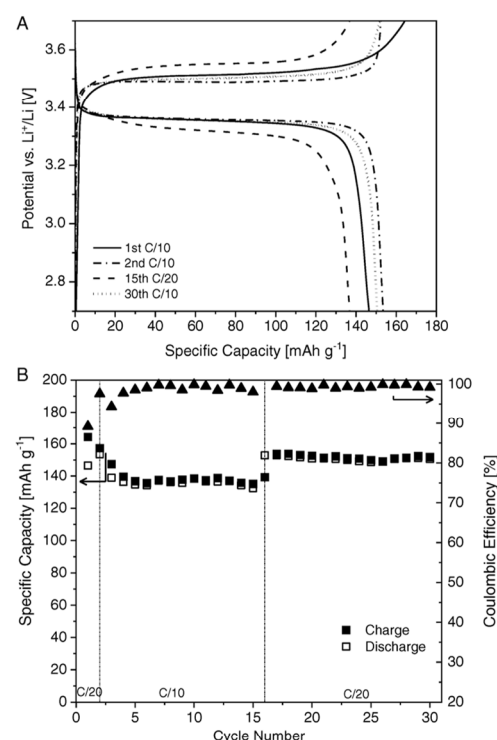


Figure 8. A) Voltage profile versus specific capacity during CC cycling of a Li/PEO_HPyr-VC/LFP cell at C/20 and C/10 rate and RT. B) Specific capacity and coulombic efficiency versus cycle number upon CC cycling of the proof-of-concept lab-scale solid-like Li/PEO_HPyr-VC/LFP Li-metal cell in which the surface of the lithium-metal electrode was wetted with few drops of a solution of $\text{PyT}_{\text{H}4}\text{TFSI}$ and LiTFSI (having a PIL:salt molar ratio equal to 4:1) added with 10% by weight of VC prior to contacting the crosslinked PEO_HPyr polymer electrolyte.

thickness of the polymer electrolyte ($\approx 120 \mu\text{m}$), and that the cell was cycled at RT. The coulombic efficiency of the first cycle is 97.5%, probably limited by processes occurring at the interface electrolyte/electrode, including the formation of the protective layer on the Li-metal surface promoted by the presence of VC. By the second cycle at C/10 rate onward, the coulombic efficiency increases, reaching values ≥ 98.5 and $\geq 99.2\%$ at C/10 and C/20 rate, respectively, which accounts for the high reversibility of the charge/discharge processes. The specific discharge capacity at C/20 rate is 154 and 151 mAh g^{-1} after 2 and 30 cycles, respectively. These values are close to the practical specific capacity of the LFP used in this work, which is about 158mAh g^{-1} .^[11a] At C/10 rate, the specific discharge capacity delivered by the cell is about 136mAh g^{-1} , and the overpotential is about 200 mV, due to the clear limitations associated with the internal resistance of the cell, which can be decreased upon further optimization beyond the scope of this article. Nevertheless, it is important to remark that the performance of this proof-of-concept cell, being the first example of a PIL-based solid polymer electrolyte operating with a Li-metal electrode, is already comparable with that reported for cells with analogous electrodes (in our case, in addition, we used a standard LFP electrode, without any ion conductive binder) and solid electrolytes based on AILs (see Table S1, Supporting Information, for a more detailed comparison).

Future work will be dedicated to the investigation of the protective layer formed by VC on the surface on the Li-metal surface and the modification of the preparation procedure of the polymer electrolyte, to directly incorporate the proper quantity of VC in the reaction mixture and obtain a thin film enabling cell operation at higher current densities.

3. Conclusion

This work reports, for the first time, about the preparation and characterization of a crosslinked polymer electrolyte encompassing $\text{Pyr}_{\text{H4}}\text{TFSI}/\text{LiTFSI}$ PIL-based mixture and its effective use at ambient conditions in lab-scale EDLCs and, for the very first time, in proof-of-concept lithium-metal batteries. We have shown that this novel solid electrolyte displays elasticity, robustness, and safety due to non-flammability, along with high ionic conductivity at low temperature and thermal stability in a wide temperature range. As in the case of liquid PILs, the ESW of the polymer electrolyte is limited by the acidic proton in the PIL. Nevertheless, this is not hindering the application of this innovative solid electrolyte in energy storage devices.

Indeed, we realized the first example of an all-solid-state EDLC operating with the crosslinked $\text{PEO}_{\text{H}}\text{Pyr}$ -based electrolyte. We have shown that this device displays excellent performance in terms of capacitance output at RT, comparable to that achievable with the liquid PIL. This performance is coupled with largely enhanced stability, in addition to the advantages listed in the previous paragraph. Offering the typical benefits of an all-solid system such as flexibility, compactness, and improved safety (no risk of leakage), this unoptimized system appears already very attractive not least due to the larger temperature range in which it can be utilized, compared with the liquid PIL.

Furthermore, we presented the first example of a PIL-based lithium-metal battery assembled with an LFP cathode and a Li-metal anode. This proof-of-concept system has been realized by protecting the Li-metal anode with a VC-containing electrolyte, which is electrochemically polymerized during the initial charge. The system displayed almost full specific capacity output and stable cycling at different current rates at RT. The use of a solid electrolyte incorporating a PIL appears, therefore, as a feasible strategy to suppress the high reactivity of these ILs toward alkali metals, and to allow the introduction of PIL-based electrolytes in metal batteries.

International developments at European Union (EU) level and abroad to reduce air pollution and CO_2 production are pushing toward a rapid implementation of electrification of transport, and the rush for better technology correspondingly necessitates improved, safe traction battery systems operating in a broad temperature range. In this respect, stable, low-cost, all-solid-state lithium-metal batteries are a key enabling technology providing high energy/power density output, which can easily be coupled with all-solid-state EDLC in an integrated architecture for even enhanced performance. The results of this study clearly enlighten that PIL-based crosslinked polymer electrolytes are a new and very interesting class of safe, stable, low-cost solid electrolytes that can definitely serve the purpose. Clearly, we are still at the proof-of-concept stage, and in the near future, additional efforts will be needed to understand the properties of these solid electrolytes, e.g., ion mobility, and their interactions with the electrode materials to further improve the performance of PIL-based systems.

4. Experimental Section

Synthesis of the IL: The PIL was synthesized with a procedure similar to that reported in a previous study.^[12] In a first step, 10.55 g of the yellowish precursor 1-butylpyrrolidine (98%, obtained by Aldrich) was distilled at 60°C and 20 mbar. After the distillation, colorless 1-butylpyrrolidine (7.55 g/59.34 mmol) was put in a two-neck flask on a magnetic stirring plate. The flask was topped by a reflux condenser and a 50 mL dropping funnel, which was filled with 5.35 mL HCl (35%).

HCl was added dropwise and slowly under stirring, while the mixture was cooled with an ice bath. After the complete addition, the ice bath was removed, and the solution was stirred for 2 h. Residual water and reactants were removed under reduced pressure, leaving 1-butylpyrrolidine chloride as a solid.

The 1-butylpyrrolidine chloride was solved in 8 mL of H_2O and then put into a two-neck flask, equipped with a reflux condenser and a 50 mL dropping funnel; 19.33 g of LiTFSI (99.95%, obtained by Aldrich) was solved in 18 mL of H_2O and filled into the dropping funnel. The LiTFSI solution was added to 1-butylpyrrolidine dropwise, and the mixture was stirred for 3 h. During this reaction, two phases were formed: an organic one containing $\text{Pyr}_{\text{H4}}\text{TFSI}$, at the bottom and an aqueous one on top. To remove the aqueous from the organic one, a separating funnel was used.

Subsequently, the PIL was washed five to six times with water, to remove residual LiCl. To test on complete removal, AgNO_3 was added to the washing water.

As a last step, residual water was removed by reduced pressure and heating (60°C , 3.0×10^{-3} mbar).

Preparation of the Polymer Electrolyte: To prepare the polymer electrolytes, LiTFSI (Solvionic, battery grade) was first carefully mixed with PEO (Mn 200 000 Da, Merck, dried under vacuum at 55°C for two days prior use), and the mixture was melt and mixed at 80°C until complete homogenization, resulting in a highly viscous paste. The solution of the

photoinitiator BP (*Merck*) dissolved in Pyr_{H4}TFSI was then added to the paste. Continuous mixing at 80 °C yielded homogeneous blends. The weight percentages of PEO, Pyr_{H4}TFSI, LiTFSI, and BP are 41, 41, 16, and 2 wt%, respectively. The molar ratio among the components PEO:Pyr_{H4}TFSI:LiTFSI is approximately 16.7:1.7:1. The operations mentioned earlier were carried out in an argon filled glove box (Jacomex GP concept, <1 ppm H₂O and <1 ppm O₂). The blend was then processed into a film by hot-pressing for 15 min at 10 bar and 70 °C between two polypropylene sheets with adhesive tape as spacers in sealed bags and crosslinked upon irradiation by UV light (UV curing) for 6 min at 40 mW cm⁻² using a medium-pressure Hg lamp (*Helios Quartz*).

Scanning Electron Microscope: The SEM pictures were taken and EDX mapping done using a *pro X* from *PhenomTM*.

Surface Profile: The surface profile was measured using a *Zeiss SmartProof 5* profilometer. The calculations were done using the software *ZEN smartproof* by *Zeiss*.

Thermogravimetric Analysis: The thermogravimetric analysis (TGA) was performed with a *PerkinElmer STA 6000* using nitrogen or oxygen as carrier gas with a total flow rate of 20 mL min⁻¹. For each measurement, about 15 mg of solid or liquid electrolyte was filled in a platinum crucible. For TGA measurements, the samples were heated to 500 °C with a gradient of 10 °C min⁻¹. For isothermal measurements, a gradient of 30 °C min⁻¹ was used to reach 60 °C, which was hold for 24 h.

Electrochemical Measurements: In all cases, the cells with the self-standing crosslinked polymer electrolytes were assembled without any additional spacer or separator. The proof-of-concept lab-scale solid-like Li-metal cell was assembled, placing the polymer electrolyte membrane directly in contact with the lithium-metal anode, whereas the other side was placed in contact with the LFP electrode disk, stacking the cell components in a standard sandwiched configuration. For the Li-metal cell with Li/PEO₄HPyr-VC/LFP configuration, we followed the same procedure reported earlier, with the addition of pre-treatment on the anode: the surface of the lithium-metal electrode was wetted with few drops of a solution of Pyr_{H4}TFSI and LiTFSI (having a PIL:salt molar ratio equal to 4:1) containing 10% by weight of VC prior to contacting the crosslinked PEO₄HPyr polymer electrolyte. The cells with liquid electrolyte were equipped with glass microfiber filters (*Whatman*, 150 μm) as separators, drenched with 150 μL electrolyte. All cells were assembled in an argon filled glove box (*MBraun LABmasterpro ECO glove boxes*, <1 ppm H₂O and <1 ppm O₂).

The ionic conductivity of the polymer electrolyte was evaluated from the impedance response of the symmetric cells (ECC-Std cells by *EL-CELL GmbH*) assembled by sandwiching PEO₄HPyr between two stainless steel (SS-316) blocking electrodes. The impedance spectra were recorded at an oscillating voltage of 10 mV in the frequency range between 3 × 10⁵ and 1 Hz, using a *VMP3* electrochemical workstation (*Biologic*). The test was carried out while increasing the temperature in 10 °C steps from -20 to 80 °C using an environmentally controlled climate chamber (*BINDER, MK53 E2*). The cell was kept for at least 90 min at each given temperature for proper equilibration. The impedance spectra were analyzed using the *ECLab V10.44* software. The bulk resistance (*R_b*) was extracted from the intercept (on the real impedance axis) of the signal due to the double layer capacity at the blocking electrodes. The ionic conductivity (*σ*) was calculated using Equation (2)

$$\sigma = \frac{t}{R_b \cdot A} \quad (2)$$

The thickness (*t*) of the samples is the average of three measurements carried out with a micrometer (*Mitutoyo* gauge). The area (*A*) of the samples is 2.54 cm².

The ESW of the electrolytes was measured in a three-electrode *Swagelok* cell using a platinum working electrode, an oversized activated carbon electrode as the counter electrode, and a silver pseudo-reference electrode. Activated carbon electrodes were prepared following a procedure identical to that used by Krause et al.^[20] The dry composition of the electrodes is 90 wt% of AC (*DLC Super, Norit*), 5 wt% of conducting agent (*Super C65, Imerys*), and 5 wt% of binder (carboxymethyl cellulose,

Dow). The mass loading of the electrodes is between 2.6 and 3.5 mg cm⁻², and the electrode area equals to 1.13 cm². After a 12-h open circuit voltage (OCV) measurement to reach equilibrium, the cells were swept from OCV toward either positive or negative direction at 0.1 mV s⁻¹ until a potential of -6 V versus OCV and 6 V versus OCV was reached, respectively. These measurements were carried out at 40 °C, both for the liquid as well as for the solid electrolyte, to ensure the former to be molten while keeping the results comparable.

The electrochemical behavior of the EDLCs at RT was evaluated in a three-electrode *Swagelok* cell using activated carbon electrodes prepared as described earlier. The cyclic voltammetry measurements were carried out at different scan rates (0.5, 1, 5, 2.5, and 10 mV s⁻¹), and the CC experiments were carried out at different current densities (0.1, 0.5, 1, 2, 5, and 10 mA g⁻¹). The stability tests were also performed via CC measurements with a specific current of 1 mA g⁻¹. First, 5000 CC cycles were executed. For the float tests, only 50 cycles were measured but with a 20 h period of holding the cell at its designated operative voltage afterward. This was repeated until a period of roughly 600 h at the maximum voltage was reached, calculating the capacitance after each 50th cycle of the CC step.

Lab-scale cells with Li-metal anodes and LFP cathodes were assembled by simply sandwiching the components in ECC-Std cells (*EL-Cell GmbH*). The area of LFP (*Clariant-LP2*) and Li-metal (200 μm, *Chemetal*, now *Albemarle*) electrodes is 2.54 cm². CC tests were carried out with an *ARBIN BT2000* battery tester. The cutoff voltage values were set to 2.7 and 3.7 V versus Li^{+/}Li. The cathodes were prepared by a standard method from an *N*-methyl pyrrolidone (NMP; *Merck*) slurry containing LFP, conductive carbon (*Shawinigan Black AB50, Chevron Corp*), and polyvinylidene fluoride (Mn 534000, *Merck*) at 70:20:10 weight ratio, respectively. The slurry was deposited onto an Al foil, dried overnight, cut into disks, and vacuum dried at 120 °C for one day prior use to remove water and residual NMP. The resulting AC loading is about 1.0 mg cm⁻².

Supporting Information

Supporting Information is available from the Wiley Online Library or from the author.

Acknowledgements

T.S. and A.B. wish to thank the Friedrich-Schiller University for the support. C.G., M.F., and G.L. acknowledge financial support by the Si-DRIVE Project, which received funding from the EU's Horizon 2020 research and innovation program under GA 814464. Open access funding enabled and organized by Projekt DEAL.

Conflict of Interest

The authors declare no conflict of interest.

Keywords

electrochemical capacitors, lithium-metal batteries, polymer electrolytes, protic ionic liquids, solid-state devices

Received: August 21, 2020
Published online: September 29, 2020

- [1] a) M. Anouti, M. Caillon-Caravanier, Y. Dridi, H. Galiano, D. Lemordant, *J. Phys. Chem. B* **2008**, *112*, 13335; b) D. M. Fox, J. W. Gilman, A. B. Morgan, J. R. Shields, P. H. Maupin, R. E. Lyon, H. C. De Long, P. C. Trulove, *Ind. Eng. Chem. Res.* **2008**,

- 47, 6327; c) H. Sun, G. Zhu, X. Xu, M. Liao, Y.-Y. Li, M. Angell, M. Gu, Y. Zhu, W. H. Hung, J. Li, *Nat. Commun.* **2019**, *10*, 1.
- [2] a) M. A. Susan, M. Yoo, H. Nakamoto, M. Watanabe, *Chem. Lett.* **2003**, *32*, 836; b) H. Nakamoto, M. Watanabe, *Chem. Commun.* **2007**, *24*, 2539–2541.
- [3] a) L. Timperman, H. Galiano, D. Lemordant, M. Anouti, *Electrochem. Commun.* **2011**, *13*, 1112; b) X. Lu, G. Burrell, F. Separovic, C. Zhao, *J. Phys. Chem. B* **2012**, *116*, 9160; c) N. Böckenfeld, M. Willeke, J. Pires, M. Anouti, A. Balducci, *J. Electrochem. Soc.* **2013**, *160*, A559.
- [4] a) T. Vogl, C. Vaalma, D. Buchholz, M. Secchiaroli, R. Marassi, S. Passerini, A. Balducci, *J. Mater. Chem. A* **2016**, *4*, 10472; b) M. Arnaiz, A. Bothe, S. Dsoke, A. Balducci, J. Ajuria, *J. Electrochem. Soc.* **2019**, *166*, A3504.
- [5] T. Vogl, S. Menne, R.-S. Kühnel, A. Balducci, *J. Mater. Chem. A* **2014**, *2*, 8258.
- [6] T. Stettner, S. Gehrke, P. Ray, B. Kirchner, A. Balducci, *ChemSusChem* **2019**, *12*, 3827.
- [7] P. A. Z. Suarez, C. S. Consorti, R. F. de Souza, J. Dupont, R. S. Gonçalves, *J. Braz. Chem. Soc.* **2002**, *13*, 106.
- [8] S. Menne, M. Schroeder, T. Vogl, A. Balducci, *J. Power Sources* **2014**, *266*, 208.
- [9] a) Y.-S. Ye, J. Rick, B.-J. Hwang, *J. Mater. Chem. A* **2013**, *1*, 2719; b) S. Chen, K. Wen, J. Fan, Y. Bando, D. Golberg, *J. Mater. Chem. A* **2018**, *6*, 11631; c) F. Ma, Z. Zhang, W. Yan, X. Ma, D. Sun, Y. Jin, X. Chen, K. He, *ACS Sustain. Chem. Eng.* **2019**, *7*, 4675; d) J. R. Nair, F. Colò, A. Kazzazi, M. Moreno, D. Bresser, R. Lin, F. Bella, G. Meligrana, S. Fantini, E. Simonetti, *J. Power Sources* **2019**, *412*, 398; e) E. Simonetti, M. De Francesco, M. Bellusci, G. T. Kim, F. Wu, S. Passerini, G. B. Appetecchi, *ChemSusChem* **2019**, *12*, 4946; f) G. Yang, Y. Song, Q. Wang, L. Zhang, L. Deng, *Mater. Des.* **2020**, *190*, 108563.
- [10] a) A. Martinelli, A. Matic, P. Jacobsson, L. Börjesson, A. Fericola, S. Panero, B. Scrosati, H. Ohno, *J. Phys. Chem. B* **2007**, *111*, 12462; b) S.-Y. Lee, A. Ogawa, M. Kanno, H. Nakamoto, T. Yasuda, M. Watanabe, *J. Am. Chem. Soc.* **2010**, *132*, 9764; c) U. A. Rana, M. Forsyth, D. R. MacFarlane, J. M. Pringle, *Electrochim. Acta* **2012**, *84*, 213; d) Z. Wojnarowska, J. Knapik, M. Díaz, A. Ortiz, I. Ortiz, M. Paluch, *Macromolecules* **2014**, *47*, 4056.
- [11] a) K. Mishra, S. Hashmi, D. Rai, *J. Solid State Electrochem.* **2014**, *18*, 2255; b) T. J. Trivedi, D. Bhattachariya, J. S. Yu, A. Kumar, *ChemSusChem* **2015**, *8*, 3294.
- [12] M. Falco, C. Simari, C. Ferrara, J. R. Nair, G. Meligrana, F. Bella, I. Nicotera, P. Mustarelli, M. Winter, C. Gerbaldi, *Langmuir* **2019**, *35*, 8210.
- [13] a) J. Nair, L. Porcarelli, F. Bella, *Interfaces* **2015**, *7*, 961; b) L. Porcarelli, C. Gerbaldi, F. Bella, J. Nair, *Sci Rep.* **2016**, *6*, 19892.
- [14] a) J.-H. Shin, W. A. Henderson, C. Tizzani, S. Passerini, S.-S. Jeong, K.-W. Kim, *J. Electrochem. Soc.* **2006**, *153*, A1649; b) G.-T. Kim, G. B. Appetecchi, F. Alessandrini, S. Passerini, *J. Power Sources* **2007**, *171*, 861; c) G.-T. Kim, G. B. Appetecchi, M. Carewska, M. Joost, A. Balducci, M. Winter, S. Passerini, *J. Power Sources* **2010**, *195*, 6130.
- [15] G. A. Elia, U. Ulissi, F. Mueller, J. Reiter, N. Tsiouvaras, Y. K. Sun, B. Scrosati, S. Passerini, J. Hassoun, *Chem. Eur. J.* **2016**, *22*, 6808.
- [16] a) A. Brandt, S. Pohlmann, A. Varzi, A. Balducci, S. Passerini, *MRS Bull.* **2013**, *38*, 554; b) A. Brandt, J. Pires, M. Anouti, A. Balducci, *Electrochim. Acta* **2013**, *108*, 226; c) A. Brandt, A. Balducci, *J. Power Sources* **2014**, *250*, 343; d) F. Béguin, V. Presser, A. Balducci, E. Frackowiak, *Adv. Mater.* **2014**, *26*, 2219.
- [17] Z. Lin, E. Goikolea, A. Balducci, K. Naoi, P.-L. Taberna, M. Salanne, G. Yushin, P. Simon, *Mater. Today* **2018**, *21*, 419.
- [18] a) N. Handa, T. Sugimoto, M. Yamagata, M. Kikuta, M. Kono, M. Ishikawa, *J. Power Sources* **2008**, *185*, 1585; b) Y. J. Ju, C. H. Lien, K. H. Chang, C. C. Hu, D. S. H. Wong, *J. Chin. Chem. Soc.* **2012**, *59*, 1280; c) J. Krummacker, C. Schütter, L. Hess, A. Balducci, *Curr. Opin. Electrochem.* **2018**, *9*, 64; d) A. Balducci, in *Ionic Liquids II*, Springer, Cham **2017**, pp. 1–27.
- [19] L. Timperman, P. Skowron, A. Boisset, H. Galiano, D. Lemordant, E. Frackowiak, F. Béguin, M. Anouti, *Phys. Chem. Chem. Phys.* **2012**, *14*, 8199.
- [20] A. Krause, P. Kossyrev, M. Oljaca, S. Passerini, M. Winter, A. Balducci, *J. Power Sources* **2011**, *196*, 8836.

3. Conclusion

The development of high performing but also safer electrolytes is an essential task for the realization of electrochemical energy storage devices. One possibility to increase the safety in a variety of energy storage devices is the implementation of ILs. In the past, this approach has been proven to be effective in many instances yet limited to research. Obviously, this is related to their high cost but also their high viscosity, limiting the power performance of each targeted device. The use of PILs might offer a chance to dampen these drawbacks, firstly by a relatively easy synthesis, what can be seen as advantage regarding the cost. Furthermore, their protic nature is the source of unique transport mechanisms in ILs, with the possibility to yield much higher conductivities. Additionally, the coordination of metal-ions is less distinct, leading to higher mobilities of these ions, which is a key criterium for metal-ion batteries. Unfortunately, these latter advantages, derived by the presence of an available proton, come with the costly drawback of a low ESW, making the implementation of PILs in every electrochemical energy storage device a non-trivial task.

While the foundation for PILs as electrolyte in supercapacitors and batteries has already been established in the past, there are still many obstacles and difficulties to overcome. This thesis addresses some of them and thus promote the use of PILs as electrolytes, since the application of them has been always rather scarce, mainly attributed to their seemingly unsuitable nature for this task.

To give a better impression about their applicability, Publikation 1 chronicles the advances of PILs as electrolyte in electrochemical energy storage devices and summarizes the developed types of PILs and the resulting devices. It also highlights important tasks yet unresolved, amongst others the implementation of PILs in post-lithium devices.

While the use of PILs in EDLCs has been regarded as very skeptical, Publikation 2 shows a method to improve the main reason for that, its low power capability. With the addition of small amounts of water to a hydrophobic PIL, $[\text{Pyr}_{\text{H4}}][\text{TFSI}]$, the transport properties are drastically improved and the m.p. lowered below RT. Through this, the rate capability of EDLCs could be increased significantly, while the OPV was lowered only marginally. The developed system thus shows a high power with a moderate energy density combined with improved safety characteristics.

The mixture of [Pyr_{H4}][TFSI] was also analyzed via molecular dynamic calculations, showing different behavior of the water molecules, depending on the amount of water solved. While at low amounts of water the H₂O molecules are isolated between PIL molecules, higher amounts of water will lead to H₂O clusters. This was further investigated in Publikation 3, revealing a significant difference in molecule behavior from isolated water molecules and the clusters.

To expand the application of PILs to post-lithium devices, a preliminary proof-of-concept for sodium-ion based devices has been carried out in Publikation 4. In this case, mixtures of [Pyr_{H4}][TFSI] and diglyme, a common solvent for sodium-ion batteries, combined with 0.5 M NaTFSI with varying ratios of PIL have been prepared and fully characterized. Afterwards, their use in combination with AC-based EDLCs has been tested, for later applications in sodium-ion hybrid devices. To refine the work further, aprotic versions of these electrolytes using [Pyr₁₄][TFSI] have also been investigated to compare AILs and PILs for this application. Foremost, it could be shown that both electrolyte systems, protic as well as aprotic, are suitable for the application in sodium-ion EDLCs. Furthermore, depending on the solvent : IL ratio, the power performance of the system can be influenced and, at least for this supercapacitor application, AIL based electrolytes offer the better properties.

Publikation 5 considered the synthesis of either new or yet uncharacterized PILs with the aim to improve and expand the use of PILs. Based on literature data and proven anion/cation types, four different PILs based on imidazolium cations have been successfully synthesized and fully characterized for the use as electrolyte. Furthermore, their application as LIB electrolyte has been investigated. Only one PIL has been found to effectively work, showing the difficulty to find suitable PILs, when minding the vast possibilities of anion/cation combinations.

Another post-lithium battery application for PILs was investigated in Publikation 7. Mixtures of [Pyr_{H4}][TFSI] or [Pyr₁₄][TFSI] together with PC with 0.1 M Ca(TFSI)₂ have been characterized and successfully employed in Ca-based EDLCs. Here, the AIL and PIL were comparable in terms of power capability, with the former having an advantage in energy performance. Unfortunately, only the aprotic electrolyte was able to enable calcium insertion-desertion in TiS₂ electrodes, due to the limited OPV of the PIL, resulting in electrolyte decomposition. Furthermore, it was shown that not only Ca-intercalation is occurring while cycling in the

[Pyr₁₄][TFSI]-based electrolyte, but also co-intercalation of the [Pyr₁₄]⁺-cation, leading to deterioration of the TiS₂ electrode.

To further enhance the safety properties of an IL based electrolyte, the effects of incorporating both PIL and AIL in a silica matrix have been examined in Publikation 8. Depending on the presence of LiTFSI, the m.p. of confined [Pyr_{H4}][TFSI] was lowered or increased, the former in the absence, the latter in the presence of LiTFSI. Contrary, the m.p. of [Pyr₁₄][TFSI] was always lowered when confined, with or without the addition of LiTFSI. This behavior was further investigated using Raman spectroscopy, revealing a different coordination of Li-ions in the AIL and PIL based electrolyte. While the Li-ions interact stronger with the silica host matrix in the AIL, the available proton within the [Pyr_{H4}]⁺-cation is competing with the Li-ions. This leads to lower coordination numbers of Li-ions within the AIL when confined, while it does not change when the PIL is confined. This shows that the ΔpK_a value of a PIL plays an important role, and that changing it will lead to different effects when confined in a silica matrix.

Publikation 9 also concerns the confinement of a PIL ([Pyr_{H4}][TFSI]), this time in a PEO based UV-crosslinked polymer matrix. This solid electrolyte shows high conduction, a broad stable temperature window and a comparable ESW to the liquid [Pyr_{H4}][TFSI]. For the first time, a pure PIL-based solid electrolyte was deployed for both - EDLC and LIB. The former system was able to yield similar capacitances compared to an EDLC using liquid [Pyr_{H4}][TFSI] as electrolyte, but was lacking in rate capability, due to the operation at RT as well as being unoptimized in terms of electrode/electrolyte interface. The battery system consisted of an LFP cathode and a lithium-metal anode, which was never used in combination with a PIL before. It has been shown that the use of VC as additive leads to the formation of an SEI, preventing electrolyte decomposition. The system was able to deliver high capacities while displaying good reversibility.

Finally, the result of Publikation 9, the possibility to combine lithium-metal with a PIL, was further investigated in Publikation 6. Electrolytes composed of [Pyr_{H4}][TFSI] and [Pyr_{H4}][FSI] together with LiTFSI and LiFSI, respectively, were mixed with VC. After characterizing the chemical-physical properties of the electrolytes, they were employed in symmetrical lithium-metal cells. While both systems showed reversible lithium stripping-plating, a better performance and lower overpotentials were found for the [Pyr_{H4}][FSI] based electrolyte. This was also confirmed in cells employing lithium-metal anodes and LFP cathodes, in which the

[TFSI]⁻-based electrolyte was not able to provide reversible cycling of the electrodes, contrary to the [FSI]⁻-based electrolyte. The latter electrolyte was then used in combination with an NMC cathode, even further enhancing the power and energy performance of this PIL-LIB system.

4. Outlook

The results of this thesis show that the employment of PILs as electrolytes in electrochemical energy storage devices definitely has great potential, while being quite challenging.

One of the most promising paths for PILs regarding supercapacitors appears to be the combination with water. Foremost, this approach can easily diminish the lack in power capability caused by high viscosities. But it also provides the possibility for more intriguing improvements besides faster vehicular mechanisms. As it has been shown in the past, mechanisms in PILs like the Grotthuss effect are able to enhance the conductivity of an electrolyte system significantly. With the addition of water, these effects can be further strengthened. And while in this work the PIL-water mixture was composed of a hydrophobic PIL, future work should be carried out with hydrophilic PILs, to ensure a possible homogeneous hydrogen-bond network throughout the whole electrolyte.

An important task in the future regarding battery systems employing PILs will be the understanding of the role of additives on the formation of interfacial layers, e.g., SEI. While it has been successfully shown that the use of VC and VEC can lead to reversible and high performing battery systems, the exact mechanisms and the influences on the SEI composition are completely unknown. However, understanding these processes is a key factor in improving the established systems and even expanding the number of systems suitable for PIL-based electrolytes. This latter point is especially important for post-lithium devices, since it has been shown that these are very difficult undertakings in combination with PILs. Great potential could be found in the combination of PIL-based electrolytes in yet rather unexplored sectors, e.g., sulfur-based systems or even lithium-air batteries.

Finally, the identification of suitable PILs for the application in electrochemical-based development, is still extremely unoptimized. More precisely, the synthesis process is nowadays still based on a trial-and-error principle, a problem which IL research as a whole is confronted with. Only through time consuming syntheses of large amounts of ILs and their full characterization suitable candidates can be recognized. A solution for this problem is the identification through computational screening methods, an approach which is still in infancy and yet limited to AILs. Nevertheless, this tool could improve the application of PILs tremendously, considering the extremely high combination possibilities.

5. References

1. Morton, M.D. and C.K. Hamer, *Ionic liquids—The beginning of the end or the end of the beginning?—A look at the life of ionic liquids through patent claims*. Separation and Purification Technology, 2018. **196**: p. 3-9.
2. Davy, H., *The Collected Works of Sir Humphry Davy*. Vol. 1. 1839: Smith, Elder.
3. Liu, G. and D.B. Müller, *Centennial evolution of aluminum in-use stocks on our aluminized planet*. Environmental science & technology, 2013. **47**(9): p. 4882-4888.
4. Ramsay, W., *XXXIV. On picoline and its derivatives*. The London, Edinburgh, and Dublin Philosophical Magazine and Journal of Science, 1876. **2**(11): p. 269-281.
5. Walden, P., *Ueber die Molekulargröße und elektrische Leitfähigkeit einiger geschmolzenen Salze*. Bulletin de l'Académie Impériale des Sciences de St.-Petersbourg, 1914. **8**(6): p. 405-422.
6. Hurley, F.H. and T.P. Wier Jr, *Electrodeposition of metals from fused quaternary ammonium salts*. Journal of The Electrochemical Society, 1951. **98**(5): p. 203.
7. Gale, R., B. Gilbert, and R. Osteryoung, *Raman spectra of molten aluminum chloride: 1-butylpyridinium chloride systems at ambient temperatures*. Inorganic Chemistry, 1978. **17**(10): p. 2728-2729.
8. Koch, V., L. Miller, and R. Osteryoung, *Electroinitiated Friedel-Crafts transalkylations in a room-temperature molten-salt medium*. Journal of the American Chemical Society, 1976. **98**(17): p. 5277-5284.
9. Hussey, C.L., J.K. Erbacher, and L.A. King, *High energy density pelletized aluminum chloride thermal batteries*. Final Report, 1976.
10. Erbacher, J.K., C.L. Hussey, and J.C. Nardi, *New Low Temperature, High Energy Density Battery Systems*. 1978, FRANK J SEILER RESEARCH LAB UNITED STATES AIR FORCE ACADEMY COLO.
11. Wilkes, J.S., *A short history of ionic liquids—from molten salts to neoteric solvents*. Green Chemistry, 2002. **4**(2): p. 73-80.
12. Wilkes, J.S. and M.J. Zaworotko, *Air and water stable 1-ethyl-3-methylimidazolium based ionic liquids*. Journal of the Chemical Society, Chemical Communications, 1992(13): p. 965-967.
13. Bonhote, P., et al., *Hydrophobic, highly conductive ambient-temperature molten salts*. Inorganic chemistry, 1996. **35**(5): p. 1168-1178.
14. Seddon, K.R., *Ionic liquids for clean technology*. Journal of Chemical Technology & Biotechnology: International Research in Process, Environmental AND Clean Technology, 1997. **68**(4): p. 351-356.
15. Plechkova, N.V. and K.R. Seddon, *Applications of ionic liquids in the chemical industry*. Chemical Society Reviews, 2008. **37**(1): p. 123-150.
16. Welton, T., *Ionic liquids: a brief history*. Biophysical reviews, 2018. **10**(3): p. 691-706.
17. Rebelo, L.P., et al., *On the critical temperature, normal boiling point, and vapor pressure of ionic liquids*. The Journal of Physical Chemistry B, 2005. **109**(13): p. 6040-6043.
18. Deetlefs, M. and K. Seddon, *Ionic liquids: fact and fiction*. Chimica Oggi-Chemistry Today, 2006. **24**(2): p. 16.
19. Zhao, D., Y. Liao, and Z. Zhang, *Toxicity of ionic liquids*. Clean—soil, air, water, 2007. **35**(1): p. 42-48.
20. Bystrzanowska, M., et al., *How green are ionic liquids?—A multicriteria decision analysis approach*. Ecotoxicology and environmental safety, 2019. **174**: p. 455-458.
21. Koel, M., *Ionic liquids in chemical analysis*. 2008: CRC press.
22. Wang, H., G. Gurau, and R.D. Rogers, *Ionic liquid processing of cellulose*. Chemical Society Reviews, 2012. **41**(4): p. 1519-1537.
23. Zhang, X., et al., *Carbon capture with ionic liquids: overview and progress*. Energy & Environmental Science, 2012. **5**(5): p. 6668-6681.

24. Brogan, A.P. and J.P. Hallett, *Solubilizing and stabilizing proteins in anhydrous ionic liquids through formation of protein–polymer surfactant nanoconstructs*. Journal of the American Chemical Society, 2016. **138**(13): p. 4494-4501.
25. Gao, M.R., J. Yuan, and M. Antonietti, *Ionic Liquids and Poly (ionic liquid) s for Morphosynthesis of Inorganic Materials*. Chemistry–A European Journal, 2017. **23**(23): p. 5391-5403.
26. Karimi, B., et al., *Ionic liquids in asymmetric synthesis: an overall view from reaction media to supported ionic liquid catalysis*. ChemCatChem, 2018. **10**(15): p. 3173-3205.
27. Karuppasamy, K., et al., *Ionic liquid-based electrolytes for energy storage devices: A brief review on their limits and applications*. Polymers, 2020. **12**(4): p. 918.
28. Irge, D.D., *Ionic liquids: A review on greener chemistry applications, quality ionic liquid synthesis and economical viability in a chemical processes*. Am. J. Phys. Chem, 2016. **5**: p. 74-79.
29. Angell, C.A., Y. Ansari, and Z. Zhao, *Ionic liquids: past, present and future*. Faraday discussions, 2012. **154**: p. 9-27.
30. Mecerreyes, D., *Polymeric ionic liquids: Broadening the properties and applications of polyelectrolytes*. Progress in Polymer Science, 2011. **36**(12): p. 1629-1648.
31. Ye, Y.-S., J. Rick, and B.-J. Hwang, *Ionic liquid polymer electrolytes*. Journal of Materials Chemistry A, 2013. **1**(8): p. 2719-2743.
32. Gupta, N., Y.N. Liang, and X. Hu, *Thermally responsive ionic liquids and polymeric ionic liquids: Emerging trends and possibilities*. Current Opinion in Chemical Engineering, 2019. **25**: p. 43-50.
33. Greaves, T.L. and C.J. Drummond, *Protic ionic liquids: properties and applications*. Chemical reviews, 2008. **108**(1): p. 206-237.
34. Greaves, T.L., et al., *Protic ionic liquids: solvents with tunable phase behavior and physicochemical properties*. The Journal of Physical Chemistry B, 2006. **110**(45): p. 22479-22487.
35. Greaves, T.L. and C.J. Drummond, *Protic ionic liquids: evolving structure–property relationships and expanding applications*. Chemical reviews, 2015. **115**(20): p. 11379-11448.
36. Belieres, J.-P. and C.A. Angell, *Protic ionic liquids: preparation, characterization, and proton free energy level representation*. The Journal of Physical Chemistry B, 2007. **111**(18): p. 4926-4937.
37. Fumino, K., A. Wulf, and R. Ludwig, *The potential role of hydrogen bonding in aprotic and protic ionic liquids*. Physical Chemistry Chemical Physics, 2009. **11**(39): p. 8790-8794.
38. Hayes, R., et al., *The nature of hydrogen bonding in protic ionic liquids*. Angewandte Chemie International Edition, 2013. **52**(17): p. 4623-4627.
39. Fumino, K., S. Reimann, and R. Ludwig, *Probing molecular interaction in ionic liquids by low frequency spectroscopy: Coulomb energy, hydrogen bonding and dispersion forces*. Physical Chemistry Chemical Physics, 2014. **16**(40): p. 21903-21929.
40. Yoshizawa, M., W. Xu, and C.A. Angell, *Ionic liquids by proton transfer: Vapor pressure, conductivity, and the relevance of $\Delta p K_a$ from aqueous solutions*. Journal of the American Chemical Society, 2003. **125**(50): p. 15411-15419.
41. Yoshizawa, M., W. Xu, and C.A. Angell, *Ionic Liquids by Proton Transfer: Vapor Pressure, Conductivity, and the Relevance of $\Delta p K_a$ from Aqueous Solutions*. Journal of the American Chemical Society, 2003. **125**(50): p. 15411-15419.
42. Anouti, M., et al., *Synthesis and characterization of new pyrrolidinium based protic ionic liquids. Good and superionic liquids*. The Journal of Physical Chemistry B, 2008. **112**(42): p. 13335-13343.
43. Ingenmey, J., S. Gehrke, and B. Kirchner, *How to harvest Grotthuss diffusion in protic ionic liquid electrolyte systems*. ChemSusChem, 2018. **11**(12): p. 1900-1910.
44. Schreiner, C., et al., *Fractional Walden rule for ionic liquids: examples from recent measurements and a critique of the so-called ideal KCl line for the Walden plot*. Journal of Chemical & Engineering Data, 2010. **55**(5): p. 1784-1788.

45. Harris, K.R., *On the Use of the Angell–Walden Equation To Determine the “Ionicity” of Molten Salts and Ionic Liquids*. The Journal of Physical Chemistry B, 2019. **123**(32): p. 7014-7023.
46. Mariani, A., et al., *The unseen evidence of reduced ionicity: The elephant in (the) room temperature ionic liquids*. Journal of Molecular Liquids, 2020: p. 115069.
47. Earle, M.J. and K.R. Seddon, *Ionic liquids. Green solvents for the future*. Pure and applied chemistry, 2000. **72**(7): p. 1391-1398.
48. Rocha, M.A., et al., *High-accuracy vapor pressure data of the extended [C_nC₁im][Ntf₂] ionic liquid series: trend changes and structural shifts*. The Journal of Physical Chemistry B, 2011. **115**(37): p. 10919-10926.
49. Ludwig, R. and U. Kragl, *Do we understand the volatility of ionic liquids?* Angewandte Chemie International Edition, 2007. **46**(35): p. 6582-6584.
50. Horikawa, M., et al., *Vaporization of protic ionic liquids studied by matrix-isolation Fourier transform infrared spectroscopy*. The Journal of Physical Chemistry A, 2014. **118**(18): p. 3280-3287.
51. Zaitsau, D.H., et al., *Dispersion and hydrogen bonding rule: why the vaporization enthalpies of aprotic ionic liquids are significantly larger than those of protic ionic liquids*. Angewandte Chemie International Edition, 2016. **55**(38): p. 11682-11686.
52. MSS Esperança, J., et al., *Volatility of Aprotic Ionic Liquids · A Review*. Journal of Chemical & Engineering Data, 2010. **55**(1): p. 3-12.
53. Cao, Y. and T. Mu, *Comprehensive investigation on the thermal stability of 66 ionic liquids by thermogravimetric analysis*. Industrial & engineering chemistry research, 2014. **53**(20): p. 8651-8664.
54. Clough, M.T., et al., *Thermal decomposition of carboxylate ionic liquids: trends and mechanisms*. Physical Chemistry Chemical Physics, 2013. **15**(47): p. 20480-20495.
55. Fox, D.M., et al., *Flammability and thermal analysis characterization of imidazolium-based ionic liquids*. Industrial & engineering chemistry research, 2008. **47**(16): p. 6327-6332.
56. Liaw, H.-J., et al., *Relationship between flash point of ionic liquids and their thermal decomposition*. Green Chemistry, 2012. **14**(7): p. 2001-2008.
57. Diallo, A.O., et al., *Revisiting physico-chemical hazards of ionic liquids*. Separation and purification technology, 2012. **97**: p. 228-234.
58. Angell, C., *Molten Salts: From Fundamentals to Applications*. NATO Science Series, II: Mathematics, Physics and Chemistry, 2002: p. 305-320.
59. Xu, W., E.I. Cooper, and C.A. Angell, *Ionic liquids: ion mobilities, glass temperatures, and fragilities*. The Journal of Physical Chemistry B, 2003. **107**(25): p. 6170-6178.
60. Luo, H., J.-F. Huang, and S. Dai, *Studies on thermal properties of selected aprotic and protic ionic liquids*. Separation Science and Technology, 2008. **43**(9-10): p. 2473-2488.
61. Xu, W. and C.A. Angell, *Solvent-free electrolytes with aqueous solution-like conductivities*. Science, 2003. **302**(5644): p. 422-425.
62. McFarlane, D., et al., *High conductivity molten salts based on the imide ion*. Electrochimica Acta, 2000. **45**(8-9): p. 1271-1278.
63. Matveev, V.V., et al., *NMR investigation of the structure and single-particle dynamics of inorganic salt solutions in a protic ionic liquid*. Journal of Molecular Liquids, 2019. **278**: p. 239-246.
64. Kohno, Y. and H. Ohno, *Ionic liquid/water mixtures: from hostility to conciliation*. Chemical Communications, 2012. **48**(57): p. 7119-7130.
65. Du, Z., et al., *Investigation of physicochemical properties of lactam-based brønsted acidic ionic liquids*. The Journal of Physical Chemistry B, 2005. **109**(41): p. 19542-19546.
66. Zhou, Z.-B., H. Matsumoto, and K. Tatsumi, *Low-melting, low-viscous, hydrophobic ionic liquids: N-alkyl (alkyl ether)-N-methylpyrrolidinium perfluoroethyltrifluoroborate*. Chemistry letters, 2004. **33**(12): p. 1636-1637.
67. Muller, P., *Glossary of terms used in physical organic chemistry (IUPAC Recommendations 1994)*. Pure and applied chemistry, 1994. **66**(5): p. 1077-1184.

68. Reichardt, C., *Empirische parameter der lösungsmittelpolarität*. Angewandte Chemie, 1965. **77**(1): p. 30-40.
69. Muldoon, M.J., et al., *Improving carbon dioxide solubility in ionic liquids*. The Journal of Physical Chemistry B, 2007. **111**(30): p. 9001-9009.
70. Khupse, N.D. and A. Kumar, *Contrasting thermosolvatochromic trends in pyridinium-, pyrrolidinium-, and phosphonium-based ionic liquids*. The Journal of Physical Chemistry B, 2010. **114**(1): p. 376-381.
71. Bini, R., et al., *A rationalization of the solvent effect on the Diels–Alder reaction in ionic liquids using multiparameter linear solvation energy relationships*. Organic & biomolecular chemistry, 2008. **6**(14): p. 2522-2529.
72. Zhang, S., et al., *Hydroxyl ionic liquids: the differentiating effect of hydroxyl on polarity due to ionic hydrogen bonds between hydroxyl and anions*. The Journal of Physical Chemistry B, 2010. **114**(11): p. 3912-3920.
73. Lee, J.-M. and J.M. Prausnitz, *Polarity and hydrogen-bond-donor strength for some ionic liquids: effect of alkyl chain length on the pyrrolidinium cation*. Chemical Physics Letters, 2010. **492**(1-3): p. 55-59.
74. Shukla, S.K., N.D. Khupse, and A. Kumar, *Do anions influence the polarity of protic ionic liquids?* Physical Chemistry Chemical Physics, 2012. **14**(8): p. 2754-2761.
75. Yu, G., et al., *Viscosity of ionic liquids: Database, observation, and quantitative structure-property relationship analysis*. AIChE Journal, 2012. **58**(9): p. 2885-2899.
76. Ohno, H. and M. Yoshizawa, *Ion conductive characteristics of ionic liquids prepared by neutralization of alkylimidazoles*. Solid State Ionics, 2002. **154**: p. 303-309.
77. Boli, E., T. Katsavrias, and E. Voutsas, *Viscosities of pure protic ionic liquids and their binary and ternary mixtures with water and ethanol*. Fluid Phase Equilibria, 2020. **520**: p. 112663.
78. Dong, Y., et al., *Azepanium based protic ionic liquids: Synthesis, thermophysical properties and COSMO-RS study*. Journal of Molecular Liquids, 2018. **264**: p. 24-31.
79. Miran, M.S., et al., *Electrochemical properties of protic ionic liquids: correlation between open circuit potential for H₂/O₂ cells under non-humidified conditions and $\Delta p K_a$* . RSC advances, 2013. **3**(13): p. 4141-4144.
80. Smith, J., et al., *Rheology of protic ionic liquids and their mixtures*. The Journal of Physical Chemistry B, 2013. **117**(44): p. 13930-13935.
81. Rupp, A., et al., *Size matters! On the way to ionic liquid systems without ion pairing*. Chemistry—A European Journal, 2014. **20**(31): p. 9794-9804.
82. Zhao, C., et al., *Electrochemistry of room temperature protic ionic liquids*. The Journal of Physical Chemistry B, 2008. **112**(23): p. 6923-6936.
83. Tang, B., et al., *Critical assessment of superbase-derived protic ionic liquids as electrolytes for electrochemical applications*. Electrochimica Acta, 2019. **298**: p. 413-420.
84. Harris, K.R., *Can the transport properties of molten salts and ionic liquids be used to determine ion association?* The Journal of Physical Chemistry B, 2016. **120**(47): p. 12135-12147.
85. Watanabe, H., et al., *Effect of Brønsted Acidity on Ion Conduction in Fluorinated Acetic Acid and N-Methylimidazole Equimolar Mixtures as Pseudo-protic Ionic Liquids*. The Journal of Physical Chemistry B, 2020. **124**(49): p. 11157-11164.
86. Watanabe, H., et al., *Possible Proton Conduction Mechanism in Pseudo-Protic Ionic Liquids: A Concept of Specific Proton Conduction*. The Journal of Physical Chemistry B, 2019. **123**(29): p. 6244-6252.
87. Jankowski, P., W. Wiecek, and P. Johansson, *SEI-forming electrolyte additives for lithium-ion batteries: development and benchmarking of computational approaches*. Journal of molecular modeling, 2017. **23**(1): p. 1-9.
88. Wang, A., et al., *Review on modeling of the anode solid electrolyte interphase (SEI) for lithium-ion batteries*. NPJ Computational materials, 2018. **4**(1): p. 1-26.
89. Peljo, P. and H.H. Girault, *Electrochemical potential window of battery electrolytes: the HOMO–LUMO misconception*. Energy & Environmental Science, 2018. **11**(9): p. 2306-2309.

90. Béguin, F., et al., *Carbons and electrolytes for advanced supercapacitors*. *Advanced materials*, 2014. **26**(14): p. 2219-2251.
91. Suarez, P.A.Z., et al., *Electrochemical Behavior of Vitreous Glass Carbon and Platinum Electrodes in the Ionic Liquid 1-n-Butyl-3-Methylimidazolium Trifluoroacetate*. *Journal of the Brazilian Chemical Society*, 2002. **13**: p. 106-109.
92. Lane, G.H., *Electrochemical reduction mechanisms and stabilities of some cation types used in ionic liquids and other organic salts*. *Electrochimica acta*, 2012. **83**: p. 513-528.
93. Mayrand-Provencher, L., et al., *Pyridinium-based protic ionic liquids as electrolytes for RuO₂ electrochemical capacitors*. *Journal of Power Sources*, 2010. **195**(15): p. 5114-5121.
94. Wu, T., et al., *Synthesis and characterization of protic ionic liquids containing cyclic amine cations and tetrafluoroborate anion*. *Journal of the Iranian Chemical Society*, 2011. **8**(1): p. 149-165.
95. Hirao, M., H. Sugimoto, and H. Ohno, *Preparation of novel room-temperature molten salts by neutralization of amines*. *Journal of The Electrochemical Society*, 2000. **147**(11): p. 4168-4172.
96. Mayrand-Provencher, L. and D. Rochefort, *Origin and effect of impurities in protic ionic liquids based on 2-methylpyridine and trifluoroacetic acid for applications in electrochemistry*. *Electrochimica acta*, 2009. **54**(28): p. 7422-7428.
97. Venkatraman, V., et al., *Predicting ionic liquid melting points using machine learning*. *Journal of Molecular Liquids*, 2018. **264**: p. 318-326.
98. Dong, Q., et al., *ILThermo: a free-access web database for thermodynamic properties of ionic liquids*. *Journal of Chemical & Engineering Data*, 2007. **52**(4): p. 1151-1159.
99. Stettner, T. and A. Balducci, *Protic ionic liquids in energy storage devices: Past, present and future perspective*. *Energy Storage Materials*, 2021.
100. Macfarlane, D.R., et al., *Pyrrrolidinium imides: a new family of molten salts and conductive plastic crystal phases*. *The Journal of Physical Chemistry B*, 1999. **103**(20): p. 4164-4170.
101. Crosthwaite, J.M., et al., *Phase transition and decomposition temperatures, heat capacities and viscosities of pyridinium ionic liquids*. *The Journal of Chemical Thermodynamics*, 2005. **37**(6): p. 559-568.
102. Tokuda, H., et al., *Physicochemical properties and structures of room-temperature ionic liquids. 3. Variation of cationic structures*. *The Journal of Physical Chemistry B*, 2006. **110**(6): p. 2833-2839.
103. Matsumoto, H., et al., *Fast cycling of Li/LiCoO₂ cell with low-viscosity ionic liquids based on bis (fluorosulfonyl) imide [FSI]-*. *Journal of Power Sources*, 2006. **160**(2): p. 1308-1313.
104. Ruiz, V., et al., *Ionic liquid-solvent mixtures as supercapacitor electrolytes for extreme temperature operation*. *RSC Advances*, 2012. **2**(13): p. 5591-5598.
105. Fumino, K., et al., *Equilibrium of Contact and Solvent-Separated Ion Pairs in Mixtures of Protic Ionic Liquids and Molecular Solvents Controlled by Polarity*. *Angewandte Chemie International Edition*, 2013. **52**(47): p. 12439-12442.
106. Thawarkar, S., N.D. Khupse, and A. Kumar, *Comparative investigation of the ionicity of aprotic and protic ionic liquids in molecular solvents by using conductometry and NMR spectroscopy*. *ChemPhysChem*, 2016. **17**(7): p. 1006-1017.
107. Luo, J., et al., *1H-1, 2, 4-Triazole as solvent for imidazolium methanesulfonate*. *Physical Chemistry Chemical Physics*, 2012. **14**(32): p. 11441-11447.
108. Vogl, T., S. Menne, and A. Balducci, *Mixtures of protic ionic liquids and propylene carbonate as advanced electrolytes for lithium-ion batteries*. *Physical Chemistry Chemical Physics*, 2014. **16**(45): p. 25014-25023.
109. Guerfi, A., et al., *Improved electrolytes for Li-ion batteries: Mixtures of ionic liquid and organic electrolyte with enhanced safety and electrochemical performance*. *Journal of Power Sources*, 2010. **195**(3): p. 845-852.
110. Stange, P., K. Fumino, and R. Ludwig, *Ion Speciation of Protic Ionic Liquids in Water: Transition from Contact to Solvent-Separated Ion Pairs*. *Angewandte Chemie International Edition*, 2013. **52**(10): p. 2990-2994.

111. Anouti, M.r.m., J. Jacquemin, and P. Porion, *Transport properties investigation of aqueous protic ionic liquid solutions through conductivity, viscosity, and NMR self-diffusion measurements*. The Journal of Physical Chemistry B, 2012. **116**(14): p. 4228-4238.
112. Gorska, B., et al., *Effect of low water content in protic ionic liquid on ions electrosorption in porous carbon: application to electrochemical capacitors*. Physical Chemistry Chemical Physics, 2017. **19**(18): p. 11173-11186.
113. Demarconnay, L., et al., *Optimizing the performance of supercapacitors based on carbon electrodes and protic ionic liquids as electrolytes*. Electrochimica Acta, 2013. **108**: p. 361-368.
114. Timperman, L., A. Vigeant, and M. Anouti, *Eutectic mixture of protic ionic liquids as an electrolyte for activated carbon-based supercapacitors*. Electrochimica Acta, 2015. **155**: p. 164-173.
115. Thawarkar, S., et al., *Understanding the behavior of mixtures of protic-aprotic and protic-protic ionic liquids: conductivity, viscosity, diffusion coefficient and ionicity*. Journal of Molecular Liquids, 2019. **276**: p. 986-994.
116. Zhong, C., et al., *A review of electrolyte materials and compositions for electrochemical supercapacitors*. Chemical Society Reviews, 2015. **44**(21): p. 7484-7539.
117. Dai, L., et al., *Electrical characteristics of high energy density multilayer ceramic capacitor for pulse power application*. IEEE transactions on magnetics, 2005. **41**(1): p. 281-284.
118. Beguin, F. and E. Frackowiak, *Supercapacitors: Materials, Systems and Applications, 2013*. Weinheim, Germany: Wiley--VCH.
119. Pan, M.-J. and C.A. Randall, *A brief introduction to ceramic capacitors*. IEEE electrical insulation magazine, 2010. **26**(3): p. 44-50.
120. Chu, A. and P. Braatz, *Comparison of commercial supercapacitors and high-power lithium-ion batteries for power-assist applications in hybrid electric vehicles: I. Initial characterization*. Journal of power sources, 2002. **112**(1): p. 236-246.
121. Janz, G.J., *Nonaqueous electrolytes handbook*. Vol. 1. 2012: Elsevier.
122. Buscaglia, V., M.T. Buscaglia, and G. Canu, *BaTiO₃-Based Ceramics: Fundamentals, Properties and Applications*. 2020.
123. Tsurumi, T., et al., *Evaluation and statistical analysis of dielectric permittivity of BaTiO₃ powders*. Journal of the American Ceramic Society, 2006. **89**(4): p. 1337-1341.
124. Portet, C., G. Yushin, and Y. Gogotsi, *Effect of carbon particle size on electrochemical performance of EDLC*. Journal of the Electrochemical Society, 2008. **155**(7): p. A531.
125. Shukla, A., S. Sampath, and K. Vijayamohanan, *Electrochemical supercapacitors: Energy storage beyond batteries*. Current science, 2000. **79**(12): p. 1656-1661.
126. Reza, M.S., et al., *Preparation of activated carbon from biomass and its' applications in water and gas purification, a review*. Arab Journal of Basic and Applied Sciences, 2020. **27**(1): p. 208-238.
127. Schütter, C., S. Pohlmann, and A. Balducci, *Industrial requirements of materials for electrical double layer capacitors: impact on current and future applications*. Advanced Energy Materials, 2019. **9**(25): p. 1900334.
128. Chowdhury, Z.Z., et al., *Preparation of carbonaceous adsorbents from lignocellulosic biomass and their use in removal of contaminants from aqueous solution*. BioResources, 2013. **8**(4): p. 6523-6555.
129. Din, M.I., S. Ashraf, and A. Intisar, *Comparative study of different activation treatments for the preparation of activated carbon: a mini-review*. Science progress, 2017. **100**(3): p. 299-312.
130. Pandolfo, A.G. and A.F. Hollenkamp, *Carbon properties and their role in supercapacitors*. Journal of power sources, 2006. **157**(1): p. 11-27.
131. Wang, J. and S. Kaskel, *KOH activation of carbon-based materials for energy storage*. Journal of Materials Chemistry, 2012. **22**(45): p. 23710-23725.
132. Bonnefoi, L., et al., *Electrode optimisation for carbon power supercapacitors*. Journal of power sources, 1999. **79**(1): p. 37-42.
133. Chen, H., et al., *Exploring chemical, mechanical, and electrical functionalities of binders for advanced energy-storage devices*. Chemical reviews, 2018. **118**(18): p. 8936-8982.

134. Kühnel, R.-S., et al., *Anodic stability of aluminum current collectors in an ionic liquid based on the (fluorosulfonyl)(trifluoromethanesulfonyl) imide anion and its implication on high voltage supercapacitors*. *Electrochemistry communications*, 2014. **38**: p. 117-119.
135. Deimede, V. and C. Elmasides, *Separators for lithium-ion batteries: a review on the production processes and recent developments*. *Energy technology*, 2015. **3**(5): p. 453-468.
136. Zhang, S.S., *A review on the separators of liquid electrolyte Li-ion batteries*. *Journal of power sources*, 2007. **164**(1): p. 351-364.
137. Ue, M., *Chemical capacitors and quaternary ammonium salts*. *Electrochemistry*, 2007. **75**(8): p. 565-572.
138. Krummacher, J., et al., *Characterization of different conductive salts in ACN-based electrolytes for electrochemical double-layer capacitors*. *ChemElectroChem*, 2017. **4**(2): p. 353-361.
139. Brandt, A., et al., *Ionic liquids in supercapacitors*. *MRS bulletin*, 2013. **38**(7): p. 554-559.
140. Arbizzani, C., et al., *Safe, high-energy supercapacitors based on solvent-free ionic liquid electrolytes*. *Journal of Power Sources*, 2008. **185**(2): p. 1575-1579.
141. Lewandowski, A., et al., *Performance of carbon-carbon supercapacitors based on organic, aqueous and ionic liquid electrolytes*. *Journal of Power Sources*, 2010. **195**(17): p. 5814-5819.
142. Trasatti, S., *Physical electrochemistry of ceramic oxides*. *Electrochimica acta*, 1991. **36**(2): p. 225-241.
143. Conway, B.E., V. Birss, and J. Wojtowicz, *The role and utilization of pseudocapacitance for energy storage by supercapacitors*. *Journal of power sources*, 1997. **66**(1-2): p. 1-14.
144. Burke, A., *R&D considerations for the performance and application of electrochemical capacitors*. *Electrochimica Acta*, 2007. **53**(3): p. 1083-1091.
145. Chen, R., et al., *The development of pseudocapacitor electrodes and devices with high active mass loading*. *Advanced Energy Materials*, 2020. **10**(20): p. 1903848.
146. Jache, B. and P. Adelhelm, *Use of Graphite as a Highly Reversible Electrode with Superior Cycle Life for Sodium-Ion Batteries by Making Use of Co-Intercalation Phenomena*. *Angewandte Chemie International Edition*, 2014. **53**(38): p. 10169-10173.
147. Nitta, N., et al., *Li-ion battery materials: present and future*. *Materials today*, 2015. **18**(5): p. 252-264.
148. Lu, P. and S.J. Harris, *Lithium transport within the solid electrolyte interphase*. *Electrochemistry Communications*, 2011. **13**(10): p. 1035-1037.
149. Xu, K., *Nonaqueous liquid electrolytes for lithium-based rechargeable batteries*. *Chemical reviews*, 2004. **104**(10): p. 4303-4418.
150. Ponrouch, A., et al., *Non-aqueous electrolytes for sodium-ion batteries*. *Journal of Materials Chemistry A*, 2015. **3**(1): p. 22-42.
151. Kalhoff, J., et al., *Safer Electrolytes for Lithium-Ion Batteries: State of the Art and Perspectives*. *ChemSusChem*, 2015. **8**(13): p. 2154-2175.
152. Evans, D.F., et al., *Thermodynamics of solution of nonpolar gases in a fused salt. Hydrophobic bonding behavior in a nonaqueous system*. *Journal of the American Chemical Society*, 1981. **103**(2): p. 481-482.
153. Susan, M.A., et al., *Brønsted acid-base ionic liquids and their use as new materials for anhydrous proton conductors*. *Chemical Communications*, 2003(8): p. 938-939.
154. Elwan, H.A., M. Mamlouk, and K. Scott, *A review of proton exchange membranes based on protic ionic liquid/polymer blends for polymer electrolyte membrane fuel cells*. *Journal of Power Sources*, 2020: p. 229197.
155. Randriamahazaka, H., et al., *Ions transfer mechanisms during the electrochemical oxidation of poly (3, 4-ethylenedioxythiophene) in 1-ethyl-3-methylimidazolium bis ((trifluoromethyl) sulfonyl) amide ionic liquid*. *Electrochemistry communications*, 2004. **6**(3): p. 299-305.
156. Lewandowski, A. and M. Galiński, *Carbon-ionic liquid double-layer capacitors*. *Journal of Physics and Chemistry of Solids*, 2004. **65**(2-3): p. 281-286.
157. Rochefort, D. and A.-L. Pont, *Pseudocapacitive behaviour of RuO₂ in a proton exchange ionic liquid*. *Electrochemistry communications*, 2006. **8**(9): p. 1539-1543.

158. Lindberg, S., et al., *Charge storage mechanism of α -MnO₂ in protic and aprotic ionic liquid electrolytes*. Journal of Power Sources, 2020. **460**: p. 228111.
159. Djire, A., et al., *Enhanced performance for early transition metal nitrides via pseudocapacitance in protic ionic liquid electrolytes*. Electrochemistry Communications, 2017. **77**: p. 19-23.
160. Al-Zohbi, F., et al., *Impact of the aqueous pyrrolidinium hydrogen sulfate electrolyte formulation on transport properties and electrochemical performances for polyaniline-based supercapacitor*. Journal of Power Sources, 2019. **431**: p. 162-169.
161. Ketabi, S., B. Decker, and K. Lian, *Proton conducting ionic liquid electrolytes for liquid and solid-state electrochemical pseudocapacitors*. Solid State Ionics, 2016. **298**: p. 73-79.
162. Gorska, B., P. Ratajczak, and F. Béguin, *Faradaic processes on quinone-grafted carbons in protic ionic liquid electrolyte*. Electrochimica Acta, 2019. **328**: p. 135090.
163. Sathyamoorthi, S., V. Suryanarayanan, and D. Velayutham, *Organo-redox shuttle promoted protic ionic liquid electrolyte for supercapacitor*. Journal of Power Sources, 2015. **274**: p. 1135-1139.
164. Brandt, A., et al., *An investigation about the cycling stability of supercapacitors containing protic ionic liquids as electrolyte components*. Electrochimica Acta, 2013. **108**: p. 226-231.
165. Timperman, L., et al., *Phosphonium-based protic ionic liquid as electrolyte for carbon-based supercapacitors*. Electrochemistry Communications, 2011. **13**(10): p. 1112-1115.
166. Aradilla, D., et al., *A step forward into hierarchically nanostructured materials for high performance micro-supercapacitors: Diamond-coated SiNW electrodes in protic ionic liquid electrolyte*. Electrochemistry Communications, 2016. **63**: p. 34-38.
167. Oyedotun, K.O., et al., *Comparison of ionic liquid electrolyte to aqueous electrolytes on carbon nanofibres supercapacitor electrode derived from oxygen-functionalized graphene*. Chemical Engineering Journal, 2019. **375**: p. 121906.
168. Balducci, A., et al., *High temperature carbon-carbon supercapacitor using ionic liquid as electrolyte*. Journal of Power Sources, 2007. **165**(2): p. 922-927.
169. Fung, Y. and R. Zhou, *Room temperature molten salt as medium for lithium battery*. Journal of power sources, 1999. **81**: p. 891-895.
170. Ishikawa, M., et al., *Pure ionic liquid electrolytes compatible with a graphitized carbon negative electrode in rechargeable lithium-ion batteries*. Journal of power sources, 2006. **162**(1): p. 658-662.
171. Böckenfeld, N., et al., *On the use of lithium iron phosphate in combination with protic ionic liquid-based electrolytes*. Journal of The Electrochemical Society, 2013. **160**(4): p. A559.
172. Menne, S., et al., *Protic ionic liquids as electrolytes for lithium-ion batteries*. Electrochemistry communications, 2013. **31**: p. 39-41.
173. Menne, S., et al., *Carbonaceous anodes for lithium-ion batteries in combination with protic ionic liquids-based electrolytes*. Journal of Power Sources, 2014. **266**: p. 208-212.
174. Vogl, T., et al., *The beneficial effect of protic ionic liquids on the lithium environment in electrolytes for battery applications*. Journal of Materials Chemistry A, 2014. **2**(22): p. 8258-8265.
175. Arnaiz, M., et al., *Protic and Aprotic Ionic Liquids in Combination with Hard Carbon for Lithium-Ion and Sodium-Ion Batteries*. Batteries & Supercaps, 2018. **1**(6): p. 204-208.
176. Menne, S., T. Vogl, and A. Balducci, *The synthesis and electrochemical characterization of bis (fluorosulfonyl) imide-based protic ionic liquids*. Chemical Communications, 2015. **51**(17): p. 3656-3659.
177. Menne, S., R.-S. Kühnel, and A. Balducci, *The influence of the electrochemical and thermal stability of mixtures of ionic liquid and organic carbonate on the performance of high power lithium-ion batteries*. Electrochimica Acta, 2013. **90**: p. 641-648.
178. Vogl, T., S. Passerini, and A. Balducci, *The impact of mixtures of protic ionic liquids on the operative temperature range of use of battery systems*. Electrochemistry Communications, 2017. **78**: p. 47-50.
179. Vogl, T., et al., *The use of protic ionic liquids with cathodes for sodium-ion batteries*. Journal of Materials Chemistry A, 2016. **4**(27): p. 10472-10478.

180. Arnaiz, M., et al., *Aprotic and Protic Ionic Liquids Combined with Olive Pits Derived Hard Carbon for Potassium-Ion Batteries*. *Journal of The Electrochemical Society*, 2019. **166**(14): p. A3504-A3510.
181. Monti, D., et al., *Multivalent batteries—prospects for high energy density: Ca batteries*. *Frontiers in chemistry*, 2019. **7**.

6. Appendix

List of Publications

Part of this Thesis

- [1] Stettner, T., Huang, P., Goktas, M., Adelhelm, P., & Balducci, A. (2018). Mixtures of glyme and aprotic-protic ionic liquids as electrolytes for energy storage devices. *The Journal of chemical physics*, 148(19), 193825.
- [2] Stettner, T., Walter, F. C., & Balducci, A. (2019). Imidazolium-based protic ionic liquids as electrolytes for lithium-ion batteries. *Batteries & Supercaps*, 2(1), 55-59.
- [3] Stettner, T., Gehrke, S., Ray, P., Kirchner, B., & Balducci, A. (2019). Water in Protic Ionic Liquids: Properties and Use of a New Class of Electrolytes for Energy-Storage Devices. *ChemSusChem*, 12(16), 3827-3836.
- [4] Marie, A., Said, B., Galarneau, A., Stettner, T., Balducci, A., Bayle, M., ... & Le Bideau, J. (2020). Silica based ionogels: interface effects with aprotic and protic ionic liquids with lithium. *Physical Chemistry Chemical Physics*, 22(41), 24051-24058.
- [5] Stettner, T., Dugas, R., Ponrouch, A., & Balducci, A. (2020). Ionic Liquid-Based Electrolytes for Calcium-Based Energy Storage Systems. *Journal of The Electrochemical Society*, 167(10), 100544.
- [6] Stettner, T., Lingua, G., Falco, M., Balducci, A., & Gerbaldi, C. (2020). Protic Ionic Liquids-Based Crosslinked Polymer Electrolytes: A New Class of Solid Electrolytes for Energy Storage Devices. *Energy Technology*, 8(11), 2000742.
- [7] Lingua, G., Falco, M., Stettner, T., Gerbaldi, C., & Balducci, A. (2021). Enabling safe and stable Li metal batteries with protic ionic liquid electrolytes and high voltage cathodes. *Journal of Power Sources*, 481, 228979.
- [8] Stettner, T., & Balducci, A. (2021). Protic ionic liquids in energy storage devices: Past, present and future perspective. *Energy Storage Materials*.
- [9] Gehrke, S., Ray, P., Stettner, T., Balducci, A., & Kirchner, B. (2021). Water in Protic Ionic Liquid Electrolytes: From solvent separated ion pairs to water clusters. *ChemSusChem*, 14(16), 3315.

Others

- [1] Medenbach, L., Hartmann, P., Janek, J., Stettner, T., Balducci, A., Dirksen, C., ... & Adelhelm, P. (2020). A sodium polysulfide battery with liquid/solid electrolyte: improving sulfur utilization using P2S5 as additive and tetramethylurea as catholyte solvent. *Energy Technology*, 8(3), 1901200.

Contributions at International Conferences

1. Oral Presentation: Stettner, T., Huang, P., Goktas, M., Adelhelm, P., & Balducci, A. *Mixtures of Glyme and Aprotic-Protic Ionic Liquids as Electrolytes for Energy Storage Devices*. 69th Annual Meeting of the International Society of Electrochemistry, Bologna, Italy, 2018
2. Poster: Stettner, T., Ray, P., Kirchner, B., & Balducci, A. *Influence of Water on the Properties of Protic Ionic Liquids*. Bunsentagung- 118th General Assembly of the German Bunsen Society for Physical Chemistry, Jena, Germany, 2019
3. Oral Presentation: Stettner, T., Ray, P., Kirchner, B., & Balducci, A. *Influence of Water on the Properties of Protic Ionic Liquids*, Electrochemical Conference on Energy and the Environment: Bioelectrochemistry and Energy Storage (ECEE), Glasgow, Scotland, 2019
4. Poster: Stettner, T., Lingua, G., Falco, M., Balducci, A., & Gerbaldi, C. *Protic ionic liquids based polymers electrolytes: a new class of solid electrolytes for energy storage devices*, 71st Annual Meeting of the International Society, Belgrade, Serbia, Online, 2020
5. Oral Presentation: Stettner, T., Lingua, G., Falco, M., Balducci, A., & Gerbaldi, C. *Protic Ionic Liquids as Electrolytes in Lithium Batteries*, 72nd Annual Meeting of the International Society of Electrochemistry, Jeju, Korea, Online, 2021

Supplementary Information

Publication 2

Supporting Information

Water in Protic Ionic Liquids: Properties and Use of a New Class of Electrolytes for Energy-Storage Devices

Timo Stettner,^[a, b] Sascha Gehrke,^[c] Promit Ray,^[c] Barbara Kirchner,^[c] and Andrea Balducci^{*[a, b]}

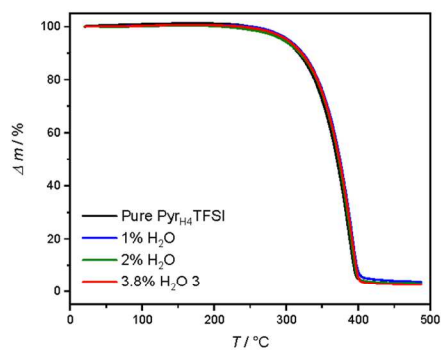


Figure S1. Thermogravimetric analysis data of the investigated water in PIL mixtures with a temperature ramp of $10\text{ }^\circ\text{C min}^{-1}$.

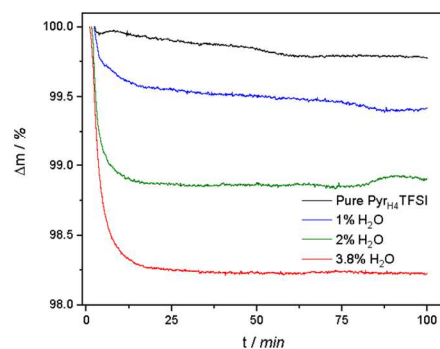


Figure S2. Isothermal analysis data of the investigated water in PIL mixtures at $100\text{ }^\circ\text{C}$ with a heating gradient of $50\text{ }^\circ\text{C min}^{-1}$.

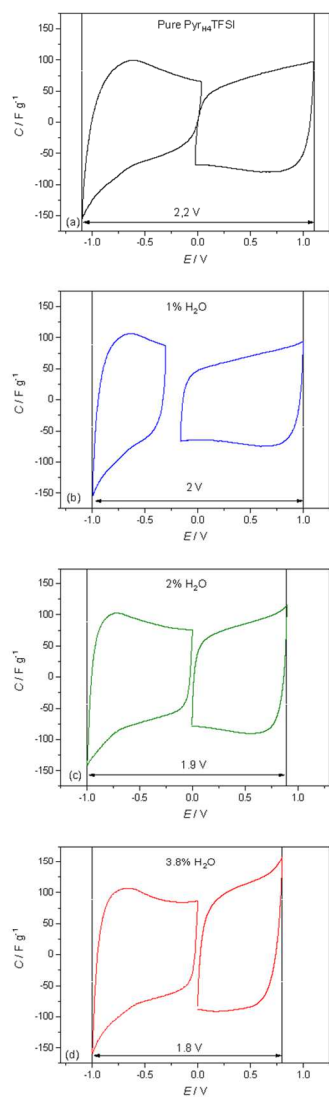


Figure S3. Specific capacitance and Coulombic efficiency of an activated carbon electrode obtained from CV at 5 mV s^{-1} at 40°C for the (a) pure $\text{Pyr}_{14}\text{TFSI}$, (b) 1 % H_2O , (c) 2 % H_2O and (d) 3.8 % H_2O based electrolyte.

Table S1. Mass ratios used for the mass balancing of the full cell EDLCs.

Electrolyte	Ratio Positive Electrode : Negative Electrode
Pure $\text{Pyr}_{14}\text{TFSI}$	1:1.31
1 % H_2O	1:1.17
2 % H_2O	1:1.75
3.8 % H_2O	1: 1.55

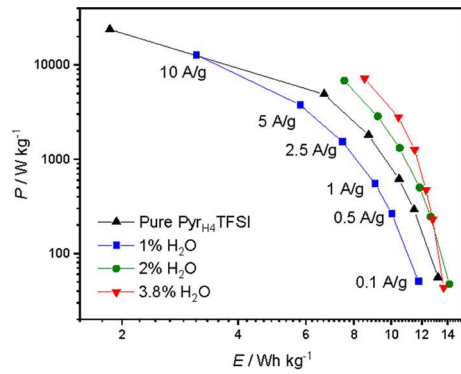


Figure S4. Ragone Plot of the investigated mixtures employed in EDLCs at 40 °C and different current densities (see Figure 7). The specific energy and power were calculated using the mass of the active material of the electrodes.

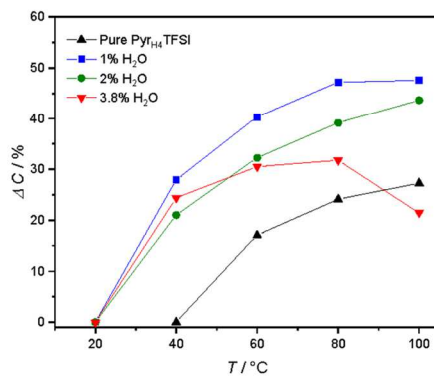


Figure S5. Influence of the temperature on the initial capacitance (starting at 20 °C for the mixture with 1, 2 and 3.8 wt% water and 40 °C for the pure Pyr_{H4}TFSI) of EDLCs using the investigated electrolytes. All tests were carried out at 1 A g⁻¹.

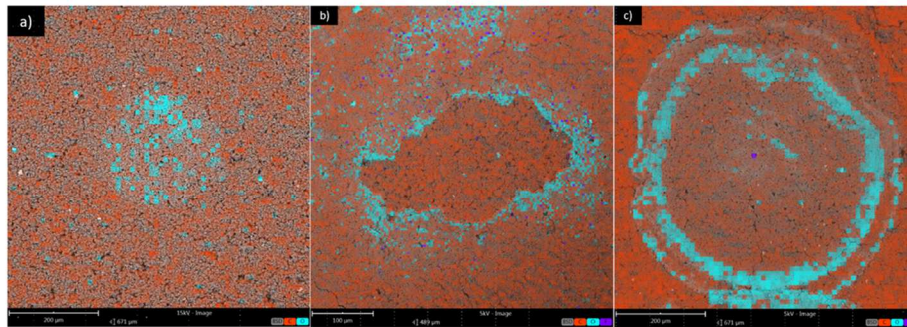


Figure S6. Energy-dispersive X-ray spectroscopy mapping of the electrodes cycled and floated in the (a) 1 % H₂O, (b) 2 % H₂O and (c) 3.8 % H₂O mixture. The orange dots represent carbon, while the blue points represent oxygen, indicating a high amount of oxygen in the drop like shapes.

Publication 3

ChemSusChem

Supporting Information

Water in Protic Ionic Liquid Electrolytes: From Solvent Separated Ion Pairs to Water Clusters

Sascha Gehrke, Promit Ray, Timo Stettner, Andrea Balducci, and Barbara Kirchner* © 2021
The Authors. ChemSusChem published by Wiley-VCH GmbH. This is an open access article under the terms of the Creative Commons Attribution License, which permits use, distribution and reproduction in any medium, provided the original work is properly cited.

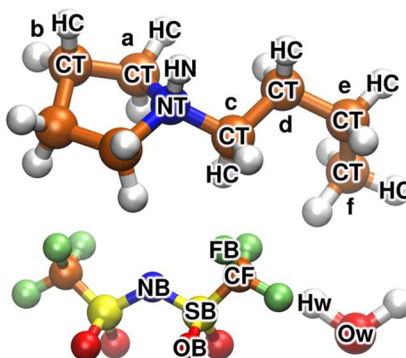


Figure S1: Atom types of the molecules applied in the simulations. Further, the CH_x groups of the cation are marked with letters from a to f.

Table 1: The scaled RESP charges applied in the article. For names of the atom types see S1.

Atom	Charge
[NTf ₂] ⁻	
CF	0.18697643
FB	-0.10657503
NB	-0.51772659
OB	-0.43203516
SB	0.85568228
[pyrH4] ⁺	
CT a	-0.00941801
CT b	-0.06069608
CT c	-0.07591409
CT d	-0.03290304
CT e	0.00364400
CT f	-0.10874314
HC a	0.08150810
HC b	0.06301608
HC c	0.07849810
HC d	0.03382304
HC e	0.03298704
HC f	0.04195005
NT	-0.05826207
HN	0.21784327
water	
Ow	-0.8476
Hw	0.4238

2 Force-Field Parameters

15 atom types
9 bond types
15 angle types
13 dihedral types

Masses

ID	Mass	MolType	Element	Symbol
1	12.011000	# MolType 1	(C2F6N04S2)	CF
2	18.998000	# MolType 1	(C2F6N04S2)	FB
3	14.000000	# MolType 1	(C2F6N04S2)	NB
4	15.999000	# MolType 1	(C2F6N04S2)	OB
5	32.066000	# MolType 1	(C2F6N04S2)	SB
6	12.011000	# MolType 2	(C8H18N)	CT
7	12.011000	# MolType 2	(C8H18N)	CT
8	12.011000	# MolType 2	(C8H18N)	CT
9	12.011000	# MolType 2	(C8H18N)	CT
10	1.008000	# MolType 2	(C8H18N)	HN
11	1.008000	# MolType 2	(C8H18N)	HC
12	1.008000	# MolType 2	(C8H18N)	HC
13	14.007000	# MolType 2	(C8H18N)	NT
14	1.008000	# MolType 3	(H2O)	HW
15	15.999000	# MolType 3	(H2O)	OW

Pair Coeffs

ID	CF	FB	NB	OB	SB	CT	CT	CT	CT	HN	HC	HC	NT	HW	OW
1	0.065999	3.500000	# MolType 1	(C2F6N04S2)	CF										
2	0.053000	2.950000	# MolType 1	(C2F6N04S2)	FB										
3	0.170000	3.250000	# MolType 1	(C2F6N04S2)	NB										
4	0.210000	2.960000	# MolType 1	(C2F6N04S2)	OB										
5	0.250000	3.550000	# MolType 1	(C2F6N04S2)	SB										
6	0.065999	3.500000	# MolType 2	(C8H18N)	CT										
7	0.065999	3.500000	# MolType 2	(C8H18N)	CT										
8	0.065999	3.500000	# MolType 2	(C8H18N)	CT										
9	0.065999	3.500000	# MolType 2	(C8H18N)	CT										
10	0.000000	0.000000	# MolType 2	(C8H18N)	HN										
11	0.030000	2.500000	# MolType 2	(C8H18N)	HC										
12	0.030000	2.500000	# MolType 2	(C8H18N)	HC										
13	0.170000	3.250000	# MolType 2	(C8H18N)	NT										
14	0.000000	0.000000	# MolType 3	(H2O)	HW										
15	0.165354	3.166000	# MolType 3	(H2O)	OW										

Bond Coeffs

1	233.030593	1.818000	# MolType 1 (C2F6N04S2)	CF - SB
2	441.921606	1.323000	# MolType 1 (C2F6N04S2)	FB - CF
3	374.880497	1.570000	# MolType 1 (C2F6N04S2)	NB - SB
4	637.069790	1.437000	# MolType 1 (C2F6N04S2)	SB - DB
5	382.002868	1.448000	# MolType 2 (CBH18N)	NT - CT
6	267.925430	1.529000	# MolType 2 (CBH18N)	CT - CT
7	339.985660	1.090000	# MolType 2 (CBH18N)	HC - CT
8	434.034417	1.010000	# MolType 2 (CBH18N)	HN - NT
9	450.000000	1.000000	# MolType 3 (H2O)	DW - HW

Angle Coeffs

1	92.934990	111.700000	# MolType 1 (C2F6N04S2)	FB - CF - SB
2	98.331740	107.100000	# MolType 1 (C2F6N04S2)	FB - CF - FB
3	80.186424	125.600000	# MolType 1 (C2F6N04S2)	SB - NB - SB
4	91.300191	103.500000	# MolType 1 (C2F6N04S2)	NB - SB - CF
5	94.287763	113.600000	# MolType 1 (C2F6N04S2)	NB - SB - DB
6	103.967495	102.600000	# MolType 1 (C2F6N04S2)	CF - SB - DB
7	115.798279	118.500000	# MolType 1 (C2F6N04S2)	DB - SB - DB
8	56.202199	109.500000	# MolType 2 (CBH18N)	NT - CT - CT
9	35.002390	109.500000	# MolType 2 (CBH18N)	HC - CT - NT
10	37.500000	110.700000	# MolType 2 (CBH18N)	CT - CT - HC
11	32.994742	107.800000	# MolType 2 (CBH18N)	HC - CT - HC
12	58.353250	112.700000	# MolType 2 (CBH18N)	CT - CT - CT
13	35.002390	109.500000	# MolType 2 (CBH18N)	HN - NT - CT
14	51.804493	107.200000	# MolType 2 (CBH18N)	CT - NT - CT
15	54.995220	109.470000	# MolType 3 (H2O)	HW - DW - HW

Dihedral Coeffs

1	7.832935	-2.490440	-0.763623	0.000000	# MolType 1 (C2F6N04S2)	SB - NB - SB - CF
2	0.000000	0.000000	0.315966	0.000000	# MolType 1 (C2F6N04S2)	NB - SB - CF - FB
3	0.000000	0.000000	0.346797	0.000000	# MolType 1 (C2F6N04S2)	DB - SB - CF - FB
4	0.000000	0.000000	-0.003555	0.000000	# MolType 1 (C2F6N04S2)	DB - SB - NB - SB
5	0.000000	0.000000	0.559990	0.000000	# MolType 2 (CBH18N)	HC - CT - NT - CT
6	0.415989	-0.128011	0.695005	0.000000	# MolType 2 (CBH18N)	CT - NT - CT - CT
7	1.300000	-0.050000	0.200000	0.000000	# MolType 2 (CBH18N)	CT - CT - CT - CT
8	0.000000	0.000000	0.300000	0.000000	# MolType 2 (CBH18N)	CT - CT - CT - HC
9	-0.190100	-0.416993	0.417997	0.000000	# MolType 2 (CBH18N)	HN - NT - CT - CT
10	2.391993	-0.673996	0.550000	0.000000	# MolType 2 (CBH18N)	CT - CT - CT - NT
11	0.000000	0.000000	0.400000	0.000000	# MolType 2 (CBH18N)	HN - NT - CT - HC
12	0.000000	0.000000	0.300000	0.000000	# MolType 2 (CBH18N)	HC - CT - CT - HC
13	-1.013002	-0.709011	0.472992	0.000000	# MolType 2 (CBH18N)	HC - CT - CT - NT

3 Mean Square Displacements

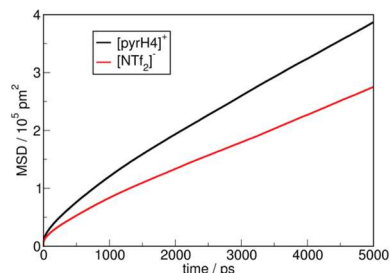


Figure S2: Mean square displacements calculated for the simulation of the pure ionic liquid at a temperature of 30° C.

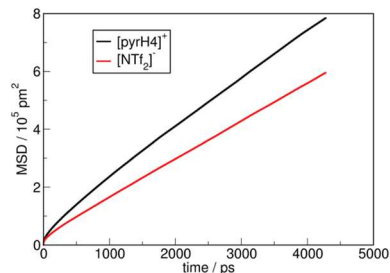


Figure S3: Mean square displacements calculated for the simulation of the pure ionic liquid at a temperature of 50° C.

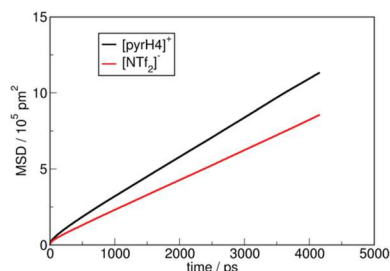


Figure S4: Mean square displacements calculated for the simulation of the pure ionic liquid at a temperature of 60° C.

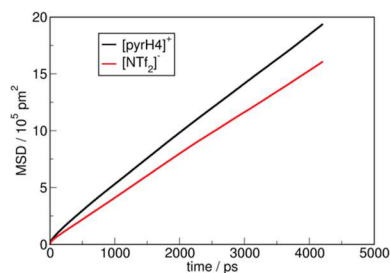


Figure S5: Mean square displacements calculated for the simulation of the pure ionic liquid at a temperature of 80° C.

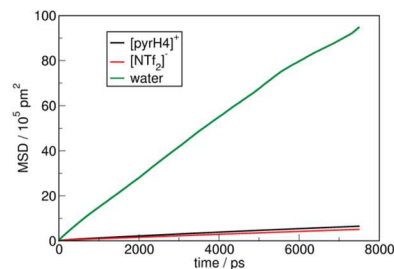


Figure S6: Mean square displacements calculated for the simulation of the ionic liquid with 0.1% water at a temperature of 30° C.

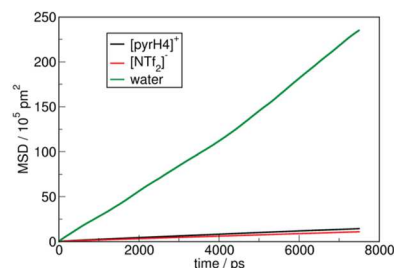


Figure S7: Mean square displacements calculated for the simulation of the ionic liquid with 0.1% water at a temperature of 50° C.

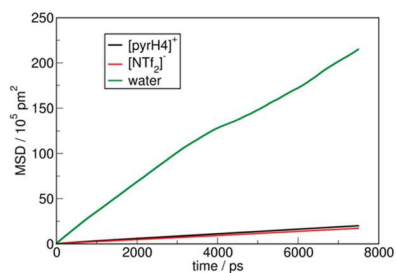


Figure S8: Mean square displacements calculated for the simulation of the ionic liquid with 0.1% water at a temperature of 60° C.

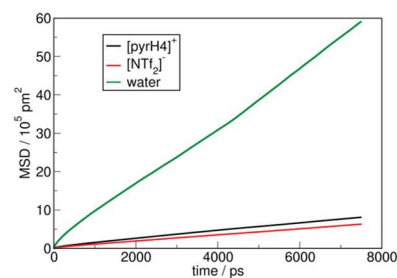


Figure S10: Mean square displacements calculated for the simulation of the ionic liquid with 1.0% water at a temperature of 30° C.

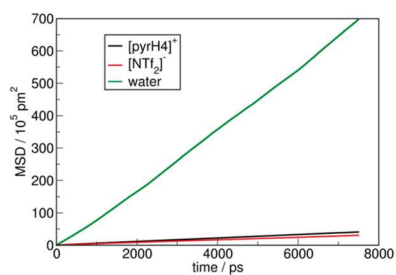


Figure S9: Mean square displacements calculated for the simulation of the ionic liquid with 0.1% water at a temperature of 80° C.

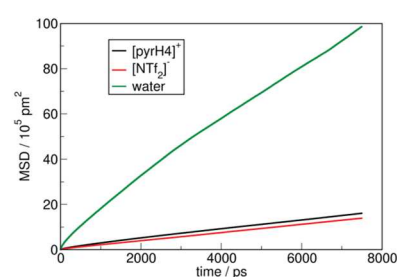


Figure S11: Mean square displacements calculated for the simulation of the ionic liquid with 1.0% water at a temperature of 50° C.

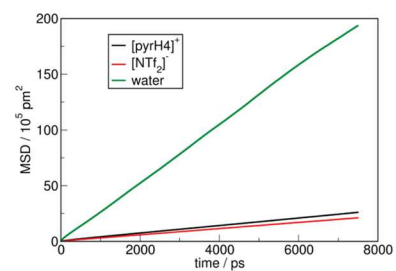


Figure S12: Mean square displacements calculated for the simulation of the ionic liquid with 1.0% water at a temperature of 60° C.

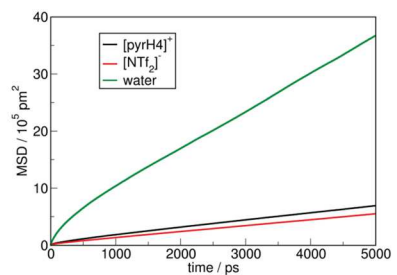


Figure S14: Mean square displacements calculated for the simulation of the ionic liquid with 2.0% water at a temperature of 30° C.

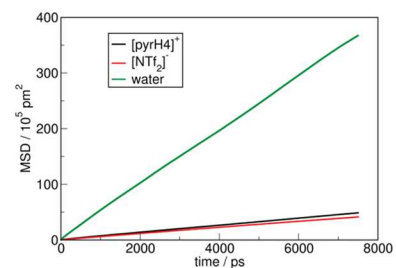


Figure S13: Mean square displacements calculated for the simulation of the ionic liquid with 1.0% water at a temperature of 80° C.

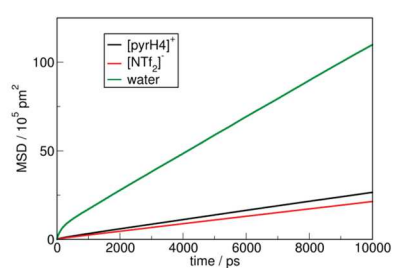


Figure S15: Mean square displacements calculated for the simulation of the ionic liquid with 2.0% water at a temperature of 50° C.

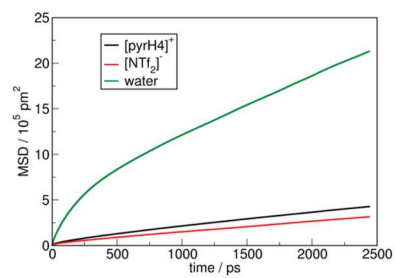


Figure S16: Mean square displacements calculated for the simulation of the ionic liquid with 3.8% water at a temperature of 30° C.

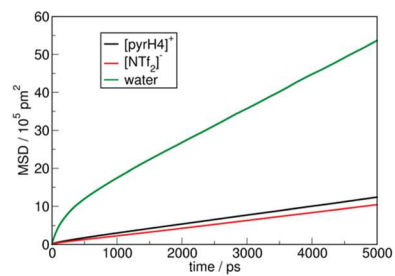


Figure S17: Mean square displacements calculated for the simulation of the ionic liquid with 3.8% water at a temperature of 50° C.

Publication 4

Mixtures of Glyme and aprotic-protic ionic liquids as electrolytes for energy storage devices

T. Stettner,^{1,2} P. Huang,^{1,2} , M. Goktas^{1,2}, P. Adelhelm ^{1,2} and A. Balducci^{1,2*}

V. Supplementary Information

TABLE II. Calculated VTF parameters of the conductivity measurements of the different electrolytes.

Electrolyte	T_0 [K]	σ_0 [mS*cm]	B_v [K]	R^2
Py _{rH4} TFSI	188	458,86	588,47	0,9999
2g/Py _{rH4} TFSI 20:80	182	441.24	558.60	0.9999
2g/Py _{rH4} TFSI 50:50	180	304.90	471.08	0.9999
2g/Py _{rH4} TFSI 80:20	161	178.19	390.74	0.9999
2g/Py _{r14} TFSI 20:80	167	623.28	732.54	0.9999
2g/Py _{r14} TFSI 50:50	157	206.16	452.79	0.9999
2g/Py _{r14} TFSI 80:20	157	158.74	402.72	0.9999

TABLE III. Calculated VTF parameters of the viscosity measurements of the different electrolytes.

Electrolyte	T_0 [K]	η_0 [mPa*s]	B_v [K]	R^2
Py _{rH4} TFSI	239	2.32	212.48	0,9987
2g/Py _{rH4} TFSI 20:80	227	1.60	246.98	0.9993
2g/Py _{rH4} TFSI 50:50	232	2.53	136.13	0.9981
2g/Py _{rH4} TFSI 80:20	276	3.08	12.11	0.8372
2g/Py _{r14} TFSI 20:80	181	0.52	536.32	0.9998
2g/Py _{r14} TFSI 50:50	181	0.56	305.38	0.9999
2g/Py _{r14} TFSI 80:20	182	0.57	262.88	0.9995

Publication 6

Enabling safe and stable Li metal batteries with protic ionic liquid electrolytes and high voltage cathodes

Gabriele Lingua^a, Marisa Falco^a, Timo Stettner^b, Claudio Gerbaldi^{a,*}, Andrea Balducci^{b,*}

^a GAME Lab, Department of Applied Science and Technology (DISAT), Politecnico di Torino, C.so Duca degli Abruzzi 24, 10129, Torino, Italy.

^b Friedrich-Schiller-University Jena, Institute for Technical Chemistry and Environmental Chemistry, Center for Energy and Environmental Chemistry Jena (CEEC Jena), Philosophenweg 7a, 07743, Jena, Germany

* Corresponding Authors: claudio.gerbaldi@polito.it; andrea.balducci@uni-jena.de;

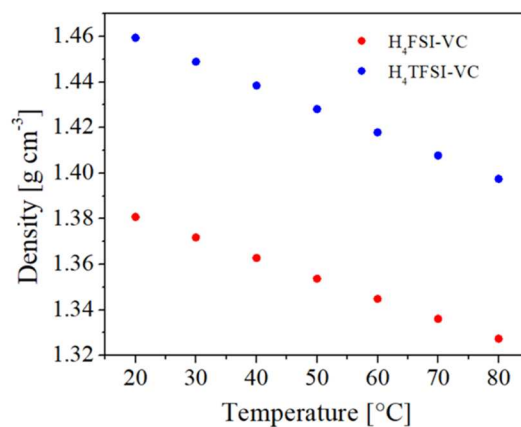


Figure S1. Influence of the temperature on the density of the VC-added PIL-based electrolytes under study.

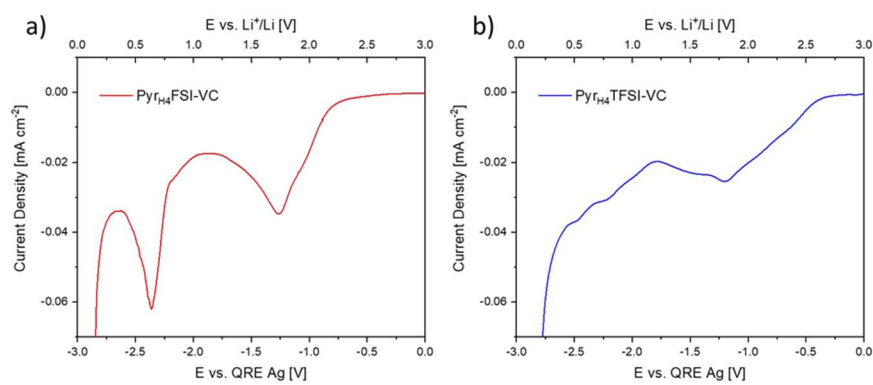


Figure S2. Magnification of the ESW of the investigated electrolytes, highlighting the decomposition of the VC and the suppressed decomposition of the PILs: a) FSI⁻ and b) TFSI⁻ based.

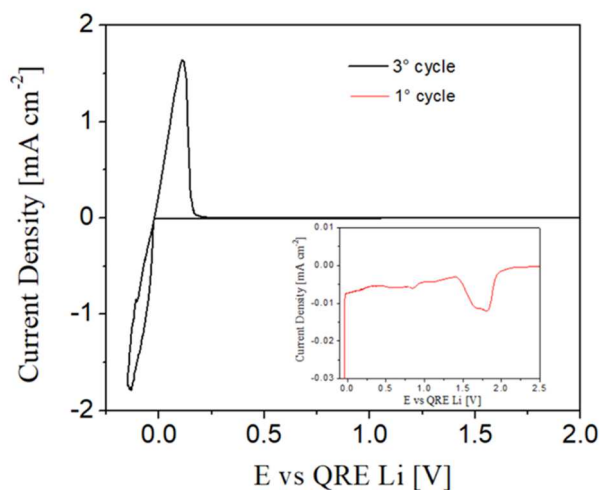


Figure S3. Cathodic stability window (CSW) of the VC-added PIL-based (H_4 FSI-VC) electrolyte; in the insert the magnification of signal between 1.5-2V during the first reduction process.

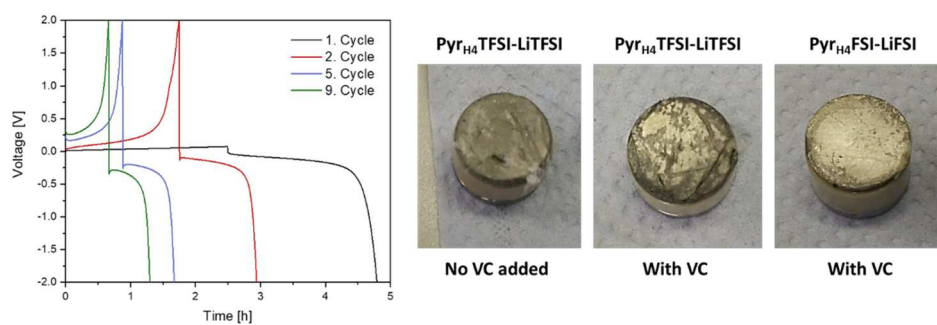


Figure S4. Stripping-plating experiment of lithium electrodes using Pyr_{H_4} TFSI with LiTFSI and no VC as additive (left hand sided plot); on the right hand side, digital photographs of Li metal surface after plating/stripping experiments with (more shiny) or without (gray and dull) VC.

The cells were opened without adopting any countermeasure to prevent contact with the air.

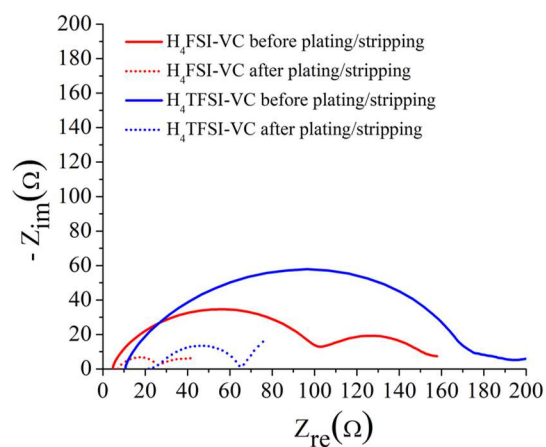


Figure S5. Nyquist impedance plots of the two PIL based electrolytes before (solid curves) and after (dotted curves) plating/stripping analysis. Measurements were conducted at ambient laboratory temperature and current density of 0.088 mA cm^{-2} .

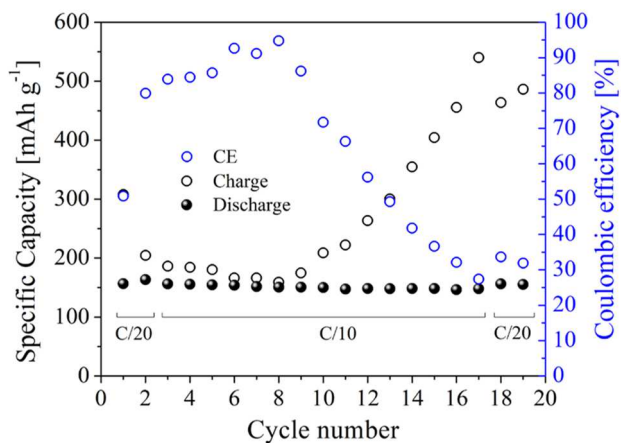


Figure S6. Galvanostatic charge/discharge cycling behavior of [Li metal/PYR₄TFSI-LITFSI-VC/NMC] cell: evolution of the specific capacity and the Coulombic efficiency at different C rates with the cycle number.

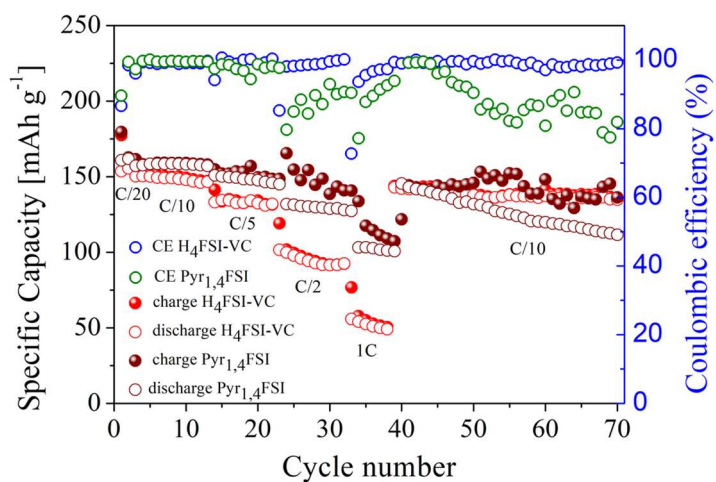


Figure S7. Comparison of the constant-current (galvanostatic) charge/discharge cycling behavior of different [Li metal/IL solution/NMC] cells assembled with H₄FSI-VC electrolyte and the corresponding one with the aprotic PYR_{1,4}FSI-LiFSI solution without VC: evolution of the specific capacity and the Coulombic efficiency at different C rates with the cycle number.

Publication 7

**Ionic liquid-based electrolytes
for calcium-based energy storage systems**T. Stettner^{1*}, R. Dugas^{2*}, A. Ponrouch^{2,3}, A. Balducci^{1,3}

¹ Institute for Technical Chemistry and Environmental Chemistry Center for Energy and Environmental Chemistry Jena
(CEEC Jena) Philosophenweg 7a, 07743 Jena, Germany

² Institut de Ciència de Materials de Barcelona (ICMAB-CSIC), Campus UAB, 08193 Bellaterra, Catalonia (Spain).

³ ALISTORE – European Research Institute, CNRS FR 3104, Hub de l’Energie, 15 Rue Baudelocque, 80039 Amiens (France)

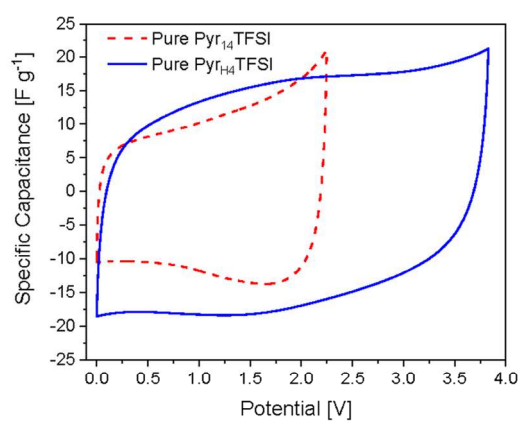
Supplementary Information

Figure S1: Cyclic Voltammetry (scan rate 1 mV s⁻¹ of EDLCs containing PYR₁₄TFSI and PYR₄TFSI. The tests have been carried out at room temperature.

Publication 8

Electronic Supplementary Material (ESI) for Physical Chemistry Chemical Physics.
This journal is © the Owner Societies 2020. Please do not adjust margins



PCCP

ARTICLE

Supplementary Information

Silica based ionogels: interfaces effects with aprotic and protic ionic liquids with lithium
A Marie, B Said, A Galarneau, T Stettner, A Balducci, M Bayle, B Humbert and J. Le Bideau

DOI: 10.1039/d0cp03599h

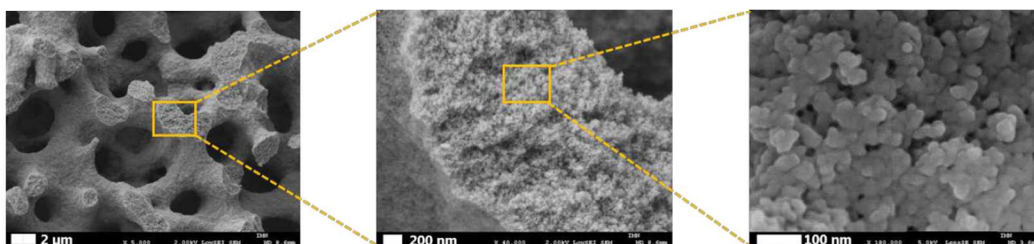


Fig. S1 SEM image of silica monolith

Table S1 Mass fraction and volume of ILs in impregnated silica

$\phi_{\text{meso (N2)}}$ (nm)	Pyr14TFSI-based ionogels		Pyr14-LITFSI-based ionogels		PyrH4TFSI-based ionogels		PyrH4-LITFSI-based ionogels	
	%wt IL	$V_{\text{Total (I4)}}$ (cm ³ /g of silica)	%wt IL	$V_{\text{Total (I4-Li)}}$ (cm ³ /g of silica)	%wt IL	$V_{\text{Total (H4)}}$ (cm ³ /g of silica)	%wt IL	$V_{\text{Total (H4-Li)}}$ (cm ³ /g of silica)
8.1	82.5 ± 0.2	3.40 ± 0.05	82.6 ± 0.3	3.32 ± 0.06	81.9 ± 0.1	3.15 ± 0.01	82.36 ± 0.02	3.24 ± 0.00
8.5	81.9 ± 0.1	3.26 ± 0.01	82.0 ± 0.4	3.19 ± 0.08	82.1 ± 0.7	3.2 ± 0.1	82.4 ± 0.6	3.3 ± 0.1
9.8	83.0 ± 0.5	3.5 ± 0.1	84.0 ± 0.4	3.7 ± 0.1	84 ± 1	3.6 ± 0.3	82.9 ± 0.7	3.4 ± 0.1
11.2	82.8 ± 0.1	3.47 ± 0.02	83.1 ± 0.2	3.44 ± 0.05	83.7 ± 0.8	3.6 ± 0.2	83.75 ± 1	3.6 ± 0.2
12.6	83.4 ± 0.1	3.62 ± 0.04	83.3 ± 0.3	3.49 ± 0.07	83.02 ± 0.05	3.41 ± 0.01	83.2 ± 0.1	3.43 ± 0.02
16.2	84.3 ± 0.1	3.87 ± 0.02	84.5 ± 0.2	3.80 ± 0.05	84.38 ± 0.01	3.770 ± 0.002	84.44 ± 0.00	3.77 ± 0.00

Density at 30°C: Pyr14TFSI 1.3906 ; Pyr14TFSI + 0.5M LITFSI 1.4319 ; PyrH4TFSI 1.4326 ; PyrH4TFSI+0.5M LITFSI 1.4397

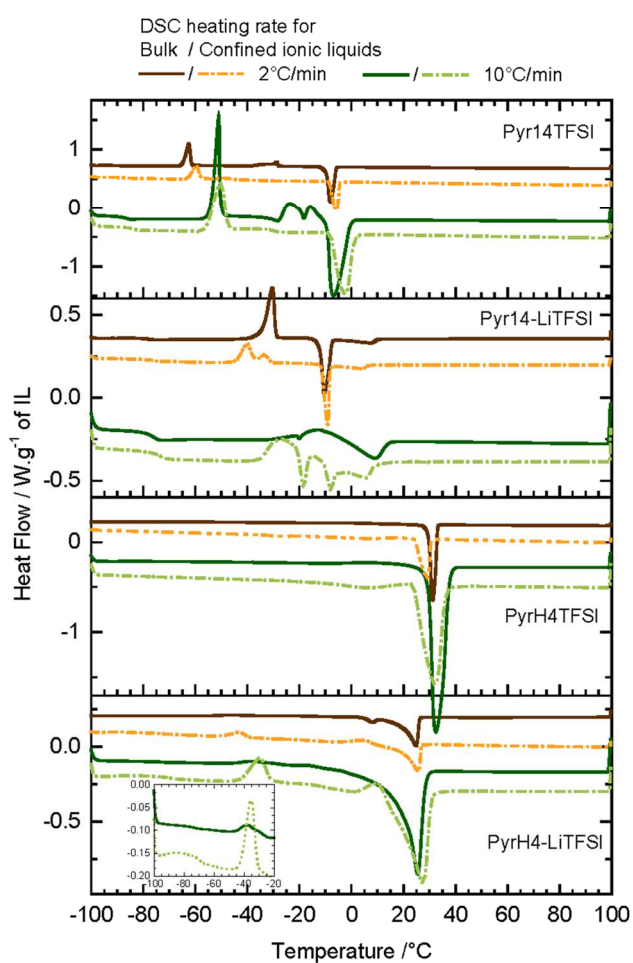


Fig. S2: DSC thermogram of ionic liquids, in bulk state and for a confinement in 11.2 nm meso-porous silica. From top to bottom: Pyr14TFSI, Pyr14-LiTFSI, PyrH4TFSI and PyrH4-LiTFSI. Inset: glass transition of PyrH4-LiTFSI.

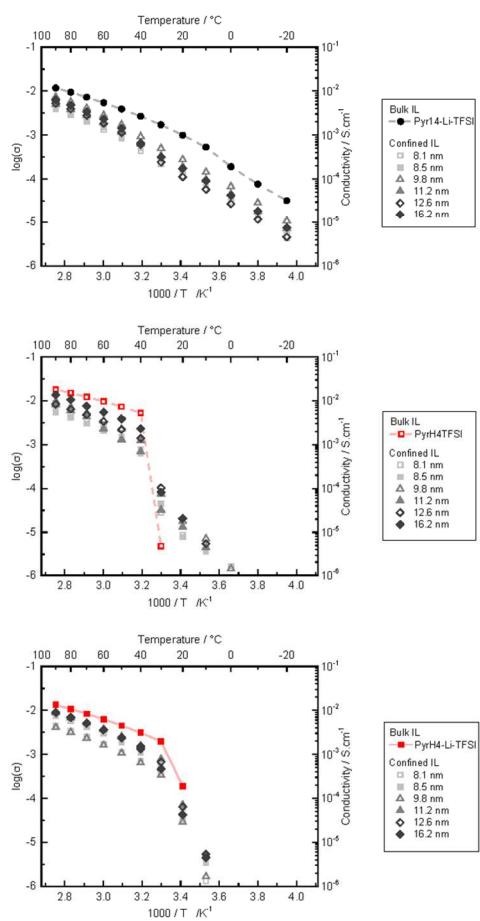


Fig. S3: Conductivity of Pyr14TFSI, PyrH4TFSI and PyrH4-Li-TFSI bulk ionic liquids and ionogels.

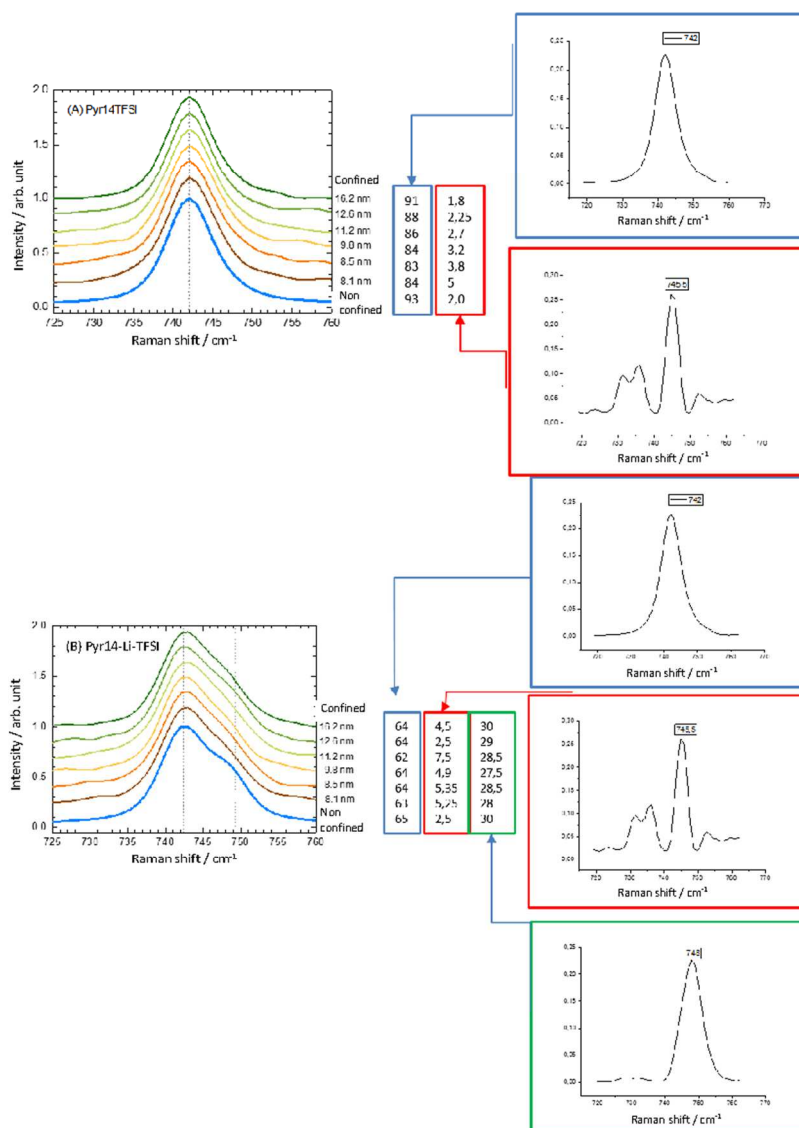


Fig. S4:-BPSS. Examples of BPSS algorithm application, for Pyr14TFSI bulk and confined (A) without Li^+ and (B) with 0.5 M of Li^+ . The weight of each source is noted in column, in front of mesopore sizes.

Please do not adjust margins

Journal Name

ARTICLE

Table S2: Fitting parameters obtained for non-confined and confined Pyr14-LiTFSI (named by meso-pore size). *fixed parameters

Fitted component	Parameter	Pyr14-LiTFSI	8.1 nm	8.5 nm	9.8 nm	11.2 nm	12.6 nm	16.2 nm
	y_0	0.016	0.009	0.005	0.008	0.008	0.005	0.007
C1	x_c^*	741.8	741.7	741.7	741.7	741.7	741.7	741.7
	A	2.24	0.63	0.53	0.55	0.80	0.57	0.66
	$6 < \omega < 8$	6.56	6.67	6.67	6.33	7.69	6.66	6.39
	μ^*	0.68	0.68	0.68	0.68	0.68	0.68	0.68
C2	x_c^*	743	743	743	743	743.01	743	743
	A	1.44	1.23	1.06	1.2	1.2	0.67	1.41
	$6 < \omega < 9$	7.50	7.77	7.77	7.73	7.78	7.77	8.00
	μ^*	0.74	0.74	0.74	0.74	0.74	0.74	0.74
C3	x_c^*	748.3	748.3	748.3	748.3	748.3	748.3	748.3
	A	1.28	0.45	0.39	0.36	0.51	0.37	0.50
	$6 < \omega < 7.2$	7.14	7	7	6.2	7.2	7	7
	μ^*	0	0	0	0	0	0	0

$$y = y_0 + A \times \left[\mu \frac{2}{\pi} \frac{\omega}{4(x-x_c)^2 + \omega^2} + (1-\mu) \frac{\sqrt{4 \ln 2}}{\omega \sqrt{\pi}} \exp\left(-\frac{4 \ln 2}{\omega^2}(x-x_c)^2\right) \right]$$

With y_0 : offset, x_c : peak centre, A : peak area, μ : profil shape factor (% of Lorentzian) and ω : FWHM.

Please do not adjust margins

Please do not adjust margins

ARTICLE

Journal Name

Table S3: Fitting parameters obtained for non-confined and confined PyrH4-LITFSI (named by meso-pore size). *fixed parameters

Fitted component	Parameter	PyrH4-LITFSI	8.1 nm	8.5 nm	9.8 nm	11.2 nm	12.6 nm	16.2 nm
	y_0	0.007	0.004	0.004	0.004	0.005	0.0034	0.004
C1	x_C^*	743.06	743.06	743.06	743.06	743.06	743.06	743.06
	A	1.98	0.44	0.76	0.95	0.86	0.41	1.11
	$\omega < 8$	7.75	7.75	7.75	7.75	7.75	7.75	7.75
	μ^*	0.68	0.68	0.68	0.68	0.68	0.68	0.68
C2	x_C^*	745	745	745	745	745	745	745
	A	1.72	0.33	0.47	0.57	0.41	0.59	0.57
	$\omega < 7$	<u>7</u>	<u>7</u>	<u>7</u>	<u>7</u>	<u>7</u>	<u>7</u>	<u>7</u>
	μ^*	0.74	0.74	0.74	0.74	0.74	0.74	0.74
C3	x_C^*	748.72	748.72	748.72	748.72	748.72	748.72	748.72
	A	0.60	0.03	0.19	0.3	0.25	0.16	0.34
	$\omega < 6.2$	<u>6</u>	<u>6</u>	<u>6</u>	<u>6</u>	<u>6</u>	<u>6</u>	<u>6</u>
	μ^*	0	0	0	0	0	0	0

Please do not adjust margins

Publication 9

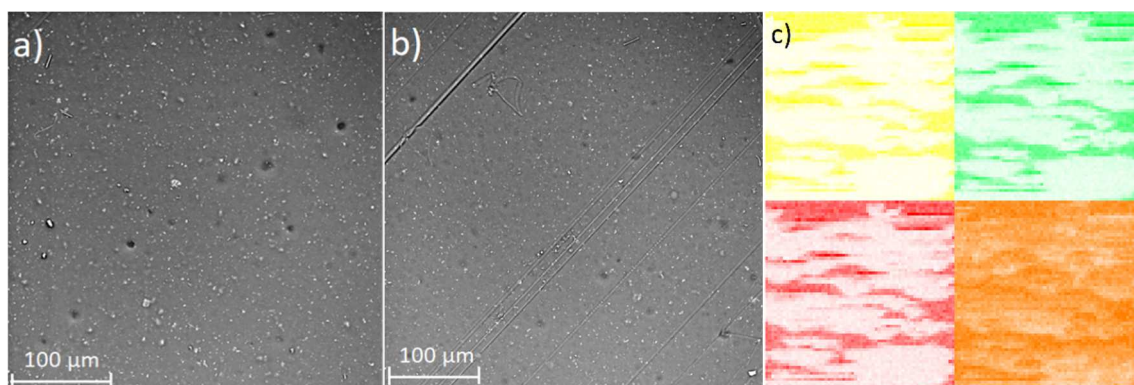


Figure S1. A) and B) SEM images of the PEO_HPyr. C) EDX mapping of B) showing the signals of fluorine (yellow), carbon (green), oxygen (red) and sulfur (orange).

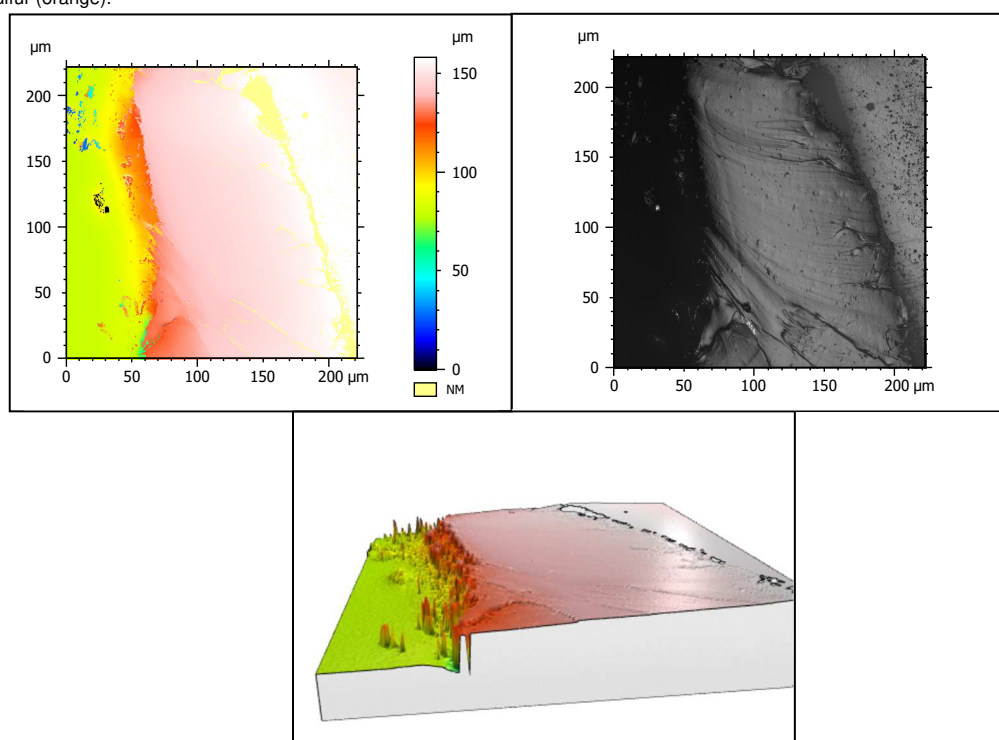


Figure S2. Surface profile of the PEO_HPyr membrane, revealing a homogenous cross section. The thickness of the membrane is around 150 µm.



Figure S3. Flammability test of the PEO based polymer electrolytes, incorporating nonflammable IL PyrH4TFSI. Only colour and size changes are visible, no flame originating from the membrane itself.

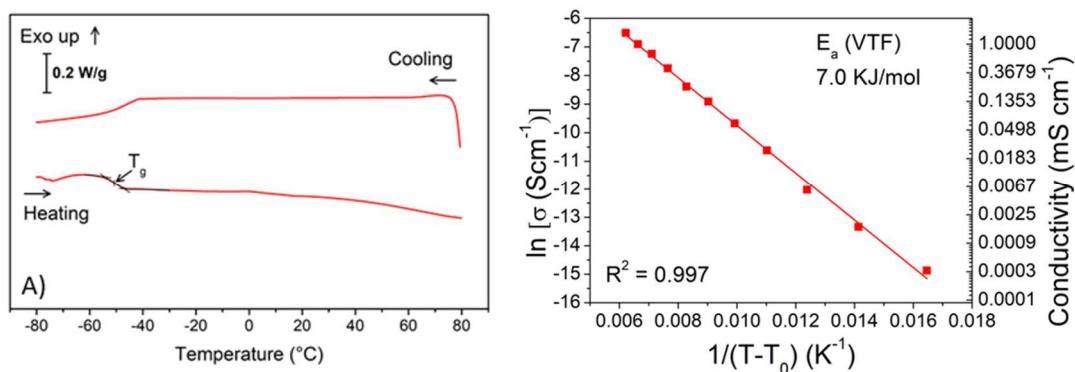


Figure S4. DSC heating and cooling scans of PEO_HPy. b) VTF plot and linear fit of the logarithm of conductivity versus $1/(T-T_0)$ for PEO_HPy.

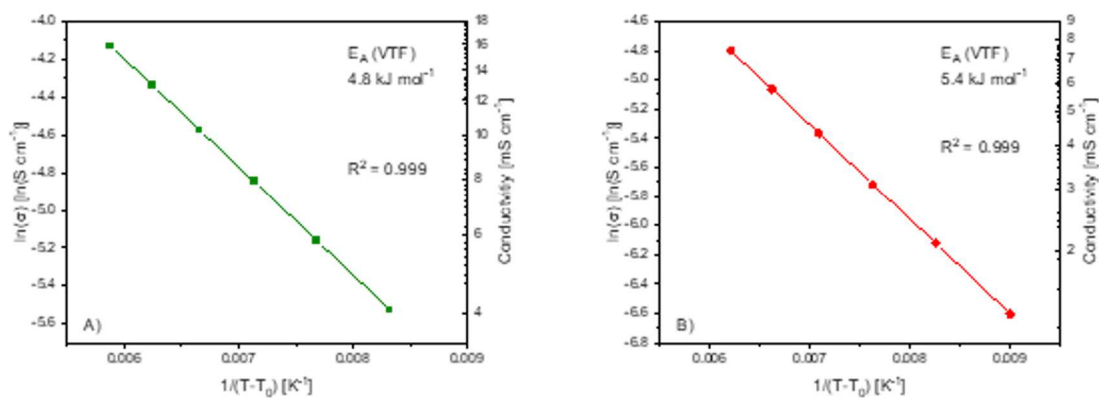


Figure S5. VTF plot and linear fit of the logarithm of conductivity versus $(T-T_0)^{-1}$ for A) PyriH₄TFSI and B) HPy.

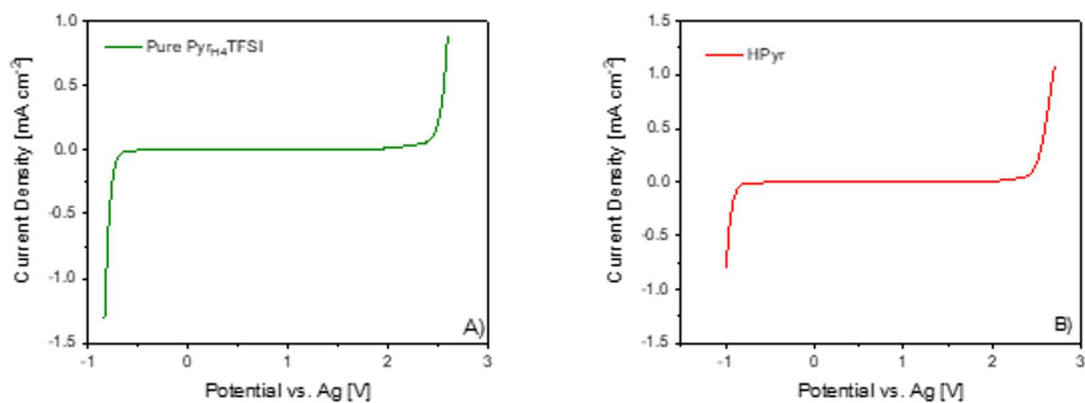


Figure S6. ESW of A) pure PyriH₄TFSI (40 °C, 0.1 mV s⁻¹) and B) the liquid electrolyte HPy (40 °C, 0.1 mV s⁻¹), measured via linear sweep voltammetry with a platinum working electrode, silver reference electrode and an oversized carbon counter electrode.

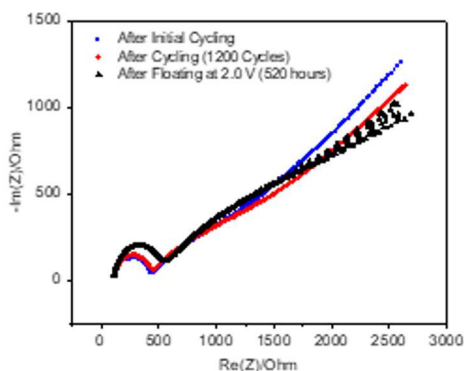


Figure S7. Nyquist plot of the EDLC using PEO_HPyr as electrolyte.

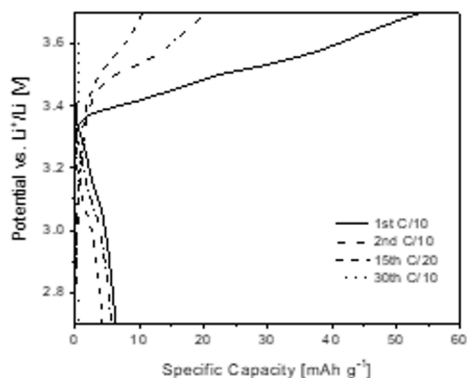


Figure S8. Voltage profile vs. specific capacity during CC cycling of a Li/PEO_HPyr/LFP cell at C/10 rate and RT.

Table S1. In this work, we present the first example ever of protic ionic liquid based polymer electrolyte membrane operating stably at high specific capacity in LFP-based Li metal cell at ambient temperature and different current regimes. For the sake of comparison, the above reported Table lists the characteristics and some specific performance of the most similar (to our knowledge) systems to our crosslinked PEO_HPyr polymer electrolyte; clearly, these systems are based on aprotic ionic liquids. It demonstrates that our newly proposed polymer electrolyte is at the level of the best reported examples in the literature so far. Other examples of similar systems have been already reported in Table of Osada et al. *Angew. Chem. Int. Ed.* 55 (2016) 500-513, thus the Reader is referred to that article for further details.

Composition (molar fraction)	C/rate	Temp. [°C]	Specific discharge capacity [mAh g ⁻¹]	No. of cycles	LFP loading [mg cm ⁻²]	Ref.
P(EO) ₁₀ LiTFSI-(Pyr ₁₄ TFSI) ₂	C/20	40	161	100	≈ 4	a)
P(EO) ₂₀ LiTFSI-(Pyp _{1.101} TFSI)	C/20	25	120	35	≈ 2	b)
P(EO) ₂₀ LiTFSI-(Pyr ₁₃ TFSI) _{1.27}	C/10	25	≈ 115	20	n.d.	c)
P(EO) ₁₀ LiTFSI-Pyr ₁₄ TFSI	C/20	30	115	20 ^{e)}	≈ 4	d)
	C/20	30	170	40	≈ 4	
P(EO) ₂₀ LiTFSI	C/20	20	5	1	≈ 4	d)
		30	10	1	≈ 4	
P(EO) _{16.7} LiTFSI-(Pyr _{H4} TFSI) _{1.8} ^{f)}	C/20	20	>150 stable ^{g)}	30	≈ 1	This work
	C/10	20	140 stable			

[a] M. Wetjen et al. / *Journal of Power Sources* 246 (2014) 846-857. [b] Y. An et al. / *Materials Chemistry and Physics* 128 (2011) 250-255. [c] A. Yongxin et al. / *J Solid State Electrochem* 16 (2012) 383-389. [d] G.B. Appetecchi et al. / *Journal of Power Sources* 196 (2011) 6703-6709. [e] Decreases to 90 mAh g⁻¹ in 10 cycles. [f] namely PEO_HPyr. [g] the LFP used in this work shows a practical specific capacity at C/20 rate in standard liquid electrolyte of 158 mAh g⁻¹.